DOCTOR OF PHILOSOPHY

Simulating the temporal and spatial variability of North Wales mussel populations

Demmer, Jonathan

Award date:
2020

Awarding institution:
Bangor University

PRIFYSGOL
BANGOR
UNIVERSITY

Simulating the temporal and spatial variability of North Wales mussel populations

by

Jonathan Demmer

School of Oceans Sciences, Bangor University, Menai Bridge, Anglesey, UK, LL59 5AB

Submitted in accordance with the requirements for the degree of Doctor of Philosophy

February, 2020

Declaration and Consent

Details of the Work

I hereby agree to deposit the following item in the digital repository maintained by Bangor University and/or in any other repository authorized for use by Bangor University.

Author Name:

……..

Title:

……..……

…….

Supervisor/Department:

.....

Funding body (if any):

.....

Qualification/Degree obtained:

…….

This item is a product of my own research endeavours and is covered by the agreement below in which the item is referred to as "the Work". It is identical in content to that deposited in the Library, subject to point 4 below.

Non-exclusive Rights

Rights granted to the digital repository through this agreement are entirely non-exclusive. I am free to publish the Work in its present version or future versions elsewhere.

I agree that Bangor University may electronically store, copy or translate the Work to any approved medium or format for the purpose of future preservation and accessibility. Bangor University is not under any obligation to reproduce or display the Work in the same formats or resolutions in which it was originally deposited.

Bangor University Digital Repository

I understand that work deposited in the digital repository will be accessible to a wide variety of people and institutions, including automated agents and search engines via the World Wide Web.

I understand that once the Work is deposited, the item and its metadata may be incorporated into public access catalogues or services, national databases of electronic theses and dissertations such as the British Library's EThOS or any service provided by the National Library of Wales.

I understand that the Work may be made available via the National Library of Wales Online Electronic Theses Service under the declared terms and conditions of use

(http://www.llgc.org.uk/index.php?id=4676). I agree that as part of this service the National Library of Wales may electronically store, copy or convert the Work to any approved medium or format for the purpose of future preservation and accessibility. The National Library of Wales is not under any obligation to reproduce or display the Work in the same formats or resolutions in which it was originally deposited.

Statement 1:

This work has not previously been accepted in substance for any degree and is not being concurrently submitted in candidature for any degree unless as agreed by the University for approved dual awards.

Signed …….. (candidate)

Date ……..

Statement 2:

This thesis is the result of my own investigations, except where otherwise stated. Where correction services have been used, the extent and nature of the correction is clearly marked in a footnote(s).

All other sources are acknowledged by footnotes and/or a bibliography.

Signed ……. (candidate)

Date …….

Statement 3:

I hereby give consent for my thesis, if accepted, to be available for photocopying, for inter-library loan and for electronic storage (subject to any constraints as defined in statement 4), and for the title and summary to be made available to outside organisations.

Signed ……. (candidate)

Date …….

NB: Candidates on whose behalf a bar on access has been approved by the Academic Registry should use the following version of **Statement 3:**

Statement 3 (bar):

I hereby give consent for my thesis, if accepted, to be available for photocopying, for inter-library loans and for electronic storage (subject to any constraints as defined in statement 4), after expiry of a bar on access.

Signed …… (candidate)

Date ……

Statement 4:

Choose **one** of the following options

a)	I agree to deposit an electronic copy of my thesis (the Work) in the Bangor University (BU) Institutional Digital Repository, the British Library ETHOS system, and/or in any other repository authorized for use by Bangor University and where necessary have gained the required permissions for the use of third party material.	
b)	I agree to deposit an electronic copy of my thesis (the Work) in the Bangor University (BU) Institutional Digital Repository, the British Library ETHOS system, and/or in any other repository authorized for use by Bangor University when the approved **bar on access** has been lifted.	
c)	I agree to submit my thesis (the Work) electronically via Bangor University's e-submission system, however I **opt-out** of the electronic deposit to the Bangor University (BU) Institutional Digital Repository, the British Library ETHOS system, and/or in any other repository authorized for use by Bangor University, due to lack of permissions for use of third party material.	

Options B should only be used if a bar on access has been approved by the University.

In addition to the above I also agree to the following:

1. That I am the author or have the authority of the author(s) to make this agreement and do hereby give Bangor University the right to make available the Work in the way described above.

2. That the electronic copy of the Work deposited in the digital repository and covered by this agreement, is identical in content to the paper copy of the Work deposited in the Bangor University Library, subject to point 4 below.

3. That I have exercised reasonable care to ensure that the Work is original and, to the best of my knowledge, does not breach any laws – including those relating to defamation, libel and copyright.

4. That I have, in instances where the intellectual property of other authors or copyright holders is included in the Work, and where appropriate, gained explicit permission for the inclusion of that material in the Work, and in the electronic form of the Work as accessed through the open access digital repository, *or* that I have identified and removed that material for which adequate and appropriate permission has not been obtained and which will be inaccessible via the digital repository.

5. That Bangor University does not hold any obligation to take legal action on behalf of the Depositor, or other rights holders, in the event of a breach of intellectual property rights, or any other right, in the material deposited.

6. That I will indemnify and keep indemnified Bangor University and the National Library of Wales from and against any loss, liability, claim or damage, including without limitation any related legal fees and court costs (on a full indemnity bases), related to any breach by myself of any term of this agreement.

Signature: …… Date: …….

Summary

The blue mussel, *Mytilus edulis*, is an economically and ecologically important shellfish species widely distributed in northern Europe. Europe's mussel shellfisheries represent 50% of the annual world-wide harvest of mussel. For the UK's largest mussel industry located in North Wales seeds are collected from wild beds throughout the Irish Sea including Morecambe Bay. However, since 2008, settlement has been unpredictable and less productive in this area (Trevor Jones, Pers. Comm.). Knowledge gaps exist on the spatial and temporal connectivity of the North Wales mussel populations, due to a lack of information on larval spawning patterns and larval dispersal pathways.

Both observational fieldwork and numerical modelling were used, for the first time, to predict the larvae dispersal of the North Wales mussel population in the Irish Sea. The study first established a robust modelling method to simulate larval dispersal in highly energetic coastal regions, through a modelling sensitivity framework. *M. edulis* spawning times according to environmental factors, together with physical factors (tides and wind), was then used to drive models that predict larval dispersal from known spawning sites in North Wales to likely settlement grounds. This novel analysis has identified the physical and biological controls on larval dispersal and connectivity among selected sites across the region.

Two hydrodynamic models were created for this study using TELEMAC-2D: one resolving the entire Irish Sea and one resolving the North Wales region including the Menai Strait at higher spatial resolution. Validation of simulated elevation and velocity against field data showed good agreement with differences < 10%. These simulated velocities were used to drive a new particle tracking model that was developed for this study. The comparison of simulated particles trajectories against drifters and 3D baroclinic hydrodynamic model showed good correlation, which means that 2D model represents well the hydrodynamics in this highly energetic region. For the first time, this study has quantified the impact of the parameterisation of the PTM on its accuracy and computational efficiency. PTM parameters tested were the spatial and temporal resolution of the velocity field, the number of particles released, the timing and location of spawning, larval behaviour, and pelagic larval duration. This study confirmed the importance of high spatio-temporal resolution modelling in the coastal zone, but also highlights their computational costs to help future similar studies to design and build experimental simulations.

The condition index (e.g. represent the evaluation of merchantable trait in blue mussel) was calculated for mussels located in the Menai Strait from March to September 2018. Results showed clear evidence of several spawning events throughout the spring and summer of 2018. This study has therefore provided a new temporal dataset that describes mussel larvae spawning in relation to the environmental factors (e.g. temperature anomaly between air temperature and sea surface temperature) that can induce spawning events in the Menai Strait. Further, spawning was more common during neap tides. Using the models. the dispersal within the Menai Strait was assessed according to different phases of the tide and to different larval release sites. Although the net flow through the Strait is directed south-westwards, results highlighted for the first time the possibility of *M.edulis* larvae dispersing in both directions through the channel and, so, potentially dispersing further within the central Irish Sea and within Liverpool Bay.

Finally, simulations of larval transport showed different spatial dispersal patterns according to the site of release along the North Wales coast. However, these spatial and temporal dispersal patterns were relatively subtle when compared with the influence of wind-driven currents. Larvae distributed in deeper waters will predominantly be transported through tidal flows. However, good agreement of the wind-influenced dispersal patterns with observational data infers that mussel larvae tend to be distributed in near surface currents – and so, the dispersal, connectivity and recruitment of mussel larvae will be highly affected by seasonal and inter-annual weather conditions.

Acknowledgements

My first acknowledgements will be for my supervisors who supported, helped and advised me wisely during the last four years, thank you Simon Neill and Shelagh Malham. A sincere thanks to Peter Robins who was always available (even when not necessary… sorry Pete) to give me energy, continuous support and ideas to write this PhD. Thanks also to Trevor Jones for his highlights on mussel farming in North Wales and funding this PhD.

Many people from the School of Ocean Sciences helped me through my PhD: Julie Webb, Stuart Jenkins, Luis Gimenez, Sophie Wilmes, Alice Goward Brown, Natasha Lucas, Alan Davies. All their advices were welcomed and helped me to progress in so many ways during the last four years. However, Matt Lewis deserves a personal acknowledgment for his kindness, time and patience. Thank you very much "office friend" for everything (I will keep the secrets about surfing with me to the grave!). Also, Big thanks to Peter Lawrence for proof reading. Special thanks to Jennifer Roberts, Gwyn Roberts, Aaron Owen and Penny Downey who help me through computer problems and administrative issues (which are more complicated than science). But also, Olga Andres from CEFAS who kindly shared her data with me.

I could not have completed my PhD if it were not for some amazing friends, so a huge thanks to all who made my life happier: the amazing couple Jendy (and now Iz!), Timbo, Mathilde, Jyodee, Andre, Annika, Sinah, Alastair, Gemma, Simon and Brian. A special thanks for my welsh family: Jack, Jamie, Owen and Rhodes. These guys make my life fun and crazy. Thanks also to Adie and Sam who make the Auckland a great place to meet people and build unforgettable memories!

I would like to mention how special North Wales is to me. I have really enjoyed spending four years in this amazing part of the UK. Enjoying the landscapes and the Irish Sea was an amazing source of inspiration. I finally found a place to call home.

The best for the last, I send a huge and enormous thanks to my family who have been supporting me from the start of the adventure to the end. I love you Mums and Dads for your faith in me and my sisters (Ondine, Megan and Faustine) who gave me strength when needed. Also, a big and sincere thanks to Kevin, Babouche, Bibine and Ludo who have been on my side since so long.

Finally, I could not conclude this acknowledgment without having a thought for Eleri, who was essential at the end of my PhD for her patience and unfailing love, I love you and Lucy.

“[…] Je me vois pour ma part comme un jeune enfant qui, errant sur les vastes rives de la connaissance, se réjouit de ramasser à l’occasion un petit galet brilliant tandis que s’étend sous ses yeux l’immense océan de la vérité inexplorée…”

La longue utopie (Terry Pratchett & Stephen Baxter)

Table of contents

Declaration and Consent *ii*

Summary *v*

Acknowledgements *vi*

Table of contents *viii*

List of figures, tables and equations *xii*

Chapter 1: General introduction *1*

1.1 The blue mussel: *Mytilus edulis* **2**

1.1.1 General biology 2

1.1.2 Reproduction and life cycle 4

1.1.3 Larval dispersal and settlement 7

1.1.3.1 Larval dispersal 7

1.1.3.2 Laval settlement 11

1.1.4 The Distribution 14

1.2 Methods to study larval dispersal **18**

1.2.1 Hydrodynamic and particle tracking models 18

1.2.1.1 Introduction and functioning of particle tracking models 18

1.2.1.2 PTM applied to ecological questions 20

1.2.2 Other methods existing 21

1.3 Study site **23**

1.3.1 The Irish Sea 23

1.3.2 The Menai Strait 31

1.4 Mussel exploitation **38**

1.4.1 Shellfisheries industry in wales 39

1.4.2 Bangor mussel companies 40

1.5 Motivation for the study **42**

Chapter 2: Hydrodynamic modelling *44*

2.1 Model grid generation **45**

2.1.1 Grid 1: Irish Sea model 46

2.1.2 Grid 2: Anglesey model 49

2.1.3 Bathymetry 51

2.2 TELEMAC modelling system 54

2.3 Model validation 58

2.3.1 Validation Method 1: Comparison of observed and simulated elevations 59

2.3.1.1 Temporal variability 61

2.3.1.2 Spatial variability 61

2.3.1.3 Validation Method 1: Discussion 63

2.3.2 Validation Method 2: Tidal analysis 64

2.3.2.1 Validation Method 2: Spatial variability 65

2.3.2.2 Validation Method 2: Discussion 65

2.4 Model sensitivity tests to improve accuracy 67

2.4.1 Effect of model time step on model accuracy 67

2.4.2 Effect of model output frequency and location on model accuracy 68

2.4.3 Effect of the coefficient of friction on the accuracy of the model 70

2.4.4 Conclusion 72

2.5 Model validation: Summary of results 73

2.5.1 Observed vs. simulated: elevation 73

2.5.2 Observed vs. simulated: velocity 79

2.5.3 Tidal analysis 89

Chapter 3: Particle tracking model 90

3.1 Introduction 91

3.1.1 PTM design 91

3.1.1.1 Creation of an orthogonal mesh from a triangular mesh 92

3.1.1.2 Determination of the position and the number of particles 94

3.1.1.3 Determination of the particle movement 95

3.1.2 Summarize of the sensitivity tests performed 96

3.2 Interpolation of velocity field 98

3.2.1 Computational efficiency 98

3.2.2 Accuracy 100

3.3 Spatial resolution 102

3.3.1 Grid resolution limit to study the Menai Strait 102

3.3.2 Impact of spatial resolution on PTM accuracy 103

3.4 Temporal resolution impact on PTM accuracy **107**

3.5 Number of particles **110**

3.5.1 Computational efficiency 110

3.5.2 Number of particles limit in the PTM 111

3.6 Released area **113**

3.6.1 Release position from a single mussel bed 113

3.6.2 Size of released patch 115

3.7 Validation of PTM via observed drifter trajectories **116**

3.7.1 Materials and methods 116

3.7.2 Results 120

3.8 Conclusions from Chapter 3 **124**

Chapter 4: Menai Strait mussels ***130***

4.1 Spawning period **132**

4.1.1 Materials and methods 132

4.1.2 Results 135

4.1.3 Discussion 141

4.2 Menai Strait PTM simulations **145**

4.2.1 Materials and methods 145

4.2.2 Results 148

4.2.3 Discussion 155

Chapter 5: Mussel beds dispersal and connectivity in North Wales ***159***

5.1 Materials and methods **161**

5.2 Results: Simulated larvae distribution **165**

5.2.1 Simulation representing larvae released at mid-water depth 165

5.2.1.1 Larval distribution 165

5.2.1.2 Distance travelled 169

5.2.1.3 Connectivity 171

5.2.2 Simulations representing larvae released at the surface in 2014 174

5.2.2.1 Larval distribution 174

5.2.2.2 Distance travelled 177

5.2.2.3 Connectivity 180

5.2.3 Simulations representing larvae released at the surface in 2018 182

5.2.3.1 Larval distribution 182
5.2.3.2 Distance travelled 185
5.2.3.3 Connectivity 188
5.2.4 Comparison of the results 191
5.3 Discussion **192**
Chapter 6: General conclusion ***201***
6.1 Particle tracking model (PTM) assessment **202**
6.2 Larval dispersal and population dynamics **203**
6.3 Management of commercial shellfisheries **204**
6.4 Final remarks **205**
References ***206***
Appendix ***225***

List of figures, tables and equations

Chapter 1:

Figure 1.1: Photo of a *Mytilus edulis* mussel bed.

Figure 1.2: Flow diagram showing a simplified food web of *Mytilus edulis L.*, red arrows show the prey of mussels, blue arrows show the predator of mussels and green arrows show prey/predator relation which does not impact mussels directly.

Figure 1.3: Photo showing *Mytilus edulis* female spawning in the water column.

Figure 1.4: Schematic showing larval and post-larval history of *M. edulis* (Wildish & Kristmanson, 1997).

Figure 1.5: Number of articles published trough time containing "larval dispersal" in their title and/or abstract.

Figure 1.6: Schematic showing the concept of larval transport, larval dispersal and reproductive population connectivity, from Pineda *et al.* (2007).

Figure 1.7: Photo showing larvae mussel attached to seaweed.

Figure 1.8: Schematic representating the proximate processes that influence larval settlement rate and population density, from Pineda (2000).

Figure 1.9: Mapping showing the worldwide distribution of the genus *Mytilus* (Gaitan-Espitia *et al.*, 2016).

Figure 1.10: Map showing the distribution of genus *Mytilus* in Europe (Michalek *et al.*, 2016).

Figure 1.11: Heat map showing *Mytilus edulis* distribution in the Irish Sea per km^2, with 1) in red, areas with the highest density; 2) in orange, areas with a medium density; and 3) in yellow, areas with a low density (from Ocean biogeographic information system). Greys area have no

known mussels. The black box and the red box represent the study area: Anglesey and the Menai Strait, respectively.

Figure 1.12: Map showing the distribution of the principal mussel beds in the Menai Strait (from Digimap).

Figure 1.13: Schematic showing vertical zonation patterns of shore area, from https://poriferabasics.weebly.com/habitat.html .

Figure 1.14: Map showing the bathymetry of the Irish Sea (meters below mean sea level), land is coloured in grey and dashed lines represent the approximate limit of the Irish Sea. (Modified from Bush, 2015).

Figure 1.15: Map showing the distribution of major sediment types in the Irish Sea, from Parker-Humphreys (2004).

Figure 1.16: Map showing Lagrangian circulation in the northern Irish Sea (a) surface and (b) bottom from Hill *et al.* (1997).

Figure 1.17: Map showing the M2 co-tidal chart of the Irish Sea, the Celtic Sea and the North Sea with dashed contours representing cotidal lines (in degrees) and solid contours representing coamplitude lines (in meters), from Neill & Hashemi (2018).

Figure 1.18: Map showing maximum amplitude of the depth-average tidal currents for a mean spring tide (m/s), from Howarth (2015).

Figure 1.19: Hydrographic map of the main water bodies, and frontal systems within the Irish Sea, modified from Golding *et al.* (2004).

Figure 1.20: Map showing average near bottom and near surface temperature (1993-2001) for summer (August) and winter (January), for the northern Irish Sea (Parker-Humphreys, 2004).

Figure 1.21: Map showing average near bottom and near surface salinity for summer and winter (Lee & Ramster, 1981).

Figure 1.22: Map of the Menai Strait (top), North Wales (bottom panels). Bathymetry contours and key towns/areas are shown. The location of the commercial mussel bed are marked in blue.

Figure 1.23: Tidal flow along the Menai Strait (from https://nwcc.info/menai-strait-tides/).

Figure 1.24: Time series of model simulation (see chapter 2 for further details) of tidal range in the Menai Strait over a spring-to-neap cycle, at three locations along the channel: Fort Belan, the Swellies and Beaumaris.

Figure 1.25: Graph showing simulated (see chapter 2 for further details) spring/neap tidal ranges in the Menai Strait at five locations along the channel: Fort Belan, Brynsiencyn (mussel bed location), the Swellies, Bangor (mussel bed location) and Beaumaris.

Figure 1.26: Time series of model simulated (see chapter 2 for further details) depth-averaged tidal flows, during a typical spring-neap tidal cycle at Fort Belan, the Swellies and Beaumaris.

Figure 1.27: Time series of Menai Strait sea surface temperature (SST) from January 2011 to November 2018 from temperature logger data located at Bangor Pier.

Figure 1.28: Map showing model simulated (see chapter 2 for further details) depth-averaged tidal flows in the Swellies (mid-channel) region of the Menai Strait: (a) High water (HW) - one hour; (b) HW (i.e. peak flood tide); and (c) HW + one hour.

Figure 1.29: Map showing the main mussel culture areas along the Atlantic coast of Europe (Smaal, 2002).

Figure 1.30: Time series of UK mussel production (tonnage), split by nation where reported.

Figure 1.31: Location of commercial mussel beds in the East part of the Menai Strait regarding to the Menai Strait Oyster and Mussel Fishery Order 1962.

Table 1.1: Life stages and characteristics of the blue mussel with in red the last stage before settlement (modified from Bayne, 1976).

Table 1.2: List of the physical and biological parameters influencing the larval dispersal and settlement.

Table 1.3: Model simulated depth-averaged tidal flows, during peak spring/neap flood/ebb tide, and the difference (i.e. tidal asymmetry) at fort Belan, the Swellies and Beaumaris.

Table 1.4: 2012 Bivalve shellfish production in the UK, broken down by species (and technique) and country. Also included are estimated farm gate price and imputed value of production.

Table 1.5: Enterprise and employment information (2012) for the UK shellfish farming industry.

Table 1.6: Coordinates of the commercial mussel bed in the Menai Strait.

Equation 1.1: Navier-Stokes equations, where u = velocity vector field, ε= thermodynamic internal energy, p = pressure, T = temperature, ρ = fluid density, μ = viscosity, K_H = heat conduction coefficient, F = external force per unit mass = acceleration.

Equation 1.2: Shallow water equations where u = velocity in the x direction; v = velocity in the y direction; g = acceleration due to gravity; η = total fluid column height and ρ = fluid density.

Chapter 2:

Figure 2.1: Irish Sea mesh (Grid 1). The boundary of the domain is composed of offshore tidal waters (red) and coastline (dark).

Figure 2.2: Grid 1 mesh resolution variation (purple line: 3,000 m, red line: 2,000 m, orange: 1,000 m, yellow: 500 m, green: 200 m and light blue: 100 m). The dashed black box region is detailed in Figure 2.3.

Figure 2.3: Grid 1: Details of the mesh density variation around Anglesey (yellow line: 500 m, green: 200 m, light blue: 100 m, dark blue: 50 m, brown: 30m). The Menai strait sub mesh used to create Grid 1 is represented by the red dashed line.

Figure 2.4: Grid 2: Menai Strait grid highlighting the increased mesh resolution (yellow line: 500 m, green line: 200m, light blue line: 100 m, dark blue line: 50 m and brown: 20 m). The limit of the domain is composed by offshore waters in red and coastline in black.

Figure 2.5: Grid 2: Details of the Swellies area and Islands in the Menai Strait. In black natural islands and in red main bridge piers considered as 'Islands' by the model.

Figure 2.6: Calculation of Mean Sea Level (MSL) using Tidal range (TR) and Chart Datum (CD).

Figure 2.7: Bathymetry of the Irish Sea grid related to MSL.

Figure 2.8: Bathymetry around Anglesey and in the Menai Strait related to MSL.

Figure 2.9: Map showing the tide gauge sites (squares) and ADCP velocity sites (triangles) used for model validation (red: sites used for Methods 1 and 2; black: sites used for Method 2 only; light blue: sites used for the Method 1 only; and green: sites used for Method 1 only on velocity). The dashed box represents the Grid 1 model domain.

Figure 2.10: Difference between observed surface elevation with tide only (OT) and observed surface elevation (O) over a period of 24 h.

Figure 2.11: Location of the 12 sites of interest used to study the effect of output frequency on model validation.

Figure 2.12: Difference of the velocity strength (black) and direction (grey) between model scenarios with 5 min output and coarser resolutions for 12 sites located in North Wales.

Figure 2.13: Box plot showing the percentage difference (i.e. model error) between simulated and observed tidal elevations, using validation Method 1. Results are based on 14 locations throughout the Irish Sea (see Figure 2.9) – showing maximum, minimum, median (crossbar) and average (cross) values. Each box plot shows a comparison with a different parameterisation for the coefficient of friction: 1 (blue), 0.4 (orange), 0.2 (grey) and 0.1 (yellow).

Figure 2.14: Box plot showing the percentage difference (i.e. model error) between simulated and observed tidal elevations, using validation Method 2 (tidal analysis). Results are based on 16 sites throughout the Irish Sea (see Figure 2.9) – showing maximum, minimum, median (crossbar) and average (cross) values. Each box plot shows a comparison with a different parameterisation for the coefficient friction: 1 (blue), 0.4 (orange), 0.2 (grey) and 0.1 (yellow).

Figure 2.15: Time series of surface elevation during March 2015 at Ilfracombe for simulated data from the Irish Sea model (blue solid line) and observed data (orange dashed line).

Figure 2.16: Time series of surface elevation during March 2015 at Millport for simulated data from the Irish Sea model (blue solid line) and observed data (orange dashed line).

Figure 2.17: Time series of surface elevation during March 2015 at Holyhead for simulated data from the Menai Strait model (blue solid line) and observed data (orange dashed line).

Figure 2.18 Time series of surface elevation during March 2015 at Llandudno for simulated data from the Menai Strait model (blue solid line) and observed data (orange dashed line).

Figure 2.19: Time series of velocity magnitude during November 2015 at North Hoyle for simulated data from the Irish Sea model (blue solid line) and observed data (orange dashed line).

Figure 2.20: Time series of velocity magnitude during November 2015 at New borough for simulated data from the Irish Sea model (blue solid line) and observed data (orange dashed line).

Figure 2.21: Time series of velocity magnitude during November 2015 at Brickworks for simulated data from the Menai Strait model (blue solid line) and observed data (orange dashed line).

Figure 2.22: Time series of velocity magnitude during November 2015 at New borough for simulated data from the Menai Strait model (blue solid line) and observed data (orange dashed line).

Figure 2.23: Time series of velocity direction during November 2015 at Rhydwyn for simulated data from the Irish Sea model (blue solid line) and observed data (orange dashed line).

Figure 2.24: Time series of velocity direction during November 2015 at New borough for simulated data from the Irish Sea model (blue solid line) and observed data (orange dashed line).

Figure 2.25: Time series of velocity direction during November 2015 at Rhydwyn s for simulated data from the Menai Strait model (blue solid line) and observed data (orange dashed line).

Figure 2.26: Time series of velocity direction during November 2015 at Conwy bay for simulated data from the Menai Strait model (blue solid line) and observed data (orange dashed line).

Table 2.1: Results for 1) NRMSE (in %) per month for observed elevation and predicted elevation and 2) Difference between observed elevation and predicted elevation per month and per season (in %).

Table 2.2: Results for 1) NRMSE (in %) per sites for observed elevation and predicted elevation and 2) Difference between observed elevation and predicted elevation per sites (in %).

Table2.3: Parameters influencing the validation value.

Table 2.4: A description of primary tidal harmonics.

Table 2.5: Tidal analysis results for the Irish Sea model (Grid 1) for the M2 tidal constituant, with in the red the results for site located within the eastern Irish Sea and in black the results for the sites located elsewhere in the Irish Sea.

Table 2.6: Model errors (%) average across the validation sites for both validation methods for three time steps tested.

Table 2.7: Model validation for surface elevation (during March 2015) using both models (Irish Sea and Menai Strait) showing 1) RMSE; 2) NRMSE; and 3) coefficient of determination (R^2).

Table 2.8: Model validation of simualted velocity magnitude (November 2015) for both models (Irish Sea and Menai Strait) showing: 1) RMSE; 2) NRMSE; and 3) coefficient of determination (R^2).

Table 2.9: Model validation of simualted velocity direction (November 2015) for both models (Irish Sea and Menai Strait) showing: 1) RMSE; 2) NRMSE; and 3) coefficient of determination (R^2).

Table 2.10: Results of the model validation tidal analysis, for simulation of the M2 tidal constituent (%) with in red the average values for both models (Irish Sea and Menai Strait).

Equation 2.1: Equations solved by TELEMAC-2D for Cartesian coordinates with 1) h: depth water (m); 2) u and v: velocity components (m/s); 3) T: passive tracer (g/l); 4) g: gravity acceleration (m/s2); 5) vt and vT: momentum and tracer diffusion (m2/s); 6) Z: free surface elevation (m); 7) t: time (s); 8) x and y: horizontal space coordinates (m); 9) S_h: source or sink of fluid (m/s); 10) S_x and S_y: source or sink terms in dynamic equations (m/s^2); and 11) S_T: source or sink of tracer (g/l/s).

Equation2.2: Courant condition equation with 1) d: dimension of the model; 2) Δx: distance between cross sections; and 3) V: average velocity of the flow.

Equation 2.3: The courant condition used to establish an appropriate model time step, with 1) Δt the time step; 2) Δx the distance between cross sections; and 3) V the average velocity of the flow.

Chapter 3:

Figure 3.1: Schematic structure of the PTM.

Figure 3.2: Model of the Irish Sea within the black square the area of interest for the PTM.

Figure 3.3: Orthogonal mesh generated on Matlab with a constant 50 m grid resolution for the Irish Sea model. Land is represented in green and Sea is represented in blue.

Figure 3.4: Example interpolation of velocity field from north of Anglesey from unstructured mesh with Blue Kenue (A) to a structured mesh into Matlab (B). Arrows showing the direction and strength in m/s.

Figure 3.5: Particles release position for 5,000 particles in an area of 1,600m^2 with A) overview of the area of interest; and B) zoom in.

Figure 3.6: Particles movement for one timestep using advection only (in black) and advection + diffusivity (in grey). The position at t and t+1 are represented by green and red square respectively.

Figure 3.7: Computational time required to generate a structured mesh within the Matlab PTM, depending on spatial grid resolution of the Menai Strait model (in blue) and the Irish Sea model (in orange). The difference of computational time between the models is represented in yellow.

Figure 3.8: Computational time required to generate velocity files within the Matlab PTM depending on the mesh resolution with in blue 30 m, in red 40 m, in green 50 m and in yellow 100 m.

Figure 3.9: Linear and bilinear interpolation method.

Figure 3.10: Release position for 10,000 particles in the western Irish Sea, arrows represent the sense of particles distribution and numbers are the label of the last particle for each line.

Figure 3.11: Pythagore's theorem applied to calculate the distance (blue line) between the final positions of two particles.

Figure 3.12: Improvement (in %) of the PTM accuracy using: A) linear interpolation for temporal resolution with solid representing 60 min; and B) bilinear interpolation for spatial resolution.

Figure 3.13: Grid resolution of the Menai Strait with values of A) 20 m, B) 50 m, C) 100 m, D) 200 m, E) 300 m; and F) 500 m.

Figure 3.14: Box plot showing the distance of the final position between the finest resolution and coarser resolutions for spatial variation resolution. Darker are the box plots and coarser was the resolution. Results are based on 10,000 particles – showing maximum, minimum, median (crossbar) and average (cross) values.

Figure 3.15: Distance of the final position for 10,000 particles depending on the release position between the finest resolution and the coarsest resolution. Particles are ranked with: 1) in yellow error from 0 km to 0.5 km; 2) in orange error from 0.5 km to 2 km; and 3) error from 2 km to 40 km.

Figure 3.16: Impact of velocity on final position difference between the simulation using 50 m grid resolution and 1,000 m grid resolution with: 1) in black the difference of the final position between 50 m grid resolution and 1,000 m grid resolution (in m); 2) in orange speed among x ($*10^4$ m/s); and 3) in green speed among y ($*10^4$ m/s). The spatial distribution of particles is represented by 1) the red arrow for South-North direction; and 2) grey and white stripes for east and west position respectively.

Figure 3.17: Box plot showing the distance of the final position between the finest resolution and coarser resolutions for temporal variation resolution. Darker are the box plots and coarser was the resolution. Results are based on 10,000 particles – showing maximum, minimum, median (crossbar) and average (cross) values.

Figure 3.18: Distance of the final position for 10,000 particles depending on the release position between the finest resolution and the coarsest resolution. Particles are ranked with: 1) in yellow error from 0 km to 0.5 km; 2) in orange error from 0.5 km to 2 km; and 3) error from 2 km to 40 km.

Figure 3.19: Impact of velocity on final position difference between the simulation using 5 min resolution and 60 min resolution with: 1) in black the difference of the final position between 5 min resolution and 60 min resolution (in m); 2) in orange speed among x ($*10^4$ m/s); and 3) in green speed among y ($*10^4$ m/s). The spatial distribution of particles is represented by 1) the red arrow for South-North direction; and 2) grey and white stripes for east and west position respectively.

Figure 3.20: Time to run a PTM depending on 1) the number of particles; and 2) the scale of the grid with in blue 30 m, in red 40 m, in white 50 m and in yellow 100 m.

Figure 3.21: Map of the Menai Strait with the limit of five areas of interest for the convergence test with the blue cross corresponding to the release position.

Figure 3.22: Difference of the particles distribution (in %) per area depending on the number of particles tested with areas represented: 1) in white for area 1; 2) in red for area 2; 3) in grey for area 3; 4) in yellow for area 4; and 5) in blue for area 5.

Figure 3.23: Map of the residual currents of the northeastern entrance of the Menai Strait. The black area corresponds to the limit of the commercial Bangor mussel bed.

Figure 3.24: Map of the northeastern entrance of the Menai Strait with in green the release positions: Beaumaris (A), Bangor harbour (B) and Bangor pier (C). The red area corresponds to the limit of the commercial Bangor mussel bed.

Figure 3.25: Map of the northeastern entrance of the Menai Strait at Bangor harbour representing the size of released patches: 1) $4e^{-5}$ km^2 (green); 2) $1.6e^{-3}$ km^2 (blue); 3) $1e^{-2}$ km^2 (black); 4) $4e^{-2}$ km^2 (white); 5) $1.6e^{-1}$ km^2 (magenta); and 5) 1 km^2 (yellow).

Figure 3.26: Drifters trajectories with: 1) in blue Drifter_1 (released in 2018); and 2) in black Drifter_2 (released in 2019). First and last position are represented by red and green respectively.

Figure 3.27: Best particle trajectory (in blue) and best finale position (in orange) of 7,000 particles simulated compared to Drifter 1 (A) and Drifter 2 (B) (both in black). The starting position is representing by a red dot. Final positions are indicated by: 1) by a green triangle for the best trajectory; 2) by a green dot for the best final position; and 3) by a purple dot for the drifter.

Figure 3.28: Plot showing RE of distance travelled by particles (10,000) released on the Irish Sea grid between the finest resolution and coarser resolutions with: 1) in orange, the results for temporal resolution; and 2) in blue, results for spatial resolution.

Figure 3.29: Graph showing the temperature difference between the surface and the bottom in the Irish Sea during March and April average for 24 years (1990 to 2014).

Table 3.1: Summarize of the tests performed to optimize the time and improve the accuracy of the PTM.

Table3.2: Sensitivity on the release location at the scale of a mussel bed in the Menai Strait. Results show the distribution (%) of 7,000 particles released from three locations (A,B,C) per area after one week simulation.

Table 3.3: Sensitivity test on: 1) advection only (Test 1); and 2) wind approximation using two different equations (Test 2) for Drifter 1 and Drifter 2. RMSE are presented for both Test 1 and Test 2 with in red the best values highlighted for both drifters.

Table 3.4: Sensitivity test on coefficient diffusivity (in m^2/s) for Drifter 1 and Drifter 2. Results show the relative error (RE) for 7,000 particles simulated for: 1) the average; 2) the minimum; 3) the maximum; and 4) the range.

Equation 3.1: Approximation of the wind impact on surface current tested with U_{wind} and V_{wind} which are the x any wind component respectively downloaded from Ceda.

Equation 3.2: Approximation of the surface velocity with U_{model} and V_{model} velocity from Telemac hydrodynamic model.

Equation 3.3: Random displacement model for longitudinal and lateral diffusion (x and y respectively) with 1) Δt is the time step (in s); 2) A is a random in the range [0,1]; 3) r is the standard deviation of $A\cos(2\pi A)$ with a value of $1/\sqrt{6}$; and 4) K is the coefficient diffusion (m^2/s).

Equation 3.4: Particle position at t+1 depending on 1) particle position at t; 2) surface velocity ($U_{surface}$ and $V_{surface}$); 3) wind impact velocity ($U_{windimpact}$ and $V_{windimpact}$); and 4) diffusivity ($x_{diffusivity}$ and $y_{diffusivity}$).

Chapter 4:

Figure 4.1: Area of the sample collection (yellow dotted square) in the Menai Strait. The logger location is represented by a yellow dot.

Figure 4.2: Method of mussel measurement.

Figure 4.3: Mussel distribution among Sample_1 (in blue) and Sample_2 (in orange) depending on: A) shell length; and B) shell width.

Figure 4.4: Evolution of meat yield (MY, solid line) and condition index (CI, dotted line) for Sample_1 (in blue) and Sample_2 (in orange).

Figure 4.5: Evolution of 1) Meat yield for sample_1 (in blue) and sample_2 (in orange) over spring/summer 2018 on both figure A and B; 2) Sea surface temperature (SST) in green on figure A; and 3) Air temperature (AT) in yellow on figure B. The portion of the curves in dashed line corresponds to period when data were not collected. Red arrows point days of massive spawning events.

Figure 4.6: Evolution of: A) Moon phases in % with full moon represented by 100 % and new moon represented by 0 %; B) Water elevation in m; and C) Wind strength and direction by arrows. Red dots represent the massive spawning events and yellow dots represent the trickle spawning events.

Figure 4.7: Particle release position in the Menai Strait (green patches) and areas of interest delimited by red dotted lines. Example of particles scattered in an area of 0.1 km2 from Brynsiencyn are presented in the sub-figure B.

Figure 4.8: Bangor water elevation from the 3rd of March 2018 to the 19th of March 2018. Released time of particles for the eight simulations are represented in red for starting time and in green for the ending time.

Figure 4.9: Density distribution of mussel larvae after one week with released area represented by a red dot: (A) Bangor mussel bed; (B) the Swellies; (C) Plas Newydd; (D) Plas Menai; (E) Brynsiencyn; and (F) Abermenai point.

Figure 4.10: Particles distribution in % for 6 areas of interest depending on the release site: The areas of interest are: 1) South of the menai Strait; 2) Caernarfon; 3) Plas newydd; 4) the Swellies; 5) Bangor; and 6) North of the Menai Strait. The sites of released are represented in: 1) black for Bangor mussel bed; 2) light black for the Swellies; 3) dark grey for Plas Newydd; 4) medium grey for Plas menai; 5) light grey for Brynsiencyn; and 6) white for Abermenai point.

Figure 4.11: Density distribution of mussel larvae after one week depending on the tidal phase during particle release: (A) neap ebb; (B) neap flood; (C) neap HW; (D) neap LW; (E) spring ebb; (F) spring flood; (G) spring HW; and (H) spring LW.

Figure 4.12: Particles distribution in % for 6 areas of interest depending on the release tide. The areas of interest are: 1) South of the Menai Strait; 2) Caernarfon; 3) Plas Newydd; 4) the Swellies; 5) Bangor; and 6) North of the Menai Strait. Particles were released during: (A) spring tide in grey and neap tide in black; (B) flood tide in grey and ebb tide in black; and (C) LW in grey and HW in black.

Figure 4.13: Difference of the residual current between simulations starting during spring tide and simulation starting during neap tide. Results present the difference for: A) V component in m/s; B) U component in m/s; C) direction in degrees; and D) magnitude in m/s. Warm colours (red to yellow) show a positive difference when spring is higher than neap. Green colours show when both residuals are equal. Cold colours (Light blue to dark blue) show when neap is higher than spring.

Figure 4.14: Residual current in the Menai Strait for a week of simulation starting during ebb: A) North of the Menai Strait; B) The Swellies; C) Caernarfon; and D) South of the Menai Strait. Residual currents are represented by arrows for the direction and colours for the strength.

Table 4.1: Details of sample collection for the meat yield experiment per sample with in the red the total of mussels and weight sampled cumulated.

Table 4.2: Biggest drop of CI with the corresponding: 1) Date; 2) MY variation in % for both samples; 3) CI variation in % for both samples; 4) SST difference between the day of spawning

and the day before in ºC; 5) AT difference between the day of spawning and the day before in ºC; and 6) Difference between AT and SST in ºC.

Table 4.3: Small fluctuation of CI in red with the corresponding: 1) Date; 2) MY variation in % for both samples; 3) CI variation in % for both samples; 4) SST difference between the day of spawning and the day before in ºC; 5) AT difference between the day of spawning and the day before in ºC; and 6) Difference between AT and SST in ºC.

Equation 4.1: Equations used to calculate the commercial meat yield (MY) and the condition index (CI), from Duinker *et al.* (2008).

Chapter 5:

Figure 5.1: Location of particle release/settlement sites (red dots), settlement sites only (orange dots) and wind station data (green dots).

Figure 5.2: Cumulative distance (CD) and net transport (NT) calculated for particle i during n timestep with black dot representing particle position at each time step (t) and red line representing the distance (d) travelled by particle during two time step.

Figure 5.3: Maps showing the density distribution of mussel larvae released at the midwater column (advected by tide only) from 10 released areas (red dots) during: (A) week 1; (B) week 2; (C) week 3; (D) week 4; (E) week 5; and (F) week 6.

Figure 5.4: Maps showing the density distribution of mussel larvae released at the midwater column (advected by tide only) after 6 weeks simulation from 10 released areas (red dots): (A) Mostyn; (B) North Hoyle; (C) Gwynt Y Mor; (D) Rhyl Flat; (E) Llandudno; (F) Conwy; (G) Bangor; (H) Red Wharf Bay; (I) Brynsiencyn; and (J) Holyhead.

Figure 5.5: Cumulative distances travelled by cohort of 7,000 particles when release at the mid-water column during week 1 (A), week 2 (B), week 3 (C), week 4 (D), week 5 (5); and week 6(F). Sites are coloured according to their location: Mostyn (grey), Offshore wind farms (red), Great Orme (green), Menai Strait (yellow), Anglesey (blue). Results are based on 7,000 particles – showing maximum, minimum, median (crossbar) and average (cross) values.

Figure 5.6: Net transport (NT) distances of particles per week when released at mid-water depth (A); at the surface in 2014 (B); and at the surface in 2018 (C). Results are based on: 70,000 particles (A) and 210,000 particles (B and C) – showing maximum, minimum, median (crossbar) and average (cross) value.

Figure 5.7: Connectivity matrices for larvae release in the mid-water column in March-April 2018 during (a) week 3, (b) week 4, (c) week 5 and (d) week 6. Connectivity between larvae from a source (column) with a sink (row) is highlighted by colour scale with high connectivity in red, low connectivity in blue and no connectivity in white. Self-recruitment (e.g. retention within the release site) is indicated by cells that cross the diagonal dashed line. Sites are colour coded as: red = source and sink sites and orange = sink sites only.

Figure 5.8: Maps showing the density distribution (%) of particles (representing mussel larvae dispersing near the surface) when released during March and April 2014 from 10 released areas (red dots) during: (A) week 1; (B) week 2; (C) week 3 (D) week 4; (E) week 5; and (F) week 6.

Figure 5.9: Maps showing the density distribution of mussel larvae released at the surface (advected by tide and wind-driven current) during March-April 2014 after 6 weeks simulation from 10 released areas (red dots): (A) Mostyn; (B) North Hoyle; (C) Gwynt Y Mor; (D) Rhyl Flat; (E) Llandudno; (F) Conwy; (G) Bangor; (H) Red Wharf Bay; (I) Brynsiencyn; and (J) Holyhead.

Figure 5.10: Cumulative distance (CD) travelled by particles (representing mussel larvae dispersing near the surface) when released during March and April in 2014 during week 1 (A), week 2 (B), week 3 (C), week 4 (D), week 5 (E) and week 6 (F). Sites are coloured according to their location: Mostyn (grey), Offshore wind farms (red), Great Orme (green), Menai Strait (yellow), Anglesey (blue). Results are based on 21,000 particles – showing maximum, minimum, median (crossbar) and average (cross) value.

Figure 5.11: Connectivity matrices for particles (representing mussel larvae dispersing near the surface) when released from 10 sources site (1-10) during March and April in 2014, during (a) week 3, (b) week 4, (c) week 5 and (d) week 6. Connectivity between larvae from a source (column) with a sink (row) is highlighted by colour scale with high connectivity in red, low connectivity in blue and no connectivity in white. Self-recruitment (e.g. retention within the

release site) is indicated by cells that cross the diagonal dashed line. Sites are colour coded as: red = source and sink sites and orange = sink sites only.

Figure 5.12: Maps showing the density distribution (%) of particles (representing mussel larvae dispersing near the sea surface) released from 10 sites (red dots) during March to April 2018 during: (A) week 1; (B) week 2; (C) week 3; (D) week 4; (E) week 5; and (F) week 6.

Figure 5.13: Maps showing the density distribution of mussel larvae released at the surface (advected by tide and wind-driven current) during March-April 2018 after 6 weeks simulation from 10 released areas (red dots): (A) Mostyn; (B) North Hoyle; (C) Gwynt Y Mor; (D) Rhyl Flat; (E) Llandudno; (F) Conwy; (G) Bangor; (H) Red Wharf Bay; (I) Brynsiencyn; and (J) Holyhead.

Figure 5.14: Cumulative distance (CD) travelled by particles (representing mussel larvae dispersing near the sea surface) during March-April 2018 during week 1 (A), week 2 (B), week 3 (C), week 4 (D), week 5 (5) and week 6 (F). Sites are coloured according to their location: Mostyn (grey), Offshore wind farms (red), Great Orme (green), Menai Strait (yellow), Anglesey (blue). Results are based on 21,000 particles – showing maximum, minimum, median (crossbar) and average (cross) value.

Figure 5.15: Connectivity matrices for particles (representing mussel larvae dispersing near the surface) when released from 10 sources site (1-10) during March and April in 2018, during (a) week 3, (b) week 4, (c) week 5 and (d) week 6. Connectivity between larvae from a source (column) with a sink (row) is highlighted by colour scale with high connectivity in red, low connectivity in blue and no connectivity in white. Self-recruitment (e.g. retention within the release site) is indicated by cells that cross the diagonal dashed line. Sites are colour coded as: red = source and sink sites and orange = sink sites only.

Figure 5.16: Wind rose corresponding to the PLD of larvae during March and April 2014 from 3 wind stations (Valley, Rhyl and Crosby). The direction is based on where the wind blow to. The wind strength (m/s) is represented by colour scale. The frequency is represented by the inner circle.

Figure 5.17: Wind rose corresponding to the PLD of larvae during March and April 2018 from 3 wind stations (Valley, Rhyl and Crosby). The direction is based on where the wind blow to.

The wind strength (m/s) is represented by colour scale. The frequency is represented by the inner circle.

Figure 5.18: Residual currents from March to April 2018 in Cardigan Bay. Direction of the residual currents are presented by black arrows and strength (m/s) by colour scale.

Figure 5.19: Map showing the difference of the residual currents for magnitude (A) and direction (B) between the hydrodynamics model created to simulate larval dispersal in 2014 and 2018.

Table 5.1: Cumulative percentage (= sum of the connectivity percentage) of particles (representing mussel larvae dispersing in mid-waters in 2018) per release site which were simulated to connect with settlement site, for different PLD: week 3, week 4, week 5 and week 6.

Table 5.2: Cumulative percentage (= sum of the connectivity percentage) of particles (representing mussel larvae dispersing near the surface in 2014) per release site which were simulated to disperse to a settlement site, for different PLD: week 3, week 4, week 5 and week 6.

Table 5.3: Cumulative percentage (= sum of the connectivity percentage) of particles (representing mussel larvae dispersing near the surface in 2018) per release site which were simulated to disperse to a settlement site, for different PLD: week 3, week 4, week 5 and week 6.

Chapter 1: General introduction

The interdisciplinary of this study makes important to explain several concepts such as: 1) mussel biology and ecology; 2) method to study larval dispersal focussing on modelling techniques; 3) the physical oceanography of the Irish Sea and the Menai Strait; and 4) the importance of mussel aquaculture.

Mussel life cycle comprises a vagile phase (larvae) and a sessile phase (juvenile and adult) (Wildish & Kristmanson, 1997). The vagile phase started when mussel spawn. However, spawning of *M.edulis* varies both spatially and temporally (Lowe *et al.*, 1982). What are the factors (e.g. temperature, tide/moon) influencing spawning events? When do these events occur in North Wales? Furthermore, larvae dispersal is influenced by both biological (e.g. swimming behaviour) and physical parameters (e.g. tide and wind driven current). What parameters influence the most larval dispersal in North Wales? Is it possible to predict larval trajectory based only on physical parameters or should studies take into account larvae behaviour? How accurate are hydrodynamics modelling and particle tracking model?

Answering these questions will help to understand better mussel ecology and improve particle tracking model accuracy for scientists but also will provide information for shellfish farmers to improve their culture method.

1.1 The blue mussel: *Mytilus edulis*

1.1.1 General biology

The blue mussel, *Mytulis edulis* Linnaeus (1758) is a sessile benthic bivalve, which filters seawater to feed itself with bacteria, plankton and detritus (Bayne, 1976; Widdows *et al.*, 1979) (Figure 1.1). Mussels can be found in the intertidal zone on any substratum providing a secure anchorage (Seed, 1976) such as rocks, stones, gravels, shingles, shells, mud, sands and man-made infrastructures (e.g. wind turbines). Individuals are bonded together with threads of byssus and form large beds, which are dominant in term of biomass. Those are also a key component of many marine communities as they provide habitat for other organisms, increase seabed roughness and create sediment (Seed & Suchanek, 1992; Herman, 1993; Van der Schatte *et al.*, 2018). Thiel & Ullrich (2002) showed that mussels that have settled on hard-seabeds (e.g. rocks) provide principally substratum for associated fauna, while those that have settled on soft-seabeds (e.g. mud and sands) provide both substratum and food resources by the creation of sediment via the cycling of nutrients (Van der Schatte *et al.*, 2018). All the ecological goods and economic services that mussel beds provide help explain the importance to study *M.edulis* (Van Der Schatte *et al.*, 2018). The persistence of mussel beds depends on self-recruitment and

connectivity from surrounding mussel beds (Petraitis, 1995; Reaugh, 2006; Becker *et al.*, 2007; Commito *et al.*, 2014).

Figure 1.1: Photo of a *Mytilus edulis* mussel bed.

The greatest cause of mortality of mussels is predation (Seed, 1969) by a range of predators such as starfish (Dare, 1982; Buschbaum, 2002), crabs (Cote, 1995), birds (Dare, 1976), but also gastropods, lobsters, flatfish and seals (Seed & Suchanek, 1992) (Figure 1.2). Predator pressure level and identity of predators depend on mussel size, season, location and height relative to the shore (Hamilton *et al.*, 1999, Witman *et al.* 2003, Cockrell *et al.*, 2015). In Wales for example, birds seem to predate on mussels during winter and target larger size classes (25 to 55 mm) (Seed & Suchanek, 1992, Meire, 1993) while starfishes feed in the subtidal areas on mussels < 35mm (O'Neill *et al.*, 1983). Crabs also exhibit a different pattern by predating in both intertidal and subtidal zone but essentially during spring and summer on mussels < 25 mm (Seed, 1976; Dare & Edwards, 1976; Aagaard *et al.*, 1995). Predation directly impacts mussel settlement and consequently the proportion of self-recruitment and connectivity which must be taken into account in larval dispersal studies.

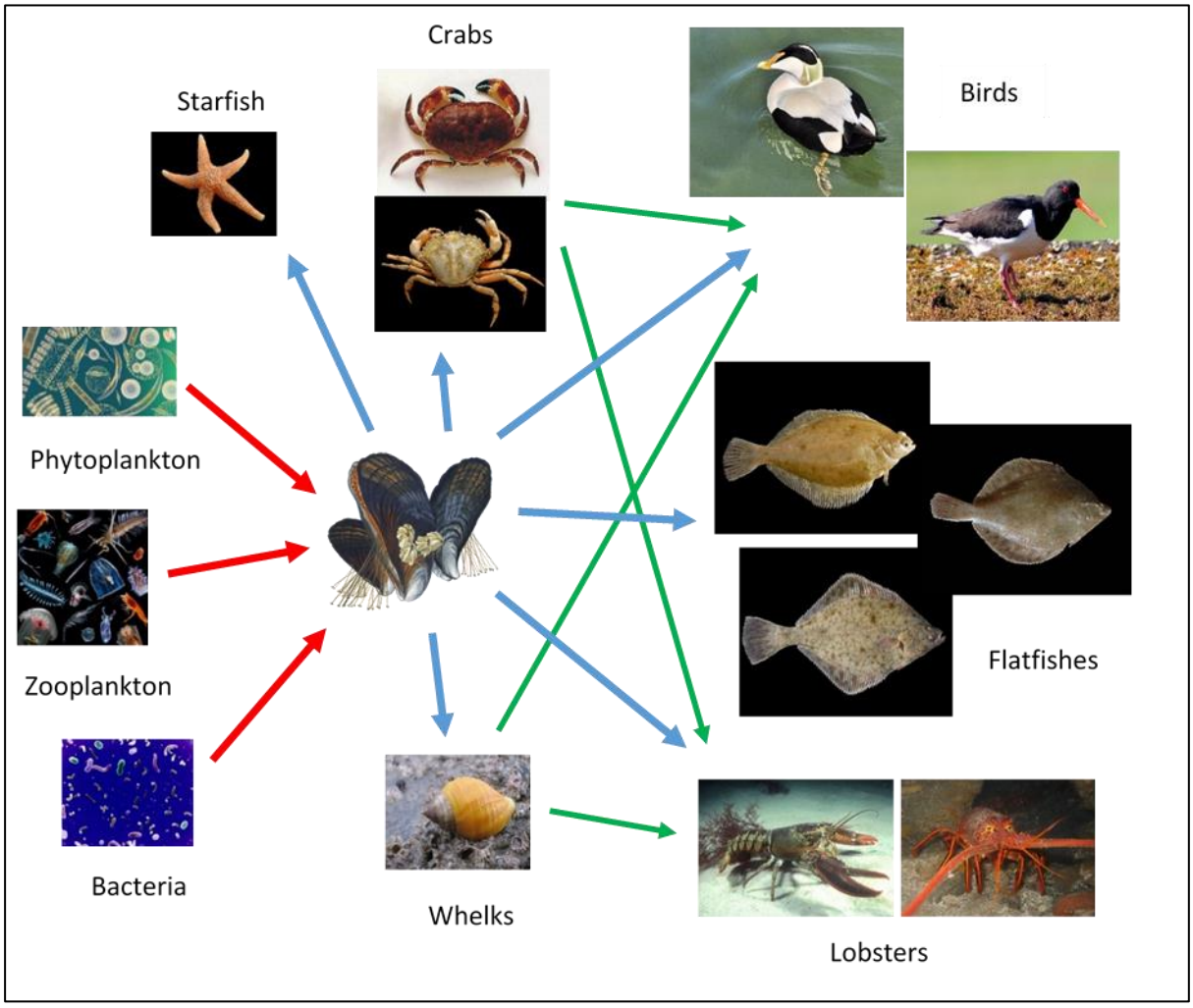

Figure 1.2: Flow diagram showing a simplified food web of *Mytilus edulis L.*, red arrows show the prey of mussels, blue arrows show the predator of mussels and green arrows show prey/predator relation which does not impact mussels directly.

1.1.2 Reproduction and life cycle

Mytilus edulis are gonochoristic with a 1:1 sex ratio, which means that the number of male and female are equal in a population, with creamy-white and orange reproductive tissue for males and females, respectively (Figure 1.3) (Seed, 1976; Sprung, 1983). After a year, mussels can be sexually mature depending on physical environment and release millions of gametes into the water column (Seed 1976). Mussel spawning strategy is based on a mass synchronised releasing of gametes, which maximizes the reproductive success of the species (De Vooys, 1999). This strategy allows the optimal fertilization of eggs and maximal survival during the pelagic larvae duration, but it is unknown exactly what the proportion of survival is and how the larvae travel in the water column.

The gametogenic cycle and spawning event of *M.edulis* varies both spatially and temporally (Lowe *et al.*, 1982). However, a similar pattern is observed among the mussel bed located in the North hemisphere (Ireland, Western Norway, Wadden Sea, Baltic Sea, Wales, France and

East coast of the United States), which consists of: 1) an accumulation of nutrient reserve during the summer; 2) gametogenesis during autumn/winter; and 3) spawning event during the spring/early summer and sometimes several spawning events during summer (Wilson & Seed, 1974; Sprung, 1983; Rodhouse *et al.*, 1984; Boromthanarat *et al.*, 1987; De Vooys, 1999; Myrand *et al.*, 2000; Thorarinsdottir *et al.*, 2013). In North Wales, *M.edulis* initially spawn in spring (March-April) followed by a fast gametogenesis until early summer. Further spawning events occur during summer until autumn (Dare, 1976; Lowe *et al.*, 1982). A partial spawning during the spring is the consequence of a gametogenesis during the winter when mussels feed on detritus. Summer spawning occurs after the mussels feed on phytoplankton and detritus (Rodhouse *et al.*, 1984). The inter-annual and spatial variations of spawning seem to be dependent on nutrient availability. Indeed, mussels that accumulate sufficient nutrients are able to have several spawning episodes in a short time (Newell *et al.*, 1982). Seed (1969) and Dare (1976) showed that larvae are present in the plankton throughout the year, although most numerous from April-July in the Irish Sea, however larvae identification was made using microscope which might induce errors (e.g. misidentify mussel larvae).

Figure 1.3: Photo showing *Mytilus edulis* female spawning in the water column.

After fertilisation in the water column, the zygotes will go through six larval stages before the first settlement (Figure 1.4 and Table 1.1) (Bayne, 1964; Bayne, 1965). The pelagic larvae duration (PLD) varies from 2-4 weeks but it can take 10 weeks or more between the fertilisation and the last settlement (Bayne, 1965; Seed, 1969). PLD is a direct consequence of the larvae abilities to develop into a pediveliger larvae to initiate the settlement. However, the metamorphosis and the growth of larvae depend on physical parameters (temperature, salinity, tidal currents, ability to find a good substrate for settlement, release location, wind climate and interaction with fluvial flow) and biological parameters (spawning patterns, food availability, larval behaviour, survival rate). Numerous articles have studied the impact of both salinity, temperature and food concentration on *M. edulis* larval growth and morphological

differentiation (Brenko & Calabrese, 1969; Beaumont & Budd, 1982; Sprung, 1984; Pechenik *et al.*, 1990; Filgueira *et al.*, 2015; Dinh & Fotedar, 2016). In North Wales, the sea temperature varies from 8ºC to 15ºC and salinity from 30‰ to 35‰ during spring/summer (Beamish, 2012; Mackenzie *et al.*, 2014). According to the literature, the mussel larvae should reach the pediveliger stage between 25 to 40 days after spawning in North Wales (Brenko & Calabrese, 1969; Beaumont & Budd, 1982; Sprung, 1984; Pechenik *et al.*, 1990; Filgueira *et al.*, 2015; Dinh & Fotedar, 2016).

The larval dispersal from North Wales mussel population is poorly understood, particularly the Menai Strait since the tidal flows are strong and complex. Known larval dispersal and settlement characteristics are described in the next section to understand the duration of the pelagic life and how it is impacted by physical and biological factors.

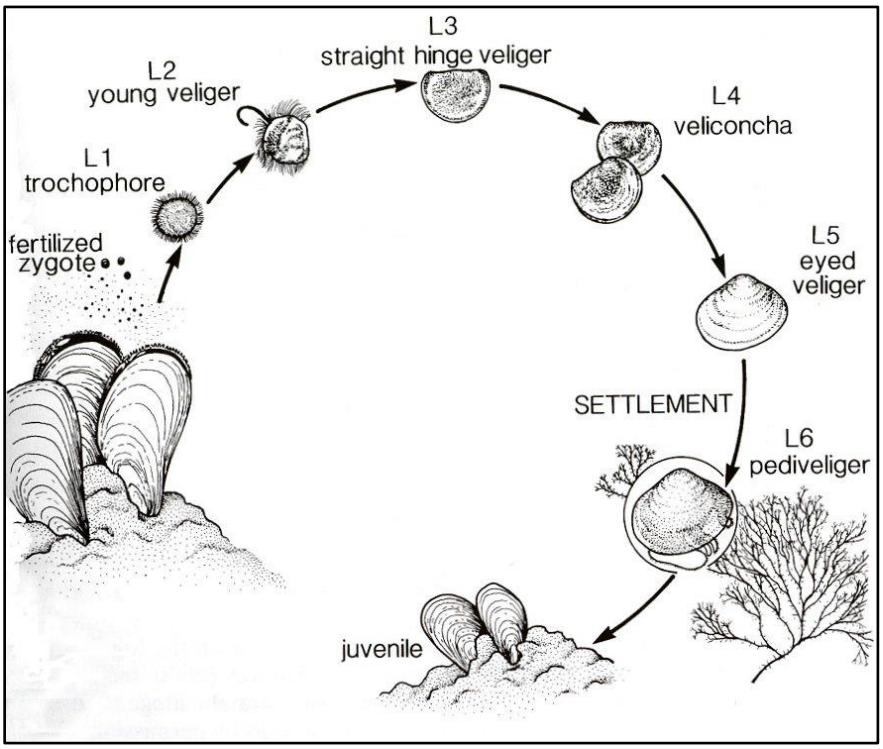

Figure 1.4: Schematic showing larval and post-larval history of *M. edulis* (Wildish & Kristmanson, 1997).

Table 1.1: Life stages and characteristics of the blue mussel with in red the last stage before settlement (modified from Bayne, 1976).

Stage	Size	Age	Characteristics
Fertilized eggs	68-70 µm	0-5 hours	Non motile
Trochophore	70-110 µm	5-48 hours	Ciliated and motile
Young Veliger	110-260 µm	40-72 hours	Feeds and swims with ciliated-velum
Straight hinge veliger			Straight-hinged shell
Veliconcha			Umbo on shell
Eyed larvae	220-260 µm	up to 40 days	Development of pigmented 'eyed spots'
Pediveliger	0.26-1.5 mm		Development of foot
Juvenile		up to 1 year	Sexually immature
Adult	up to 100 mm	up to 20 years	Sexually mature

1.1.3 Larval dispersal and settlement

1.1.3.1 Larval dispersal

The larval dispersal stage for many shellfish species remains largely unresolved in the science community, despite the high importance of larval transport in controlling the dynamics and resilience of shellfish populations (Hjort, 1926; Thorson, 1950). Since the 1980s, there has been a large increase in larval studies with a central position in the field of marine ecology (Figure 1.5) (Levin, 2006).

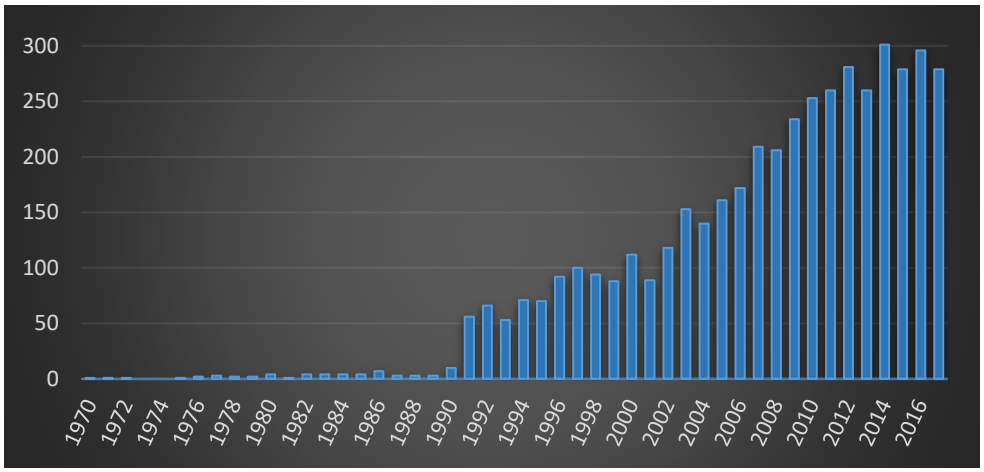

Figure 1.5: Number of articles published trough time containing “larval dispersal” in their title and/or abstract.

According to Pineda *et al.* (2007), larval dispersal from a spawning source population is a function of: 1) larval transport within the water column (which is a function of physical transport and larval behaviour); 2) larval survival; 3) spawning time and location; and 4) settlement success (Figure 1.6). Larval dispersal from a source population defines two fundamental concepts in population biology 1) self-recruitment: the capacity of juveniles to recruit to the parental population; and 2) connectivity: the potential dispersal of individuals among discrete local sub-populations (Cowen *et al*., 2006; Pineda *et al.*, 2007; Sheaves, 2009) (Figure 1.6). The relative importance of these physical and biological parameters on connectivity and self-recruitment varies greatly overtime and location. Many sources in the literature describe the physical and biological parameters which influence larval dispersal (e.g. Lane *et al.,* 1985; Gaylord *et al.,* 2002; Criales *et al.*, 2007; Harnett *et al.*, 2007; Robins *et al.*, 2012; Robins *et al*., 2013; Rhörs *et al.*, 2014; Weidberg *et al.*, 2015; Daigle *et al.*, 2016) (Table1.2):

Physical parameters: tidal currents, non-tidal currents (e.g. coastal eddies, density-driven (baroclinic) flows, wind-driven flows), water depth, coastal interactions, wave climate, seabed substrate.

Biological parameters: food availability, growth rate, metamorphosis speed, pelagic larval duration, vertical migration patterns, vertical swimming speed, mortality, settlement behaviour.

Bio-physical parameters: temperature and salinity gradients. These two parameters influence both the physical oceanography as well as the mussel biology. Indeed, the variation of temperature (spatially and temporally) creates thermal fronts and/or water stratification which constraints the larvae dispersal but also influence the larval development speed. The same phenomenon is observed with salinity variation (Harnett *et al.*, 2007; Dinh & Fotedar, 2016).

Table 1.2: List of the physical and biological parameters influencing the larval dispersal and settlement.

Parameters	
Physical	Biological
Spawning location (Coastal intertidal or subtidal, Deep ocean area)	Period and time of spawning
Size of the mussel bed	Ability to settle (e.g. early pediveliger or late pediveliger)
Sea temperature	Ability to choose a substrate
Tidal flow direction (e.g. during the ebb or flood)	Larval migration behaviour (e.g. passive, surface, diel migration)
Tidal flow strength (e.g. during neap tide or spring tide)	Larval swimming/sinking speed
Coastal residual currents (e.g. within channels, around headlands/islands, upwelling)	Predators (Absence vs Presence)
Wind-driven flows (Wind direction and strength)	Ability of survival
Water stratification and density-driven flow (tidal mixing fronts such as the Irish Sea gyre and Celtic Sea front)	Conspecifics (Absence vs presence)
River influenced flows (e.g. in estuarine or coastal waters)	Pelagic larval duration (PLD) (e.g. 6 weeks)
Wave-current interactions (e.g. during a storm)	Settlement strategy (e.g. primary settlement, secondary settlement)
Season flow variations (e.g. during spring or summer)	Duration of primary settlement (e.g. hours or days)
Seabed substrate type (e.g. rocky, mud or algae)	Competition (e.g. intra and inter-specific)

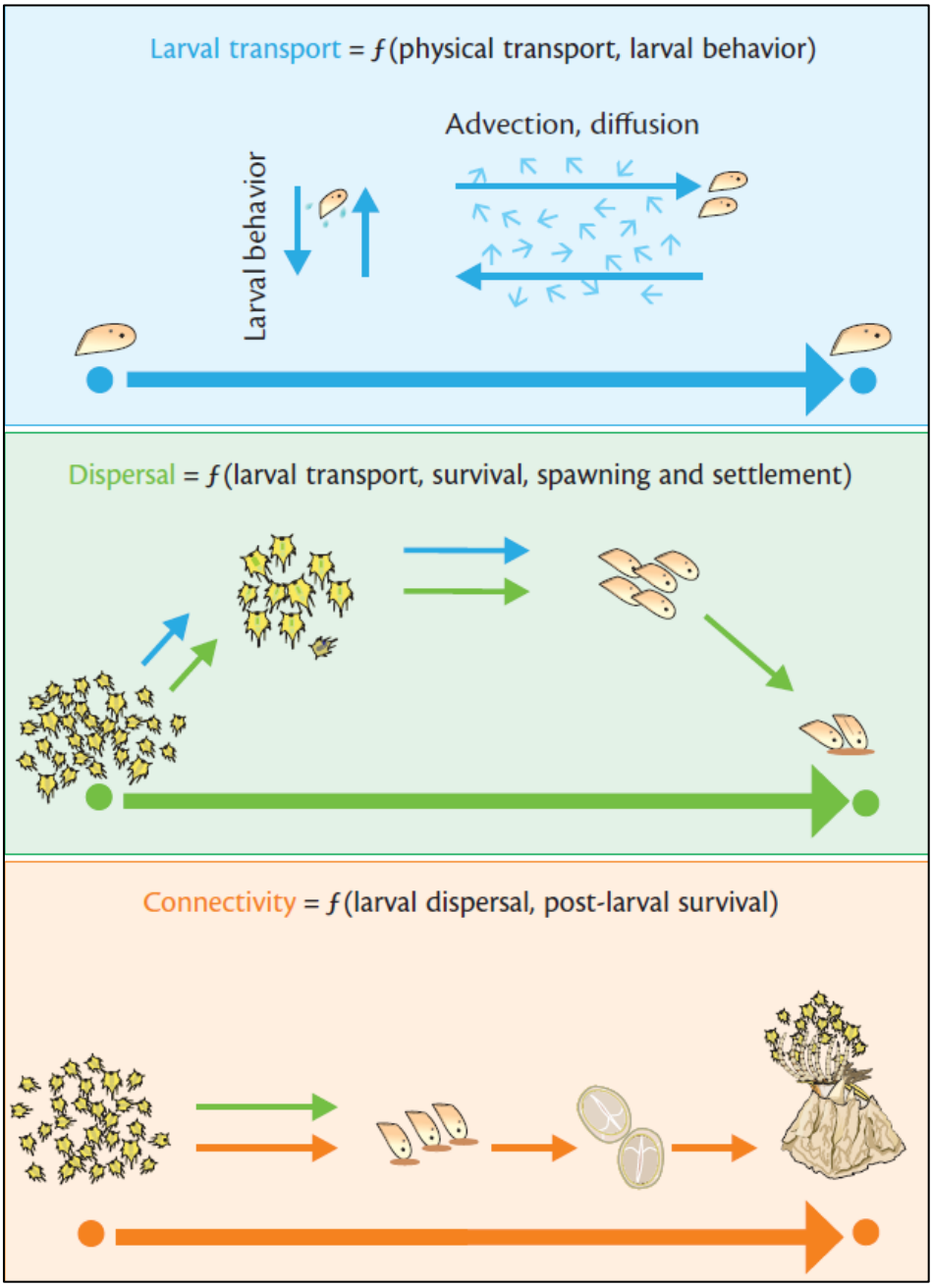

Figure 1.6: Schematic showing the concept of larval transport, larval dispersal and reproductive population connectivity, from Pineda *et al.* (2007).

The importance of the parameters in Table 1.2 on larval dispersal is both area dependant and species dependant (Metaxas, 2001; Nanninga & Berumen, 2014). The focus here was on studies which concern the genus *Mytilus spp* to understand the dominant parameters to resolve for a bio-physical particle tracking model to study *Mytilus edulis* larval dispersal in North Wales. Mcquaid & Phillips (2000) showed that *Mytilus galloprovincialis* larvae in South Africa were dispersed like passive particles with no evidence of diel migration in shallow inshore waters (< 20 m) and the wind being the main factor for dispersal. The same was observed by Weidberg *et al.* (2015) who showed that an increase of the Aghulas current (which is directed southwards along the eastern coast of South Africa) may mask any larval vertical swimming behaviour of

mussel larvae and transport larvae offshore entrained within the current. Also, Gilg & Hilbish (2003) showed that a 2D hydrodynamic model, which takes into account tide and wind stress "corresponded very well" with the genetic results to study larval dispersal of *M.edulis* in the south-western England. On the other hand, a study made in the White Sea showed that *M. edulis* larvae adapted their vertical distribution relative to the larval stage to increase settlement success but also that 65% of larvae were present in the surface 3 meters (Dobretsov & Miron, 2001). Knight *et al.* (2006) showed in the southern Irish Sea that the distribution of *Mytilus spp.* larvae in the water column (down to 24 m of the water column) was influenced by flow condition with a strong current promoting homogeneous distribution and low current increasing larvae density near the seabed. Mussel larvae are known to be slow swimmers (less than 7 mm/s: Sprung, 1984; Troost *et al.*, 2008) which helps explain why a strong current might not allowed mussel to vertically swim. Further, Chia *et al.* (1984) showed that the effectiveness of locomotory organelles (e.g. cilia: short and microscopic hairlike vibrating structure) decreases when the body size of larvae reaches 1 mm. Recent research made by James *et al.* (2019) highlighted that: 1) larval swimming must vary over a tidal cycle as they observed a homogenous distribution of larvae in the water column during flood tide and aggregation of larvae in the middle and bottom waters during ebb tide; and 2) larval size has no effect on vertical distribution pattern of *Mytilus spp.* . The contradicting evidence in literature on the importance of larval behaviour and/or hydrodynamics on larval dispersal, indicate that the influence of several parameters on larval dispersal might be area dependant. Even at a country scale mussel larvae can experienced markedly different currents and/or wind stress which will influence self-recruitment and connectivity (Becker *et al.*, 2007). No previous studies have been working on North Wales mussel population where larvae experience both strong (> 3 m/s in the Menai Strait and around northwest Anglesey) and weak currents.

1.1.3.2 Laval settlement

There is evidence to show that larval settlement is impacted by both physical and biological parameters. Previous experiments have shown that mussel larvae or post-larvae may act like passive particles if the water flow velocity is > 3.9 cm/s, but larval behaviour controls settlement under 3.9 cm/s current velocity (Pernet *et al.*, 2003). Literature suggests that in an area where waves are strong and persistent, larval behaviour are less important for settlement (Martinez *et al.*, 1994). For the physical parameters, settlement is also subject to the surface complexity of the substrates (e.g. the presence of crevices or depressions) (Young, 1983; Hunt & Scheibling, 1996; Lapointe & Bourget, 1999). A study in Canada (Hunt & Scheibling, 1996) showed that

mussel settlement on artificial substrate is mainly the consequence of physical factors (specifically current velocity) and that settlement on a natural substrate is a mix between biological factors (macroalgual/barnacle cover) and physical factors (current velocity, tidal height and flushing time). Porri *et al.* (2006) also suggested that the substrate type is important for settlement but showed that the location of the substrate is also very important as some locations received more settlers than others depending on local hydrodynamic patterns. For the biological parameters, it has been shown that: 1) when larvae or post-larvae reach a critical size they must find a substratum to attach (Herlyn *et al.*, 2008); and 2) chemical cues are released by other species (predators, competitors and substratum like algae and hydroids) (Petersen, 1984; Grizzle *et al.*, 1996; Dobretsov & Wahl, 2001) and conspecific mussels (McGrath & Gosling, 1988). Chemicals cues released by predators and competitors influence settlement negatively however those released by conspecifics and substratum impact the settlement positively (Morello & Yund, 2016). Several settlements can occur during the larvae phase duration known as primary settlement and secondary settlement (Maas Geesteranus, 1942). The primary settlement seems to be on filamentous substrata (such as filiform algae, bryozoans and hydroids) (Figure 1.7) to avoid competition for food and oxygen with adult mussels, which could be unfavourable for young spat (Bayne, 1964). However, according to Martinez *et al.* (1994), this negative effect (e.g. competition for food and oxygen) can only determine the distribution patterns but not the direct settlement.

Figure 1.7: Photo showing larvae mussel attached to seaweed.

The secondary migration (e.g. post primary settlement) allowed the post-larvae to find favourable conditions to settle indefinitely. Again, laboratory tests showed that if post larvae are not disturbed, they remained on their original point of attachment (Martinez *et al.*, 1994).

This result is correlated with an experiment made by Pernet *et al.* (2003) using a down welling system, which showed that mussel larvae are unable to overcome the regime flow and they acted like passive particles. Evidence shows that, most of the time mussel larvae settle on a mussel bed already established (De Block & Geelen, 1958), but occasionally mussel larvae settle directly on the seabed with no primary phase on filamentous substrate (McGrath *et al.*, 1988). Bayne (1964) showed settlement of late plantigrades on mussel beds at Tal-y-Foel (southern Menai Strait, UK) 2-3 weeks after settlement of early plantigrades on filamentous red algae. However, the origin of the mussel larvae was not defined in both observations. The secondary migration phase has not been considered in modelling studies. According to Pineda (2000), larval dispersal and larval settlement are linked and both determine the abundance of many benthic species. All phenomena influencing larval settlement are hierarchical in several axis as shown in Figure 1.8 with spatial and temporal scales (Pineda, 2000). No previous studies have worked on the settlement of *Mytilus edulis* in relation to the spawning time in North Wales. An experiment on both spawning and settlement could help to validate particle tracking models and understand the predominant parameters to take into account to understand larval dispersal.

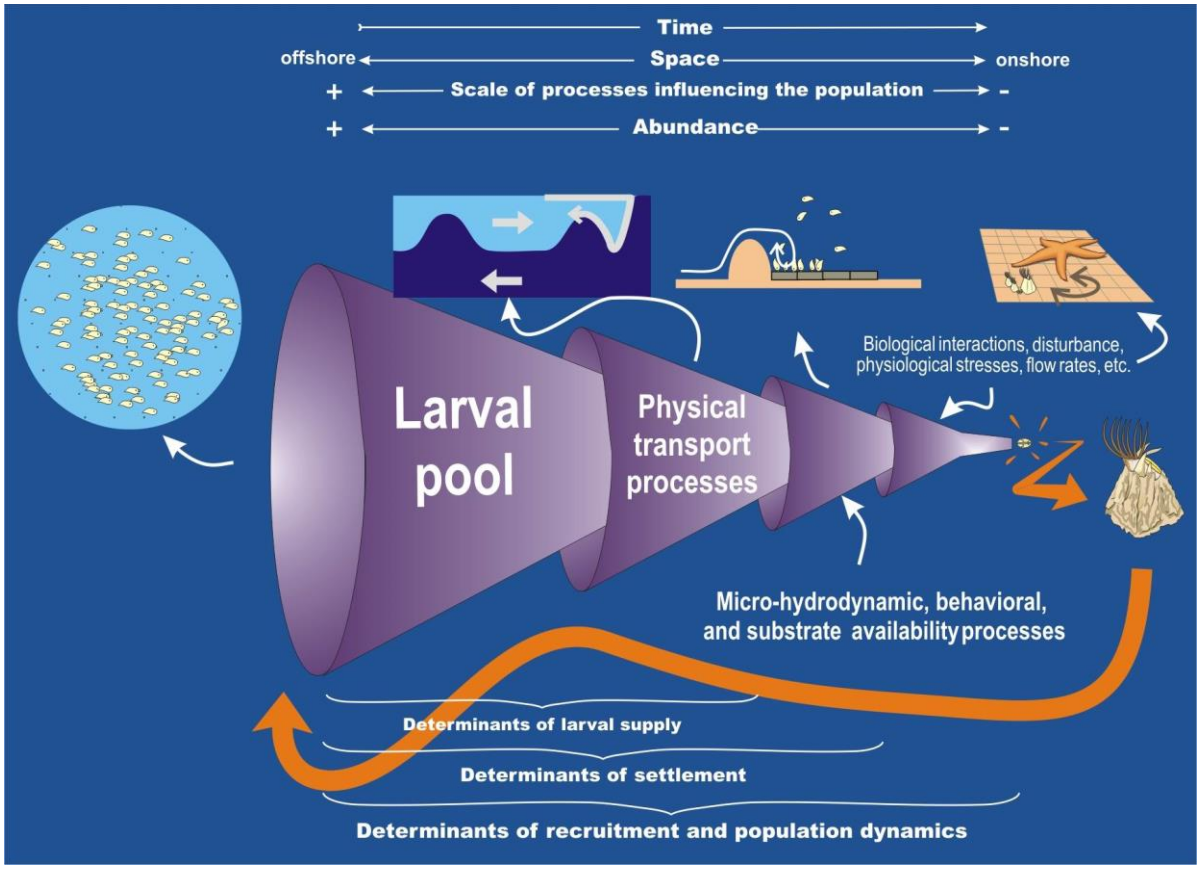

Figure 1.8: Schematic representating the proximate processes that influence larval settlement rate and population density, from Pineda (2000).

1.1.4 The Distribution

Blue mussels (*Mytilus spp.*) are globally widespread in coastal waters, with a distribution of five species in the Northern Hemisphere north of the tropic of Cancer (*M. trossulus*, *M. edulis*, *M. galloprovincialis*, *M. californianus* and *M. coruscus*) and three in the Southern Hemisphere south of the tropic of Capricorn (*M. galloprovincialis*, *M. chilensis* and *M. platensis*) (Figure 1.9) (Seed, 1976; Gosling, 1992; Gaitan-Espitia *et al.*, 2016). According to Hilbish *et al.* (2000), the antitropical distribution (no presence of *Mytilus spp.* between the tropic of Cancer and tropic of Capricorn) pattern of *Mytilus spp.* is closely related to a transequatorial migration from the Northern Hemisphere to the Southern Hemisphere through the Atlantic during the Pleistocene. Indeed, it seems that the South American mussel species are more related to *M. edulis* whereas mussels from Australia and New Zealand more related genetically and morphologically to *M. galloprovincialis* (McDonald *et al.*, 1991).

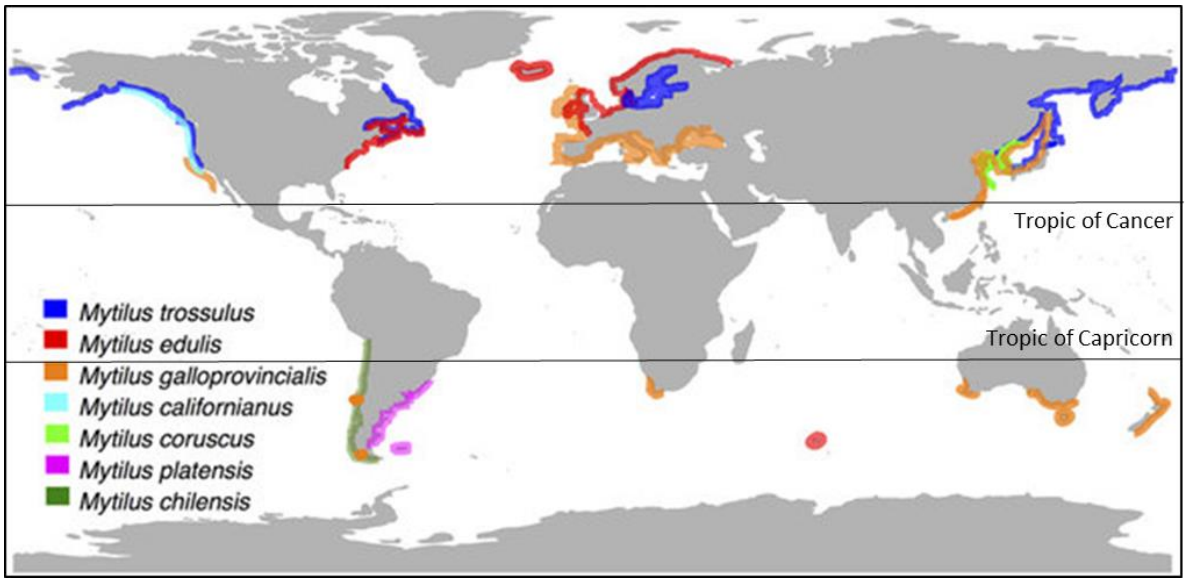

Figure 1.9: Mapping showing the worldwide distribution of the genus *Mytilus* (Gaitan-Espitia *et al.*, 2016).

In Europe, there are three mussel species from the genus *Mytilus* are present (Figure 1.10):

- *M. edulis* (Linnaeus, 1758) is a cold-temperate species (acclimated from 5°C to 20°C) and is widely distributed in the north of Europe from the Atlantic coast to the White Sea.
- *M. galloprovincialis* (Lamarck, 1819) is a warm-temperate species and is principally found in the Mediterranean Sea and in the Black Sea as well as parts of the northwest Atlantic.

- *M. trossulus* (Gould, 1850) is widespread along northern European coasts and the Baltic Sea (Vainola & Streklov, 2011).

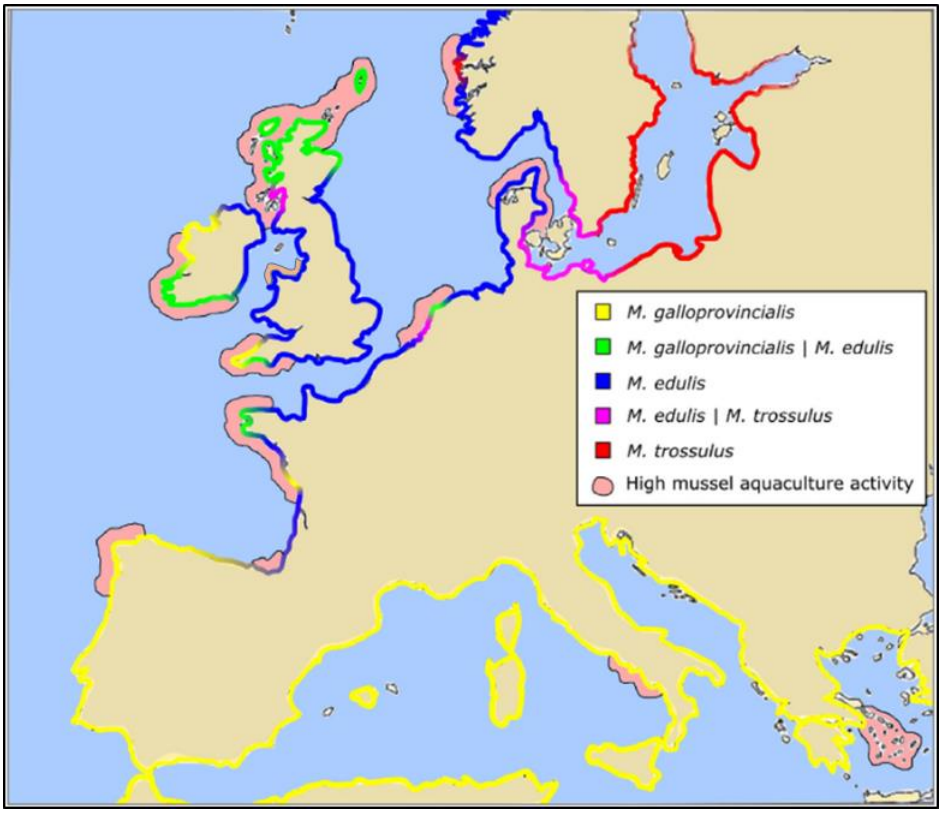

Figure 1.10: Map showing the distribution of genus *Mytilus* in Europe (Michalek *et al.*, 2016).

Hybridisation between these three species occurs readily where their distributions overlap (Gosling, 1992) (Figure 1.10). The extent of hybridisation depends on five factors: 1) spawning synchrony (Toro *et al.*, 2002); 2) larval dispersal patterns which can promote settlement of a new specie; 3) local adaptation due to environmental conditions (Riginos & Cunningham, 2005); and 4) human activities such as the increase of shipping traffic (Vainola & Streklov, 2011). Figure 1.10 shows a hybrid zone *M. edulis*/*M. trossulus* in the Baltic Sea and the hybridisation *M. edulis*/*M. galoprovincialis* along the Atlantic coast of Europe and the southwest coast of the UK (Gilg & Hilbish, 2003). In the Irish Sea, *M.edulis* are present everywhere, however the highest density of mussels are observed in the north of Ireland, North Wales and Pembrokeshire; further these populations appear to be exclusively *M. edulis* (Gosling *et al.*, 2008) (Figures 1.10 and 1.11).

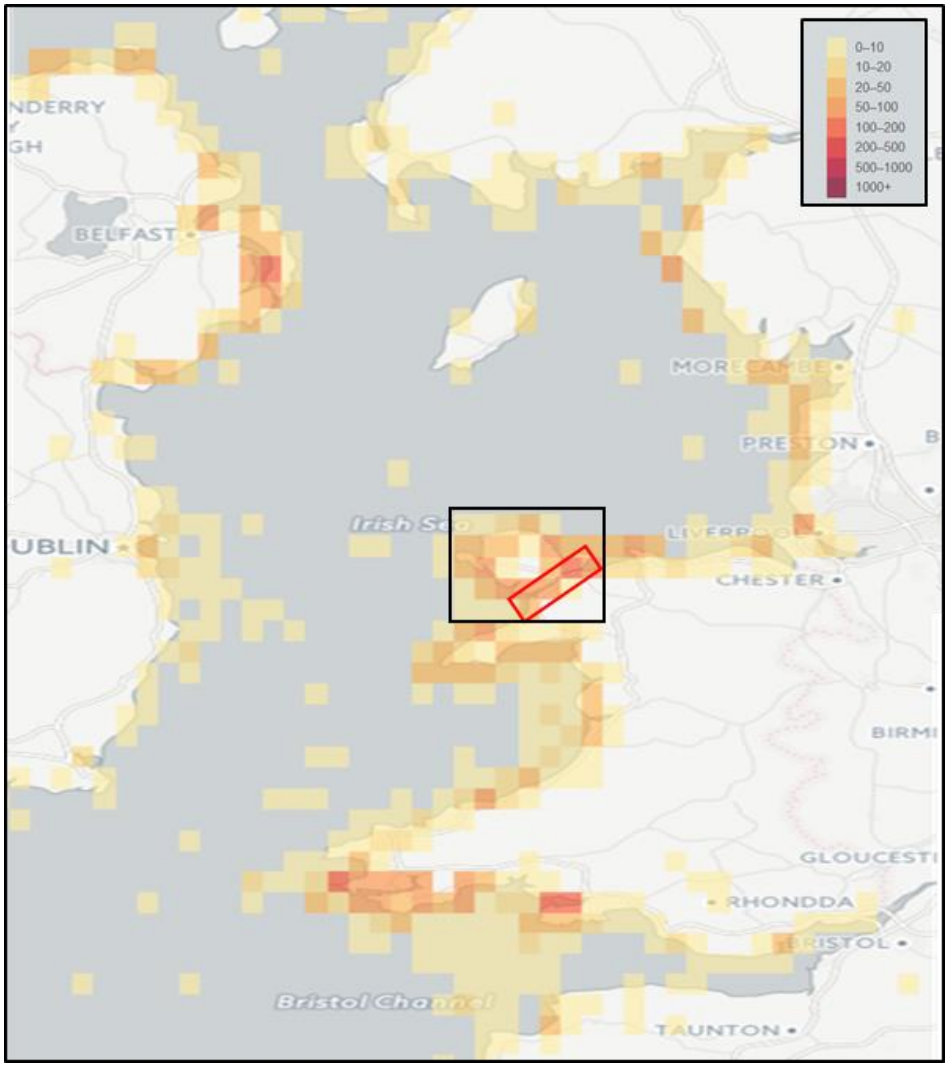

Figure 1.11: Heat map showing *Mytilus edulis* distribution in the Irish Sea per km^2, with 1) in red, areas with the highest density; 2) in orange, areas with a medium density; and 3) in yellow, areas with a low density (from Ocean biogeographic information system). Greys area have no known mussels. The black box and the red box represent the study area: Anglesey and the Menai Strait, respectively.

The focus of this study is the distribution of mussels around Anglesey, northwest Wales, in the Irish Sea. Specifically, the potential larval transport from source sites within the Menai Strait (red box on Figure 1.3). Within the Menai Strait, there are five mussel beds. The largest by area is located in the north east of the Strait and covers approximately 7 km^2 (Figure 1.12). It is managed by Bangor Mussel Producers Limited, which is the association of four companies: Extramussels Limited, Deepdock Limited, Myti Mussels Limited and Ogwen Mussel Limited. The four others mussel beds are not managed by Bangor Mussels Producers and they are located in the south west of the Menai Strait. Three of them are situated on the Anglesey coast opposite Caernarfon and Y Felinheli and one on the mainland between Caernarfon and Y Felinheli (Figure 1.12).

Figure 1.12: Map showing the distribution of the principal mussel beds in the Menai Strait (from Digimap).

At the scale of a mussel bed, *M. edulis* are distributed in the intertidal area (Figure 1.13). The reason for such a distribution depends on: 1) physiological intolerance to extreme temperature and desiccation which determine the upper limit along the shore line (Paine, 1974); 2) areas such as open water and estuaries where the energy is sufficient to provide food and remove waste (Dame, 1993; Dame & Prins, 1998); 3) predation, in the subtidal area by fish, lobster and starfish, which influences the lower limit along the shoreline (Suchanek, 1978; Richards *et al.*, 1999); and 4) interspecific competitions (Suchanek, 1978).

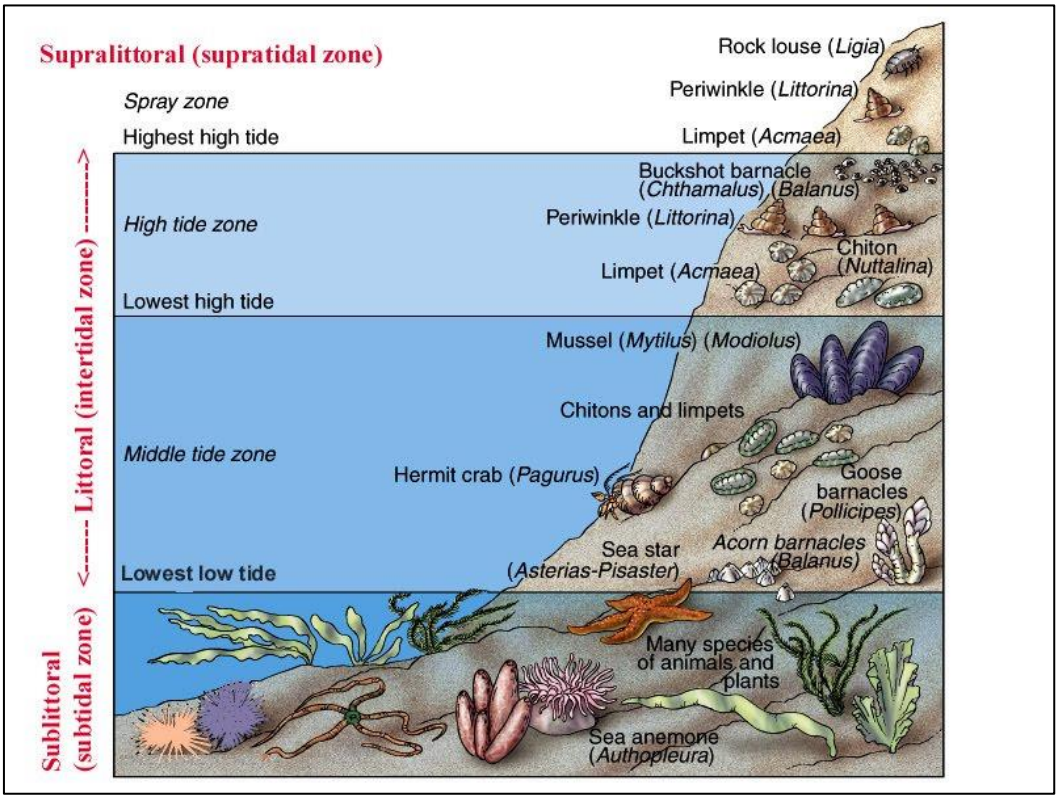

Figure 1.13: Schematic showing vertical zonation patterns of shore area.

1.2 Methods to study larval dispersal

1.2.1 Hydrodynamic and particle tracking models

1.2.1.1 Introduction and functioning of particle tracking models

Computational hydrodynamic modelling allows the simulation of the motion and properties of water. Two modelling methods can be used to describe the motion of a fluid. The Lagrangian approach tracks the position and velocity of individual parcels/particles in time and space, while the Eulerian approach focuses on fixed points in space (usually in the form of a model grid/mesh) and simulations are made of the changes to parameters in time (e.g. changes in flow velocity, water temperature, density etc…) (Durst *et al.*, 1984). In the case of simulating larvae transport, it is common to use a Lagrangian particle tracking model which tracks particles (i.e. virtual larvae) through the Eulerian flow field predicted by the hydrodynamic model (Gouesbet & Berlemont, 1999).

Hydrodynamic models follow the Navier-Stokes equations which are derived from Newton's Laws (Liu & Losada, 2002) (Equation 1.1).

$$\frac{\partial p}{\partial t} + \nabla . \rho u = 0 \quad Continuity\ Equation$$

$$\frac{\partial u}{\partial t} + (u.\nabla)u = -\frac{1}{\rho}\nabla p + F + \frac{\mu}{\rho}\nabla^2 \mathrm{u} \quad \text{Equation of Motion}$$

$$\rho\left(\frac{\partial \varepsilon}{\partial t} + u.\nabla\varepsilon\right) - \nabla.(K_H \nabla T) + p\nabla.u = 0 \quad \text{Conservation of Energy}$$

Equation 1.1: Navier-Stokes equations, where **u** = velocity vector field, ε= thermodynamic internal energy, p = pressure, T = temperature, ρ = fluid density, μ = viscosity, K_H = heat conduction coefficient, **F** = external force per unit mass = acceleration.

For shallow coastal waters, because the vertical dimension is much smaller than the horizontal scale, the Navier-Stokes equations are commonly simplified to the shallow water equations (e.g. assume hydrostatic pressure and absence of vertical velocity) (Equation 1.2).

$$\frac{\partial(\rho\eta)}{\partial t} + \frac{\partial(\rho\eta u)}{\partial x} + \frac{\partial(\rho\eta v)}{\partial y} = 0$$

$$\frac{\partial(\rho\eta u)}{\partial t} + \frac{\partial}{\partial x}\left(\rho\eta u^2 + \frac{1}{2}\rho g\eta^2\right) + \frac{\partial(\rho\eta uv)}{\partial y} = 0$$

$$\frac{\partial(\rho\eta v)}{\partial t} + \frac{\partial(\rho\eta uv)}{\partial x} + \frac{\partial}{\partial y}\left(\rho\eta u^2 + \frac{1}{2}\rho g\eta^2\right) = 0$$

Equation 1.2: Shallow water equations where u = velocity in the x direction; v = velocity in the y direction; g = acceleration due to gravity; η = total fluid column height and ρ = fluid density.

Numerical methods perform discrete calculations to solve the complexity of the ocean system of interest (e.g. an estuary or shelf sea). In the Eulerian framework, two model grid structures are common: 1) the structured grid or finite-difference (which uses quadrilateral grid size); and 2) the unstructured grid or finite-element/finite-volume (which uses variable-sized triangular elements). Both methods represent well the large-scale circulations patterns in deep water regions (Jones & Davies, 2006). Due to the simpler code structure, the finite-difference method presents a better computational time efficiency (Chen & Liu, 2003). However, this method requires a large number of grid elements/cells to resolve complex geometry such as in coastal areas (Chen *et al.*, 2007). The finite-element method has been very successful in resolving estuarine flows and coastal flows due to a better fitting of the geometric complexity, but the computational power needed is higher than the finite-difference method (Chen & Liu, 2003; Walters, 2006; Neill & Hashemi, 2018).

This study focusses on the coastal currents and their impact on larval dispersal in the Irish Sea. Due to the complexity of the coast comprising headlands, islands, channels and estuaries, and their influence on coastal currents, the finite-element method was used to obtain a fine-scale coastal resolution. Irish Sea modelling was computationally expensive, requiring the model code to be parallelised and run on high performance computing systems on Super computing Wales (https://www.supercomputing.wales). This enables the simulations to be partitioned between several computer cores, which can significantly reduce computational time or enable model resolution to be increased to improve accuracy (Yang & Khangaonkar, 2009; Xu *et al.*, 2011).

The importance of the spatial resolution of a model grid can be crucial and is an important source of model uncertainty. Indeed, Graham *et al.* (2018) showed that a finer spatial resolution mesh, increased from 7 km to 1.5 km across the northwest European continental shelf, reduced the mean bias for four out of seven tidal constituents (M2, S2, K1 and N2) which has a direct impact on the improvement of seasonal stratification and temporal variability of salinity and temperature. Jones & Davies (2005; 2010) showed that a finite-difference model underestimated the tidal amplitude at coastal gauges on average mainly to the lack of resolution offered by this method. Heaps & Jones (1977) developed a numerical model of the Irish Sea, however, the simulated currents were under-estimated mainly due to the coarse resolution of the domain (14 km^2 grid cells) (Dabrowski *et al.*, 2003). Allen & Newberger (1996; 1998) also concluded that a finer model will improve the understanding of baroclinic instabilities (mesoscale turbulence which impact ocean stratification and consequently ocean dynamics and particle transport), internal initial-gravity waves (wave along the thermocline) and coastal boundaries flow generated by wind events. Several studies made by Dabrowski *et al.* (2003; 2005; 2008; 2010) showed that a structured-grid model with a 2 km grid resolution resolved accurately the overall circulation patterns of the Irish Sea but it was too coarse to simulate the coastal flows.

1.2.1.2 PTM applied to ecological questions

Once the appropriate hydrodynamic modelling methodology has been set up for a region and validated against flow/temperature fields, separate ('off-line') Lagrangian Particle Tracking Models (PTMs) can be developed for larval dispersal, since larval dispersal does not affect the flow field. The rise of numerical methods gave the possibility to study ecological questions on larval dispersal (i.e. self-recruitment, connectivity, metapopulations, source-sink dynamics) (Swearer *et al.*, 2019). Indeed, fieldwork was almost impossible logistically to study larval

transport at different temporal and spatial scale, also numerical methods are less expensive financially (Swearer *et al.*, 2002). These PTMs can disperse particles (i.e. larvae) according to physical advection and mixing output from the hydrodynamic model, and also the larval behaviour of the pelagic phase (Lett *et al.*, 2008; Garcia-Garcia *et al.*, 2016):

- Spawning: number of eggs, spawning location and area, depth of mature animal and timings/frequency of releases.
- Movement: horizontal and vertical dispersion, egg buoyancy (difference between egg density and sea density), larval vertical migration behaviour and pelagic larval duration.
- Growth: the size of the larvae changes during depending on the food availability and the temperature, which have a direct impact on pelagic larval duration and so settlement.
- Mortality: predation rate, water conditions such as temperature, salinity and/or pollution.
- Settlement: the size of the larvae, substrate type, water depth, proximity to established bed.

Once physical and biological parameters are set up, it is possible to resolve dispersal trajectories and answer ecological questions such as: 1) Is a population sustainable? 2) Does a population can be considered as a source or a sink?; 3) How much are populations connected to each other?; and 4) Does connectivity among populations lead to metapopulation (i.e. population of population)? (Hjort, 1914; Levins 1969; Larghier, 2003; MacDonalds *et al.*, 2006). The sustainability of a population is the consequence of self-recruitment (i.e. successful settlement at the same place) and/or connectivity with one or several populations (i.e. connection between two or more populations, which are locally distinct) (Hawkins *et al.*, 2019). It has been previously shown that the connection between populations depended on spatial (e.g. distance between populations; location of larval release) and temporal scale (e.g. pelagic larvae duration) (Hjort, 1914; Kinlan *et al.*, 2005; Shima *et al.*, 2015 and Noonburg *et al.*, 2015). Numerical studies on larval dispersal are essential to resolve dispersal trajectories and calculate connectivity matrices/networks that determine the level of self-recruitment of a population and connectivity between neighbouring populations (Largier, 2003). However, it is important to simulate sufficient numbers of particles to be statistically representative of transport/connectivity/self-recruitment patterns from different sources (MacDonald *et al.*, 2006).

1.2.2 Other methods existing

Several other ways exist to obtain information on larval dispersal, which can be used to validate and/or parameterize PTMs:

- Observations of plankton distribution in the water column will give information on mortality, vertical distribution and vertical migration (Largier, 2003). Larval collection with plankton net, drogues and autonomous vehicles only give information about larvae abundance in time and space but do not answer the questions about: 1) self-recruitment and/or connectivity; and 2) taxon species (Power, 1996; Wiebe & Benfield, 2003). Further, larval collection in the field requires considerable man-hours. Furthermore, plankton nets need to be adapted to the area/species of interest (Wiebe & Benfield, 2003). In our case study, the area of North Wales includes: 1) both blue water (i.e. water with low concentrations of suspended particles) and green water (i.e. water with high concentrations of suspended particles); and/or 2) both stratified and well-mixed water (Neil *et al.*, 2012; Keen, 2015). Therefore, to effectively survey the range of environments in the region would be practically difficult and too expensive for the scope of this study.
- Genetic approaches are used to measure the similarity between spatially distinct populations and hence, provide an estimate of their connectivity (or lack of). Such methods include microsatellite screening because they are considered ideal markers to identify species, individuals and inter-familial relationships (Gilg & Hilbish, 2003; Berumen *et al.*, 2012; Pusack *et al.*, 2014; Harrison *et al.*, 2014). In North wales, *M. edulis* are found in many locations along the coast (http://data.nbn.org.uk ; habitat maps). Consequently, genetic approaches are not useful in this area as the different mussel populations could be already well mixed genetically.
- Laboratory experiments can be used to understand the larval biology. However, this method is typically performed at smaller scales (e.g. aquarium, tank) and therefore does not represent realistic oceanic environments which influence larval dispersal rates (Katz *et al.*, 1994), especially in the Menai Strait where current speeds can reach 2.60 m/s (see section 3.2).
- Microchemistry of crustacean exoskeletons, fish otoliths or mollusc shells can provide good estimates of the origin of the different organism but also information of the settlers (Largier, 2003). Marriott *et al.* (2016) showed a significant difference for 10 elements between nursery grounds of juvenile plaice in north Wales. However, this technique has never been used in North Wales on *M.edulis* yet.

The above analyses can provide essential information on larval behaviour for case-specific particle tracking modelling studies that predict larval transport and connectivity (Weidberg *et al.*, 2015).

1.3 Study site

1.3.1 The Irish Sea

The Irish Sea separates Ireland and Great Britain and covers approximately 47,000 km^2 with a volume of 2,430 km^3 (Howarth, 2015). The sea is connected to the Atlantic Ocean via the Celtic Sea in the southwest by St George's Channel and via the North Channel in the north (Bowden, 1980). The Irish Sea is approximately 300 km in the northwards direction and varies from 75 km to 200 km in the eastwards direction but decreases to 30 km in the North Channel (Howarth, 2005). The biggest island is Anglesey followed by the Isle of Man (Vincent *et al.*, 2004). The Irish Sea topography consists of a deeper channel in the west (30-50 km wide, 300 km long and up to 275 m deep) and shallower embayments in the east. The water depths remain generally shallow with an average depth of 60 m (Bush, 2015; McKay & Pattenden, 1993) (Figure 1.16). Principal shallower embayments (less than 50 m depth) are: 1) Cardigan Bay (between the Llyn peninsula and Pembrokeshire); 2) the eastern Irish Sea (east of Isle of Man including Liverpool Bay); and 3) Caernarfon Bay. The eastern Irish Sea is the most affected by freshwater input (70 % of the total fresh water in flow to the Irish Sea) from the Ribble, the Mersey and the Dee rivers (Dabrowski & Harnett, 2008). Coastal typology of the Irish Sea varies from undulating rocky coast, cliffs, sandy beaches, sand dunes, estuaries (e.g. Dee, Mersey), bays (e.g. Caernarfon, Liverpool, Morecambe) and tidal channels (e.g. the Menai Strait). Further, seabed sediment varies in the Irish Sea greatly from rocks, gravels, sands and mud (Dobson *et al.*, 1970; Mackie, 1990; Davies & Lawrence, 1993) (Figure 1.17).

The Irish Sea circulation is primarily controlled by an energetic tidal regime, which created an annual average net flux northward of 2.50 km^3/s (Figure 1.18) (Lee & Ramster, 1981; Parker-Humphreys, 2004; Dabrowski *et al.*, 2010). The tide here is semi-diurnal in nature, meaning there are two cycles per day. The semi-diurnal tidal waves (mainly the lunar (M2) and solar (S2) tidal constituents) propagate into the Irish Sea, southwards from the North Channel and northwards from St. Georges Channel (Davies & Hall, 2000; Dabrowski *et al.*, 2003). This tidal regime produces the typical spring-neap cycle: 1) spring with large tidal range resulting from the alignment of the earth, sun and moon; and 2) neap with smaller tidal range when the sun and the moon cycles are out of phase. Lower-frequency tidal constituents (e.g. diurnal) have an impact on tidal stream currents (e.g. causing the two tides per day to be of different strengths) in this area but to a lesser effect than the semi-diurnal constituents (Piano *et al.*, 2015; Howarth, 2015). Tidal velocities are governed by local bathymetry and tidal range, which varies from over 10 m in Liverpool Bay and the Bristol Channel, to amphidromic points (near zero tidal amplitude) southeast of the Irish coast and northeast of Ireland (Bush, 2015; Howarth, 2015)

(Figure 1.19). Tidal current velocities exceed 1 m/s at spring tides throughout St Georges Channel and the North Channel and can exceed 2 m/s in certain localised regions such as arounds headlands (e.g. Pembrokeshire, Llyn Peninsula and northwest Anglesey) and through tidal channels (e.g. the Menai Strait) (Figure1.20). Areas of weaker tidal currents (less than 0.5 m/s) can be found in shallower and sheltered bays (e.g. Cardigan Bay, Liverpool Bay and along the Cumbrian coast) (Figure1.20).

Although the tidal currents are strong in many regions and therefore have the potential to advect larvae long distances over a tidal phase of six hours, tidal flows are oscillatory and so the net transport due to tide alone is likely small. Residual currents result from asymmetric oscillatory tidal flows (averaged over one or several tidal cycles) or from persistent wind-driven or density-driven flows. Residual currents are apparent in the Irish Sea and can transport larvae over long distances depending on the PLD even though the instantaneous current strength is likely much smaller than tidal currents. Elliott (1991) showed the importance of residual circulation on oil spilled dispersal, however no studies have investigated the potential impact of wind-driven currents on particles in the Irish Sea over a long time period. However, several studies showed the contributions of wind forcing (direct and indirect), surface waves and density gradients (horizontal and vertical) on residual currents (Prandle & Matthews, 1990; Prandle, 1987; 1991; 1997). Geos (2001) showed that in the Irish Sea wind comes from southwest and west principally (40 %) and wind strengths are highest between December and March (wind data analysed from 1979 to 1994). The associated waves depend on the duration and the fetch of the wind. For the Irish Sea, the wave period is relatively short (maximum of 10 s; data analysed over 50 years) (Howarth, 2015). Significant residual flows are observed: 1) directed southward along the east coast of Ireland; 2) westward from South Wales towards Ireland along St. George's Channel: the Celtic Sea front; 3) directed southward from Llyn peninsula to Cardigan Bay; and 4) directed westward along the north Wales coast: Liverpool bay front (Heaps, 1972; Simpson *et al.*,1978; Heaps & Jones, 1977; Simpson & Bowers, 1981; Bush, 2015) (Figure 1.21).

Most of the Irish Sea remains well mixed throughout the year. However, stratification over the summer occurs in the east and west of the Isle of Man and in Cardigan Bay due to weak tidal currents in these areas (Figure 1.21). The stratification phenomenon in the east of the Isle of Man remains marginal as it can easily be mixed away by storms and spring tides (Howarth, 2005). In the western Irish Sea, the stratification creates a front where a circulation gyre appears (Figure 1.21). Here, a combination of deep water and weak tides (< 0.3 $m.s^{-1}$) which is insufficient to generate enough turbulent energy to maintain vertical mixing leads to warmer upper layer and cold water beneath (Simpson, 1971; Hill, 1993; Hill *et al.*, 1997). This results

in an anticlockwise circulation gyre in the western Irish Sea, which increases from spring to summer but also with an inter-annual variability in terms of times of formation (Horsburgh & Hill, 2003; Xing & Davies, 2001). These areas of thermal stratification (southern Irish Sea, western Irish Sea gyre and eastern Irish Sea) may have an important impact for planktonic larvae retention during the summer but also to isolate populations from each other (Dickey-Collas *et al.*, 1996; O'Sullivan *et al.*, 2015). However, Phelps *et al.* (2015) showed that larval vertical migration might play a role in the reduction of the retention rate by escaping the circulation which is confined to a narrow area around the thermocline.

The temperature of the Irish Sea varies seasonally (between winter and summer) but also spatially from the east to the west, with the warmest waters in the east in summer and in the west in winter (Figure 1.22). Because of the shallow water in the eastern Irish Sea, the variation of water surface temperature (data from 1993 to 2001) is higher from 16°C in summer to 6°C in winter. In contrast, the western Irish Sea varies from 13.5°C to 9.5°C between summer and winter, respectively (Figure 1.22) (Parker-Humphreys, 2004). A difference is also observed for the salinity between: 1) increase from eastern to the western Irish Sea (31.0 to 34.5 respectively); and 2) decrease from south to north (35 to 34 respectively) (Figure 1.23) (Hadziabdic & Rickards, 1999; Parker-Humphreys, 2004).

All these observations show that both barotropic (gravity-driven; e.g., tides or wind) and baroclinic (densitydriven; e.g., tidal mixing fronts) components play a fundamental roles in the water circulation in the Irish Sea and consequently may have an influence on larval dispersal (Robins *et al.*, 2013).

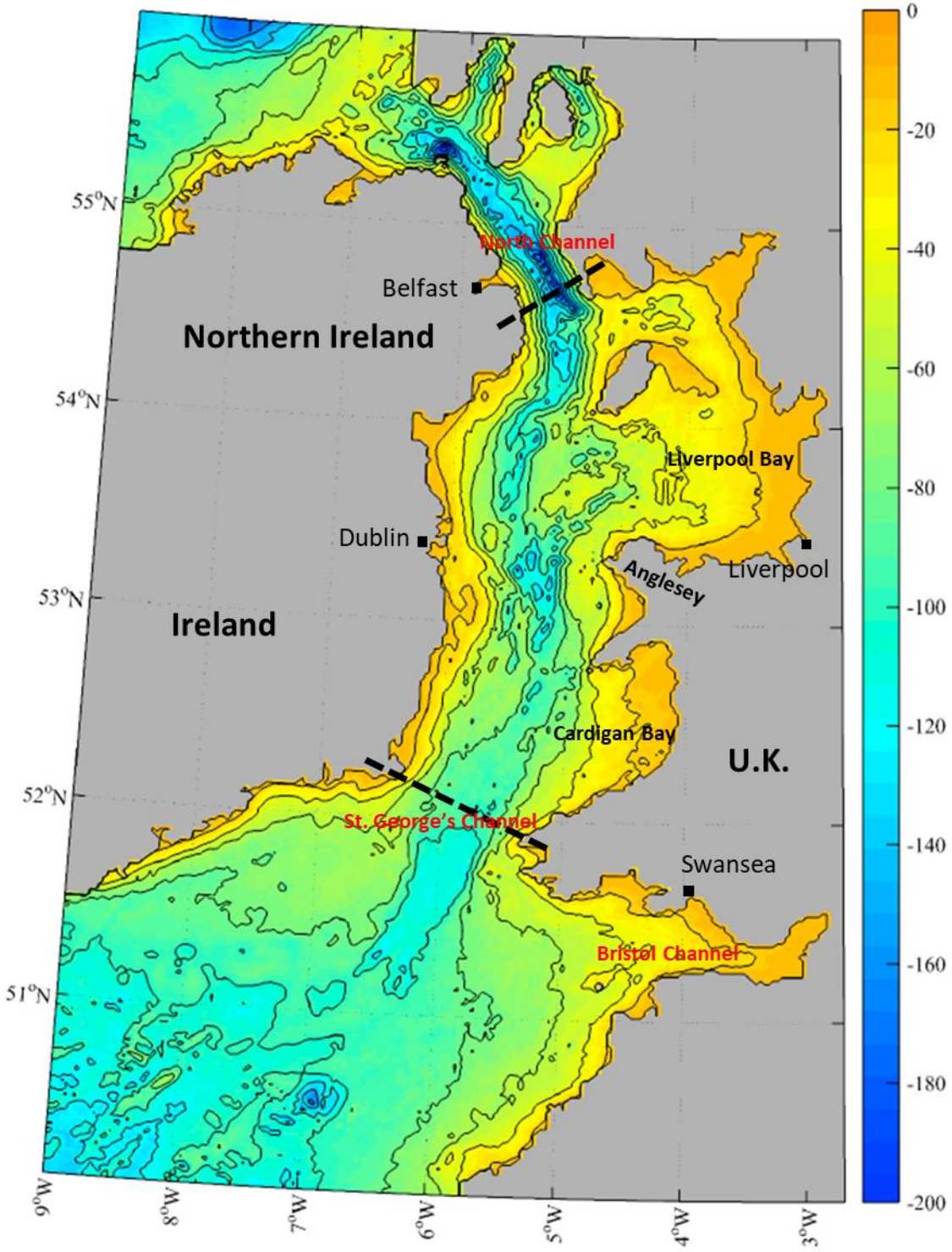

Figure 1.14: Map showing the bathymetry of the Irish Sea (meters below mean sea level), land is coloured in grey and dashed lines represent the approximate limit of the Irish Sea. (Modified from Bush, 2015).

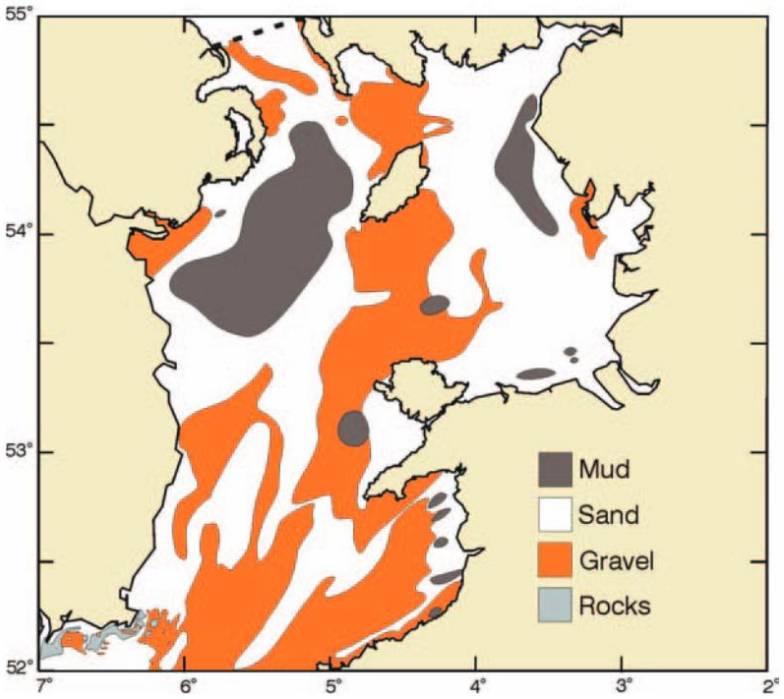

Figure 1.15: Map showing the distribution of major sediment types in the Irish Sea, from Parker-Humphreys (2004).

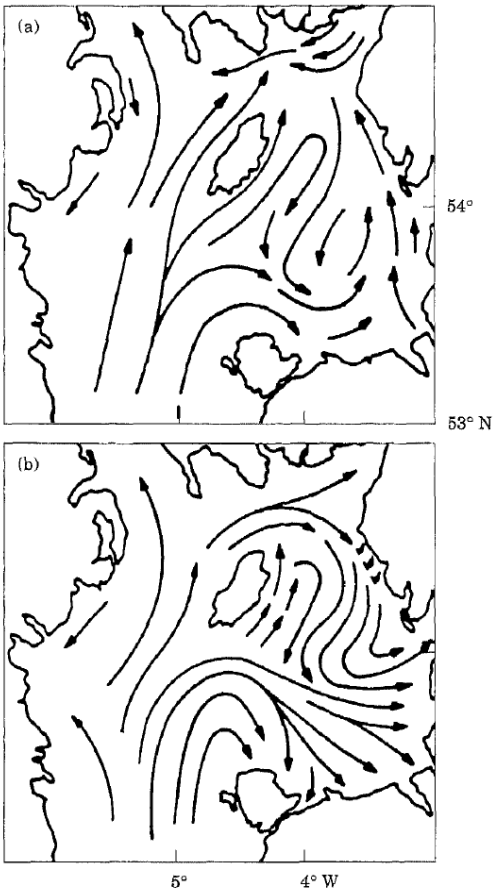

Figure 1.16: Map showing Lagrangian circulation in the northern Irish Sea (a) surface and (b) bottom from Hill *et al.* (1997).

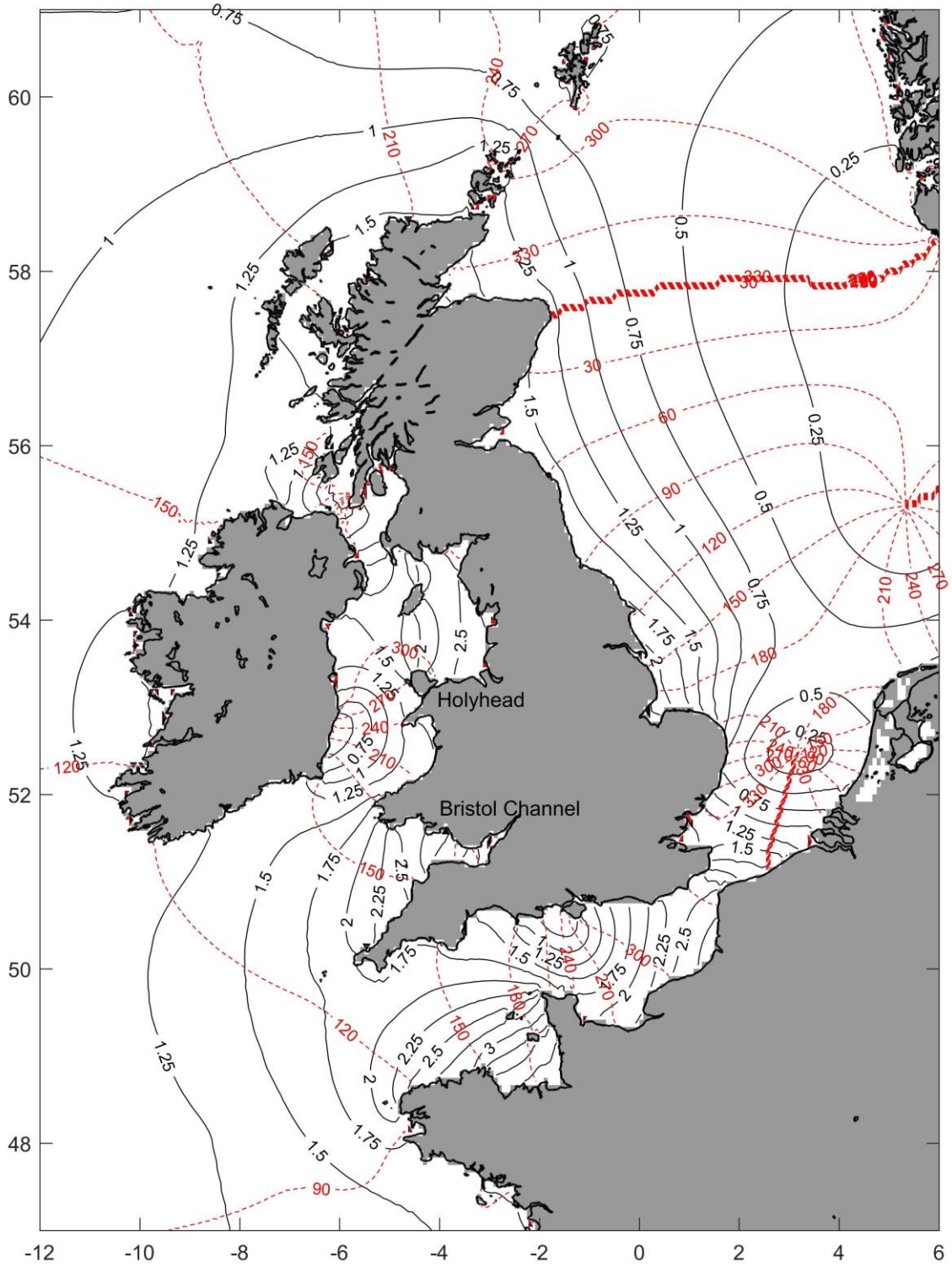

Figure 1.17: Map showing the M2 co-tidal chart of the Irish Sea, the Celtic Sea and the North Sea with dashed contours representing cotidal lines (in degrees) and solid contours representing coamplitude lines (in meters), from Neill & Hashemi (2018).

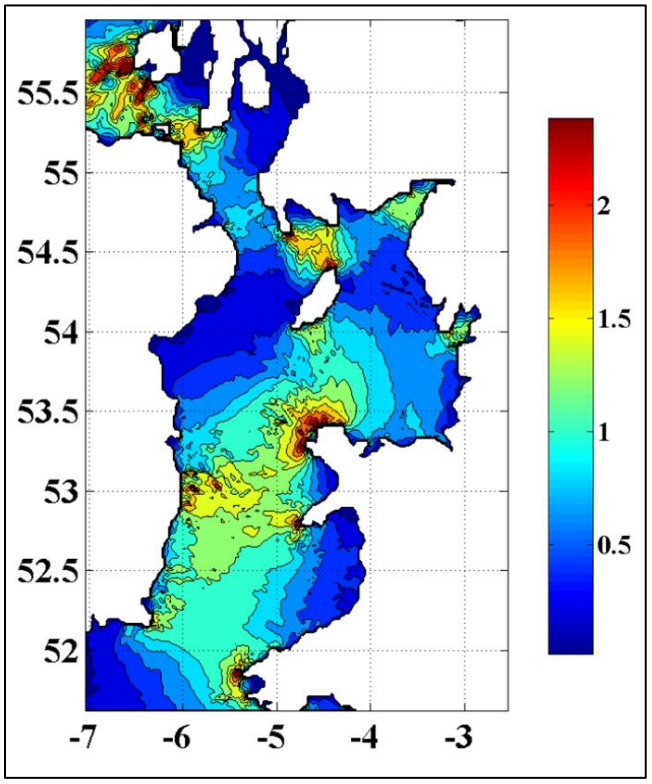

Figure 1.18: Map showing maximum amplitude of the depth-average tidal currents for a mean spring tide (m/s), from Howarth (2015).

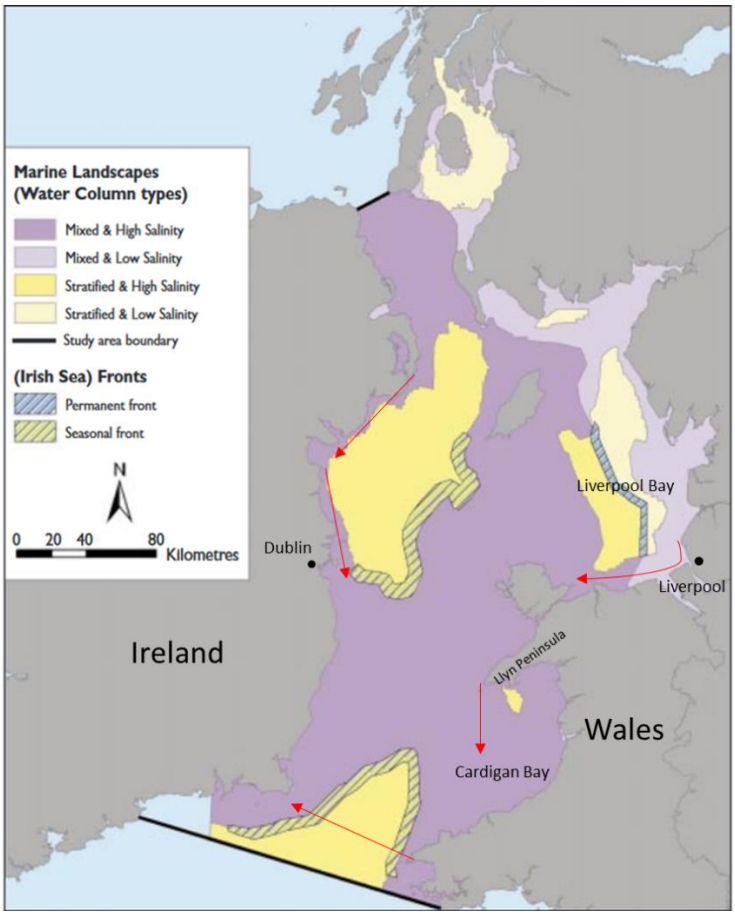

Figure 1.19: Hydrographic map of the main water bodies, and frontal systems within the Irish Sea, modified from Golding *et al.* (2004).

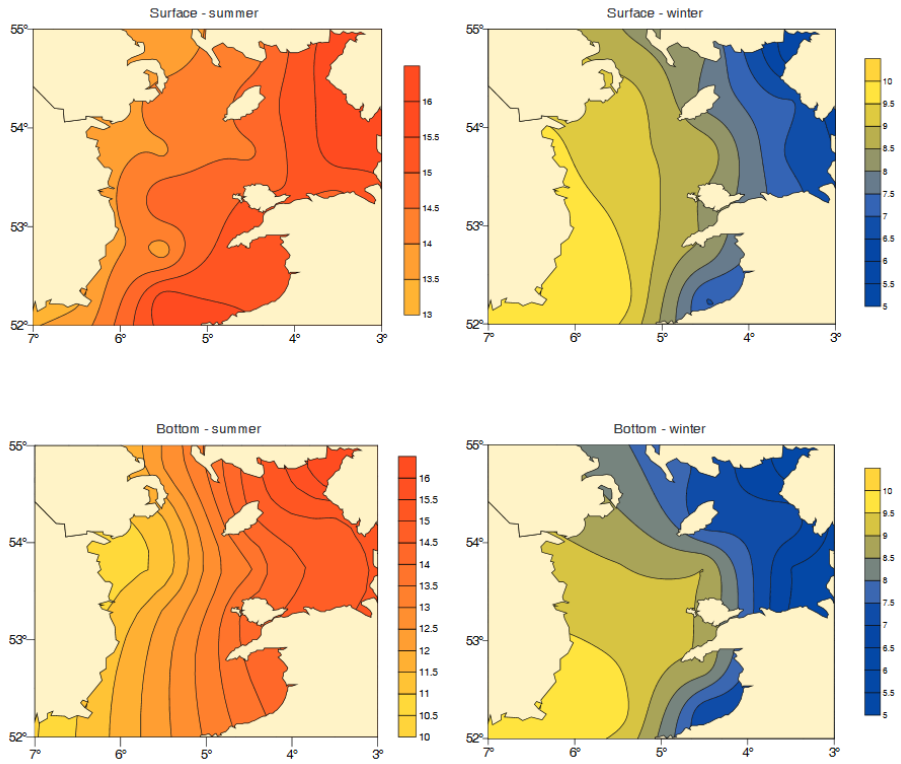

Figure 1.20: Map showing average near bottom and near surface temperature (1993-2001) for summer (August) and winter (January), for the northern Irish Sea (Parker-Humphreys, 2004).

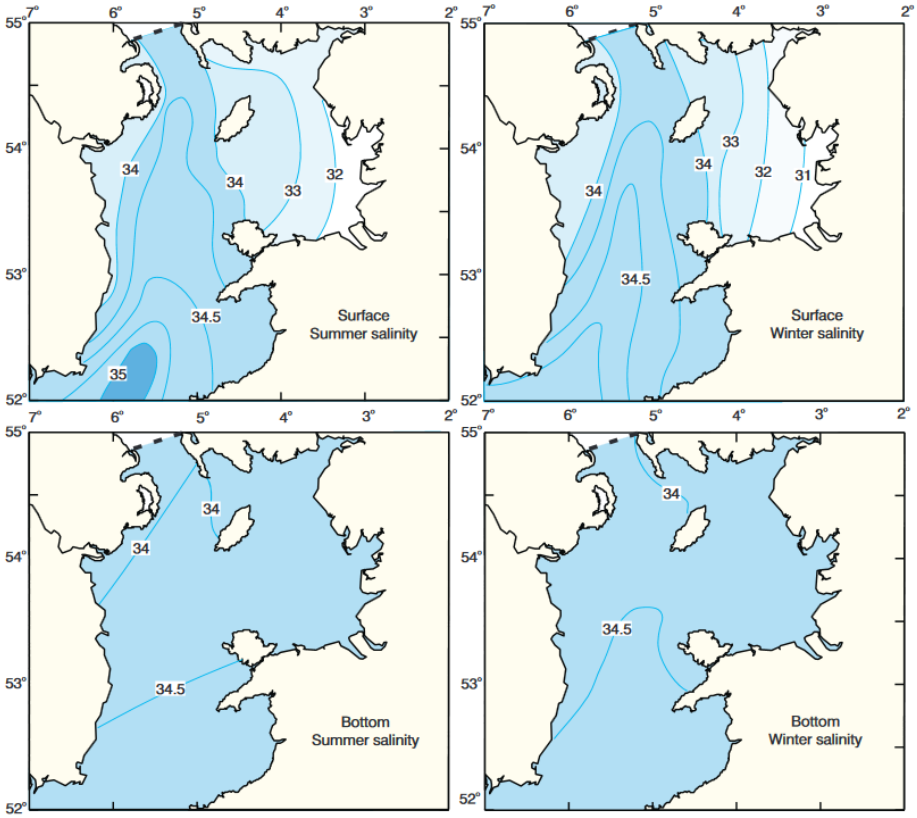

Figure 1.21: Map showing average near bottom and near surface salinity for summer and winter (Lee & Ramster, 1981).

1.3.2 The Menai Strait

The Menai Strait is the focus region for this study. Here, there is an active mussel population and shellfishery (Figures 1.12 and 1.31). Potential larval dispersal from this region will be investigated through observational and modelling approaches. The Strait is a narrow seawater channel located between the island of Anglesey and the mainland of North Wales (Figure 1.22; Kratzer *et al.*, 2003). It is the result of Pleistocene glaciations, which eroded the bedrock along a line of weakness associated with the Menai Strait fault system (Gibbson, 1987). It is approximatively 25 km long from Fort Belan, in the south-west, to Beaumaris in the northeast where it re-connects with the Irish Sea. The channel has a mean width of 800 m with a variation from 300 m (in the swellies area and at the southwest entrance) to 1.2 km (e.g. near Caernarfon) (Embleton, 1964; Kratzer *et al.*, 2003). Water depths vary from 2 meters to a maximum of 25 meters in the south west of the swellies (Harvey, 1968; Campbell *et al.*, 1998) (Figure 1.22).

The tidal flows through the Menai Strait are strong and complex – driven by the tide propagating northwards through the Irish Sea (Figure 1.23). As the tide advances northwards through the Irish Sea, it enters the southwest entrance to the Strait with fast current speeds – peak flows exceeding 1 m/s. Here, the tidal range is approximately 5 m during springs and 1.3 m during neaps (Campbell *et al.*, 1998; Rippeth *et al.*, 2001) (Figures 1.24 and 1.25). Because the tidal range and the mean water depth are of similar magnitudes, the high friction influence of the seabed slows the advancement of the tide through the channel. In the time taken for the tide to reach the Swellies (mid-channel), the tidal wave has also advanced around the north coast of Anglesey to enter the Strait at the northeast entrance, near Beaumaris (Davies & Robins, 2017). In effect, the tide floods into the channel from both ends. The tidal amplitude at the northeast entrance is greater than at the southwest entrance: 7.5 m (springs) and 2.2 m (neaps) (Figures 1.24 and 1.25). These differences in tidal range, combined with the slowing down of the tide as it travels through the channel, generates an asymmetrical tidal cycle with markedly stronger currents during the ebb phase (directed southwest) than the flood. Indeed, the ebb flow southwest is 10% to 15% stronger than the flood flow northeast (Campbell *et al.*, 1998). This means that, in Menai west, there is a greater flux of water south-westwards than north-eastwards and the net flow is south-westwards over a tidal cycle – hence, due to the tidal dynamics alone, the movement of planktonic animals such as mussel larvae are expected to be transported south-westwards through the channel over a tidal cycle (Figure 1.26 and Table 1.3).

The flow regime in the Menai Strait has previously been studied using observational techniques, such as tracking drifters (Harvey, 1968) and deploying current meters (Simpson *et al.*, 1971), but also using numerical modelling (Davies & Robins, 2017). Because of the tidal processes

described above, the Strait is subject to strong tidal currents (e.g. up to 2.5 m/s during spring tides in the Swellies and at the southwest entrance) (Harvey, 1968). All reported studies have shown that there is a net transport of water to the southwest of approximately 30 million tonnes per tidal cycle, which generates a flushing time of approximately 2-3 days (Campbell *et al.*, 1998). Due to the strong tidal currents, the Menai Strait is well mixed. Indeed, Harvey (1972) noticed a difference of 0.1ºC between the near surface and the near bottom, nevertheless he observed a semi-diurnal and diurnal variation of the temperature in the Menai Strait. Observational sea surface temperature (SST) data has been attained from a temperature logger (Cefas Data Storage Tag G6, temperature sensing) attached to Bangor Pier (53.23109 N, -4.1373 E; maintained by Bangor University) from 2011 to 2017 and showed that water temperature varied from 19ºC in summer to 4ºC in winter (Figure 1.27).

Model simulations of the depth-averaged flow through the Menai Strait has been performed (see Chapter 2 for further details). These simulations covered the period of March 2018 and have been validated against extensive data in the channel with a model error of approximately 1.1% (see Chapter 2 for further details). These results are summarised as follows (Figure 1.28 and Table 1.3):

- Maximum velocities were simulated through the Swellies and Fort Belan, with values of 2.73 m/s and 2.68 m/s directed southwest, respectively. In comparison, maximum velocities at Bangor mussel bed were 0.87 m/s.
- The greatest tidal asymmetry (i.e. when the ebb flows were greater than the flood flows) occurred in the Swellies. The tide was symmetrical at each entrance.
- During peak flows at Fort Belan, it was slack water near the mussel bed (Bangor), and vice-versa.

In the absence of wind, Davies & Robins (2017) simulated the tidally averaged residual flow (south-westwards) to be approximately 686 m^3/s during springs and 334 m^3/s during neaps. The simulated annual mean (residual) flow was 525 m^3/s towards the southwest. However, Simpson *et al.* (1971) reported that a strong south-westerly wind may reverse the direction of the residual flow, especially during neap tides.

The variability and complexity of the seabed of the Menai strait also influence the flow strength spatially and temporally which has a direct impact on sediment dispersal (Davies & Robins, 2009). Freshwater input to the Menai Strait is via several small rivers: the Ogwen (northeast) and the Seiont (southwest) being the most important. Further, freshwater input is strongly dependant on local rainfall and the annual snow melt of the surrounding mountain range (Simpson & Nunes, 1981; Robins *et al.*, 2018). However, the discharge associated is small compared with the tidal prism and/or the residual flow of seawater through the Strait (Buchan

et al., 1973). Freshwater input brings nutrients into the Strait, which help productivity of living communities such as filters feeders like mussels (Edwards, 1987; Simpson & Berx, 2007). The salinity remains fairly constant 32-34‰ in the Menai Strait but can falls below 30‰ frequently (Edwards, 1987). The salinity showed a small increase over the summer, with lowest readings during in autumn and winter (Kratzer *et al.*, 2000). However, the water column is generally well mixed and vertically homogeneous in temperature and salinity due to a high level of turbulence and Reynold stress created by a large tidal velocity (Buchan *et al.*, 1973; Rippeth *et al.*, 2001; Tweddle *et al.*, 2005).

Because of the complex interactions of tidal flows, fresh water and nutrients inputs, bahtymetry, substrate and benthic ecology, the Menai Strait is a challenge to understand the processes which influence larval dispersal. Although this challenge and key research gap is addressed in this study through state-of-the-art modelling.

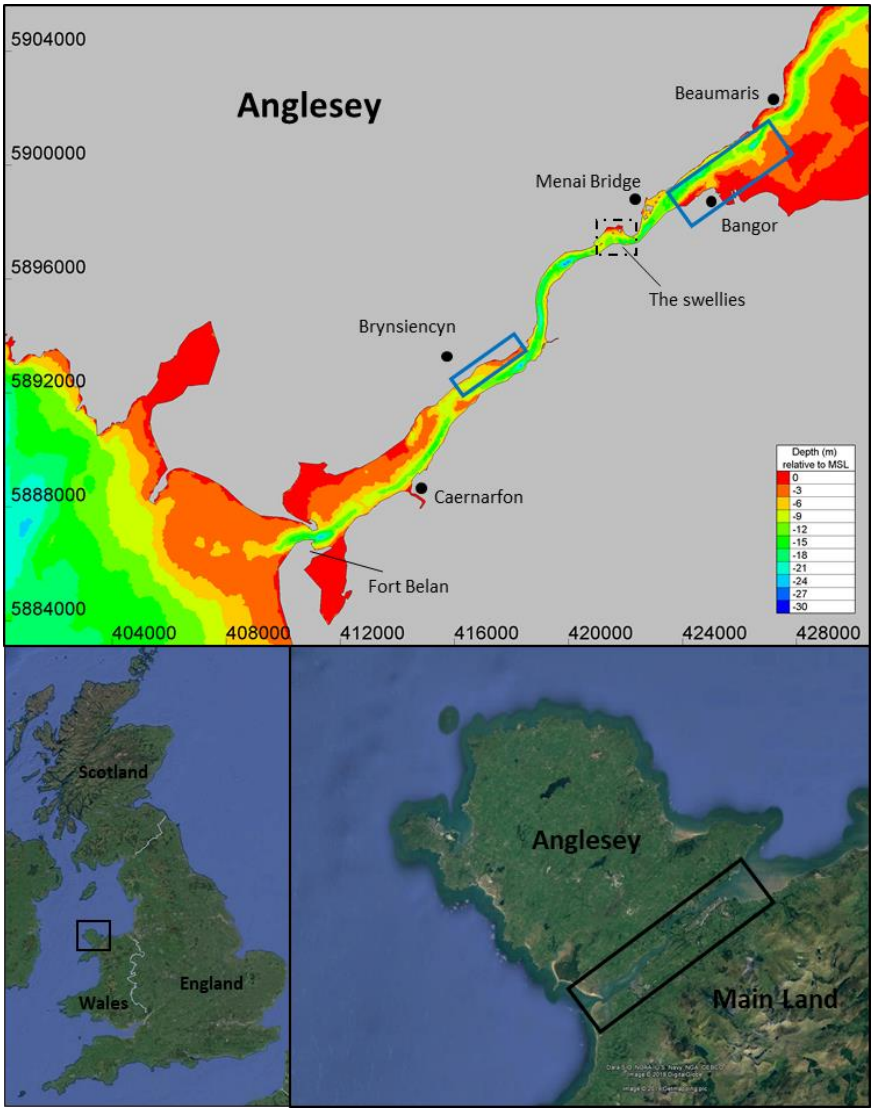

Figure 1.22: Map of the Menai Strait (top), North Wales (bottom panels). Bathymetry contours and key towns/areas are shown. The location of the commercial mussel bed are marked in blue.

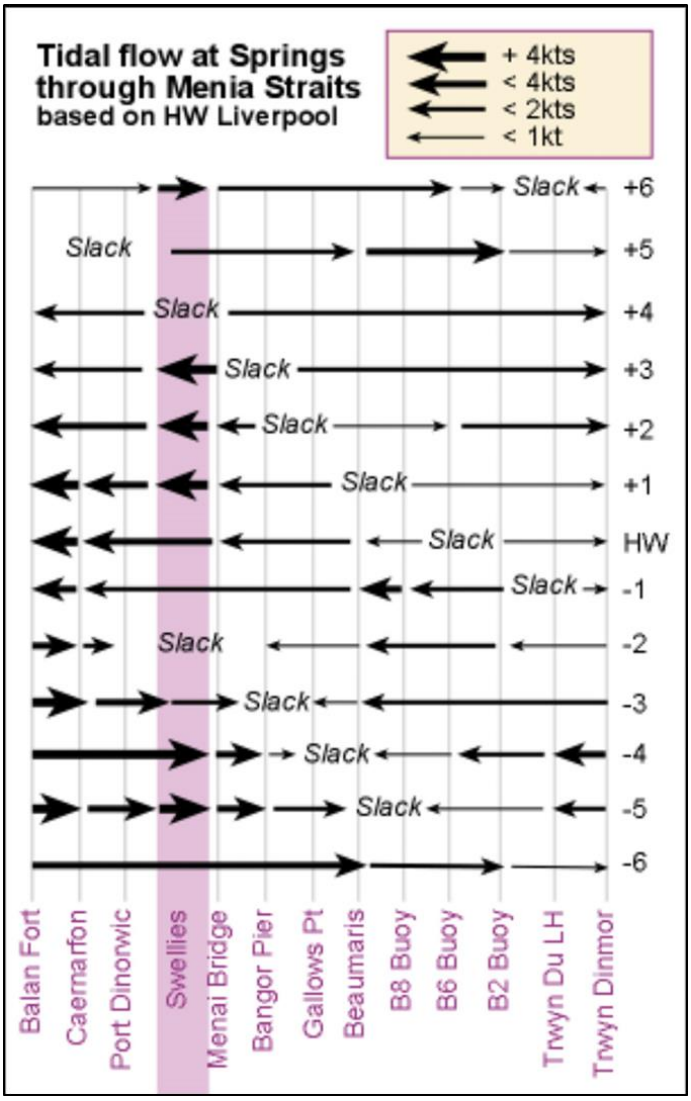

Figure 1.23: Tidal flow along the Menai Strait.

Table 1.3: Model simulated depth-averaged tidal flows, during peak spring/neap flood/ebb tide, and the difference (i.e. tidal asymmetry) at fort Belan, the Swellies and Beaumaris.

	Peak velocity (m/s)					
	Spring tide		Difference	Neap tide		Difference
	Ebb	Flood	Ebb-Flood	Ebb	Flood	Ebb-Flood
For Belan	2.45	2.68	**-0.23**	1.00	0.93	**0.07**
The Swellies	2.73	1.39	**1.34**	1.26	0.89	**0.37**
Beaumaris	0.97	0.63	**0.34**	0.45	0.28	**0.17**

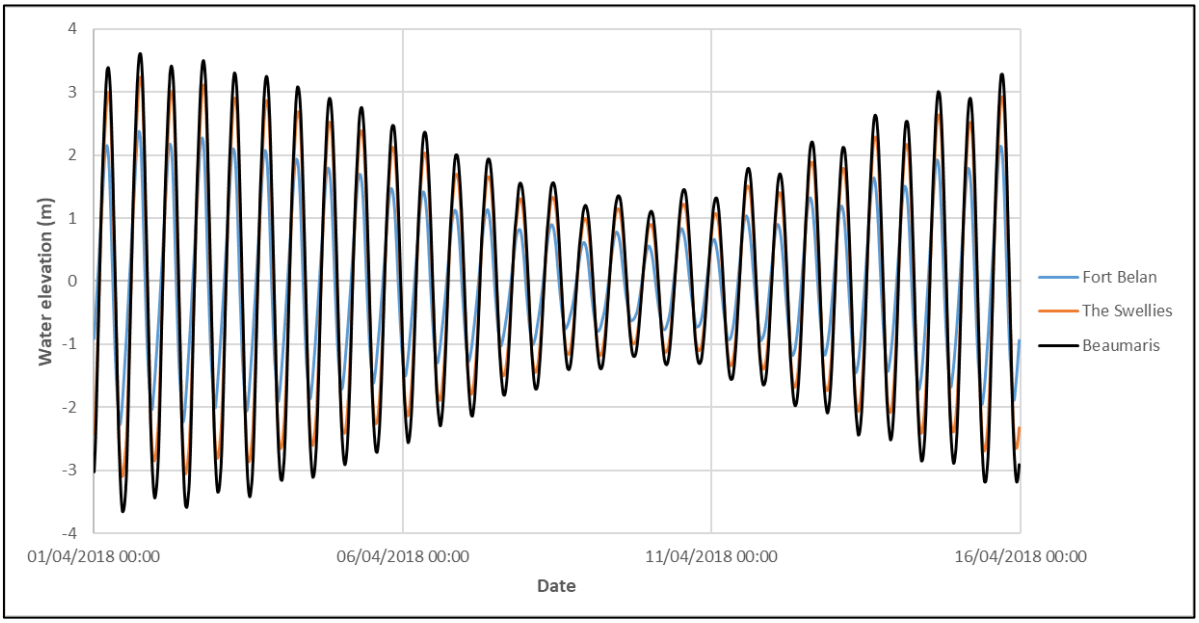

Figure 1.24: Time series of model simulation (see chapter 2 for further details) of tidal range in the Menai Strait over a spring-to-neap cycle, at three locations along the channel: Fort Belan, the Swellies and Beaumaris.

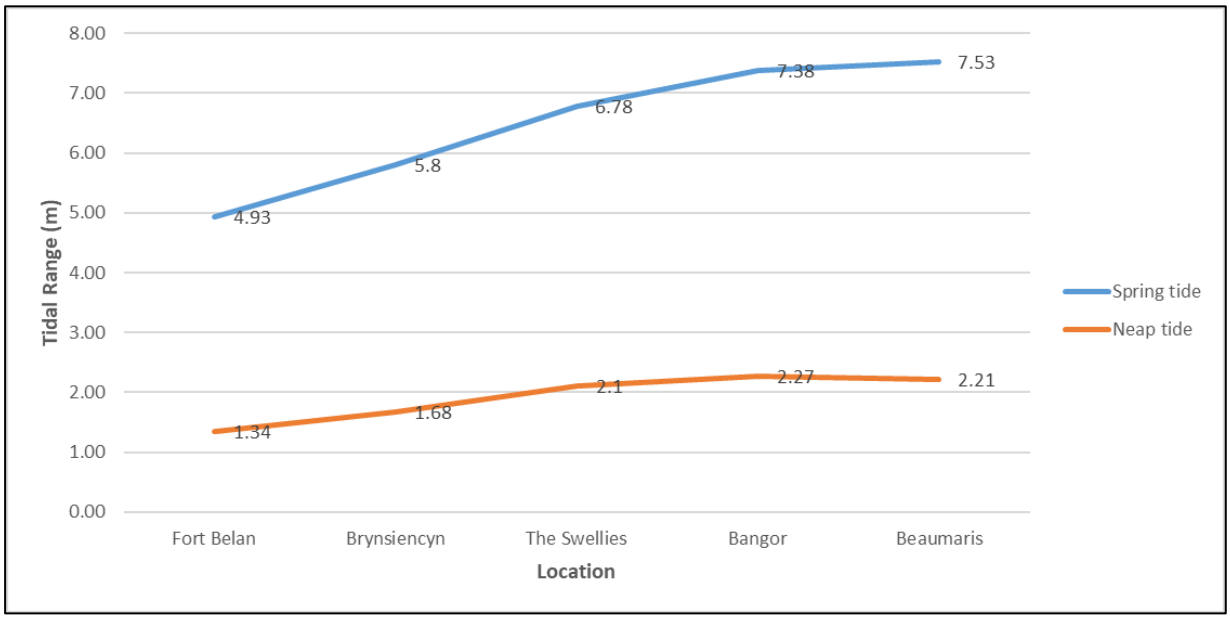

Figure 1.25: Graph showing simulated (see chapter 2 for further details) spring/neap tidal ranges in the Menai Strait at five locations along the channel: Fort Belan, Brynsiencyn (mussel bed location), the Swellies, Bangor (mussel bed location) and Beaumaris.

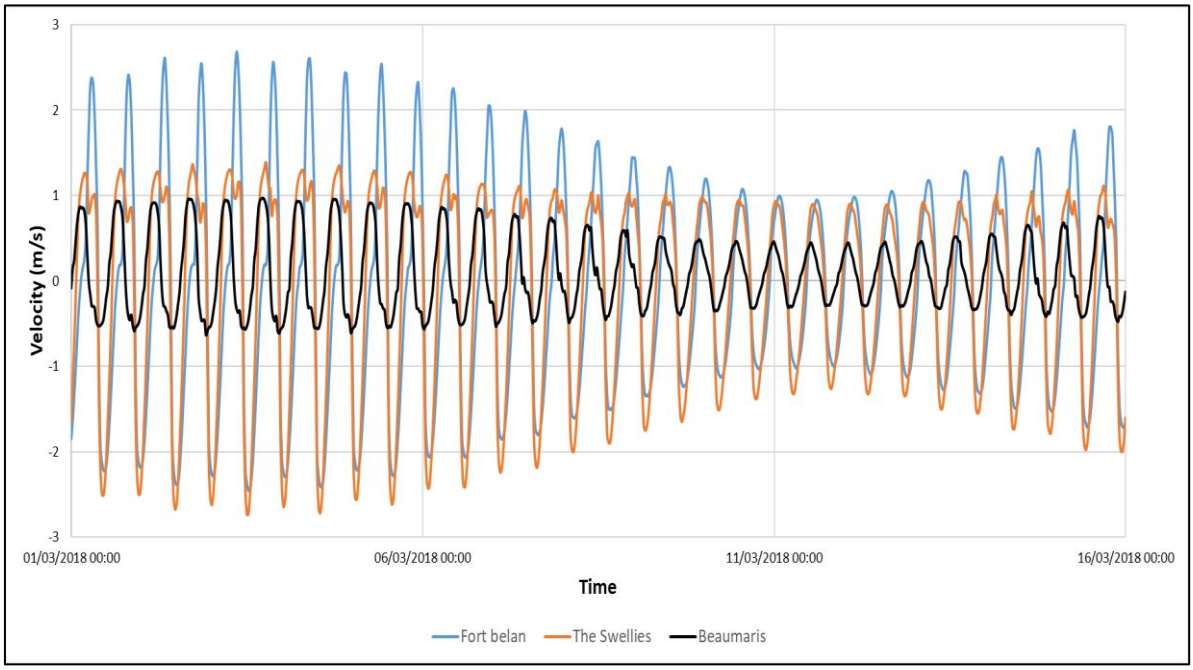

Figure 1.26: Time series of model simulated (see chapter 2 for further details) depth-averaged tidal flows, during a typical spring-neap tidal cycle at Fort Belan, the Swellies and Beaumaris.

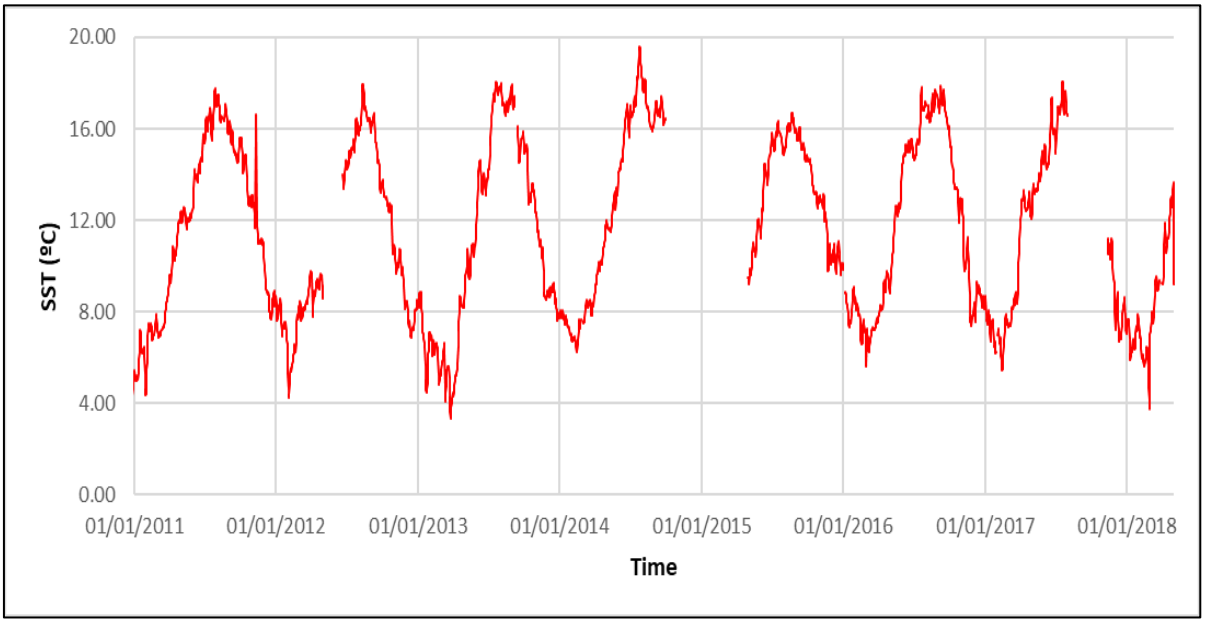

Figure 1.27: Time series of Menai Strait sea surface temperature (SST) from January 2011 to November 2018 from temperature logger data located at Bangor Pier.

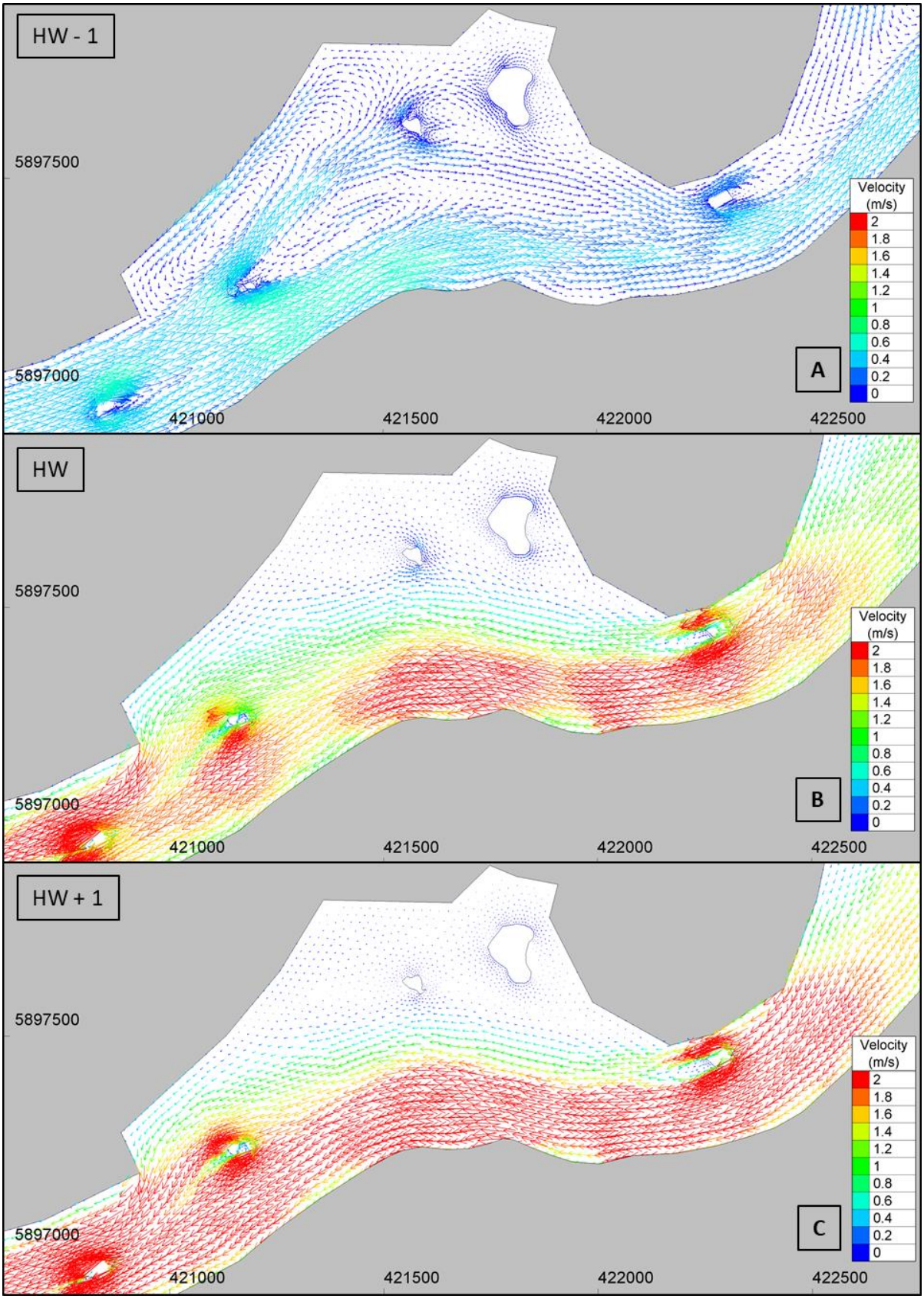

Figure 1.28: Map showing model simulated (see chapter 2 for further details) depth-averaged tidal flows in the Swellies (mid-channel) region of the Menai Strait: (a) High water (HW) - one hour; (b) HW (i.e. peak flood tide); and (c) HW + one hour.

1.4 Mussel exploitation

Mussels have been collected worldwide for food and for bait (for other fisheries) since prehistoric times (Siegfried *et al.*, 1994). Nowadays, *Mytilus edulis L.* is principally produced and/or cultured in America (Chile, U.S.A and Canada) and Europe (UK, Ireland, Spain, France, Netherlands, Norway, Sweden, Denmark and Germany). European production represents 50% of the annual world-wide harvest of mussel (Smaal, 2002; Figure 1.31). Several culture methods are used around the world based on the prevailing hydrographical, social and economic conditions (Aypa, 1990):

- *The bottom culture:* The on-bottom method is based on the collection of mussel spat also called seed mussel from an area where mussels settle to transplanted them in an area where they can have a better growth and fattening (Aldon, 1998). This technique requires an adequate tidal flow to prevent silt deposition, removal of excreta and to provide sufficient oxygen for the cultured animals (mostly in Netherlands and Wales). The mussel seeds are collecting by dredging and transported by boat to the area of culture.
- *The intertidal and shallow water culture:* This method includes: 1) the stake culture, which consists to grow mussels on bamboo poles staked at half meter depth (mostly in Thailand and Philippines); 2) the rack culture (mostly in India and Italy) which is an off-bottom technique consisting of artificial collectors (ropes) on pole or horizontal structures near natural spawning ground; and 3) "bouchot" culture also called intertidal pole culture is based on the collection of seeds on ropes which are, after mussel settlement, wound around large vertical poles (bouchots) (mostly in France) (Aldon, 1998; Asokan & Mohamed, 2009).
- *The deep water culture:* This method contains: 1) the raft culture (mostly in Spain) which consists to use rope collectors suspended from a raft anchored to the seabed; and 2) the long-line culture consist of stretching a rope horizontally near the surface and hang to it vertical ropes (known as droppers) where mussel will settle and grow. This is an alternative of raft culture in areas less protected from wave action (mostly in New Zealand) (Aldon, 1998; Asokan & Mohamed, 2009).

Figure 1.29: Map showing the main mussel culture areas along the Atlantic coast of Europe (Smaal, 2002).

1.4.1 Shellfisheries industry in wales

Since 1993, UK mussel production has risen from 5,000 tonnes to 26,000 tonnes in 2012 (Figure 1.30). The molluscan shellfish aquaculture in the UK is dominated by mussels which represent 95% of tonnage and 82% of imputed value with Wales producing the highest tonnage with 33% of the total in 2012 (Table 1.4) (Ellis, 2015). Of the 248 shellfish farming industries in 2012 in the UK, 4% were in Wales, with 5% of the 705 UK employees (Table 1.5).

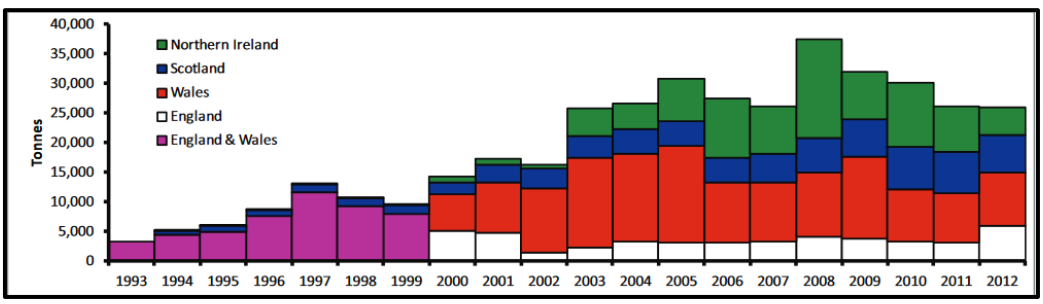

Figure 1.30: Time series of UK mussel production (tonnage), split by nation where reported.

Table 1.4: 2012 Bivalve shellfish production in the UK, broken down by species (and technique) and country. Also included are estimated farm gate price and imputed value of production.

	Species	Method	Harvest	Estimated price per tonne	Imputed value
			tonnes	£/tonne	£
ENGLAND	Mussels	On/off bottom	5,965.7	1000	5,965,700
	Pacific (cupped) oyster	On bottom	850.0	4000	3,400,000
	European (flat) oyster	On bottom	85.9	7600	653,106
	Northern quahog (=Hard clam)	On bottom	8.6	3100	26,576
	Japanese carpet shell (=Manila clam)	On bottom	5.0	3100	15,500
	NATIONAL TOTAL		6,915.2	-	10,060,882
	% UK TOTAL		25%	-	30%
WALES	Mussels	On/off bottom	8,996.0	1000	8,996,000
	Pacific (cupped) oyster	On bottom	3.0	4000	12,000
	NATIONAL TOTAL		8,999.0	-	9,008,000
	% UK TOTAL		33%	-	27%
SCOTLAND	Mussels	Off bottom	6,277.0	1200	7,532,400
	Pacific (cupped) oyster	Off bottom	216.0	4400	950,400
	European (flat) oyster	Off bottom	25.0	7600	190,000
	Great Atlantic scallop	On bottom	7.0	14300	100,100
	Queen scallop	On bottom	0.4	2500	1,000
	NATIONAL TOTAL		6,525.4	-	8,773,900
	% UK TOTAL		24%	-	26%
NORTHERN IRELAND	Mussels	Off bottom	76.6	1200	91,920
	Mussels	On bottom	4,706.0	1000	4,706,000
	Pacific (cupped) oyster	On bottom	137.3	4000	549,200
	NATIONAL TOTAL		4,919.9	-	5,347,120
	% UK TOTAL		18%	-	16%
UNITED KINGDOM TOTAL	Mussels	On/off bottom	26,021.3	-	27,292,020
	Pacific (cupped) oyster	On/off bottom	1,206.3	-	4,911,600
	European (flat) oyster	On/off bottom	110.9	-	843,106
	Northern quahog (=Hard clam)	On bottom	8.6	-	26,576
	Japanese carpet shell (=Manila clam)	On bottom	5.0	-	15,500
	Great Atlantic scallop	On bottom	7.0	-	100,100
	Queen scallop	On bottom	0.4	-	1,000
	TOTAL		27,359.5	-	33,189,902

Table 1.5: Enterprise and employment information (2012) for the UK shellfish farming industry.

	Number of Enterprises	Active Farm sites	FT employees	PT employees	Male employees	Female employees	Total
England	68	-	166	92	250	8	258
Wales	10	-	31	3	32	2	34
Scotland	153	330	171	187	313	45	358
Northern Ireland	17	-	-	-	-	-	55
UK	248	-	-	-	-	-	705

1.4.2 Bangor mussel companies

Bangor Mussel Producers Limited is an association of four businesses located in North Wales, which employs 20 staff and operates four boats from Bangor and Holyhead to farm mussel beds

along the norhteast coast of Wales: 1) Extramussel Limited; 2) Deepdock Limited; 3) Myti Mussels Limited; and 4) Ogwen Mussel Limited. The commercial mussel beds are located in the northern part of the Menai Strait between Menai Bridge, Bangor and Beaumaris (Table 1.6 and Figure 1.31). The boundary of the 1962 Menai Strait Fishery Order is divided into 6 different areas, which belong to the different companies. The cycle of culture occurs in 3 years:

- *Year 1:* Collection of seed (spat) from surrounding waters, such as 1) Morecambe Bay (major source); 2) Caernarfon Bay (previously a major source but no more seeds for the last ten years); 3) River Dee estuary; and 4) South Wales (Tenby and Port Eynon) and reseeded in the mud flats.
- *Year 2:* The mussels are moved further out to sea where there is an increased food source.
- *Year 3:* The mussels are moved to deep water and are immersed most of the time

After three years, the mussels are ready to be harvested. Currently, all Menai mussels are exported to Holland, Ireland and France. As mussels become sexually mature after one year, it is the interest of Bangor mussel companies to know: 1) when do they spawn?; 2) where do the larvae go?; 3) where do they settle?; 4) Is the population self-seeded or influence by other populations?; 5) What parameters influence the most the larval dispersal?; 6) Does the dispersal vary seasonally and annually?; and 7) in a context of climate change, how will changes impact the larval dispersal? By answering these questions, Bangor mussel companies could reduce their costs and their environmental impact.

Table 1.6: Coordinates of the commercial mussel bed in the Menai Strait.

	Latitude	**Longitude**
A	53 14’01.6’’N	04 08’49.6’’W
B	53 15’45.3’’N	04 05’02’’W
C	53 14’24.3’’N	04 04’48.6’’W
D	53 13’44.3’’N	04 08’47.2’’W

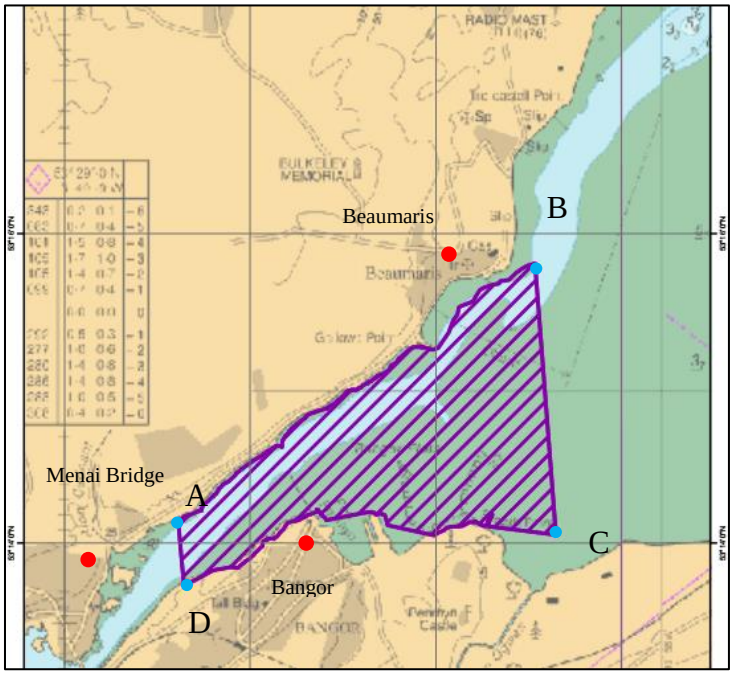

Figure 1.31: Location of commercial mussel beds in the East part of the Menai Strait regarding to the Menai Strait Oyster and Mussel Fishery Order 1962.

1.5 Motivation for the study

The United Kingdom produced 21,619 tonnes of shellfishes in 2016, which represented over 35.5 £m for the shellfisheries industry. One third of this production came from North Wales (7,945 tonnes which has been valued at 15.10 £m), which made shellfisheries aquaculture the third most economically important activity in the area (Hambrey & Evans, 2016). Several commercial bivalve species are numerous off the North Wales coast: mussels, oysters, clams, scallops, cockles and razor shells. Persistent populations of these species occur in estuaries, bays and channels, and on sand bank and rocky shores. The blue mussel (*Mytilus edulis*, Linnaeus 1758) cultivation is the principal component of Wales' aquaculture, and in the industry is growing - annual mussel production rose by approximately 7,500 tonnes for the year 2015 (Roberts *et al.*, 2015).

In addition to their economic interest, blue mussel habitats are a key component of the intertidal environment, affecting sediment deposition and providing a suitable habitat for other organisms such as bacteria, limpets, chitons, polychaetes and flatworms (Suchanek, 1985; Seed & Suchanek, 1992; Herman, 1993; Dame, 1996; Van der Schatte *et al.*, 2018). *M. edulis* is a bivalve filter feeder (e.g. filtering water and particulates) which release sperm and eggs in the water column where fertilization occurs, and larvae develop as plankton until settlement (Gosling, 2015). They are sessile as adults within geographically distinct populations that can

be connected through larval dispersal stage. However, knowledge gaps exist in the connectivity of the North Wales mussel populations, due to a lack of information on: 1) the timing of spawning events; 2) the larval dispersal pathways; and 3) the final settlement locations. It is therefore of scientific interest to understand which parameters influence the release of gametes and larval transport. Many sources in the literature describe the physical and biological parameters, which influence larval dispersal (Chapter 1, section 1.1.3.1., Table 1.2). However, the relative importance of those parameters on spawning, connectivity/self-recruitment and settlement varies greatly overtime and location and remain unresolved in North Wales.

The biggest commercial mussel bed in North Wales is located in the Menai Strait (managed by Extramussel Limited) and it is believed that a significant proportion of their seeded mussels go on to spawn naturally and disperse away from the mussel beds to settle at secondary grounds (e.g. along the Welsh, English and Irish coasts). This is because the bivalve larvae can experience strong ocean currents (e.g. > 2 m/s in the Menai Strait and around Anglesey) which will greatly influence larval dispersal (Chapter 1, section 1.3.1.). However, larval dispersal in North Wales is poorly understood, particularly the Menai Strait, which has so far been neglected in larval dispersal studies (Chapter 1, section 1.3.2.).

The mussel industry relies on wild seed mussel, which can be found in different bays along the British coast (e.g. Morecambe Bay and River Dee estuary). Further, mussel farmers have noticed that mussel seed varies spatially, temporally and quantifiably from a year to another. For example, in the last ten years, in Morecambe Bay (e.g. main spat recruitment area), seed mussel fished varied from 1,200 tonnes in to 2014 to nothing in 2018 and 2015. It is the interest of Bangor mussel company to understand the phenomena which influences the variation of mussel larvae recruitment, in order to be able to manage their stock efficiently.

The present study addresses *Mytilus edulis* larval dispersal in North Wales, providing information on: 1) the period of gametes released according to environmental factors; and 2) the influence of tidal currents, wind-driven currents and mussel behaviour on larval dispersal and connectivity among selected sites across the region.

Chapter 2: Hydrodynamic modelling

Hydrodynamic modelling is a well-established scientific tool that can be used to study larval dispersal (Largier, 2003; Coscia *et al.*, 2012; Sebille *et al.*, 2018;), and this approach has been applied in this study of *Mytilus edulis* dispersal in North Wales. Alternative methods to establish larval dispersal are beyond the scope of this study (e.g. genetics, genomics, microchemistry, invasion rate, larval biology laboratory experiments and plankton distribution) as explained in Chapter 1. The hydrodynamic models created in this study are described in this chapter. These models enable us to understand the theoretical impact of oceanographic parameters (e.g. tide-driven currents, wind-driven currents and coastal currents) on larval dispersal. The TELEMAC hydrodynamic modelling system has been used, which has the following practical advantages: 1) it is open source, allowing the source code to be modified by the user; 2) it has been used extensively for coastal applications (Hervouet, 2000; Villaret *et al.*, 2013; Langendoen *et al.*, 2016); 3) it can be coupled to open source tools for pre- and post-processing of data; and 4) it has informative modelling assistance via an active user forum base (from TELEMAC website). Firstly, accurate hydrodynamic simulations are produced and, secondly, the simulated velocity fields are used (coupled) with a separate particle tracking model (PTM) that simulates the dispersion of larvae from source to sink (described in Chapter 3). Several steps are necessary before the hydrodynamic model can be coupled with the particle tracking model: 1) bathymetric grid generation; 2) model parameterisation and formation of boundary forcing; 3) sensitivity tests on spatial and temporal parameters for model optimisation; and 4) model validation against observational oceanographic data. The TELEMAC development and validation are described in this chapter, following by a description of the PTM in Chapter 3.

2.1 Model grid generation

Two separate model grids were developed using the Blue Kenue^{TM} software (https://nrc.canada.ca/fr/recherche-developpement/produits-services/logiciels-applications/blue-kenuetm-logiciel-modelisateurs-hydrauliques). Grid 1 covers the Irish Sea (165,000 km^2) and Grid 2 covers the region around Anglesey and the Menai Strait (10,000 km^2). In particular, the Anglesey model is approximately 1/16th of the size of Grid 1 but allowed the resolution of the mesh around Anglesey Island and in the Menai Strait to be increased. Both grids adopted an unstructured configuration, meaning that computational nodes within the model domain are connected in a triangular formation with graded spatial resolution (Figures 2.2 and 2.5). As the study focuses on coastal benthic animals, an unstructured grid method is the most appropriate to resolve the complex geometry of coastal areas such as the Menai Strait, whilst adopting, coarser spatial resolution offshore where fine-spatial-scale

velocity fluctuations are less. The resolution growth rate of the mesh was < 8 % in order to allow the grid size to vary smoothly, further it was used by McCann *et al.* (2011) successively for simulation on a similar coastal domain (Bourban *et al.*, 2014). The criterion prevents sudden increases/decreases in mesh density, which renders the model computations more stable. The grids were then mapped onto bathymetric data to create a bathymetric grid that is used by the TELEMAC model to compute the hydrodynamics. Further, comparisons between the two models provide information of the effect of spatial resolution on the model validation accuracy and, hence, on the accuracy of the particle tracking model.

2.1.1 Grid 1: Irish Sea model

The Irish Sea grid (Grid 1) covers an area of approximately 165,500 km^2 and contains 206,413 nodes (Figure 2.1). The domain covers the whole Irish sea as previous studies show that larvae can potentially travel up to 300 km (Van Der Molen *et al.*, 2007). The coast boundaries of the model have been generated using Google earth Pro to ensure a good representation of the coastline, e.g. < 50 m resolution (other coastline products have a relative coarse spatial resolution such as ¼ degree for m_map in Matlab). In some outer regions of the model (e.g. Solway Firth near Carlisle), the coastline was more coarsely resolved, but ensuring coastal nodes were above the high-water line. The Irish Sea grid comprised two sub-grids: 1) the Menai Strait; and 2) the rest of the Irish Sea.

The domain extends from Colonsay Island in the north (56º 10’ 42.906’’ N) to Cornwall in the south (50º 54’ 20.276’’ N). The west boundary is 7º 23’ 27.7872’’ W and the east boundary is 2º 24’ 31.2012’’ W. The spatial resolution of the mesh varied from 30 m to 5,000 m (Figures 2.2 and 2.3). The coarser resolution (5,000 m) is located at the extreme north and south of the domain. The resolution increases gradually (< 8%) to the centre of the Irish Sea (1,000 m) and around Anglesey Island (500 m) (Figure 2.2). Figure 2.3 shows that the finest resolution (30 m) is defined in the Menai Strait as it is the area where the mussel beds are present and because of the coastal complexity of the channel. The 30 m mesh resolution within the Menai Strait resolves tidal flux through the channel but not the fine scale hydrodynamics around the islands and the bridge piers in the central channel (Figure 2.5). For this, therefore, a fine scale mesh, Grid 2, was created and is described in the next section. Grid 1 was created for the PTM simulations outside the Menai Strait to determine the wider larval dispersion through a long period (e.g. 45 days) and study the connectivity among mussel beds of interest (e.g. commercial mussel bed/ natural mussel beds/mussel beds established on humans infrastructures) within the Irish Sea.

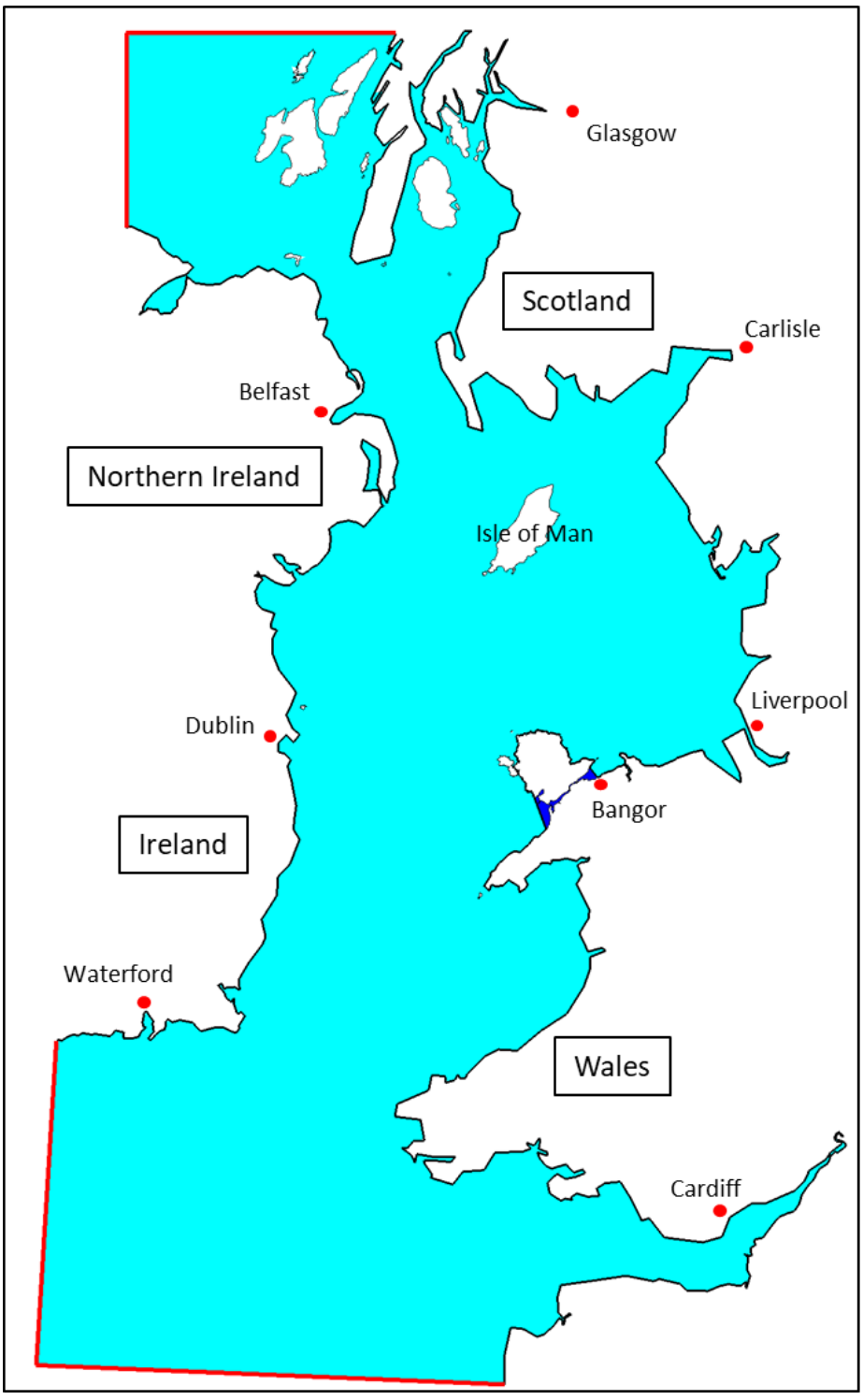

Figure 2.1: Irish Sea mesh (Grid 1). The boundary of the domain is composed of offshore tidal waters (red) and coastline (dark).

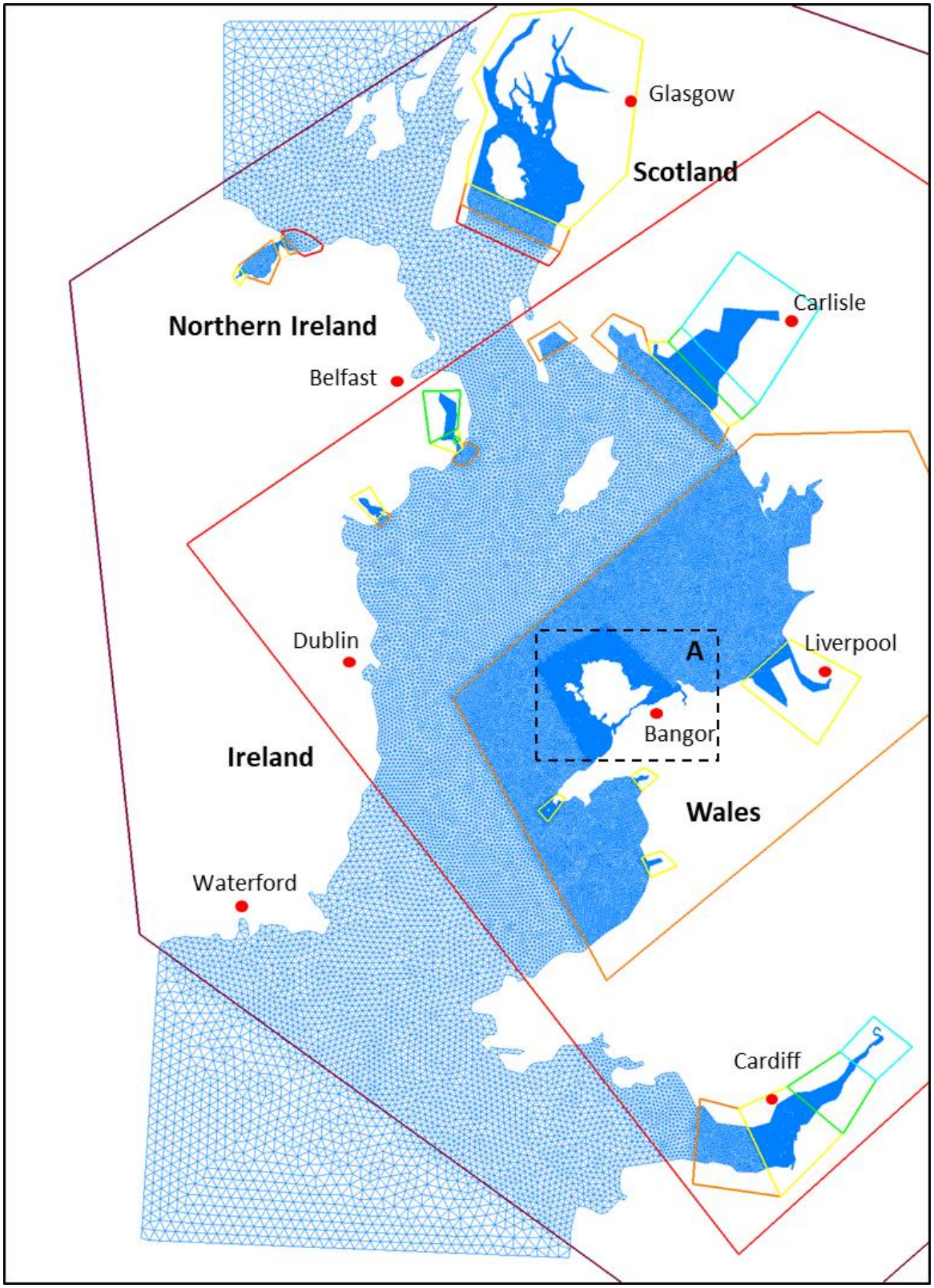

Figure 2.2: Grid 1 mesh resolution variation (purple line: 3,000 m, red line: 2,000 m, orange: 1,000 m, yellow: 500 m, green: 200 m and light blue: 100 m). The dashed black box region is detailed in Figure 2.3.

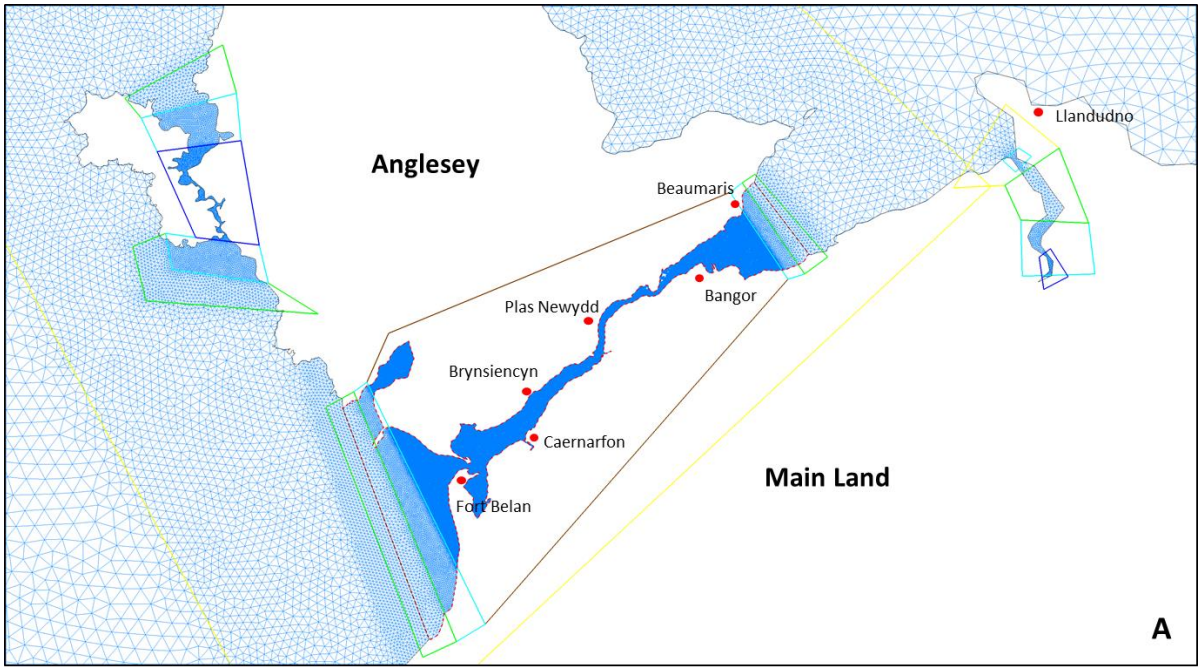

Figure 2.3: Grid 1: Details of the mesh density variation around Anglesey (yellow line: 500 m, green: 200 m, light blue: 100 m, dark blue: 50 m, brown: 30m). The Menai strait sub mesh used to create Grid 1 is represented by the red dashed line.

2.1.2 Grid 2: Anglesey model

The TELEMAC model of the Irish Sea (Grid 1) is computationally expensive because of the size of the domain and the grid resolution (206,413 nodes). Therefore, to increase the mesh resolution in the Menai Strait, a second grid was created that covers a smaller area surrounding Anglesey. Figure 2.4 represents a model approximately 1/16th of the size of the Irish Sea model (10,000 km^2) but containing, similar number of nodes (187,295). In this case, the same computational time was expected with a better accuracy of the model. The density varies from 1,000 m on the outer boundary in the Irish Sea to 100 m along the coast of Anglesey (Figure 2.4). Within the Menai Strait, the mesh density varies from 50 m near the ends of the channel to 20 m in the channel interior (Figure 2.4).

Grid 2 will be used: 1) for PTM simulations for larvae spawned within the Menai Strait during their initial pelagic larval phase (maximum one week as the particles readily reach the model boundary thereafter); and 2) study the larval dispersal within the Menai Strait under different tidal conditions.

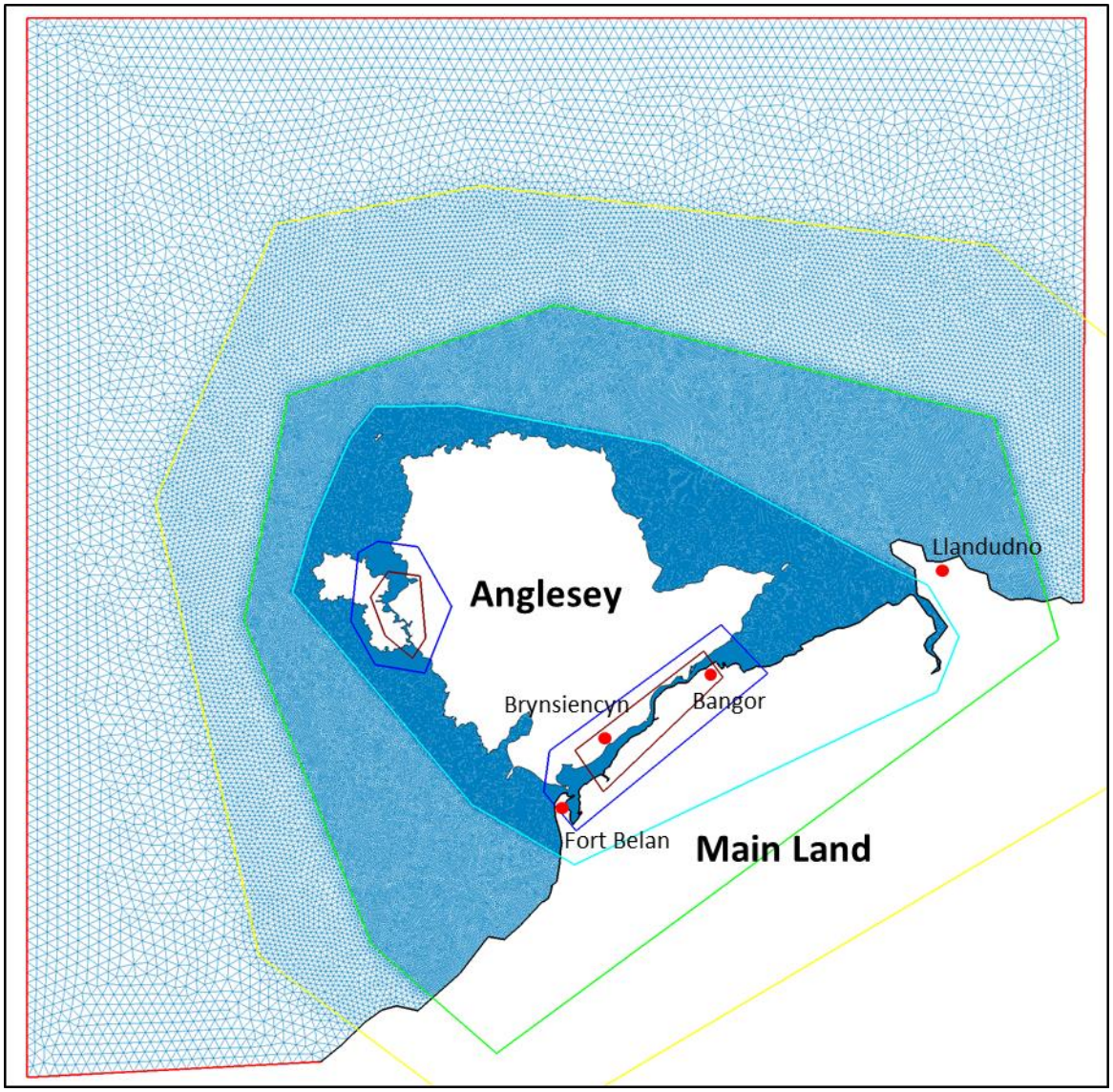

Figure 2.4: Grid 2: Menai Strait grid highlighting the increased mesh resolution (yellow line: 500 m, green line: 200m, light blue line: 100 m, dark blue line: 50 m and brown: 20 m). The limit of the domain is composed by offshore waters in red and coastline in black.

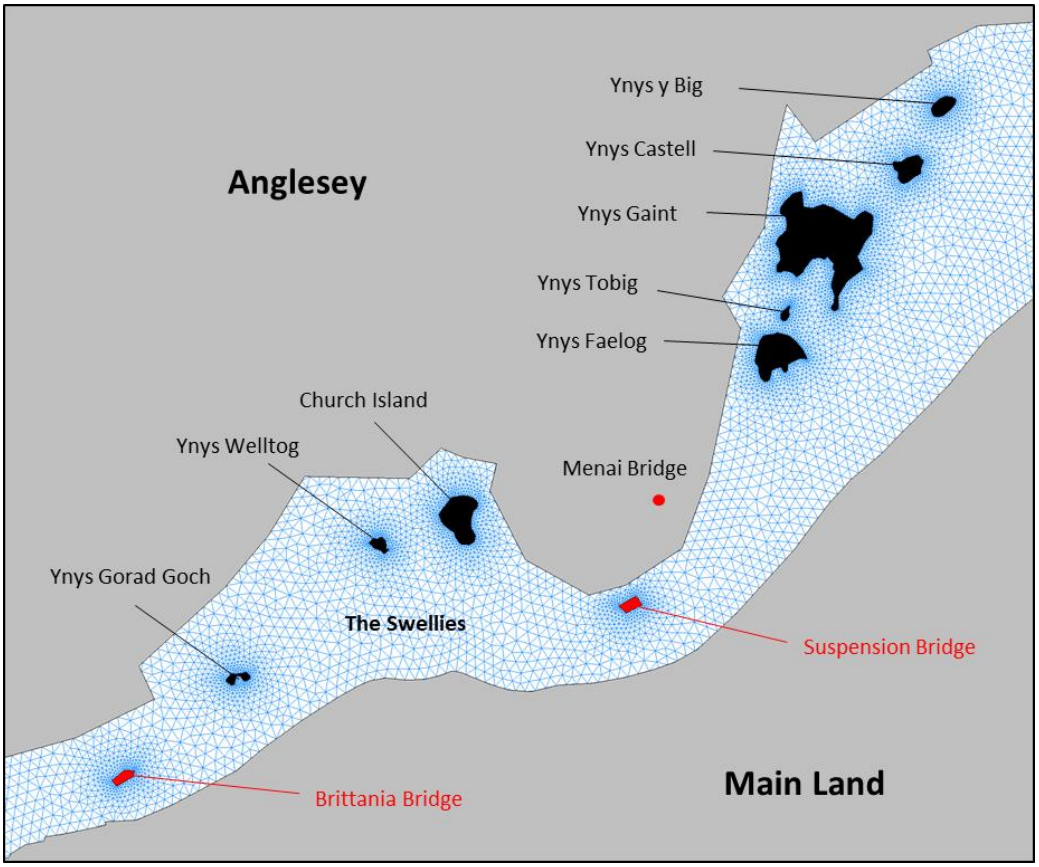

Figure 2.5: Grid 2: Details of the Swellies area and Islands in the Menai Strait. In black natural islands and in red main bridge piers considered as 'Islands' by the model.

2.1.3 Bathymetry

Grids 1 and 2 were mapped onto bathymetric data from Digimap referenced to Chart datum (CD) i.e. Lowest Astronomical Tide, LAT. This data has a spatial resolution of 1 arc second (i.e. approximately 30 m for the Irish Sea). Data comes from a seabed surface model called The Marine Themes Digital Elevation Model (DEM) using recent commercial single and multi-beam survey and LiDAR data available, with chart-derived data providing additional coverage (from Digimap website). Bathymetry data was derived from surveys undertaken by different organisations (military, scientific and/or industrial) and have been quality controlled (OceanWise ltd, 2018). Also, bathymetric data for the Menai Strait comprised an assemblage of: 1) multi-beam data collected during 2012; 2) LiDAR data collected during 2013; and 3) Admiralty bathymetric data of the offshore regions at both end of the Strait (Davies & Robins, 2017).

In order to simulate the tidal variation within the models, the bathymetry grid was converted from CD to Mean Sea level (MSL) (average level of the sea surface). Figure 2.6 shows that

MSL of the Irish Sea is obtained by adding half of the maximum Tidal Range (TD) to CD. The maximum tidal range corresponds to the vertical height difference between lowest astronomical tide (LAT) and highest astronomical tide (HAT). The tidal range varies spatially throughout the Irish Sea from few cm near Wexford (Ireland) to more than 12 m in the Bristol Channel (UK) (Ward *et al.*, 2012; Robins *et al.*, 2013). TD data was obtained from Robins *et al.* (2013) and mapped onto the Irish Sea grid created with Blue Kenue (See Appendix A). The conversion from CD to MSL has been made using Blue Kenue calculator tool, which allowed determining the new value of bathymetry in MSL at each node of the grids (Figures 2.7 and 2.8).

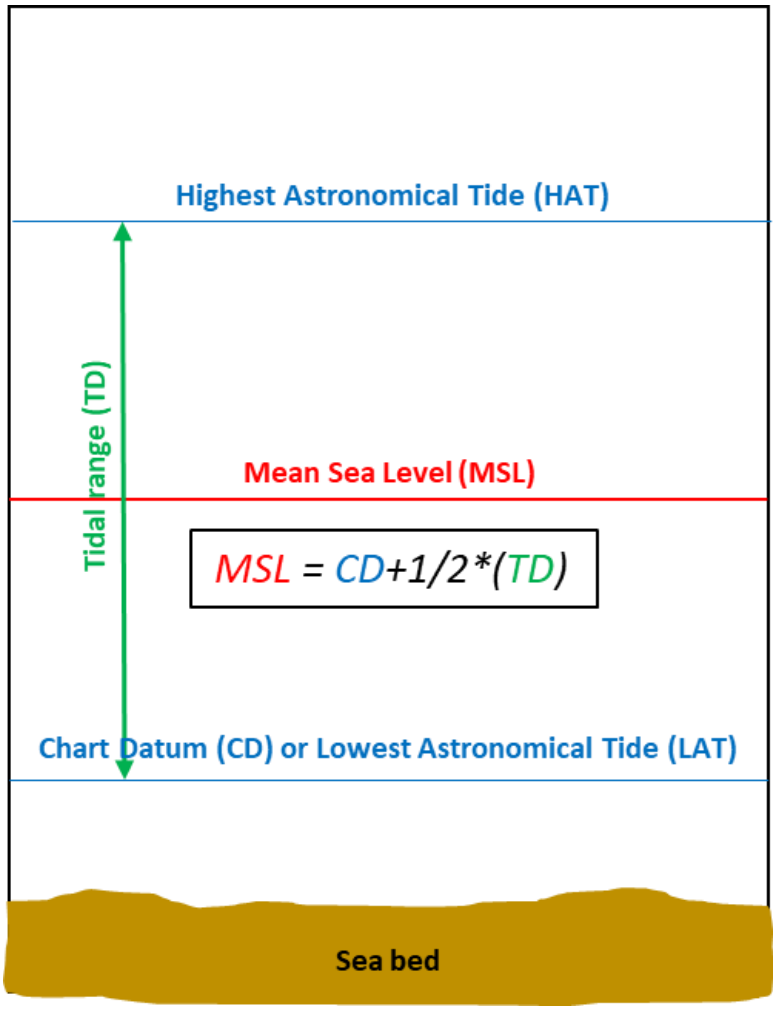

Figure 2.6: Calculation of Mean Sea Level (MSL) using Tidal range (TR) and Chart Datum (CD).

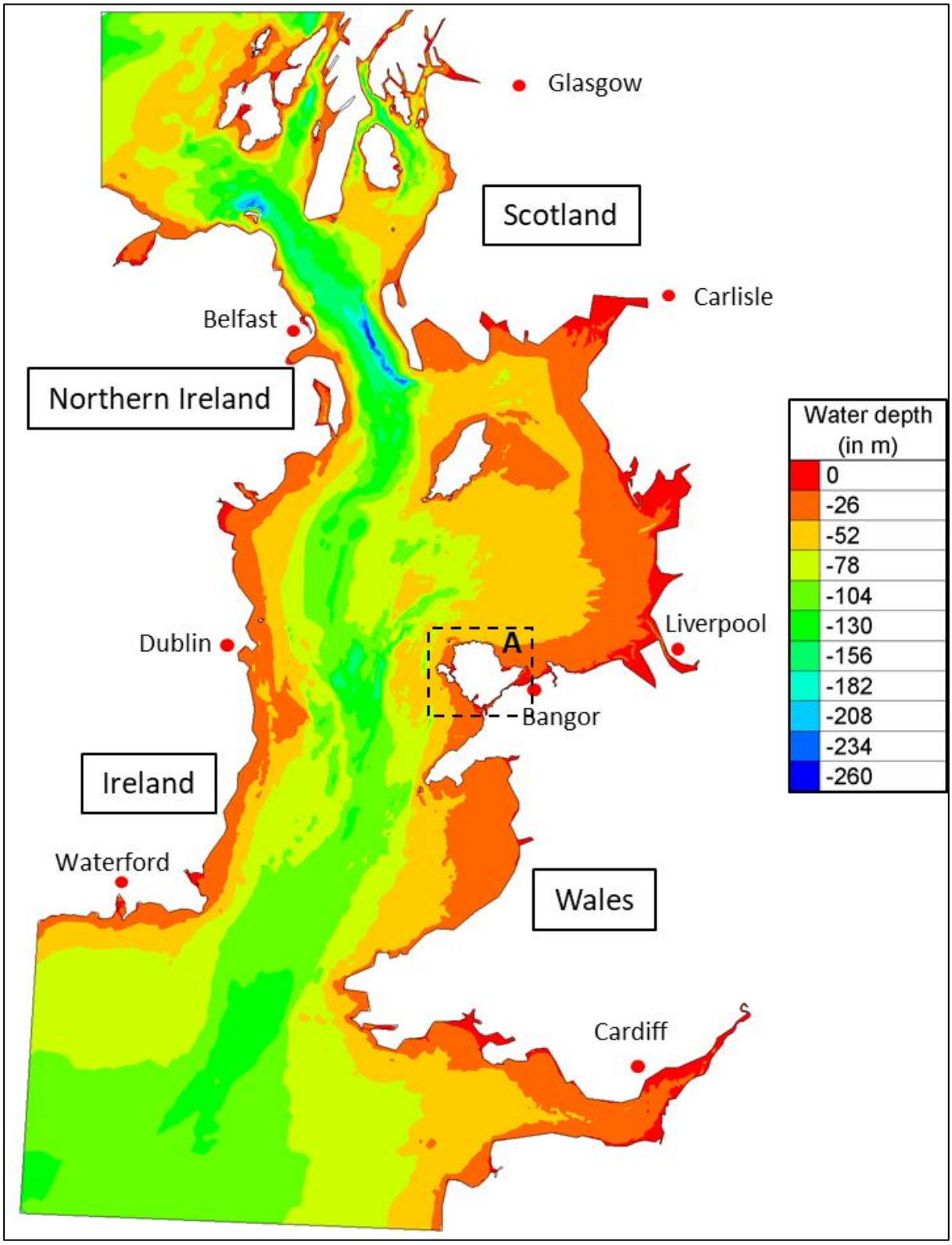

Figure 2.7: Bathymetry of the Irish Sea grid related to MSL.

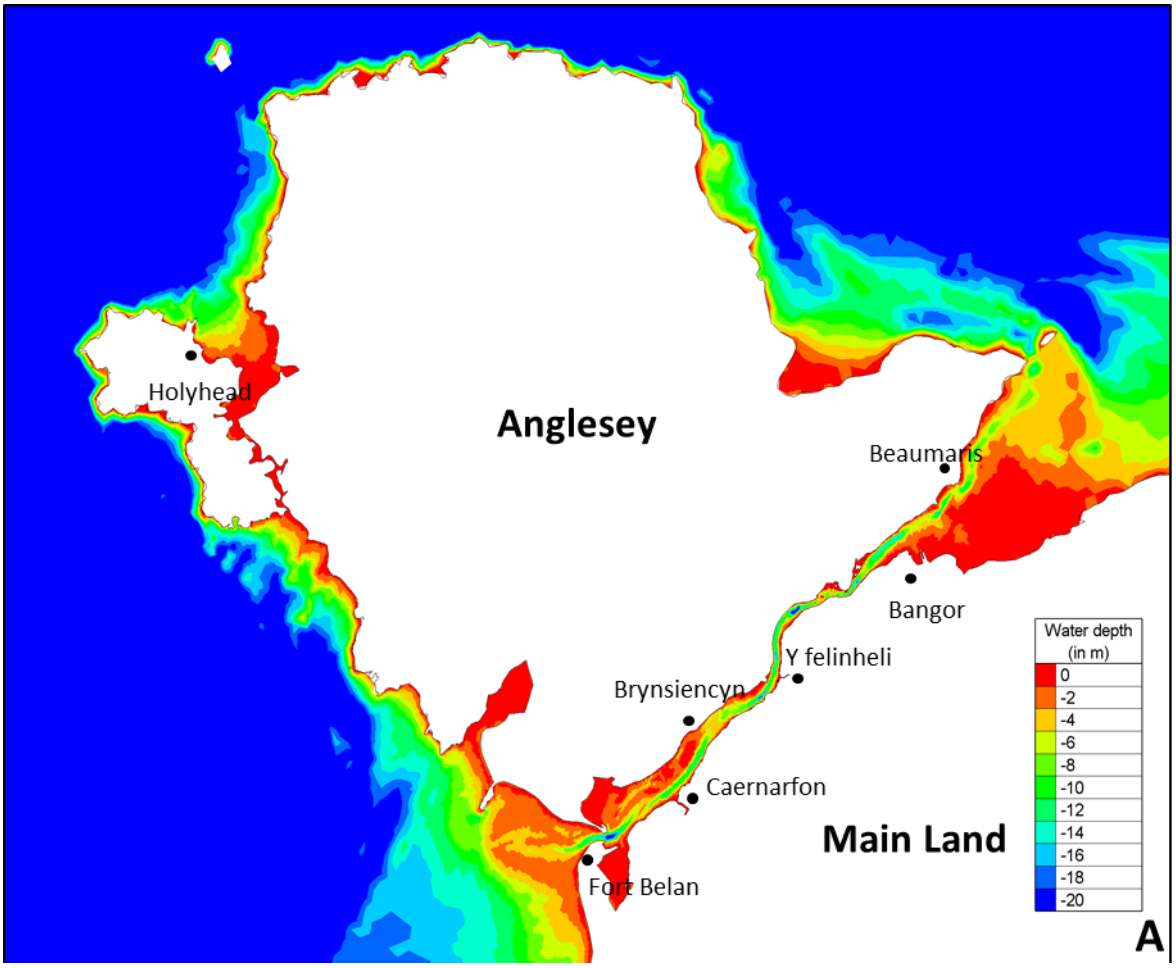

Figure 2.8: Bathymetry around Anglesey and in the Menai Strait related to MSL.

2.2 TELEMAC modelling system

The Telemac Modelling System (Hervouet, 2007) has been used here to simulate the Menai Strait and wider Irish Sea hydrodynamics. Based on finite-element algorithms, Telemac simulates the hydrodynamics, such as tidal and wind driven flows, using an unstructured numerical grid with a graded resolution (e.g. Villaret *et al.*, 2013, Davies & Robins, 2017). This unstructured computational framework is well suited to complex coastal area dynamics (e.g. narrow channels) as it allows a better resolution of the coast (Fernandes *et al.*, 2001). The Telemac system comprises different modules adapted to different fields of research. Hydrodynamic studies are supported by TELEMAC-2D and TELEMAC-3D, which perform simulations in two-dimensions (i.e. depth-avergaed) and three-dimensions (i.e. depth resolving), respectively. In addition, these modules simulate the transport of scalars such as temperature and salinity. The TELEMAC-2D code solves four hydrodynamic equations simultaneously: 1) continuity; 2) momentum along x (longitude); 3) momentum along y (latitude); and 4) conservation of multiple tracers (Equation 2.1). In addition, waves can be

studied using the TOMAWAC module, which simulates sea state in permanent or transitory conditions (Mesencal, s.d.) and sediment transport studied using the SISYPHE-2D/3D modules. Only TELEMAC-2D was used in this study, described below.

The simulations of the Menai Strait and Irish Sea hydrodynamics required parallel processing methods on a supercomputer, i.e. distributing the modelling task over several computer processors in order to speed-up the computational time. This was achieved through the Supercomputing Wales programme, which allowed use of the supercomputer hub based in Cardiff. Once the bathymetric model grids were developed, the computation of TELEMAC involved designing experimental simulations, whereby constraining parameters were assigned via an input text file (a steering file) (Ata *et al.*, 2014). In addition, the user can make modifications to the source code. In the study, the steering file was divided in 7 parts which were adapted for simulating different scenarios (See Appendix B):

- **Inputs files**: 1) GEOMETRY FILE (bathymetric mesh, e.g. Figure 2.7); 2) BOUNDARY CONDITION FILE (description of the type of each boundary of the mesh, e.g. offshore tidal or land); 3) FORTRAN FILE (containing modifications to the TELEMAC code) and associated DATA FILES (containing data on realistic wind forcing, for example); 4) PARALLEL PROCESSORS (which state the number of processors used by the supercomputer hub, in this case multiplications of 40 cores); and 5) PREVIOUS COMPUTATION FILE (which gives the initial state of the computation, e.g. a new simulation or a follow-on from a previous simulation sometimes called a 'hot-start').
- **Outputs**: 1) RESULTS FILE (name and format of the ouput files); 2) VARIABLES FOR GRAPHIC PRINTOUTS (list of variables to be stored in the results file); 3) GRAPHIC PRINTOUT PERIOD (defined temporal period for outputs); 4) TIME STEP (model time step of the computation); 5) NUMBER OF TIMESTEPS (total duration of the computation); and 6) MASS-BALANCE (gives information on the mass fluxes).
- **Initial conditions**: 1) INITIAL CONDITIONS (describes the initial state of the model (e.g. water depth and velocity values at each nodes of the domain) at the start of the simulation); and 2) INITIAL ELEVATION (initial value of the free surface elevation). (N.b. these parameters are not used for hot starts)
- **Tidal forcing**: 1) GEOGRAPHIC SYSTEM (determines the type of coordinates of the mesh, e.g. Cartesian (WGS84) or spherical (latitude/longitude)); 2) UTM ZONE NUMBER IN GEOGRAPHIC SYSTEM (specification of the geographic system area); 3) OPTION FOR TIDAL BOUNDARY CONDITIONS (activates the use of one of the available database); 4) TIDAL DATA BASE (specifies the database used); 5)

ORIGINAL DATE OF TIME and ORIGINAL HOUR OF TIME (time and hour calibration to prescribe a real tide to the model); and 6) PRESCRIBED ELEVATIONS (defines elevation of open boundaries).

- **Physical parameters**: 1) LAW OF BOTTOM FRICTION (defines the friction law used to compute friction on the bed); 2) TURBULENCE MODEL (specifies the viscosity of the domain); 3) CORIOLIS (take into account the inertia effect of the Coriolis force); and 4) WIND (simulation of flow under the influence of a blowing wind on the water surface)
- **Numerical parameters**: 1) TIDAL FLATS (wetting/drying intertidal nodes in the computational field); 2) TYPE OF ADVECTION (scheme used to solve the advection step); 3) SOLVER ACCURACY (defines the accuracy required during solution of the propagation step); 4) DISCRETIZATIONS IN SPACE (specifies the type of discretization); 5) PROPAGATION (take into account the propagation phenomena); 5) IMPLICITATION FOR DEPTH and VELOCITY (set the value of the implication coefficient); and 6) MAXIMUM NUMBER OF ITERATIONS FOR SOLVER (defines the maximum permissible number of iterations when solving the propagation step).

Simulations were performed during the period of mussel spawning events occurring in spring and summer (from 1st March to 31st October). Each simulation covered a two-month period to capture the pelagic larval duration time scale. Simulations were limited to two months to avoid large output file sizes (e.g. > 6 GB). Consequently, the keywords COMPUTATION CONTINUED and PREVIOUS COMPUTATION FILE were used to maintain continuity between successive simulations over the season. The TIME STEP (Δt) used for all simulations was optimised following sensitivity tests (See Section 2.3). Indeed, the stability, accuracy and optimisation of a model can be achieved by satisfying the courant condition (Equation 2.2). A too coarse time step (e.g. > 1 hour) will cause numerical diffusion and model instability, while a too fine (e.g. < 10 seconds) might lead to a long computational time. Simulated variables (e.g. water depth (H) and depth-averaged velocity (U and V) were output for all simulations and stored on the supercomputer. However, the temporal output resolution (GRAPHIC PRINTOUT PERIOD) was determined via a sensitivity test, presented in Section 2.3. The output time step was chosen to maximize the accuracy of the evolving water depth and velocity as well as to minimize the computational time and the size of the output files. All simulations ran using the World Geodetic System 1984 (WGS84) spatial format (GEOGRAPHIC SYSTEM = 2). The INITIAL CONDITIONS were defined as 'CONSTANT ELEVATION' with INITIAL ELEVATION = 0 (i.e. zero MSL). The TIDAL DATA BASE used for the boundary conditions

was TPXO, which provides amplitudes of earth-relative sea-surface elevation for 13 tidal harmonic constituents with a resolution of 1/30º (Egbert & Erofeeva, 2002). TPXO refers to the TOPEX/POSEIDON satellite mission to map the ocean surface topography using both direct observational data and dynamical information (Egbert *et al.*, 1994). This method allows to predict astronomical tide and to be applied at the boundaries for simulation in the past and in the future. The tidal prediction (setting ORIGINAL DATE OF TIME and ORIGINAL HOUR OF TIME) were defined depending on the time period of interest. This information allows TELEMAC to perform tidal prediction and calculate the time-varying free surface elevation and horizontal velocities at each boundary node. The changes are then propagated spatially and temporally into the model domain. As the Menai Strait is an energetic tidal channel with a turbulent flow regime, the Nikuradse formula was used in the key word LAW OF BOTTOM FRICTION for both models of the Menai Strait and the Irish Sea. However, the FRICTION COEFFICIENT impact on model accuracy has been studied in Section 2.3, in order to choose the formula, which is appropriate for the Irish Sea domain.

Equation 2.1: Equations solved by TELEMAC-2D for Cartesian coordinates with 1) h: depth water (m); 2) u and v: velocity components (m/s); 3) T: passive tracer (g/l); 4) g: gravity acceleration (m/s2); 5) vt and vT: momentum and tracer diffusion (m2/s); 6) Z: free surface elevation (m); 7) t: time (s); 8) x and y: horizontal space coordinates (m); 9) S_h: source or sink of fluid (m/s); 10) S_x and S_y: source or sink terms in dynamic equations (m/s^2); and 11) S_T: source or sink of tracer (g/l/s).

$$\frac{\partial h}{\partial t} + u.\nabla(h) + hdiv(u) = S_h \qquad \text{Continuity}$$

$$\frac{\partial u}{\partial t} + u.\nabla(u) = -g\frac{\partial Z}{\partial x} + S_x + \frac{1}{h}div(h\vartheta_t\nabla u) \qquad \text{Momentum along x}$$

$$\frac{\partial v}{\partial t} + u.\nabla(v) = -g\frac{\partial Z}{\partial y} + S_y + \frac{1}{h}div(h\vartheta_t\nabla v) \qquad \text{Momentum along y}$$

$$\frac{\partial T}{\partial t} + u.\nabla(T) = S_T + \frac{1}{h}div(h\vartheta_t\nabla T) \qquad \text{Tracer conservation}$$

Equation 2.2: Courant condition equation with 1) d: dimension of the model; 2) Δx: distance between cross sections; and 3) V: average velocity of the flow.

$$\Delta t \leq \frac{1}{\sqrt{d}}\frac{\Delta x}{c_{\max}} \quad \text{with} \quad c_{\max} = \frac{3}{2}V$$

2.3 Model validation

Ocean models require validation against field observations in order to evaluate their accuracy and level of uncertainty. Field observations are assumed to be realistic but with a small level of uncertainty due to instrument errors (accuracy of the measurement and/or limited sensitivity) (Nystrom *et al.*, 2007). In this study, both models (Grids 1 and 2) were validated via the following methods: Method 1) comparison of simulated velocities and surface elevation against time series observations and Method 2) comparison of simulated and observed tidal constituents using tidal analysis techniques. Sensitivity tests have been performed for both methods using Grid 1 as it allows analysis of a greater number of sites (25) than for Grid 2 (11 sites). Both validation methods have been used to assess the temporal and spatial model accuracy. Throughout the Irish Sea, 18 coastal tide gauges sites and seven offshore sites measuring velocities were used for the validation. Of the 18 tide gauge sites, 13 were used for both validation methods, four sites for Method 2 only and one site only for Method 1 (Figure 2.9).

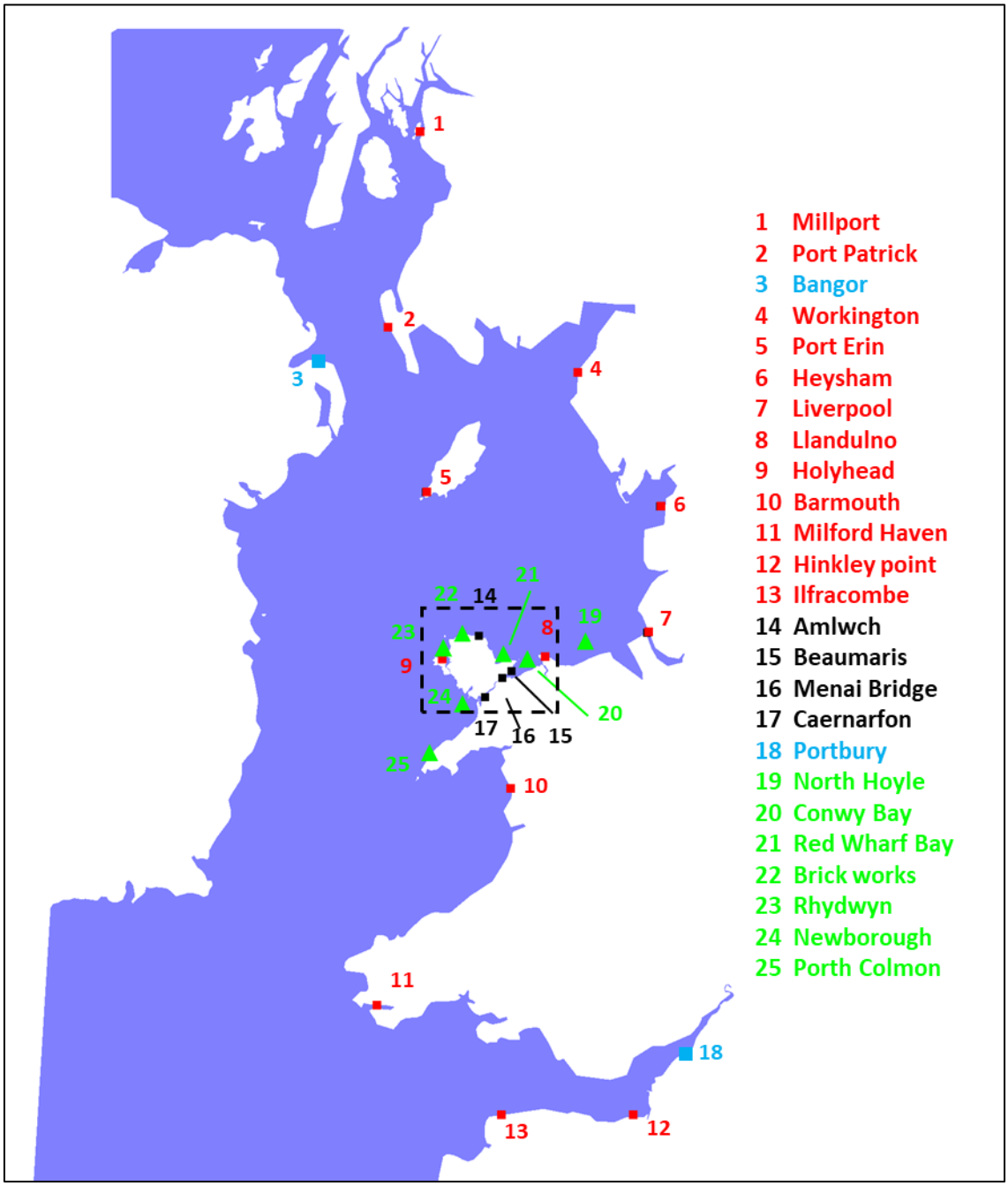

Figure 2.9: Map showing the tide gauge sites (squares) and ADCP velocity sites (triangles) used for model validation (red: sites used for Methods 1 and 2; black: sites used for Method 2 only; light blue: sites used for the Method 1 only; and green: sites used for Method 1 only on velocity). The dashed box represents the Grid 1 model domain.

2.3.1 Validation Method 1: Comparison of observed and simulated elevations

Simulated surface elevations were compared with tide gauge data, which have been proved to give good results of seasonal cycle of sea water level on the coast and finer temporal data than satellite data (Tsimplis & Woodworth, 1994; Plas & Tsimplis, 1999; Schouten *et al.*, 2005; Fenoglio-Marc *et al.*, 2005). Tide gauges data are sampled at coastline, which facilitated the study of tide and swell (Kim *et al.*, 2011). Since the simulations were constrained with tidal

forcing only, and the observed data was subjected to other forces such as atmospheric effects, the aim of this section is to assess if the non-tidal forcing markedly affected the model accuracy. Tide gauge data for the year 2015 was downloaded from the British Oceanographic Data Center (BODC) website (Form BODC website). Data included the observed surface elevation (O) and non-tidal residuals (R) (water elevation due to meteorological events such as wind, waves and/or surges) (Figure 2.10). The model of the Irish Sea simulates only the water elevation due to the tide. Other weather conditions (such as wind, waves and/or river input) were not computed. The observed surface elevation with tide only (OT) was calculated by subtracting R from O. Then, validation results between the observed surface elevation (O) were compared with observed elevation with tide only (OT) for: 1) each month of the year 2015; and 2) 14 sites. Validation has been calculated via regression analysis to calculate the coefficient of determination (R^2) followed by the calculation of the Root Mean Square Error (RMSE in m) and the Normalized Root Mean Square Error (NRMSE in %). The comparison between simulated and observed data was calculated every 30 minutes, which corresponds to the output frequency of the TELEMAC 2D model.

An ANOVA test was performed to analyse if a significant difference was observed between sites and season, which supposed that: 1) samples are independent; 2) the error values are normally distributed; and 3) variance is the same between samples. The error values are normally distributed with R^2 = 0.97 for seasonal variability in validation, and R^2 = 0.97 for spatial variability in validation.

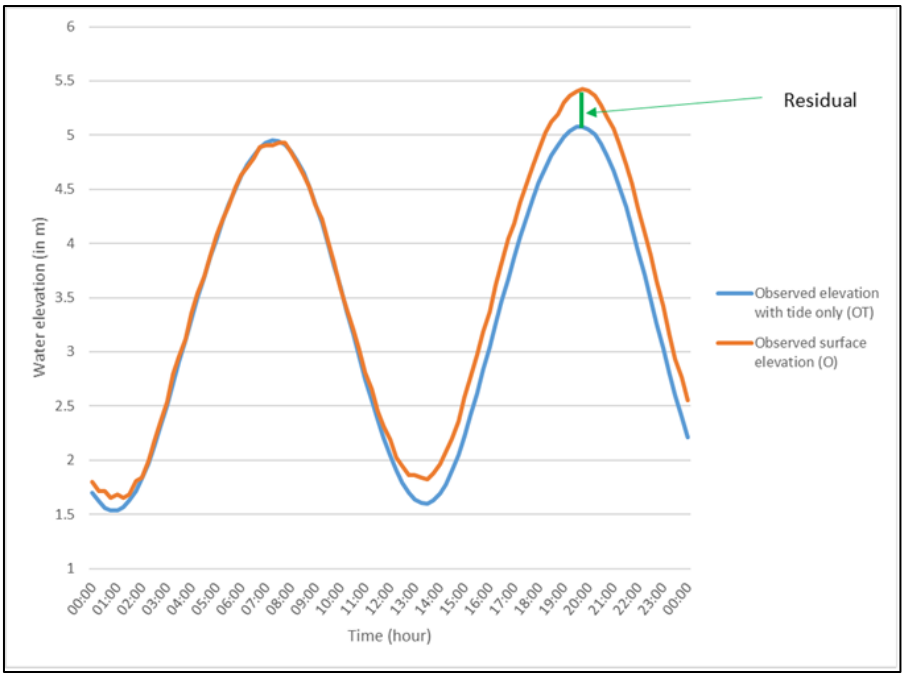

Figure 2.10: Difference between observed surface elevation with tide only (OT) and observed surface elevation (O) over a period of 24 h.

2.3.1.1 Temporal variability

Model validation was improved for each month of 2015 when the non-tidal signal (R) was removed from the observed surface elevations (O) (Table 2.1). The results per season showed a highly significant difference ($p < 0.0001$). Indeed, in winter and in autumn the improvement of validation is respectively 25.5% and 27.1%, conversely to summer (3.3%). Furthermore, an intermediate value for spring is observed of 14.5% (Table 2.1).

Table 2.1: Results for 1) NRMSE (in %) per month for observed elevation and predicted elevation and 2) Difference between observed elevation and predicted elevation per month and per season (in %).

Season	**Month**	**Average NRMSE (in %)**		**Difference (in %)**	**Average difference per season (in %)**	**P-value**
		Observed vs. simulated elevation	**Observed (tide only) vs. simulated elevation**			
Winter	*January*	6.39	4.74	34.78	25.49	**< 0.0001**
	February	5.68	4.67	21.60		
	March	5.51	4.59	20.10		
Spring	*April*	4.86	4.42	9.84	14.48	
	May	4.70	4.08	15.07		
	June	4.68	3.95	18.54		
Summer	*July*	4.24	4.20	0.91	3.32	
	August	4.69	4.46	5.17		
	September	4.93	4.74	3.87		
Autumn	*October*	5.02	4.38	14.47	27.06	
	November	5.56	4.30	29.50		
	December	5.38	3.92	37.22		

2.3.1.2 Spatial variability

Model validation of surface elevations have been grouped depending on: 1) deterioration of the validation; 2) improvement of the validation of 20%; 3) improvement of the validation of 20%-40%; and 4) improvement of the validation of > 40%. The ANOVA test showed a highly significant difference ($p < 0.0001$) between these four distinct groups (Table 2.2). The first group included Hinkleypoint and Portbury, which showed a deterioration of the validation values of -8.5% and -3.3%, respectively. The second group comprised Liverpool, Llandudno and Heysham. The results showed a slight improvement of the validation when the non-tidal residuals were removed from the observed surface elevation (2.8% for Liverpool, 4.9% for Llandudno and 5.7% for Heysham). The third group included five disparate sites (Ilfracombe, Barmouth, Porterin, Workington and Holyhead) with an improvement of the validation results by 26.5% on average. The last group included Millport, Portpatrick, Bangor and Milford haven, which showed the highest improvement of the validation results by 52.4% on average (Table 2.2). The difference between the validation against observed elevation and tide-only elevation varied from -8.5% (Hinkley point) to 60.9% (Milford haven).

Table 2.2: Results for: 1) NRMSE (in %) per sites for observed elevation and predicted elevation; and 2) Difference between observed elevation and predicted elevation per sites (in %).

Groups	**Station number**	**Sites**	**Average NRMSE (in %)**		**Difference (in %)**	**P-value**
			Observed vs. simulated elevation	**Observed (tide only) vs. simulated elevation**		
1	12	*Hinkley point*	4.89	5.34	-8.46	**< 0.0001**
	18	*Portbury*	8.53	8.82	-3.26	
2	7	*Liverpool*	7.37	7.17	2.82	
	8	*Llandudno*	4.56	4.34	4.93	
	6	*Heysham*	7.15	6.76	5.72	
3	13	*Ilfracombe*	2.53	2.10	20.82	
	10	*Barmouth*	6.00	4.93	21.86	
	5	*Porterin*	3.99	3.11	28.30	
	4	*Workington*	3.45	2.68	28.58	
	9	*Holyhead*	3.89	2.93	32.82	
4	1	*Millport*	6.56	4.61	42.35	
	2	*Portpatrick*	5.24	3.58	46.53	
	3	*Bangor*	5.27	3.30	59.78	
	11	*Milford haven*	2.46	1.53	60.87	

2.3.1.3 Validation Method 1: Discussion

Once the non-tidal contribution to the surface elevation was removed from the tide gauge record, the simulated tidal elevations matched the observations with an error of 4.4% on average. Note that these simulations were tidally forced only. Models that include atmospheric forcing can be validated directly against observations without removing the non-tidal contribution.

The temporal variability of the model performance correlated with the seasons because in the UK it is generally less windy/stormy during summer than during winter/autumn months. Consequently, the observed summer surface elevation is generally a better representation of the tide-only surface elevations. These results highlight the importance of accounting for the non-tidal effects on hydrodynamics for particle tracking modelling especially during winter and autumn. However, the tide-only model suits periods of summer when mussel larvae are numerous in the water column.

The spatial variability of the model performance among 14 sites around the Irish Sea can be explained using site specific characterisations, which influence non-tidal surface elevation: 1) Tidal range; and 2) Atlantic wave exposure (Table 2.3). The main explanation of the variability between the four groups is the tidal range value. Indeed, the sites in the group 1 and 2 are located in areas of high tidal range (hypertidal: > 6 m) and the sites in group 4 are in areas of low tidal range (mesotidal: < 4 m). Hypertidal sites have a smaller influence of non-tidal residuals on observed surface elevations. Further, the sites in group 2 (Liverpool, Llandudno and Heysham) are located in areas sheltered from the Atlantic surges and more generally sheltered from south-westerly storms. This explains why the non-tidal residuals were smaller here. On the contrary, group 3 contains sites that are located in areas of medium tidal range (macrotidal: 4 m to 6 m) and are exposed to long period waves and storms from the Atlantic (Table 2.3). This exposure explains the influence of non-tidal constituents (waves and wind) on observed surface elevations. The results from group 1, composed with Hinkley point and Port Bury, are in an area where the tidal range reaches 10 m. This extreme tidal range might explain the deterioration of the results as the model underestimated the tide impact on water elevation in this area. To conclude, the results highlighted the importance of wind and/or surges on hydrodynamics spatially. Indeed, particle tracking models must be adapted to the area of interest as the current velocities might be influenced differently by non-tidal residuals (e.g. varying wind direction and strength; varying wave exposure).

Table2.3: Parameters influencing the validation value.

Groups	Sites	Tidal range	Atlantic surges exposure
1	*Hinkley point*	**High**	Sheltered
	Portbury	**High**	Sheltered
2	*Liverpool*	**High**	**Sheltered**
	Llandudno	**High**	**Sheltered**
	Heysham	**High**	**Sheltered**
3	*Ilfracombe*	Medium	**Exposed**
	Barmouth	Medium	**Exposed**
	Porterin	Medium	**Exposed**
	Workington	Medium	**Exposed**
	Holyhead	Medium	**Exposed**
4	*Millport*	**Low**	Sheltered
	Portpatrick	**Low**	Exposed
	Bangor	**Low**	Exposed
	Milford haven	**Low**	Exposed

2.3.2 Validation Method 2: Tidal analysis

Global ocean tides are driven by the relative configuration and motions of the earth-moon-sun system (Pugh, 1996). Tidal analysis, or harmonic analysis of the tide, is a mathematical procedure that isolates the different periodic oscillations which make up the tide (either the surface tide or tidal flows) at a given constituents (amplitude and phase), are caused by the orbits of the Moon (M2) and the sun (S2). Other tidal harmonics that typically influence the character of the tide are (Amin, 1976; Le Provost, 2001): N2, K2, K1, O1, P1 and Q1 (Table 2.4). Nonlinear manifestations of these oscillations can occur as the tide interacts with shallow water or complex topography, causing higher harmonics to develop; e.g. M2 (period of 12.42 hours), M4 develops with exactly half the period (6.21 hours). Tidal analysis is commonly used to validate ocean models against known tidal constituents at specific locations, e.g. calculated from coastal tide gauge data or from offshore velocity moorings.

To calculate the main tidal constituents listed above that are simulated by ocean models, simulations are typically computed for at least 30 days and can resolve any period in time since the resultant constituent amplitudes and phases are constants. In this study, the tidal analysis has been performed using the T-tide Matlab toolbox (Pawlowicz *et al.*, 2002). This method

requires an input time series (e.g. simulated surface elevation at the same location of the known tidal constituents) and the start date and time step of this data. One year of simulated data was used. Using these parameters, T-tide calculates the amplitude and phase for any specified tidal harmonics. These values can then be compared with the known values to test the accuracy of the model locally to the data. In this study, tidal analysis validation was focused on the tidal amplitude of the principal lunar semidiurnal tidal constituent, M2. The difference between the observed (taken from Admiralty tidal stream atlas) and the simulated data is shown as a percentage for all sites. The average results per site are described below.

2.3.2.1 Validation Method 2: Spatial variability

Considering all 16 sites analysed, a significant difference ($p = 0.0002$) of model performance was calculated between sites located within the eastern Irish Sea and those located elsewhere. Difference between observations and the model were on average -13.9% for the eastern Irish Sea sites and on average -3.5% for those elsewhere (Table 2.5). The poorest performance of the model was at Liverpool (-21.4%). All sites underpredicted the M2 tidal constituent in our model, except for Barmouth.

2.3.2.2 Validation Method 2: Discussion

According to several studies modelling the hydrodynamics of the Irish Sea, (Davies & Aldridge, 1993; Green & McCave, 1995; Osuna & Wolf, 2005), a coefficient of friction value between 0.003 and 0.004 permitted a good representation of the hydrodynamics. However, the coefficient is typically higher for shallow regions, indeed, Davies & Robins (2017) showed that a spatially and temporally constant coefficient of friction value of 0.32 for their model of the Menai Strait gave good hydrodynamic validation results. Therefore, as the present study focusses on the the Menai Strait region, a constant coefficient of friction value of 0.3 was used here. The largest modelled errors (> 10%) were located in areas of shallow water such as Liverpool, Caernarfon, Heysham, Llandudno, Workington, Beaumaris and Menai (Table 2.5). As the Irish Sea model presents a high variability of water depth (from 200 m to 1 m), the coefficient of friction value must be adapted to the areas of deep water and shallow water especially in the Eastern Irish Sea. As the model underpredicted the tidal elevations for the area of interest (Menai Strait and the eastern Irish Sea), several sensitivity tests were carried out: 1) model time step; 2) output frequency; and 3) the coefficient of friction, in order to improve the accuracy of the model. These tests are described in the next section.

Table 2.4: A description of primary tidal harmonics.

Tidal harmonics	Period (hours)	Description	Periodic nature
M2	12.42	Principal lunar	Semi-diurnal
N2	12.66	Principal solar	Semi-diurnal
S2	12	Large lunar elliptic	Semi-diurnal
K2	11.97	Luni-solar	Semi-diurnal
K1	23.93	Luni-solar diurnal	Diurnal
O1	25.82	Principal lunar diurnal	Diurnal
P1	24.07	Principal solar diurnal	Diurnal
Q1	26.87	Large lunar elliptic	Diurnal

Table 2.5: Tidal analysis results for the Irish Sea model (Grid 1) for the M2 tidal constituant, with in the red the results for site located within the eastern Irish Sea and in black the results for the sites located elsewhere in the Irish Sea.

Sites	Observed M2 tidal amplitude (m)	Modelled M2 tidal amplitude (m)	Difference (%)	P-value
Liverpool	3.12	2.45	-21.35	**0.0002**
Caernarfon	1.61	1.32	**-18.15**	
Heysham	3.17	2.60	-17.94	
Llandudno	2.67	2.22	-16.89	
Beaumaris	2.54	2.18	**-14.19**	
Menai	2.33	2.06	**-11.39**	
Workington	2.73	2.47	-9.54	
Holyhead	1.81	1.66	**-8.36**	
Amlwch	2.30	2.13	**-7.49**	
Hinkley point	3.80	3.57	-6.07	
Port Patrick	1.34	1.26	-5.79	
Ilfracombe	3.08	2.94	-4.39	
Port Erin	1.76	1.69	-4.14	
Milford haven	2.24	2.15	-4.04	
Millport	1.13	1.10	-2.41	
Barmouth	1.47	1.50	2.22	

2.4 Model sensitivity tests to improve accuracy

These sensitivity tests were performed for model validation but also to optimise computational efficiency. These sensitivity tests were achieved using Grid 1 (Figure 2.11). In order to compare the accuracy of the different simulations, two approaches were used: validation Method 1 for surface elevation and velocity, and validation Method 2 for surface elevation only (both methods described in the previous Section 2.3).

2.4.1 Effect of model time step on model accuracy

To investigate how the model time-step influences the accuracy of the simulated hydrodynamics, five different scenarios were simulated with different time step values: 1 second, 2 seconds, 3 seconds, 4 seconds and 5 seconds. One month (November 2015) was simulated as the field data on velocity has been collected during this period. The values of both validation methods were compared using: 1) 14 sites for the simulation time period on elevation; 2) 7 sites for the simulation time period on velocity; and 3) 16 sites for the tidal analysis (Figure 2.9).

A time step of 4 seconds and 5 seconds caused the model to go unstable. Indeed, this can happen when the time step does not satisfy the courant condition (Equation 2.1). In the Menai Strait (Y Felinheli specifically; see figure 2.8) the distance between mesh nodes (Δx in the x-direction) is approximately 10 m with an average velocity (V) of 1.7 m/s. Using equation 2.1, these values gave a Δt of 3.9 s. This demonstrates why the model was unstable when the time step was > 3.9 s. For both validation methods, no significant difference was observed between the three other time steps (1 s; 2 s and 3 s) (Table 2.6). However, the computational time to run the model depends on the chosen time step (Table 2.6). Indeed, the computational time was reduced by 57% between the 3 s output simulation and 1 s output simulation.

$$\Delta t \leq \Delta x/(\frac{3}{2} * V)$$

Equation 2.3: The courant condition used to establish an appropriate model time step, with 1) Δt the time step; 2) Δx the distance between cross sections; and 3) V the average velocity of the flow.

Table 2.6: Model errors (%) average across the validation sites for both validation methods for three time steps tested.

			Telemac model time step (Δt)		
			1 s	**2 s**	**3 s**
Validation Method 1	Surface elevation (%)		4.29	4.29	4.29
	Velocity (%)	Strength	9.77	9.77	9.77
		Direction	11.19	11.18	11.22
Validation Method 2	M2 tidal constituent (%)		-10.07	-10.07	-10.07
	S2 tidal constituent (%)		-10.19	-10.19	-10.19
Computational time (s)			13947	7840	5910

2.4.2 Effect of model output frequency and location on model accuracy

In this section, the output frequency of the simulated variables (U, V, H) were tested to study their effect on the accuracy of the model. Six simulations were performed using Grid 1, each for 8 days and outputting variables at different frequencies (5 min, 10 min, 15 min, 20 min, 30 min and 60 min). In each case, velocity time series were extracted at 12 different locations through the Menai Strait and the surrounding coast (Figure 2.11). It was assumed that the simulation with finest output frequency resolution (5 min) produced the most accurate velocities, and these results were compared with the coarser output (10 min; 15 min; 20 min; 30 min and 60 min) for both velocity strength and direction (Figure 2.12).

Results showed that the output frequency affected the accuracy of the model with a maximum difference of 0.6% and 0.3% for the velocity strength and the direction, respectively, for all the simulations, which is assumed to be negligible. However, both velocity strength and direction showed an increase of the difference (error) for the sites located within the Menai Strait (4, 5, 6 and 7) compared with the sites outside of the Menai Strait. The maximum difference was observed at location 5 (south entrance to the Strait) with 3.3% for the velocity strength, while the maximum difference for the direction was observed in the Swellies with 0.9% (site 6) (Figure 2.12). Results are shown on average for all output frequencies tested as no significant difference was observed between them. The complexity and the strength of the currents in the Menai Strait, especially in the Swellies area (see Chapter 1, Section 3.2: The Menai Strait), can explain the differences observed (Figure 2.12). Despite the small differences in simulated flow between these scenarios, these differences could lead to significant differences in the trajectory

of particles (and therefore larvae) over a period of several weeks (i.e. the timeframe of shellfish larval cycles).

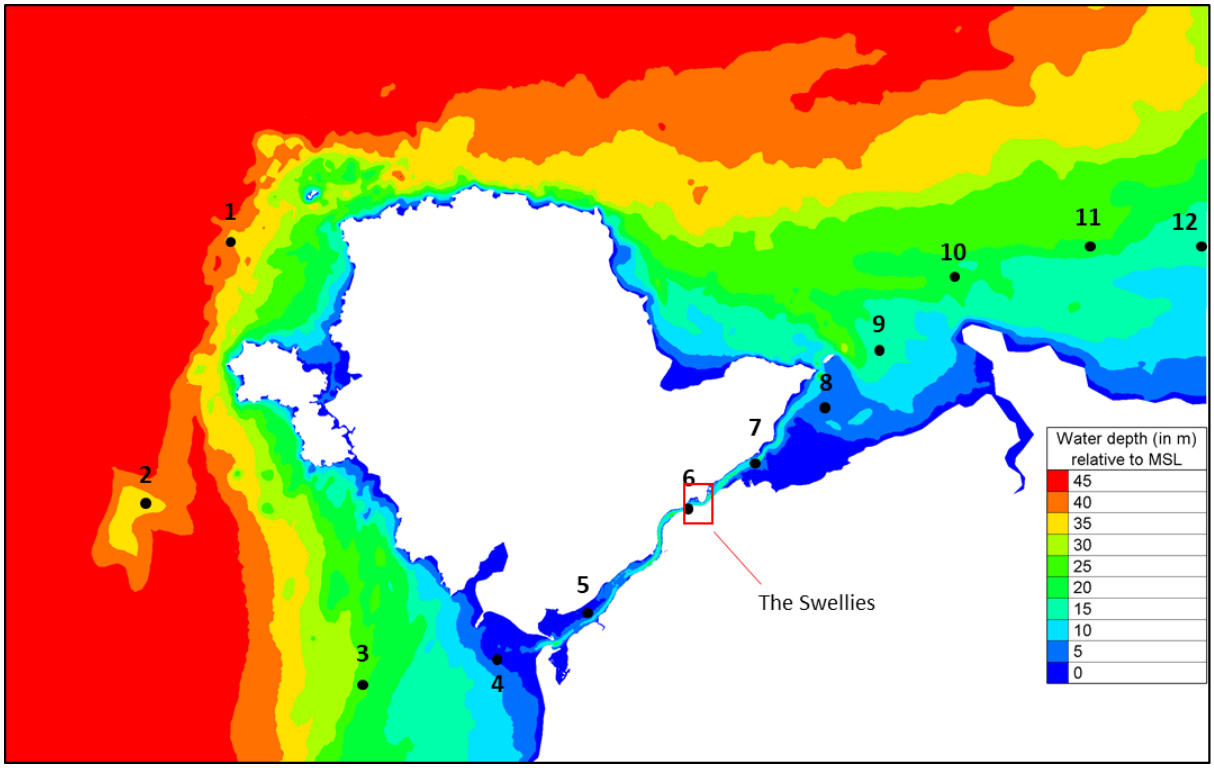

Figure 2.11: Location of the 12 sites of interest used to study the effect of output frequency on model validation.

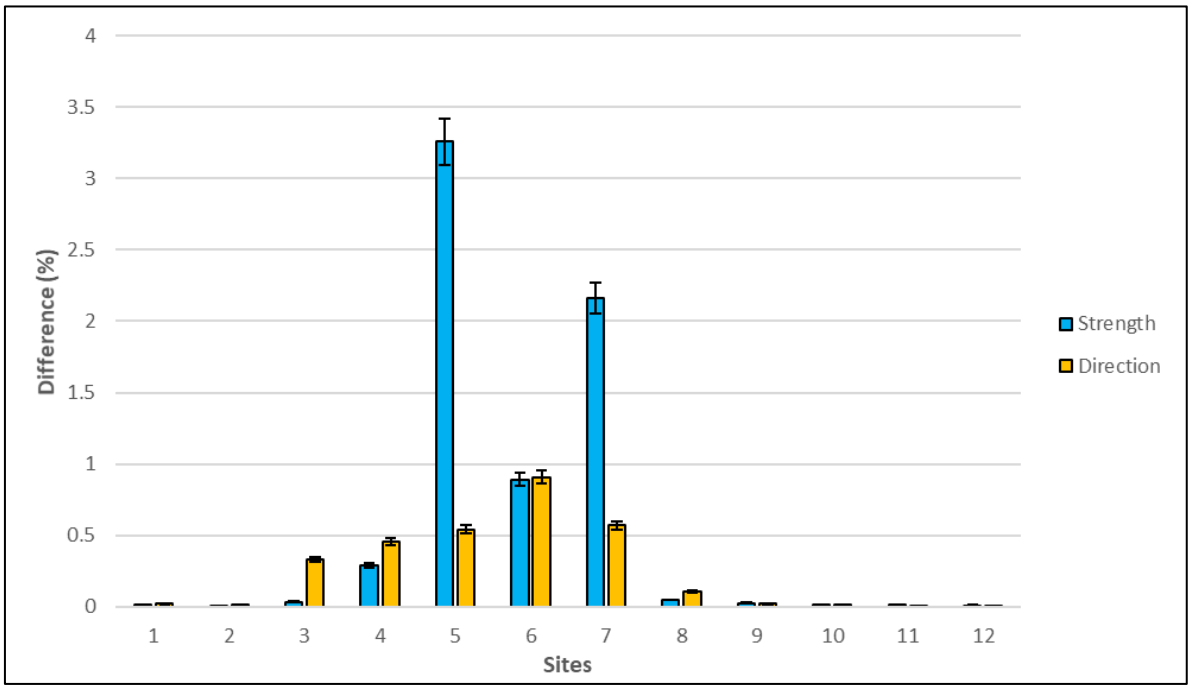

Figure 2.12: Difference of the velocity strength (black) and direction (grey) between model scenarios with 5 min output and coarser resolutions for 12 sites located in North Wales.

2.4.3 Effect of the coefficient of friction on the accuracy of the model

In hydrodynamic modelling, the value of the coefficient of friction for the bottom boundary of the model has an strong impact on the near-bed flow and, hence, the tidal currents throughout the water column (both strength and direction) and in-turn on surface elevations (Davies & Aldridge, 1993). Further, appropriate values for the coefficient of friction vary depending on the specific law of friction used in the model; but for all laws of friction, the coefficient is a function of the specific bed features (i.e. the width and depth of ripples or dunes, for example) and the sediment type (e.g. sands or gravels). TELEMAC 2D offers a range of friction law (e.g. Chezy's law, Manning's law, Strickler's law and Nikuradse's law) which can be used for hydrodynamics model. In this study, Nikuradse's law was used as it had been proved to be efficient for oceanographic studies, furthermore it is well suited for rough turbulent flow as regime flow encountered in the Menai Strait (Nikuradse, 1933; Davies & Robins, 2017). Nikuradse turbulence model is based on the size of grain at the bottom relating friction factor to bed roughness (Nikuradse, 1933). As limited data exists on the variability of the seabed in the Irish Sea (Ward *et al.*, 2015; Wilson *et al.*, 2017), but also because the features vary greatly, a fixed coefficient of friction was chosen for the entire domain. The scientific literature gives numerous values for the coefficient of friction depending on the area of interest within the Irish Sea (Davies & Aldridge, 1993; Green & McCave, 1995; Osuna & Wolf, 2005; Lewis *et al.*, 2017; Piano *et al.*, 2017). However, the most common value used in ocean model is 0.32 (Soulsby *et al.*, 1993).

Form this observation, the coefficient of friction value was varied to give the most accurate simulation of the hydrodynamics, throughout the domain, when compared with the observations. Telemac-2D was run using Grid 1 for four scenarios, each time varying the coefficient of friction (1.0, 0.4, 0.2 and 0.1). The upper limit was chosen to represent an unrealistic high value and the minimum limit has been chosen to represent a sandy bottom, which is mostly the composition of the bottom Irish Sea (Figure 1.16, Fernandes *et al.*, 2001). The model ran for one month, November 2015. Simulated velocities and elevations were validated using both validation methods (see Section 2.3).

Applying validation method 1, the accuracy of the simulated surface elevations was improved when the coefficient of friction decreased (Figures 2.13 and 2.14). On average across the validation sites, results showed an improvement in the error from 7.4% (coefficient 1) to 5.7% (coefficient 0.1). For validation Method 2 (tidal analysis), the results improved from -13.4% (coefficient 1) and -4.3% (coefficient 0.1). Looking at the results for all validation sites, the greatest errors were obtained for the shallow water regions in the eastern Irish Sea (Llandudno,

Liverpool and Heysham) and in the Menai Strait (Beaumaris, Caernarfon and Menai Bridge). However, the greatest improvement, from the initial simulation described in Section 2.3, was also observed in those areas (from -22.3% to -9.7% using the tidal analysis method).

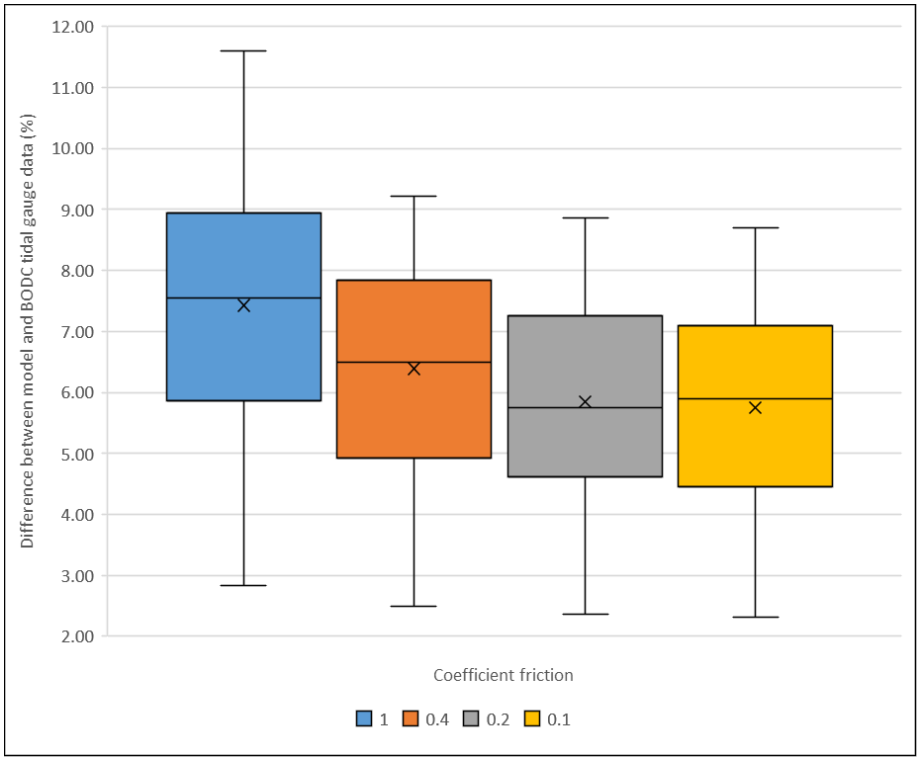

Figure 2.13: Box plot showing the percentage difference (i.e. model error) between simulated and observed tidal elevations, using validation Method 1. Results are based on 14 locations throughout the Irish Sea (see Figure 2.9) – showing maximum, minimum, median (crossbar) and average (cross) values. Each box plot shows a comparison with a different parameterisation for the coefficient of friction: 1 (blue); 0.4 (orange); 0.2 (grey); and 0.1 (yellow).

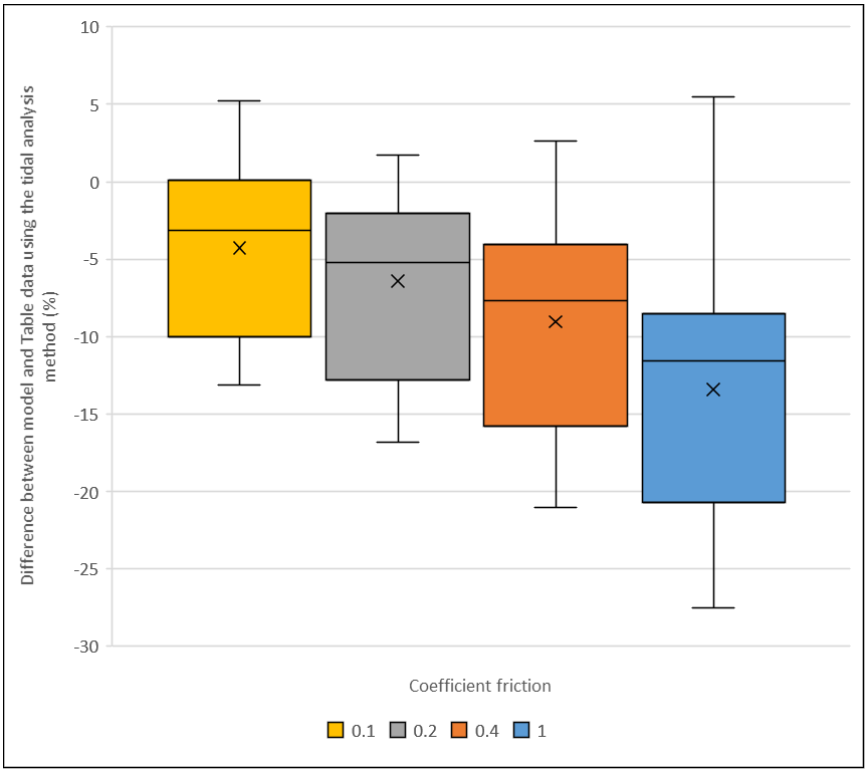

Figure 2.14: Box plot showing the percentage difference (i.e. model error) between simulated and observed tidal elevations, using validation Method 2 (tidal analysis). Results are based on 16 sites throughout the Irish Sea (see Figure 2.9) – showing maximum, minimum, median (crossbar) and average (cross) values. Each box plot shows a comparison with a different parameterisation for the coefficient friction: 1 (blue); 0.4 (orange); 0.2 (grey); and 0.1 (yellow).

2.4.4 Conclusion

This section on model sensitivity has shown that the coefficient of friction markedly affected the accuracy of the simulated surface elevations. Indeed, using Grid 1 (Irish Sea) with Nikuradse's law, the model validation for surface elevations improved from 7.4% (min = 2.8%, max = 8.8%) using a coefficient of 1, to 5.7% (min = 2.3%, max = 6.4%) using a coefficient of 0.1. The model validation for tidal analysis elevations improved from -13.4% (min = -27.5%, max = 5.5%) using a coefficient of 1, to -4.3% (min = -13.1%, max = -5.2%) using a coefficient of 0.1. Literature showed that a coefficient friction of 0.1 using Nikuradse law correspond to a bottom composed mostly by sand, which corresponds to the composition of the bottom of the Irish sea for most of it (Figure 1.16; Fernandes *et al.*, 2001). Therefore, for further TELEMAC-2D simulations in this study (both Grid 1 and Grid 2), the coefficient of friction will have a value of 0.1 using Nikuradse's law of friction. Additionally, the chosen model time step (which was varied in the range 1 s to 5 s) affected the computational efficiency and stability, with Δt = 2 s being optimal. Consequently, further simulations will compute using a 2 s time step and with a 30 minutes output frequency.

2.5 Model validation: Summary of results

The period of interest to study mussel larvae dispersal in North Wales is spring/summer when the first spawning occurs, e.g. from 01st March to 31st October (Dare & Edwards, 1975). Consequently, the validation results presented here have been performed during March 2015 validation against time series and for the tidal analysis. Validation results for velocity (strength and direction) have been calculated for the month of November 2015 as data have been collected during mid-October to November 2015 by the Prince Madog (i.e. scientific boat of the School of Ocean Sciences) using ADCP method (i.e. Acoustic Doppler Current Profiler).

2.5.1 Observed vs. simulated: elevation

The model validation for surface elevation (during March 2015), presented in Table 2.7 shows that across all 14 validation sites:

1) The root mean squared error (RMSE) is 0.45 m (Irish Sea) and 0.35 m (Menai Strait)

2) The normalized root mean squared error (NRMSE) is 5.7% (Irish Sea) and 4.8% (Menai Strait)

3) The coefficient of determination (R^2) was 0.92 (Irish Sea) and 0.99 (Menai Strait).

The best fit is observed at Ilfracombe and worst fit is observed at Millport using the Irish Sea model (Figures 2.15 and 2.16). Using the Menai Strait model the best fit is observed at Holyhead and the worst at Llandudno (Figures 2.17 and 2.18).

Table 2.7: Model validation for surface elevation (during March 2015) using both models (Irish Sea and Menai Strait) showing 1) RMSE; 2) NRMSE; and 3) coefficient of determination (R^2).

Sites	Grid 1: Irish Sea			Grid 2: Menai Strait		
	RMSE (in m)	NRMSE (in %)	R^2	RMSE (in m)	NRMSE (in %)	R^2
Ilfracombe	0.23	2.31	0.99	-	-	-
Workington	0.40	4.37	0.96	-	-	-
Llandudno	0.42	4.77	0.97	0.35	5.50	0.99
Milford haven	0.37	4.92	0.96	-	-	-
Porterin	0.30	4.85	0.96	-	-	-
Hinklepoint	0.35	2.86	0.99	-	-	-
Holyhead	0.28	4.48	0.96	0.34	4.04	1.00
Heysham	0.72	6.93	0.92	-	-	-
Portpatrick	0.33	6.97	0.91	-	-	-
Bangor (Ireland)	0.29	7.45	0.90	-	-	-
Barmouth	0.35	6.95	0.90	-	-	-
Liverpool	0.69	6.88	0.92	-	-	-
Millport	0.37	8.69	0.84	-	-	-
Portbury	1.16	8.04	0.74	-	-	-
Average	**0.45**	**5.75**	**0.92**	**0.35**	**4.77**	**0.99**

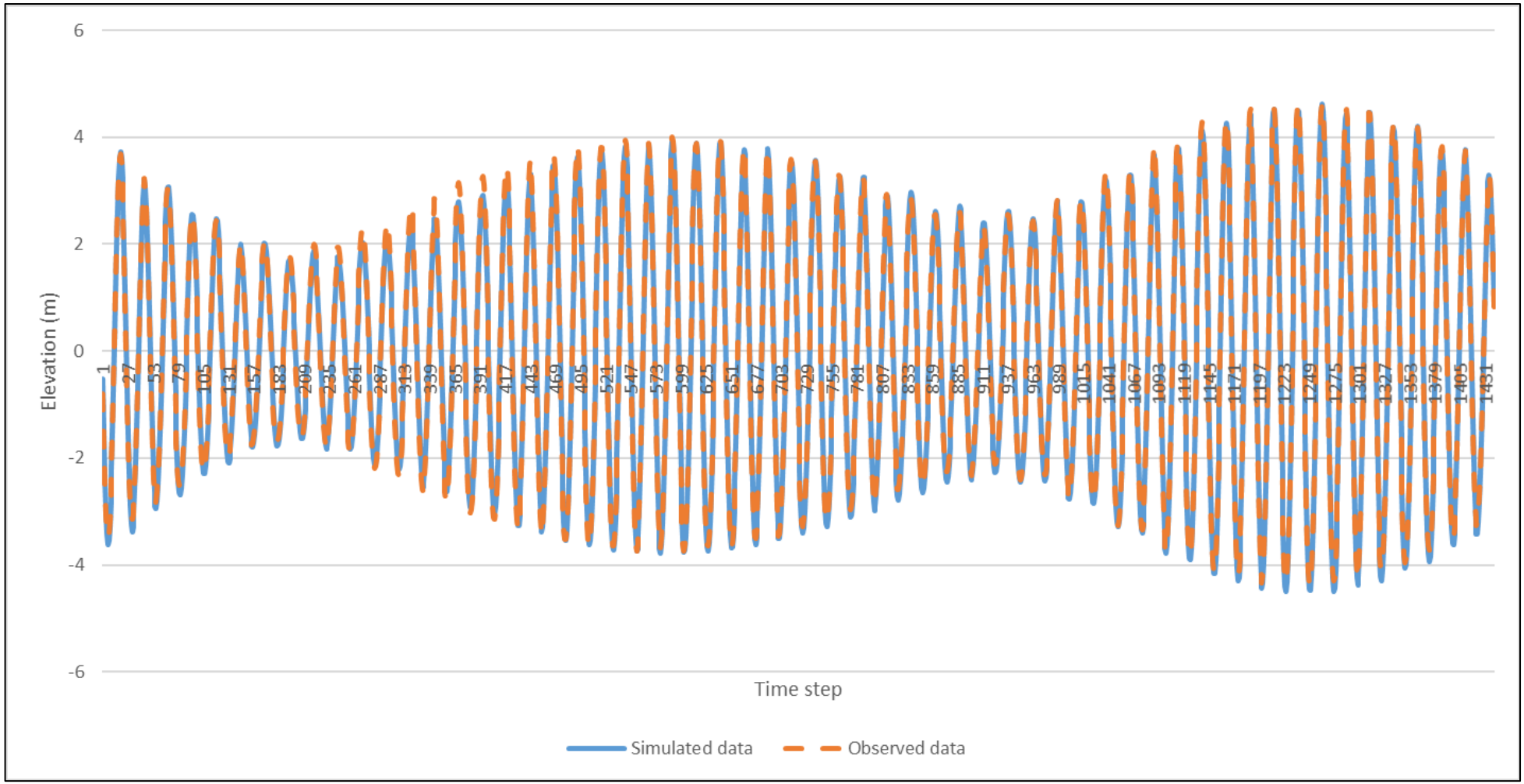

Figure 2.15: Time series of surface elevation during March 2015 at Ilfracombe for simulated data from the Irish Sea model (blue solid line) and observed data (orange dashed line).

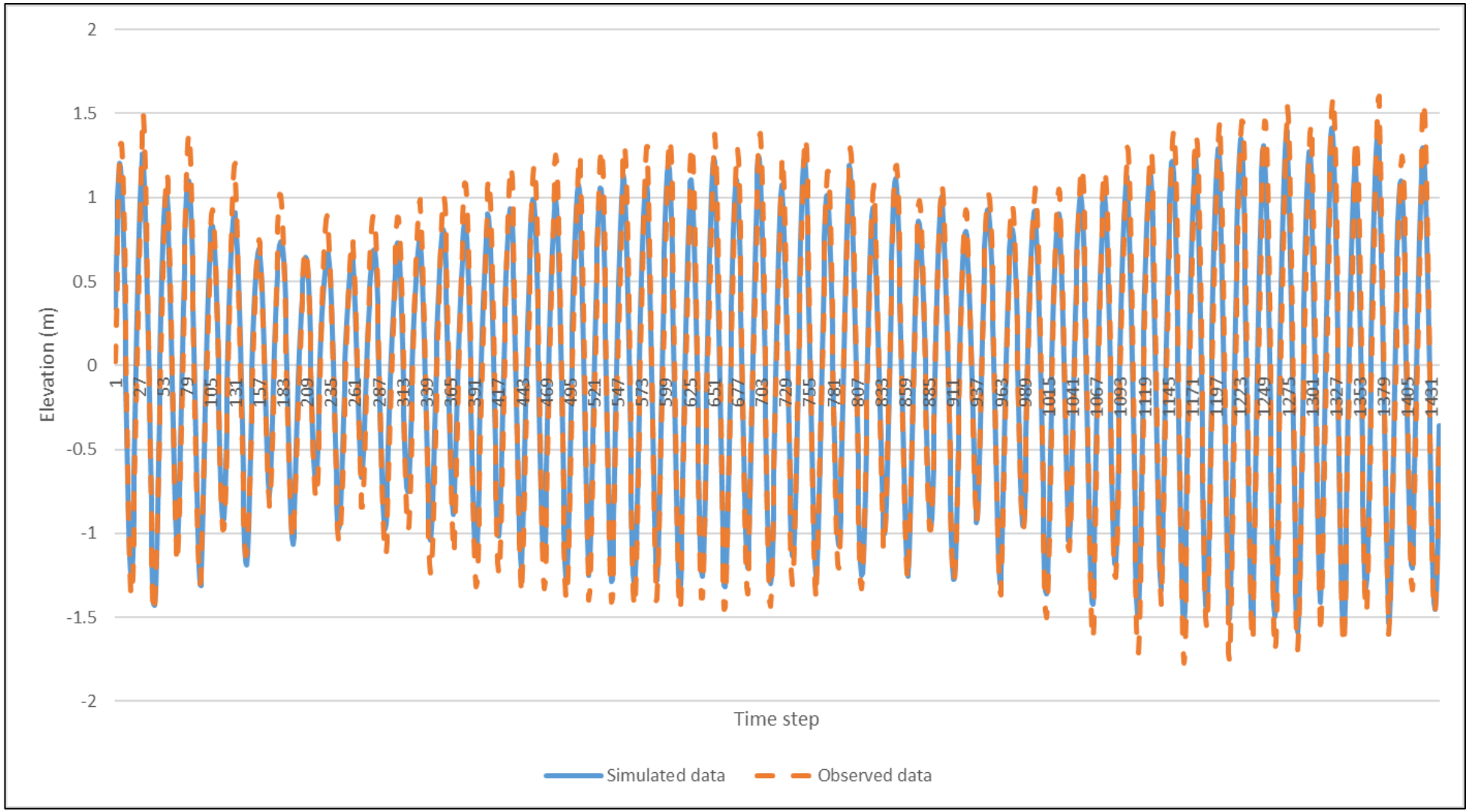

Figure 2.16: Time series of surface elevation during March 2015 at Millport for simulated data from the Irish Sea model (blue solid line) and observed data (orange dashed line).

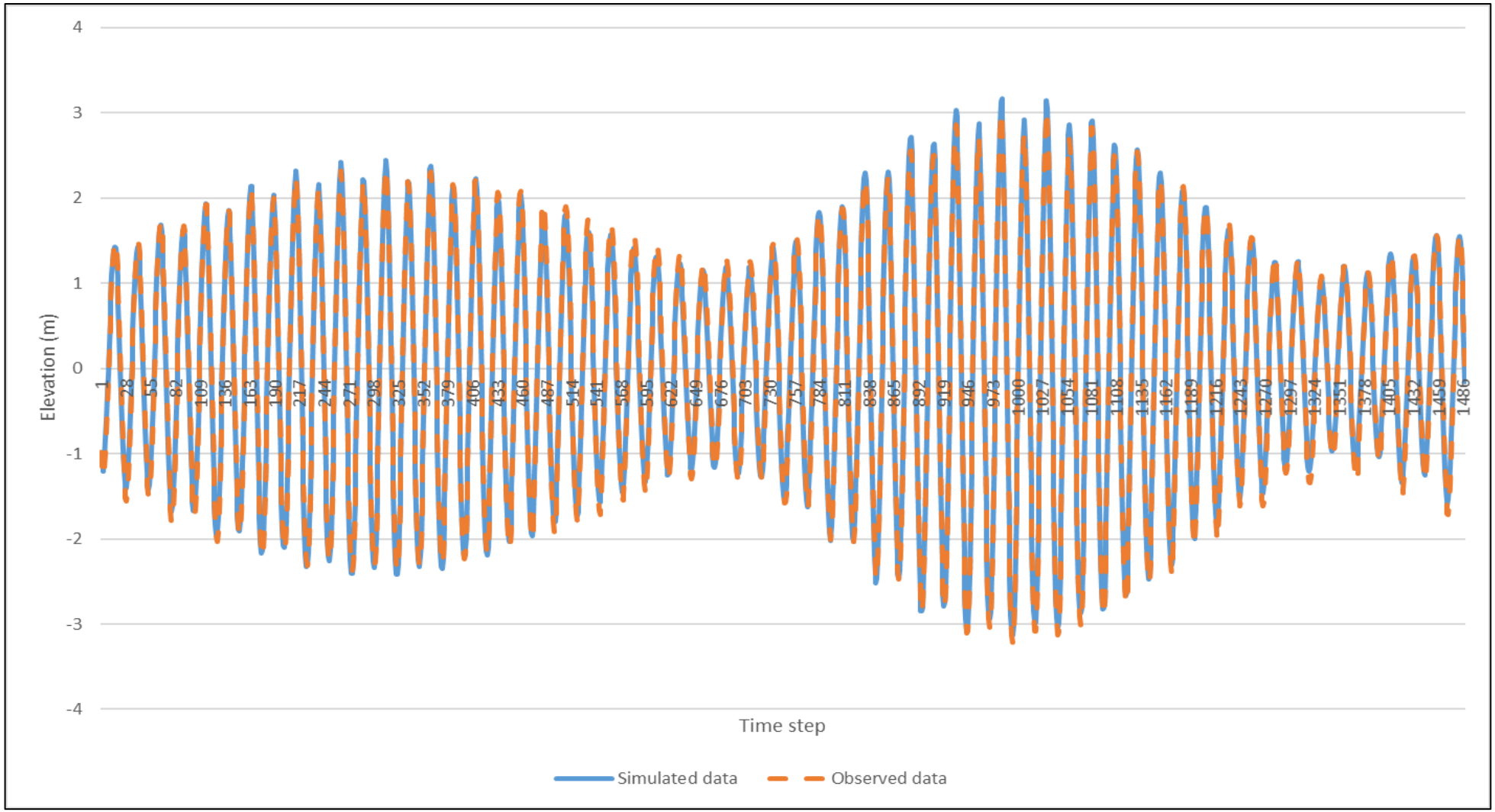

Figure 2.17: Time series of surface elevation during March 2015 at Holyhead for simulated data from the Menai Strait model (blue solid line) and observed data (orange dashed line).

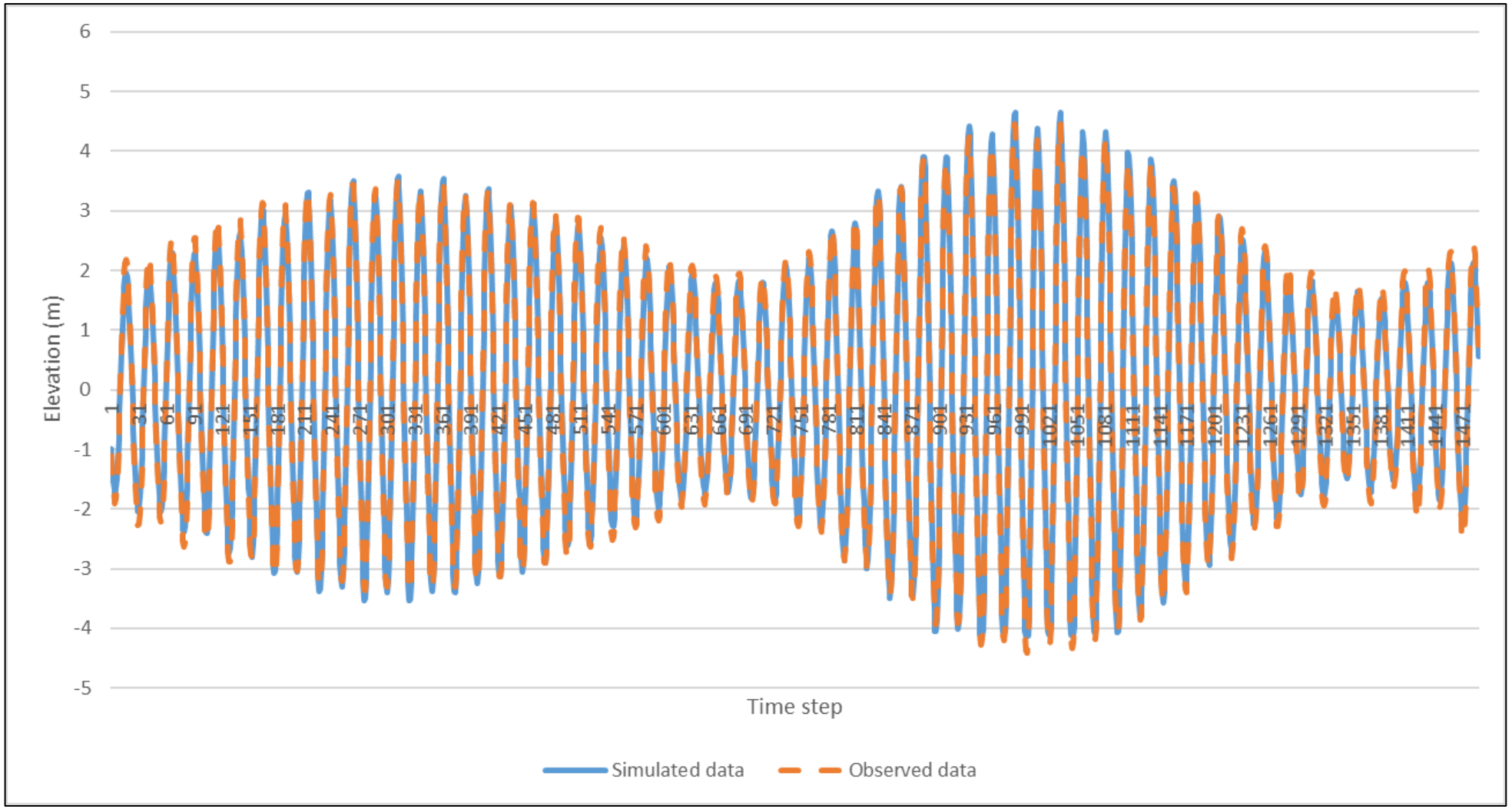

Figure 2.18: Time series of surface elevation during March 2015 at Llandudno for simulated data from the Menai Strait model (blue solid line) and observed data (orange dashed line).

2.5.2 Observed vs. simulated: velocity

In contrast to the previous results, the Irish Sea model (Grid 1) had better validation results for velocity (for both strength and direction) than the Menai Strait model (Grid 2) (Tables 2.8 and 2.9). Indeed, for simulated velocity magnitude NRMSE were 9.8% (Irish Sea model) and 13.6% (Menai Strait model) averaged across all sites (Table 2.8). The sites averaged NRMSE calculated for the velocity direction were 11.2% (Irish Sea model) and 17.7% (Menai Strait model) (Table 2.9).

For the velocity magnitude the best fit is observed at North Hoyle and the worst fit is observed at New borough using the Irish Sea model (Figures 2.19 and 2.20). Using the Menai Strait model the best fit, for the velocity magnitude, is observed at Brickworks and the worst at New borough (Figures 2.21 and 2.22).

Velocity direction is best simulated at Rhydwyn and worst simulated at New borough using the Irish Sea model (Figures 2.23 and 2.24). Using the Menai Strait model the best fit, for the velocity direction, is observed at Rhydwyn and the worst at onwy Bay (Figures 2.25 and 2.26).

Table 2.8: Model validation of simualted velocity magnitude (November 2015) for both models (Irish Sea and Menai Strait) showing: 1) RMSE; 2) NRMSE; and 3) coefficient of determination (R^2).

Sites	Grid 1: Irish Sea			Grid 2: Menai Strait		
	RMSE (m/s)	NRMSE (%)	R^2	RMSE (m/s)	NRMSE (%)	R^2
North Hoyle	0.04	5.75	0.97	-	-	-
Conwy Bay	0.04	9.01	0.96	0.08	14.58	0.69
Red Wharf Bay	0.06	12.42	0.84	0.07	13.28	0.77
Brick works	0.11	7.38	0.92	0.21	10.65	0.79
Rhydwyn	0.10	9.44	0.88	0.16	13.19	0.69
Newborough	0.06	15.94	0.68	0.07	16.52	0.56
Porth Colmon	0.09	8.47	0.93	-	-	-
Average	**0.07**	**9.77**	**0.88**	**0.12**	**13.64**	**0.70**

Table 2.9: Model validation of simualted velocity direction (November 2015) for both models (Irish Sea and Menai Strait) showing: 1) RMSE; 2) NRMSE; and 3) coefficient of determination (R^2).

Sites	Grid 1: Irish Sea			Grid 2: Menai Strait		
	RMSE (degree)	**NRMSE (%)**	**R^2**	**RMSE (degree)**	**NRMSE (%)**	**R^2**
North Hoyle	41.44	11.72	0.82	-	-	-
Conwy Bay	37.35	10.53	0.86	65.77	23.41	0.58
Red Wharf Bay	46.12	13.10	0.75	55.85	16.17	0.65
Brick works	18.09	10.14	0.95	30.48	16.77	0.87
Rhydwyn	17.15	6.34	0.95	46.77	13.02	0.72
Newborough	49.39	13.73	0.82	69.48	19.30	0.67
Porth Colmon	44.37	12.71	0.75	-	-	-
Average	**36.27**	**11.18**	**0.84**	**53.67**	**17.74**	**0.70**

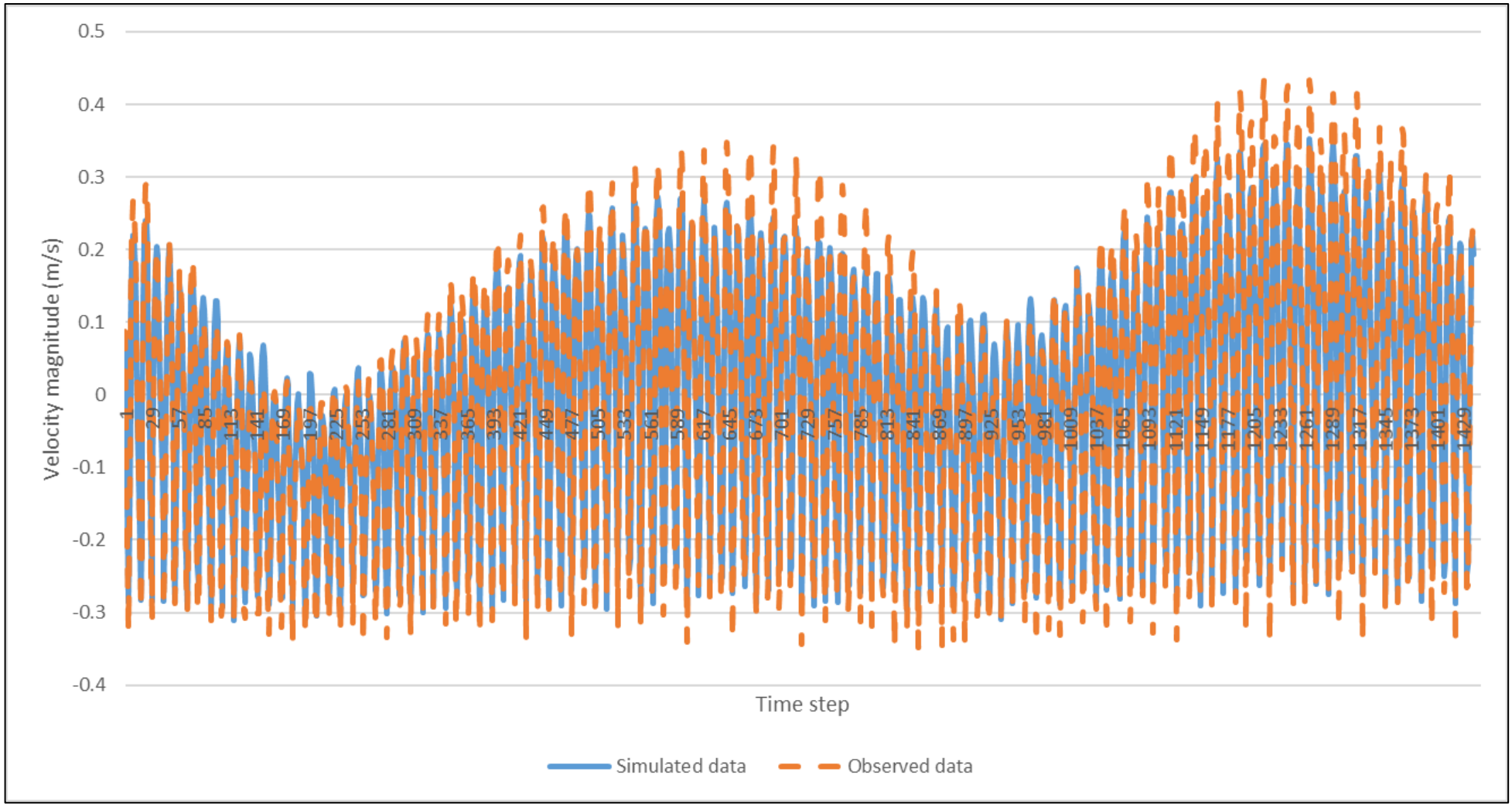

Figure 2.19: Time series of velocity magnitude during November 2015 at North Hoyle for simulated data from the Irish Sea model (blue solid line) and observed data (orange dashed line).

Figure 2.20: Time series of velocity magnitude during November 2015 at New borough for simulated data from the Irish Sea model (blue solid line) and observed data (orange dashed line).

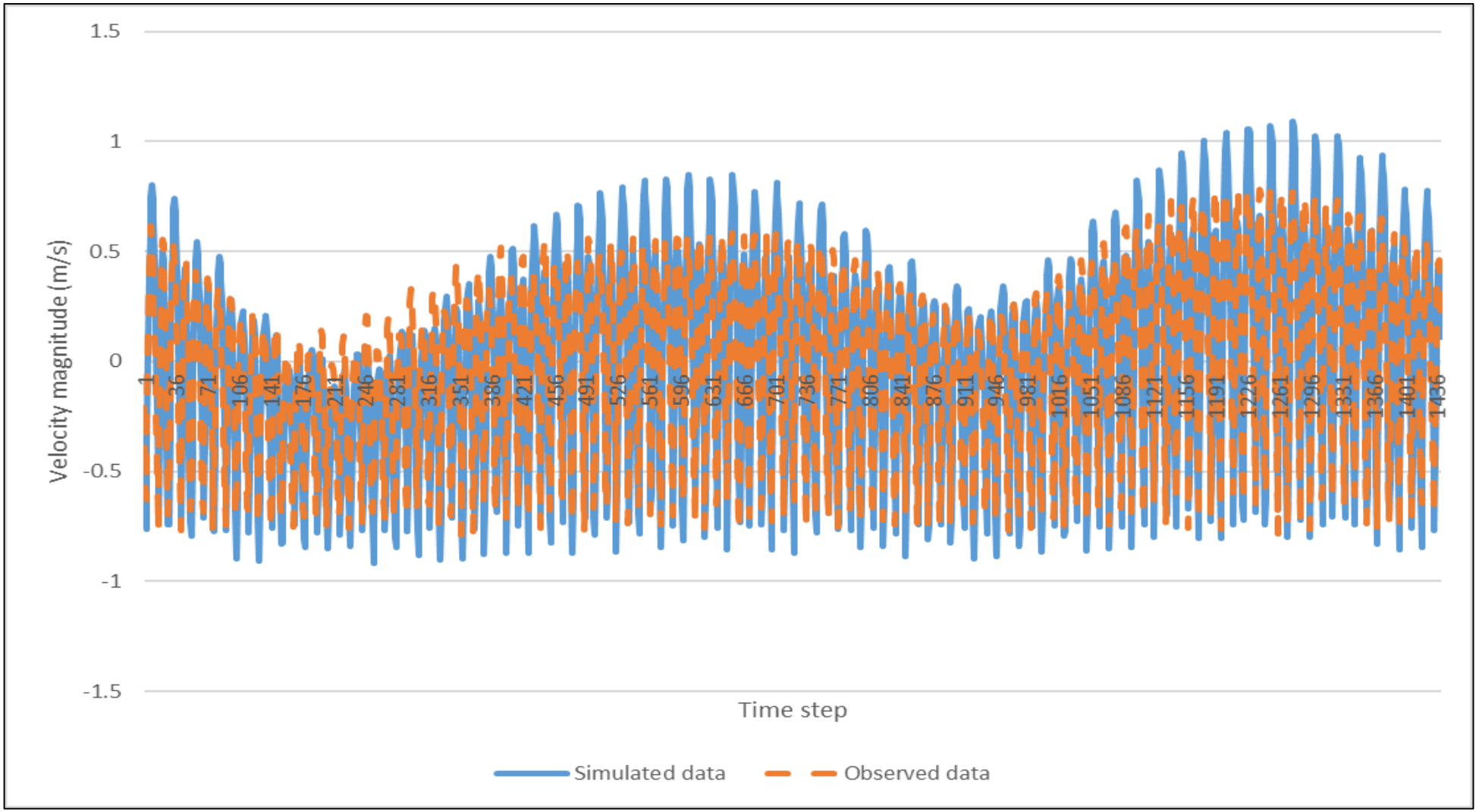

Figure 2.21: Time series of velocity magnitude during November 2015 at Brickworks for simulated data from the Menai Strait model (blue solid line) and observed data (orange dashed line).

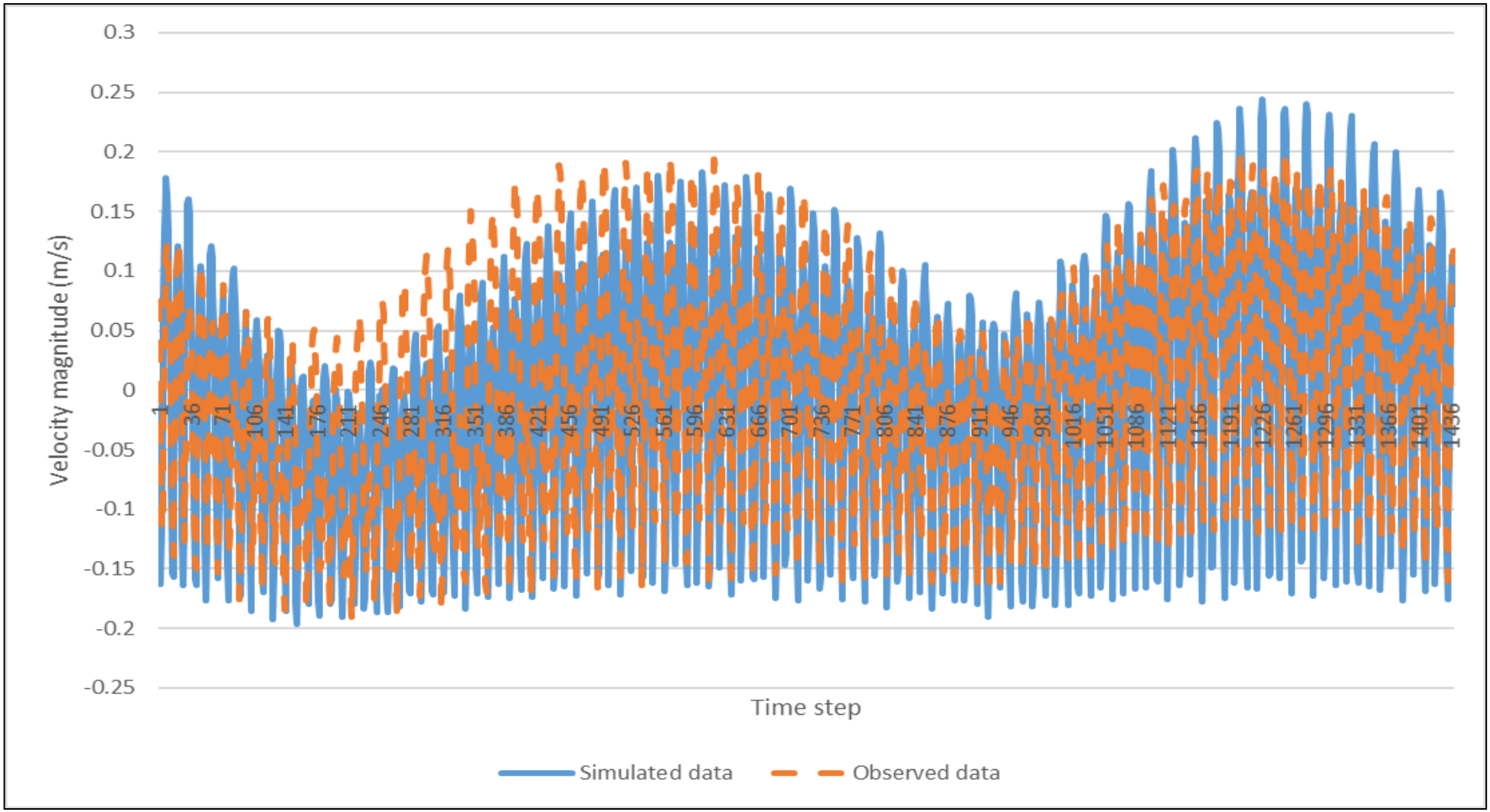

Figure 2.22: Time series of velocity magnitude during November 2015 at New borough for simulated data from the Menai Strait model (blue solid line) and observed data (orange dashed line).

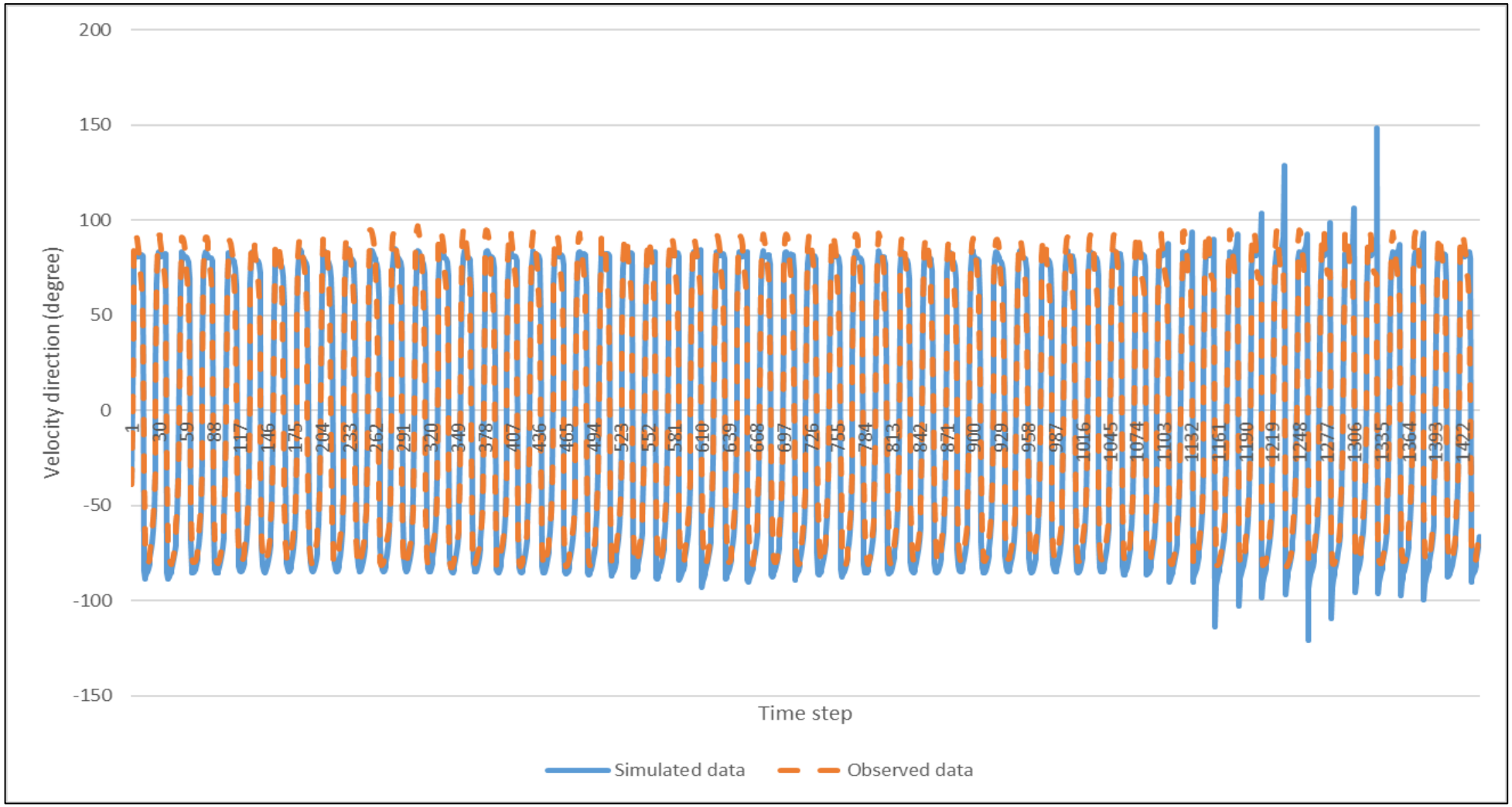

Figure 2.23: Time series of velocity direction during November 2015 at Rhydwyn for simulated data from the Irish Sea model (blue solid line) and observed data (orange dashed line).

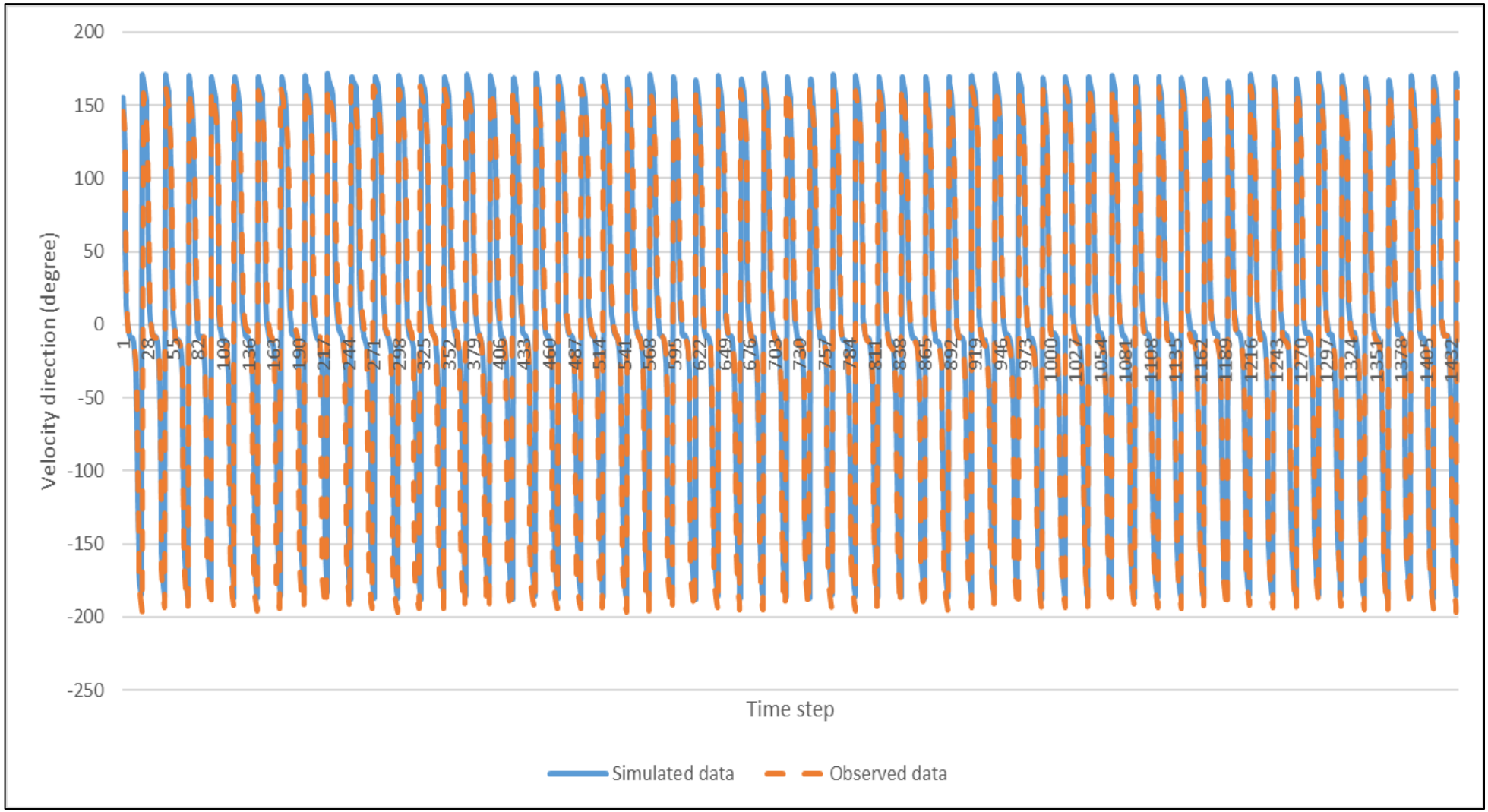

Figure 2.24: Time series of velocity direction during November 2015 at New borough for simulated data from the Irish Sea model (blue solid line) and observed data (orange dashed line).

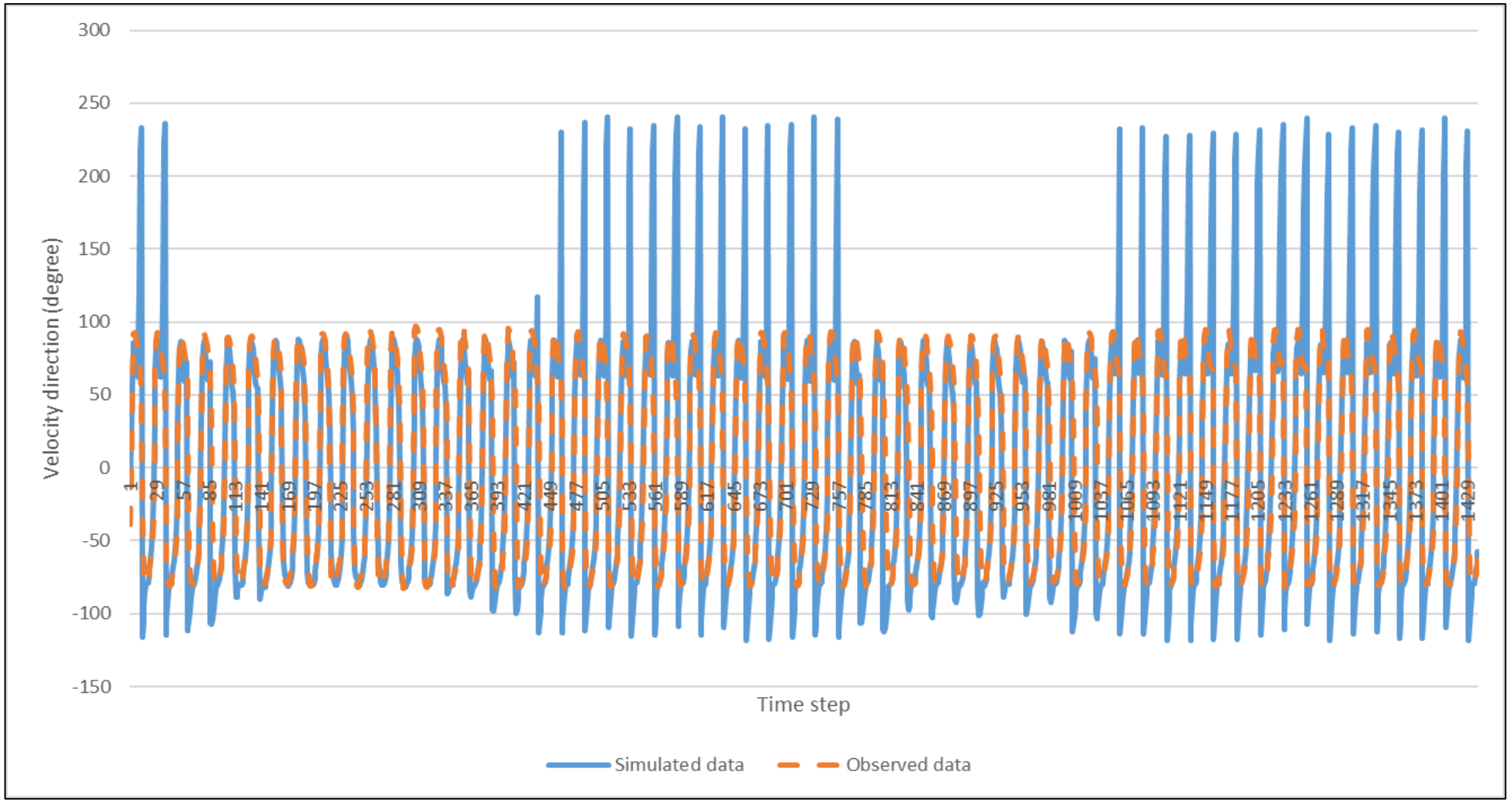

Figure 2.25: Time series of velocity direction during November 2015 at Rhydwyn for simulated data from the Menai Strait model (blue solid line) and observed data (orange dashed line).

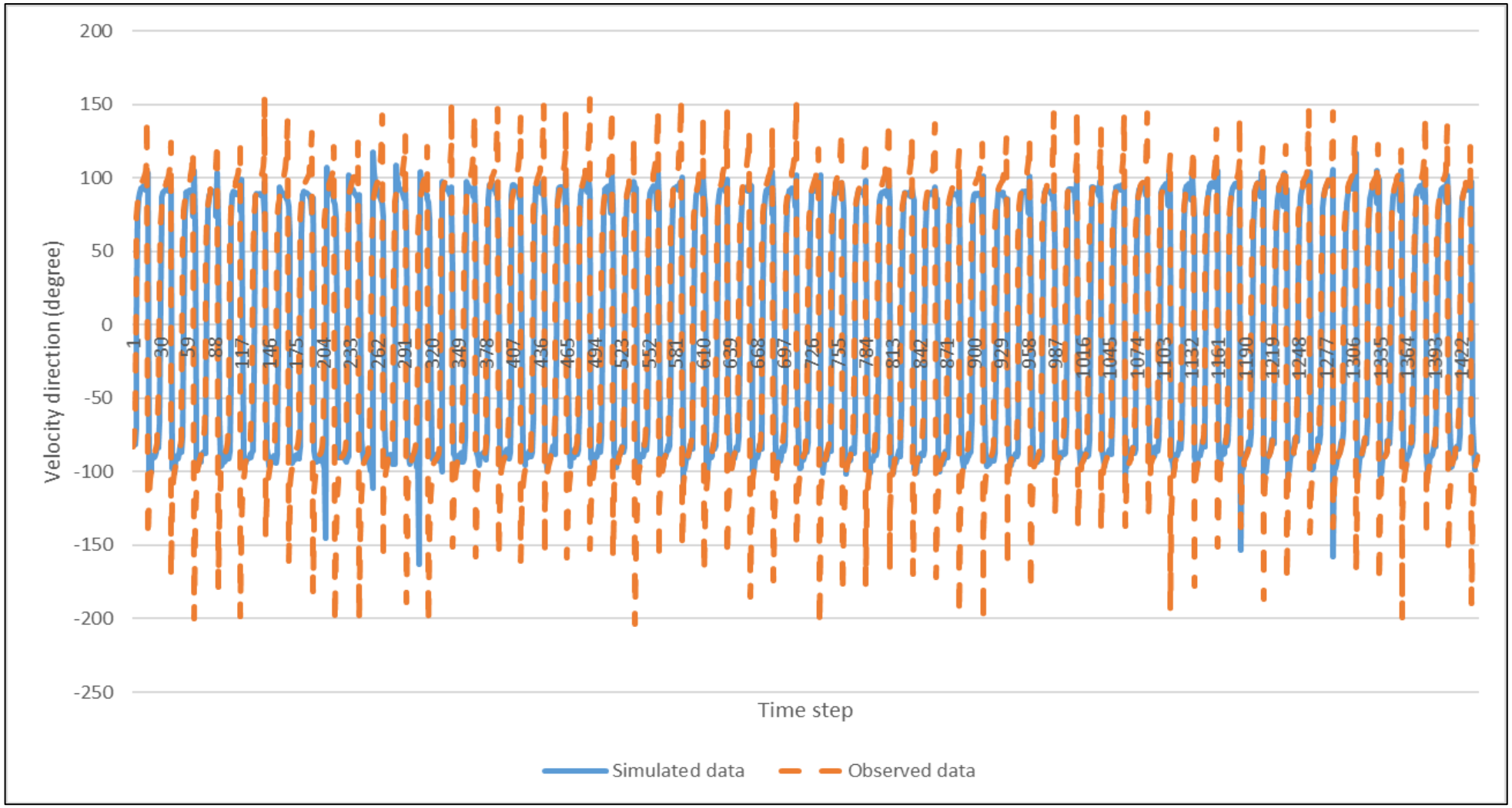

Figure 2.26: Time series of velocity direction during November 2015 at Conwy Bay for simulated data from the Menai Strait model (blue solid line) and observed data (orange dashed line).

2.5.3 Tidal analysis

According to the tidal analysis validation results, both models underpredicted the M2 tidal constituent. However, the underestimation of the model was small, on average, with errors of -4.3% for the Irish Sea model and 1% for the Menai Strait model (Table 2.10).

Table 2.10: Results of the model validation tidal analysis, for simulation of the M2 tidal constituent (%) with in red the average values for both models (Irish Sea and Menai Strait).

Site	Grid 1: Irish Sea			Grid 2: Menai Strait		
	Tide table data (m)	Model data (m)	Difference (%)	Tide table data (m)	Model data (m)	Difference (%)
Ilfracombe	3.08	3.01	-2.40	-	-	-
Workington	2.73	2.64	-3.20	-	-	-
Llandudno	2.67	2.36	-11.60	2.67	2.64	-1.30
Milford Haven	2.24	2.13	-4.70	-	-	-
Port Erin	1.76	1.79	2.00	-	-	-
Hinkleypoint	3.80	3.83	0.90	-	-	-
Holyhead	1.81	1.73	-4.40	1.81	1.79	-1.20
Heysham	3.17	2.82	-11.10	-	-	-
Port Patrick	1.34	1.35	0.90	-	-	-
Barmouth	1.47	1.44	-2.30	-	-	-
Liverpool	3.12	2.71	-13.10	-	-	-
Millport	1.13	1.19	5.20	-	-	-
Amlwch	2.30	2.25	-2.20	2.30	2.32	0.80
Beaumaris	2.54	2.37	-6.70	2.54	2.46	-2.90
Menai Bridge	2.33	2.26	-3.10	2.33	2.32	-0.30
Caernarfon	1.61	1.41	-12.50	1.61	1.59	-1.10
Average			**-4.27**			**-1.00**

Chapter 3: Particle tracking model

3.1 Introduction

In this chapter, the efficiency of the PTM was studied within the context of accuracy and computational efficiency. Indeed, the process of running the PTM code is time consuming and needed optimising. According to literature, higher resolution (spatial and temporal) improves model performance and so particle trajectory accuracy (Vadivieso Da Costa & Blanke, 2004; Andrejev *et al.*, 2011; Qin *et al.*, 2014; Putman & He, 2013; Kvile *et al.*, 2018; Dauhajre *et al.*, 2019). The aim is to find a balance, which gives acceptable results in the minimum of time. First the structure of the PTM will be presented. Then, the chapter will be articulated according to the literature (Simons *et al.*, 2013; Sebille *et al.*, 2018), which states that four main factors influence the accuracy of a PTM: 1) the interpolation scheme; 2) the spatial resolution; 3) the temporal resolution; and 4) the number of particles released.

3.1.1 PTM design

A particle tracking model is a numerical tool, which disperse particles (e.g. marine larvae) according to physical advection and mixing output from the hydrodynamic model (i.e. TELEMAC-2D) (Lett *et al.*, 2008; Garcia-Garcia *et al.*, 2016). The analyse of larvae trajectories cannot be done in the field with measurement, consequently numerical studies are essential to resolve larval dispersal (Katz *et al.*, 1994; Power, 1996; Wiebe & Benfield, 2003). The particle tracking model was created using Matlab. The PTM is composed of three parts: 1) Interpolating the TELEMAC velocity data from a triangular mesh to an orthogonal mesh; 2) Determination of particle position and parameterisation; and 3) Determination of the particle movement (Figure 3.1 and Appendix C).

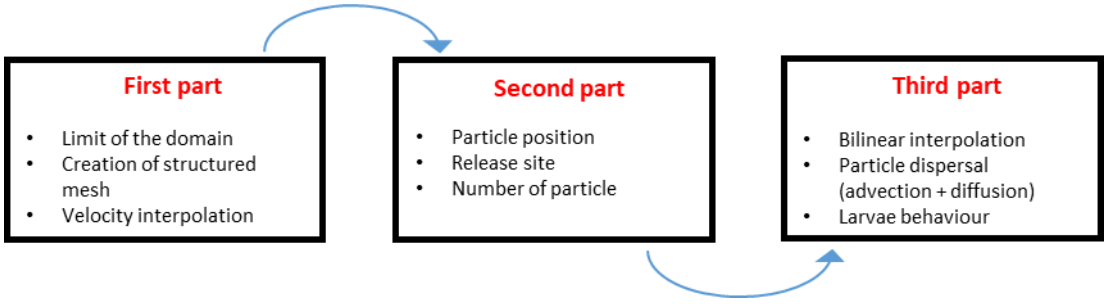

Figure 3.1: Schematic structure of the PTM.

3.1.1.1 Creation of an orthogonal mesh from a triangular mesh

The first part consists in (see Appendix C):

- **Define the limit of the domain:** For the Irish Sea model, the domain of study will be limited as presented in Figure 3.2, while for the Menai Strait model the area of study was the entire mesh domain (see Chapter 2, Figure 2.5).
- **Create on orthogonal mesh:** Here, I defined the resolution of the orthogonal mesh, which was constant over the domain. 20 meters and 50 meters were the resolution chosen for the Menai Strait model and the Irish Sea model respectively (Figure 3.3).
- **Velocity interpolation:** Output from TELEMAC (water depth (H) and velocity (U and V), which is based on a spatially unstructured mesh, was then interpolated onto an orthogonal grid (Figure 3.4).

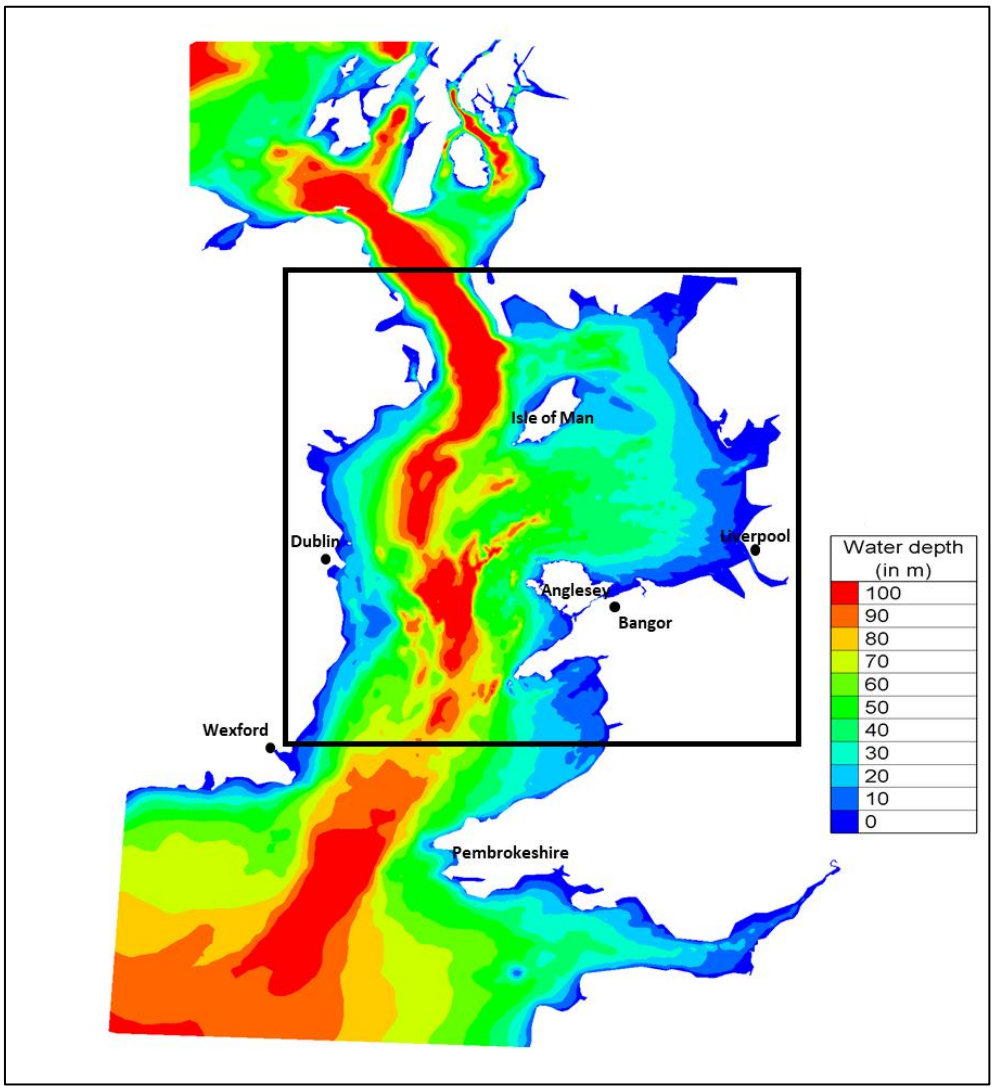

Figure 3.2: Model of the Irish Sea within the black square the area of interest for the PTM.

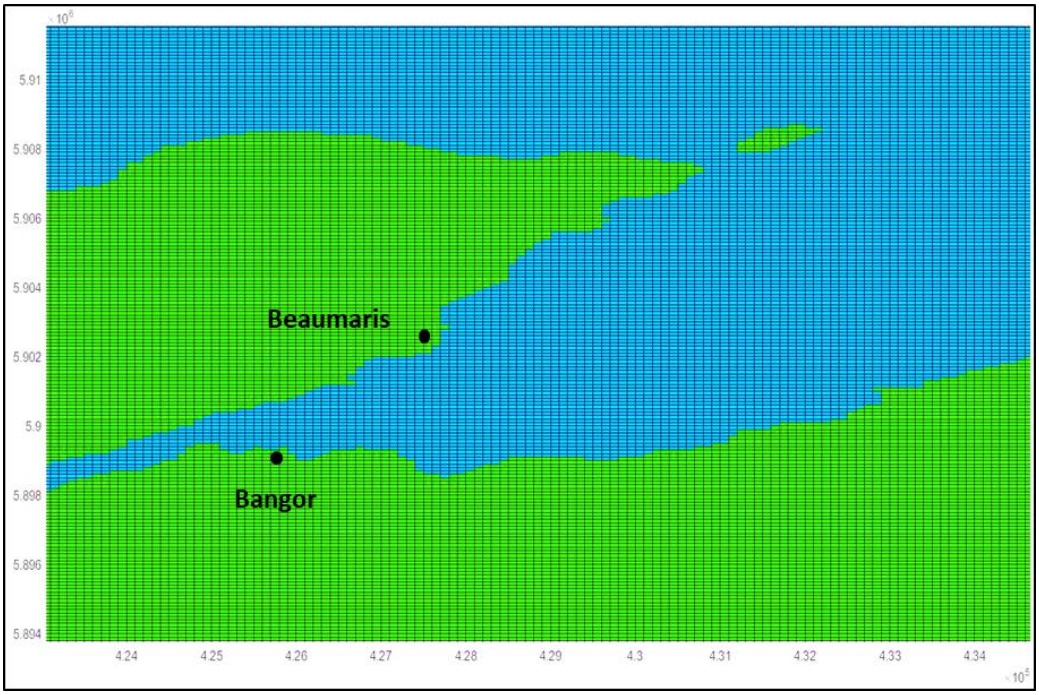

Figure 3.3: Orthogonal mesh generated on Matlab with a constant 50 m grid resolution for the Irish Sea model. Land is represented in green and Sea is represented in blue.

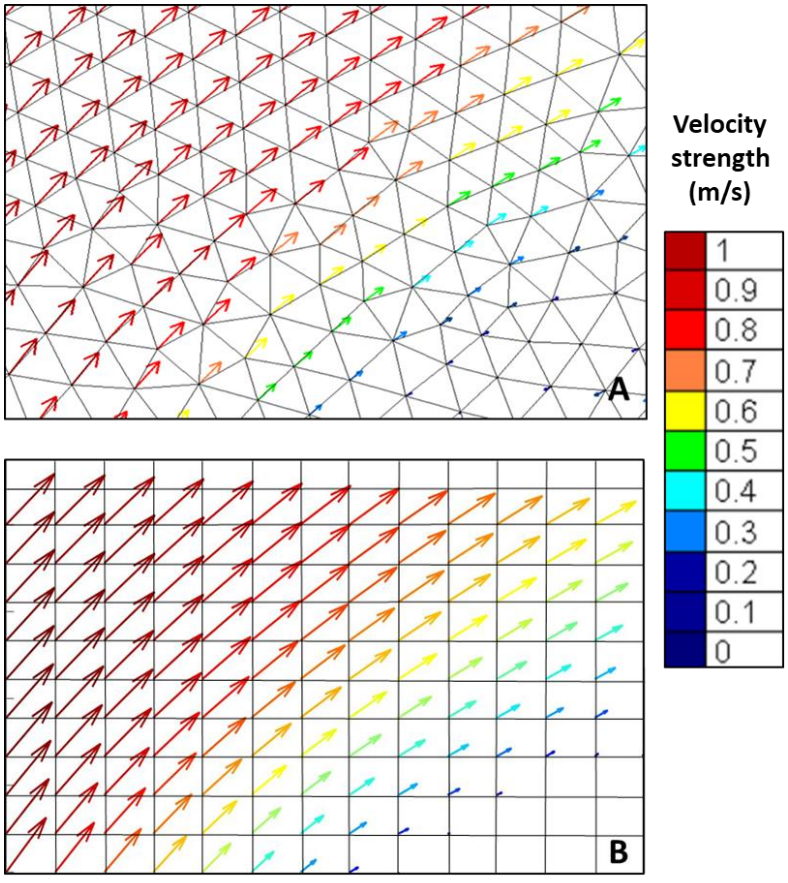

Figure 3.4: Example interpolation of velocity field from north of Anglesey from unstructured mesh with Blue Kenue (A) to a structured mesh into Matlab (B). Arrows showing the direction and strength in m/s.

3.1.1.2 Determination of the position and the number of particles

The second part of the PTM: 1) determines the number of particles used; 2) creates a matrix to record the position of all particles for each timestep along x and y; and 3) defines the release position of the particles. Particles were assigned a random release from a fixed point within a limited area. Figure 3.5 shows 5,000 particles randomly dispersed in an area of 1,600 m^2 located near Bangor pier in the Menai Strait (coordinates (in UTM): x = $4.26299*10^5$ and y = $5.899455*10^6$) (see Appendix C).

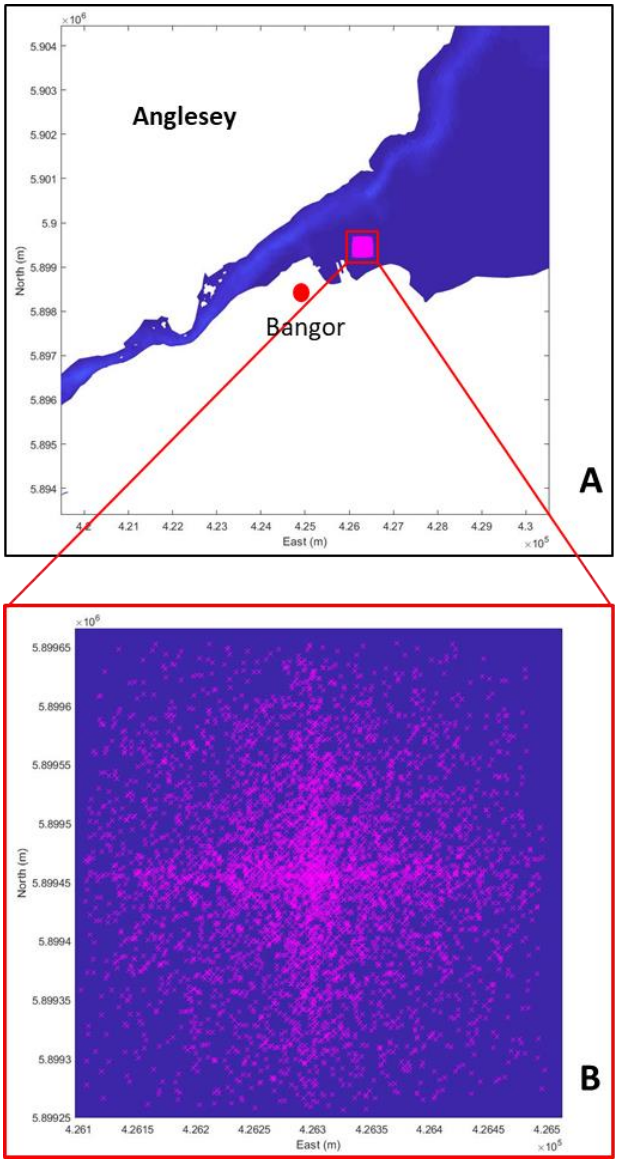

Figure 3.5: Particles release position for 5,000 particles in an area of 1600m^2 with A) overview of the area of interest and B) zoom in.

3.1.1.3 Determination of the particle movement

The motion of particles through space and time is defined in the third section. Figure 3.6 showed the movement of 5 particles released from the same position to the north of Anglesey (coordinates (in UTM): x = $3.9*10^5$ and y = $5.93*10^6$) for one time-step (Δt = 30 min) for: 1) advection only; and 2) advection + diffusivity (i.e. stochastic term from Proctor *et al.* (1994) with a constant coefficient of diffusion). Several parameters were studied, and the results have been discussed later in the thesis to understand the robustness and sensitivity of the PTM. Specifically, I will investigate:

- Does simulated tidal advection explain particle movement realistically, or is additional dispersion of particles based on a parameterisation of diffusion required? Kozalka *et al.* (2009; 2010) showed that using a sufficiently high spatial and temporal resolution hydrodynamic model of tidal currents (where grid-scale turbulent diffusion is parameterised within the model), a PTM does not need to include additional diffusion terms. The models created in this study use a varying spatial resolution grid; consequently, it is important to understand the effect of including additional sub-grid-scale particle diffusion.
- Ocean models work with discretized grids, which do not represent the continuous velocity field inside the grid cells (Sebille *et al.*, 2018). Therefore, is it necessary to interpolate the simulated fields (velocity, water depth) to the sub-grid-scale position of the particle?
- How should particles that encounter land be simulated?

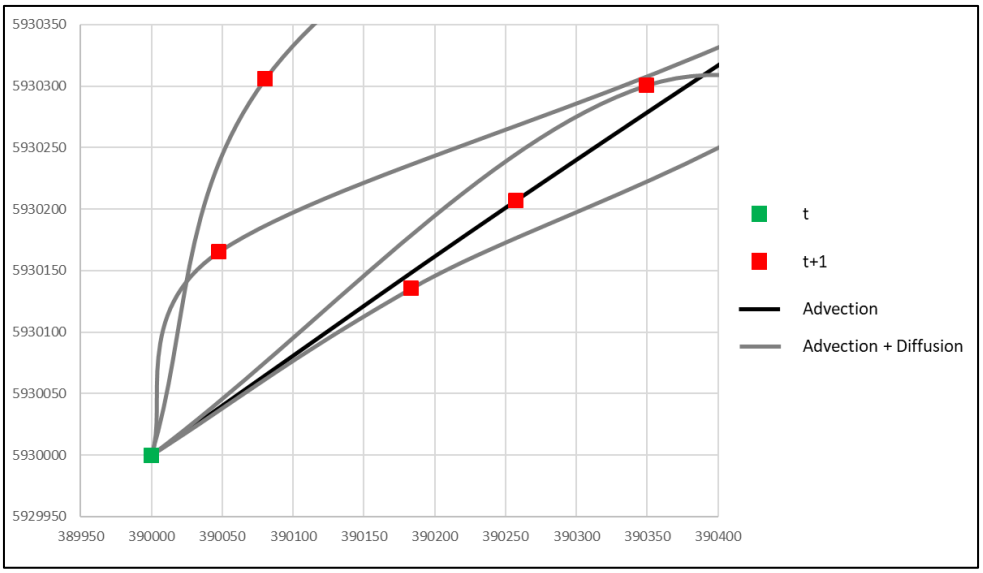

Figure 3.6: Particles movement for one timestep using advection only (in black) and advection + diffusivity (in grey). The position at t and t+1 are represented by green and red square respectively.

3.1.2 Summarize of the sensitivity tests performed

The PTM, defined above, was tested for computational efficiency and accuracy (Table 3.1). The computational efficiency of the PTM was based on PC run time (using the “tic” function in MATLAB). Sensitivity tests on accuracy studied the impact of spatial and temporal resolution. Also, the tests were performed on the first and third parts of the PTM as the second part doesn’t affect the PTM run time or its accuracy. Finally, the results obtained were used to validate the PTM against observed drifter trajectories.

Table 3.1: Summarize of the tests performed to optimize the time and improve the accuracy of the PTM.

Section title	Name of the test	Number of particles	Part of the PTM tested	PTM runtime (in hours)	Timestep (in min)	Grid resolution (in m)	Model used
Interpolation of velocity field - Computational efficiency	Test-1	0	1	-	-	From 10 to 300	Both
	Test-2	0	1	From 5 to 100	30	From 30 to 300	Menai Strait
Interpolation velocity field - Accuracy	Temporal dimension	10000	3	192	From 60 to 5	1000	Irish Sea
	Spatial dimension	10000	3	192	60	From 50 to 1000	Irish Sea
Spatial resolution	Grid resolution limit to study the Menai Strait	0	1	-	-	From 20 to 500	Menai Strait
	Impact on PTM accuracy	10000	3	96	60	From 50 to 1000	Irish Sea
Temporal resolution	Impact on PTM accuracy	10000	3	96	From 5 to 60	1000	Irish Sea
Number of particles	Computational efficiency	From 50 to 100000	3	25	30	From 30 to 100	Menai Strait
	Number limit in the PTM	From 50 to 15000	3	336	30	20	Menai Strait
Validation of the PTM via observed drifter trajectories	Test-1	7000	3	Drifter_1: 51 Drifter_2: 66	5	20	Drifter_1: Menai Strait Drifter_2: Irish Sea
	Test-2	7000	3	Drifter_1: 51 Drifter_2: 66	5	20	Drifter_1: Menai Strait Drifter_2: Irish Sea
	Test-3	7000	3	Drifter_1: 51 Drifter_2: 66	5	20	Drifter_1: Menai Strait Drifter_2: Irish Sea
Released area	Position from single mussel bed	7000	3	168	30	20	Menai Strait
	Size of released patch	7000	3	168	30	20	Menai Strait

3.2 Interpolation of velocity field

3.2.1 Computational efficiency

This test concerns the first part of the PTM where the TELEMAC output variables were loaded and interpolated from an unstructured spatial mesh to an orthogonal (i.e. structured) spatial mesh. Two tests were performed on the computational time efficiency to generate: Test-1: a structured mesh spatial resolution: 10 m, 15 m, 20 m, 30 m, 40 m, 50 m, 75 m, 100 m, 150 m, 200 m and 300 m (Figure 3.7) and Test-2: number of velocity files (from 10 to 200) (Figure 3.8). Test 1 was performed on two models: 1) the Menai Strait model (Figure 2.5) and 2) the Irish Sea model (Figure 3.2), while Test 2 was only performed on the Menai Strait model.

Test-1: To create an orthogonal mesh, there was an exponential increase in computational time as a function of spatial grid resolution, $R^2 = 0.98$ on average for both models (Figure 3.7). Computationally, the maximum spatial resolution was 10 m for these model domains due to storage memory within Matlab. The minimum resolution of 300 m was set, as coarser mesh resolutions did not resolve the Menai Strait (Figure 3.13). The computational time difference between the two models followed a linear increase with $R^2 = 0.88$ (Figure 3.7). For all interpolation procedures, the Irish Sea model took longer because the domain is bigger (32,000 km^2) than the Menai Strait model (10,000 km^2).

Test-2: Results showed an exponential increase of the computational time relative to the number of velocity files generated with $R^2 = 0.98$ on average for all the grid resolutions tested (Figure 3.8). However, a linear increase in computational time was observed depending on the grid resolution with $R^2 = 0.98$ (data not shown).

The maximum resolution of TELEMAC unstructured mesh was 20 m (in the Menai Strait). This resolution was chosen for interpolation for subsequent PTM based on the Menai Strait model. This resolution sufficiently resolves the circulation through the Strait and hence larval transport. For the Irish Sea model, which is focussed on the larger-scale circulation, resolution of 50 m was deemed sufficient. In this case, it was possible to calculate the theoretical computational time it will take to plan future simulations.

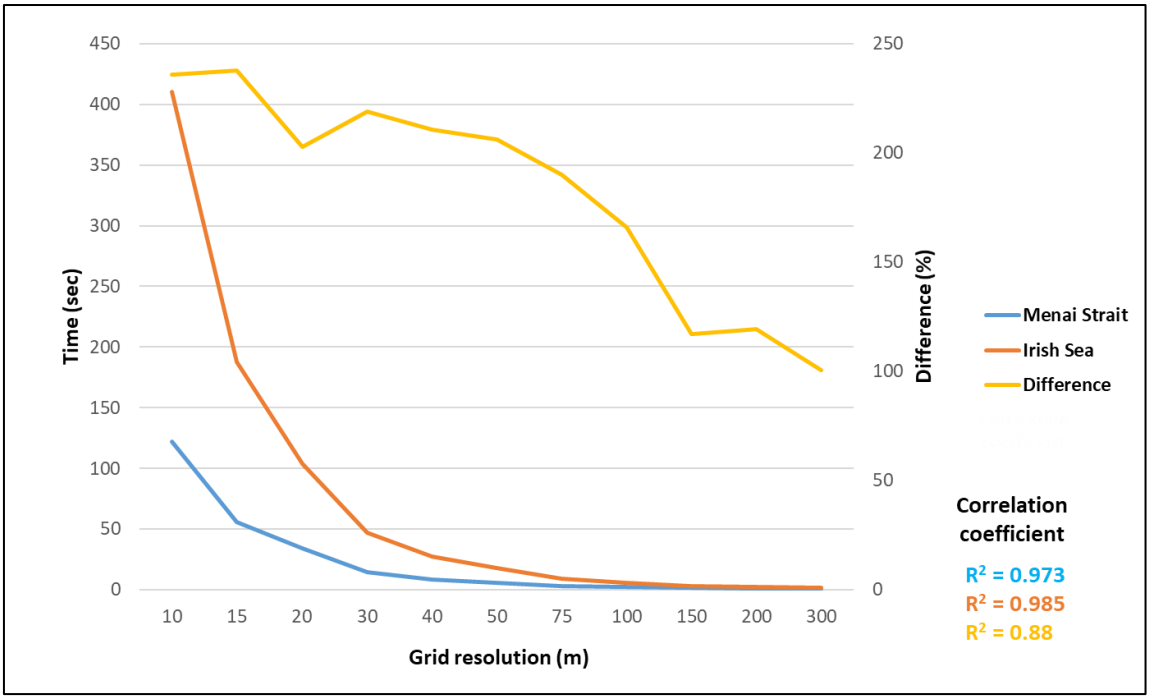

Figure 3.7: Computational time required to generate a structured mesh within the Matlab PTM, depending on spatial grid resolution of the Menai Strait model (in blue) and the Irish Sea model (in orange). The difference of computational time between the models is represented in yellow.

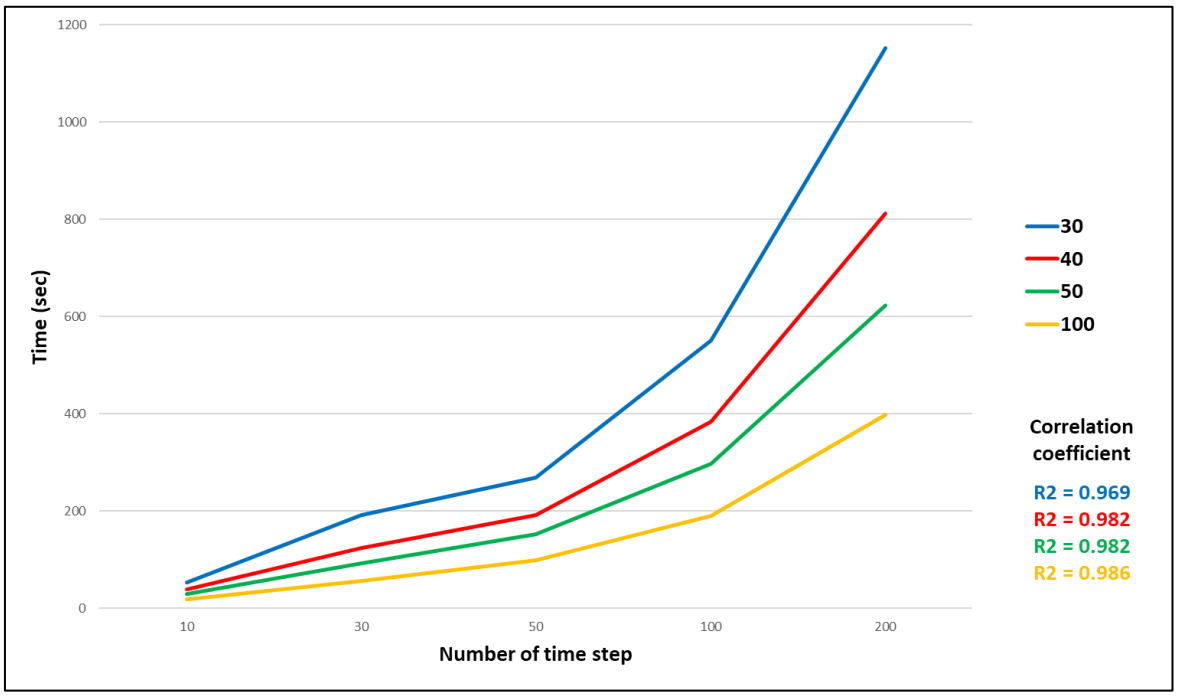

Figure 3.8: Computational time required to generate velocity files within the Matlab PTM depending on the mesh resolution with in blue 30 m, in red 40 m, in green 50 m and in yellow 100 m.

3.2.2 Accuracy

Ocean models use discretized spatial grids, where velocities are computed, e.g. at the corner or edge of the grid cell. Additionally, instantaneous velocity data are output at the specified output frequency. Consequently, it is important that the PTM reconstruct the continuous velocity field at the spatial/temporal resolution of the dispersed particles (Griffies *et al.*, 2000). Two methods of interpolation were used:

- **Temporal dimension:** Velocity output from the ocean model were linearly interpolated from 60 min to 30 min, 20 min, 15 min, 10 min and 5 min. The spatial grid resolution used was 50 m (Figure 3.9).
- **Spatial dimension:** Velocity fields output from the ocean model were bilinearly interpolated from the edges of the grid cell to define velocity at the particle position inside the cell (Goode, 1990; Sebille *et al.*, 2018) (Figure 3.9).

For each PTM, 10,000 particles were released and positioned in a grid formation spread over the western part of the Irish Sea for 8 days (Figure 3.10). For each simulation, the last position of all particles was recorded and used in the subsequent analysis. The relative error (RE) was calculated as described on figure 3.11. For both spatial and temporal resolution tests, particle dispersal were compared with the highest resolution case, which was 50 m and 5 min for spatial and temporal tests respectively.

Interpolation decreases RE of the last positions of all the particles on average for most simulations tested (Figure 3.12). Interpolation to finer temporal resolution of the velocity field showed a linear improvement of RE with $R^2 = 0.997$. Indeed, interpolating velocities from 60 min to 5 min reduced the relative error by 33.8% (Figure 3.12 A). However, RE increased by 15% when 60 min output model was interpolated to 30 min. Interpolating to finer spatial resolutions (< 500 m) of the velocity field reduced RE, although interpolation to > 500 m showed little change in RE (Figure 3.12 B). These results, for the first time, quantify the impact on model accuracy of both linear and bilinear interpolation on temporal and spatial resolution of velocity fields respectively. Also, results show the limit of bilinear interpolation on model accuracy according to the grid resolution.

Linear:

$$y = y_0 + (x - x_0)\frac{y_1 - y_0}{x_1 - x_0}$$

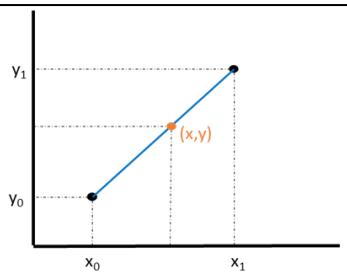

Bilinear:

$$f(R_1) \approx \frac{x_2 - x}{x_2 - x_1} f(Q_{11}) + \frac{x - x_1}{x_2 - x_1} f(Q_{21}) \text{ where } R_1 = (x, y_1)$$

$$f(R_2) \approx \frac{x_2 - x}{x_2 - x_1} f(Q_{12}) + \frac{x - x_1}{x_2 - x_1} f(Q_{22}) \text{ where } R_2 = (x, y_2)$$

$$f(P) \approx \frac{y_2 - y}{y_2 - y_1} f(R_1) + \frac{y - y_1}{y_2 - y_1} f(R_2)$$

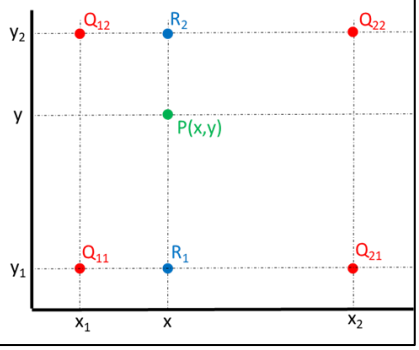

Figure 3.9: Linear and bilinear interpolation method.

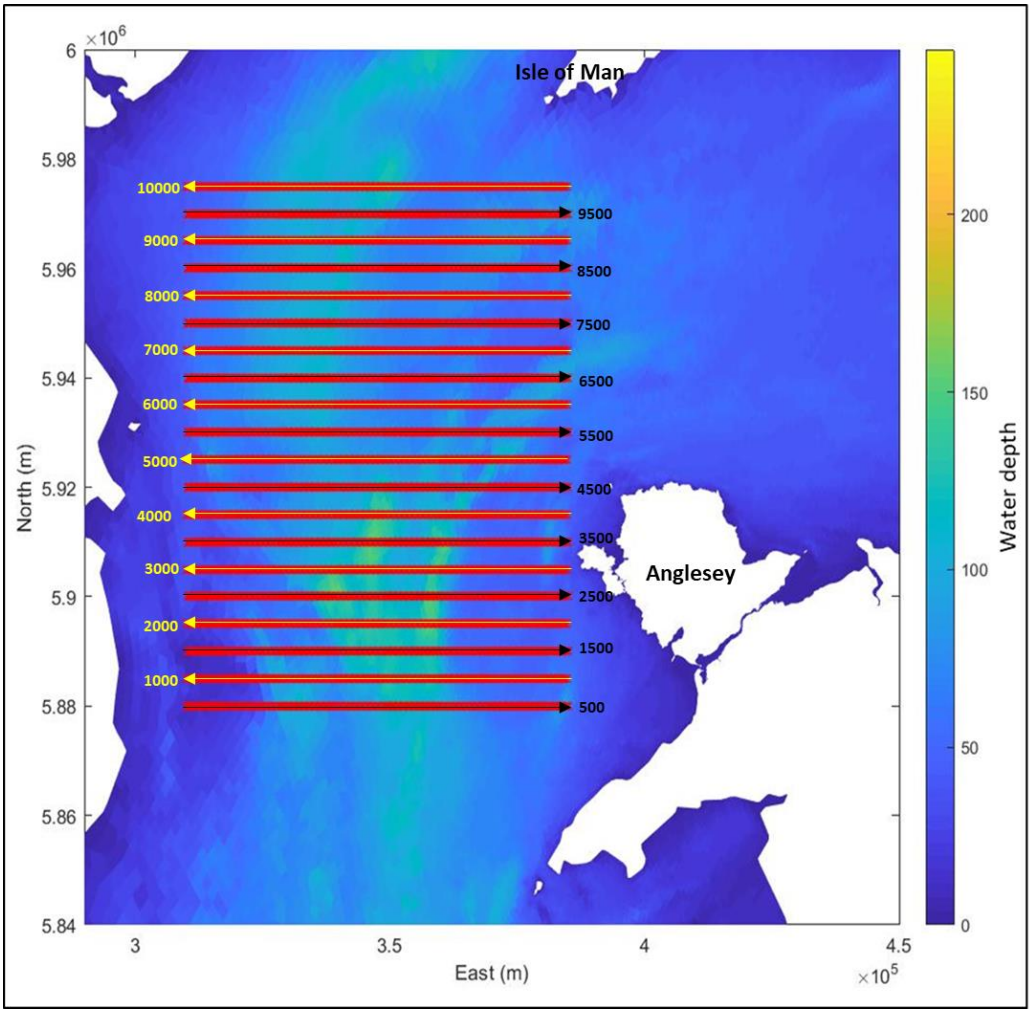

Figure 3.10: Release position for 10,000 particles in the western Irish Sea, arrows represent the sense of particles distribution and numbers are the label of the last particle for each line.

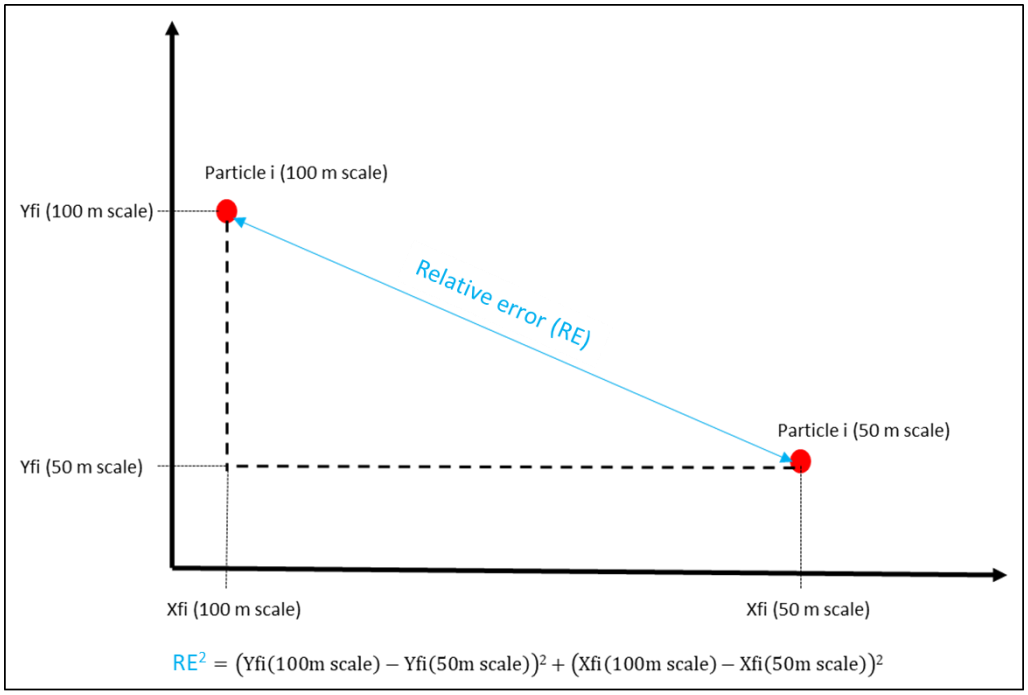

Figure 3.11: Pythagore's theorem applied to calculate the relative error (RE) (blue line) between the final positions of two particles.

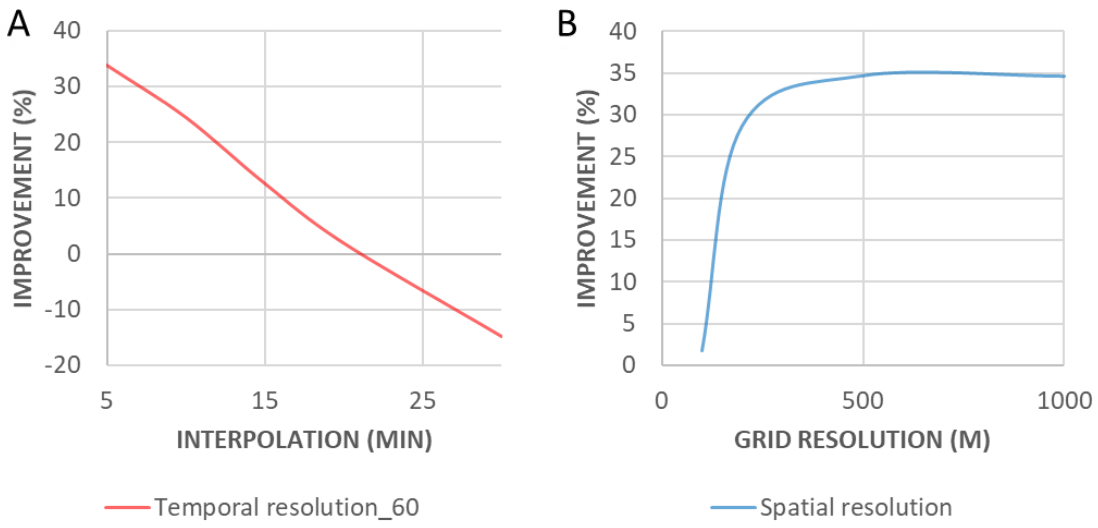

Figure 3.12: Improvement (in %) of the PTM accuracy using: A) linear interpolation for temporal resolution with solid representing 60 min; and B) bilinear interpolation for spatial resolution.

3.3 Spatial resolution

3.3.1 Grid resolution limit to study the Menai Strait

The Menai Strait is a narrow channel with a width variation from 300 m in the Swellies to 1.2 km near Caernarfon (Figure 1.23, Chapter 1). The limit of the grid resolution was tested to study the particle dispersal in the Menai Strait. Six structured grids were generated varying in

resolution from 20 m to 500 m (Figure 3.13). Results showed that a 200 m grid resolution or coarser did not resolved the islands in the Menai Strait (Figures 3.13 D-F). Further, from 300 m to coarser grid resolution, the Menai Strait appeared to be closed at the Swellies (Figures 3.13 E-F). The results highlighted that the grid resolution required to resolve the Menai Strait is < 100 m.

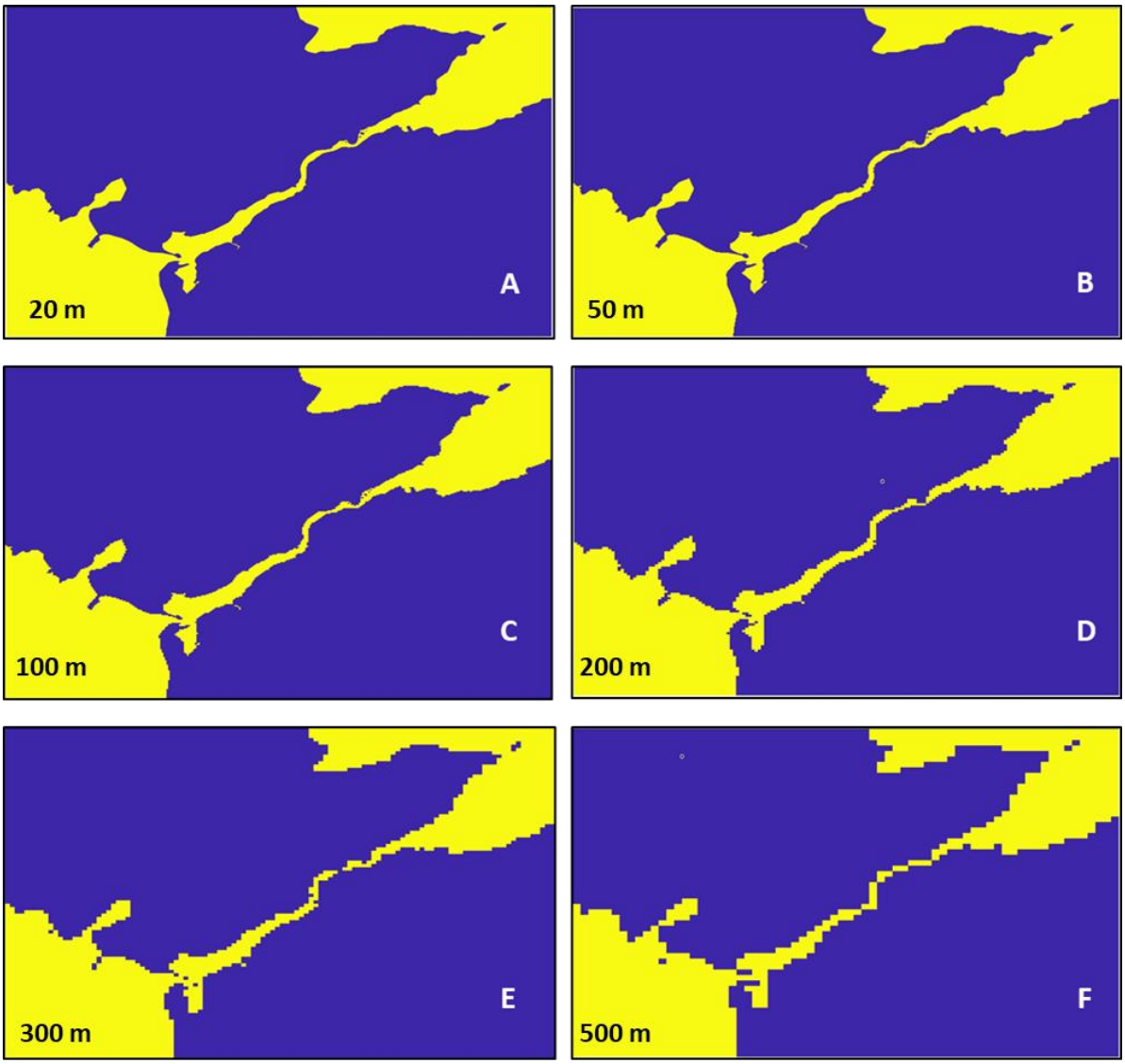

Figure 3.13: Grid resolution of the Menai Strait with values of A) 20 m; B) 50 m; C) 100 m; D) 200 m; E) 300 m; and F) 500 m.

3.3.2 Impact of spatial resolution on PTM accuracy

Five grid resolutions were tested from 50 m to 1,000 m, using a 60 min time step for velocity fields output from the TELEMAC model. Each, PTM was run for 4 days and for 10,000 particles, positioned in a similar way as described in the previous section (see section 3.2.2, Figure 3.10). This area has been chosen to avoid particles interacting with the coast during the

simulation. For each simulation, the last position of all particles was recorded and the relative error (RE) was calculated as described in figure 3.11. Particle dispersal were compared with the highest resolution case (e.g. 50 m).

Figure 3.14 shows that a coarser spatial resolution impacts exponentially the difference of the final position of the particles on average (R^2 = 0.99) (i.e. increased the error). The results showed that RE varied from 34.6 m to 483.2 m on average, for the simulations ran with a 100 m grid resolution and 1,000 m grid resolution, respectively (Figure 3.14). In addition, the range of RE varied exponentially (R^2 = 0.99) from 1.23 km to 15.57 km for the simulation with 100 m and 1,000 m grid resolution respectively. It means that coarser grid increased the possibility to have error > 5 km considered as extreme RE. However, the distance travelled on average for all the particles remained constant for all simulation with a value of 6.85 km ± 0.004 km. The RE varied spatially as shown on figure 3.15. Indeed, the particles located near Anglesey and near to the Irish Coast (south of Dublin) presented a larger relative error (from 2 km and 40 km, in red). Particles located in the middle of the Irish Sea showed the smallest error (from 0 km to 0.5 km, in yellow). A third group is located in the north west part of the Irish Sea, where particles final position presented an error from 0.5 km to 2 km (in orange) (Figure 3.15). Results showed that the relative error (RE) decreased for particles released from South to North, which was correlated with a decrease of the northwards velocity (time averaged velocity among Y axis) (green curve) (Figure 3.16). Further, the relative error also declined from west to east following the reduction of eastwards velocity (time averaged velocity among X axis) (orange curve) (Figure 3.16).

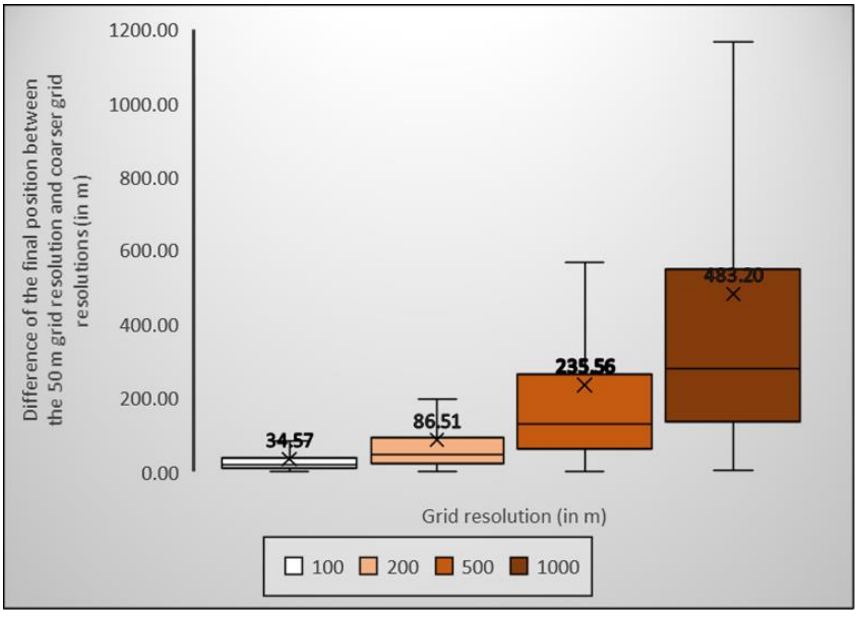

Figure 3.14: Box plot showing the distance of the final position between the finest resolution and coarser resolutions for spatial variation resolution. Darker are the box plots and coarser was the resolution. Results are based on 10,000 particles – showing maximum, minimum, median (crossbar) and average (cross) values.

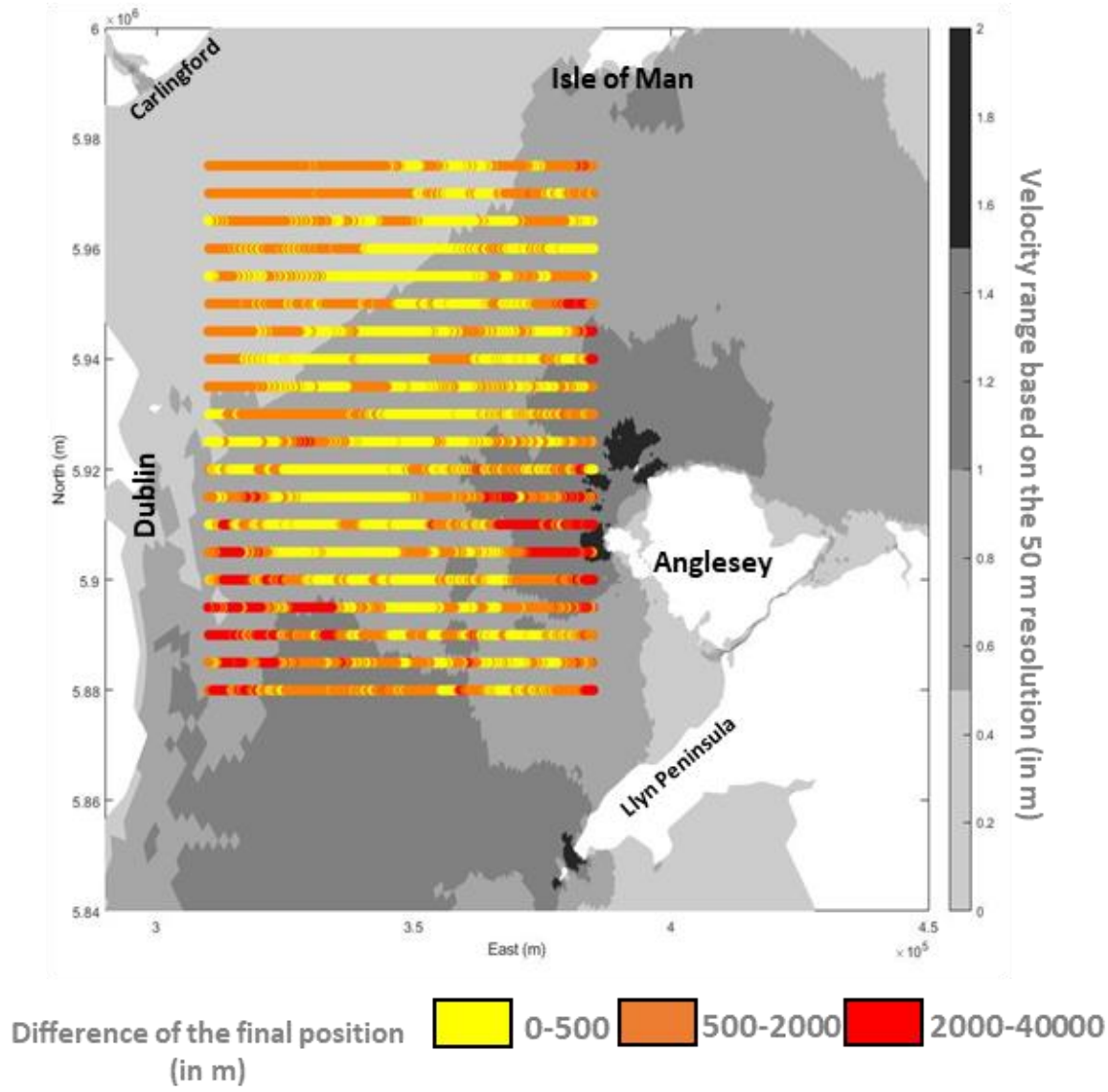

Figure 3.15: Distance of the final position for 10,000 particles depending on the release position between the finest resolution and the coarsest resolution for spatial variation resolution. Particles are ranked with: 1) in yellow error from 0 km to 0.5 km; 2) in orange error from 0.5 km to 2 km; and 3) error from 2 km to 40 km.

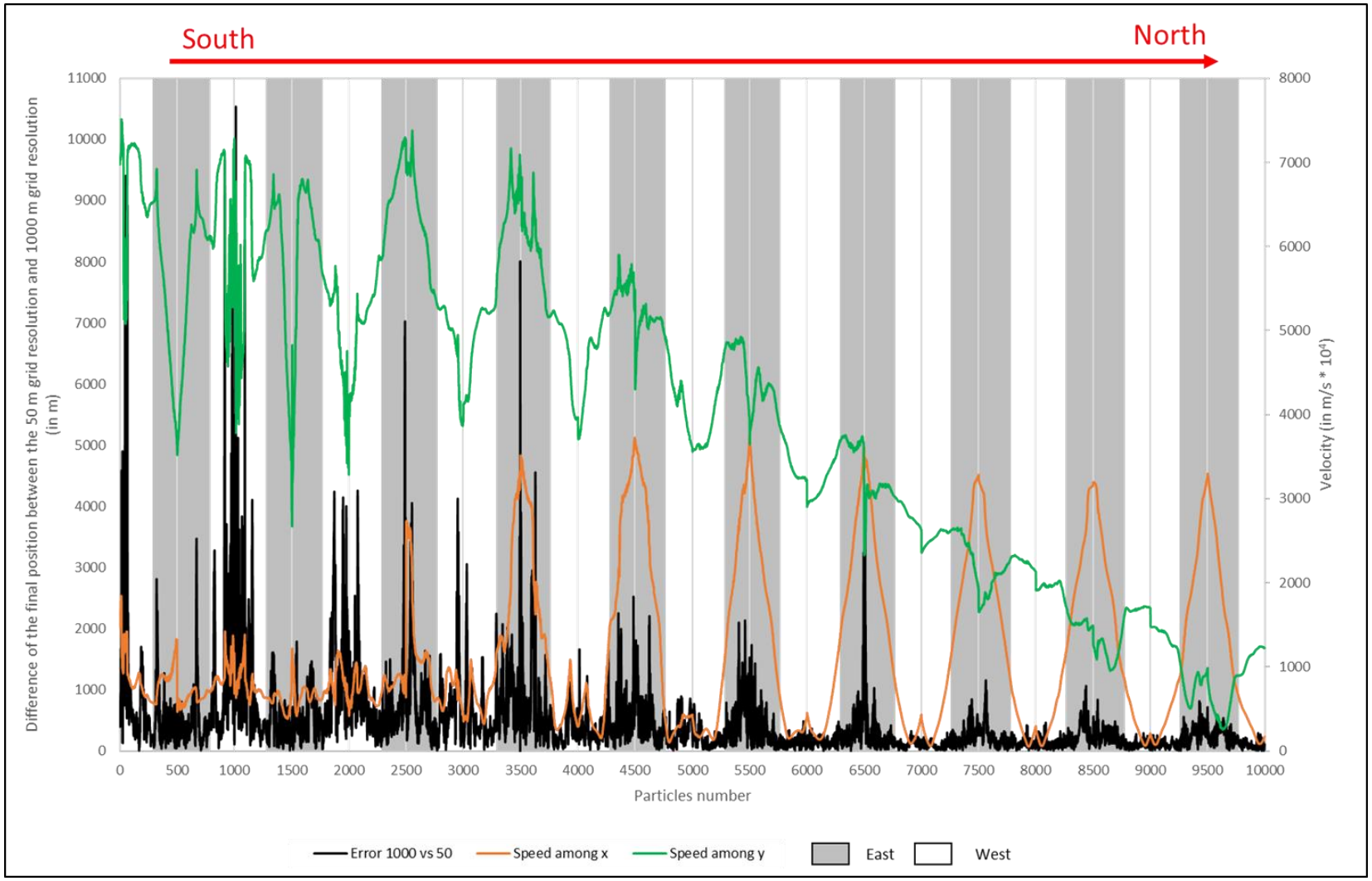

Figure 3.16: Impact of velocity on final position difference between the simulation using 50 m grid resolution and 1,000 m grid resolution with: 1) in black the difference of the final position between 50 m grid resolution and 1,000 m grid resolution (in m); 2) in orange speed among x ($*10^4$ m/s); and 3) in green speed among y ($*10^4$ m/s). The spatial distribution of particles is represented by 1) the red arrow for South-North direction; and 2) grey and white stripes for east and west position respectively

3.4 Temporal resolution impact on PTM accuracy

The same method developed in the section 3.2 was applied to study the impact of temporal resolution on the model accuracy (see section 3.2.2, Figures 3.10 and 3.11). Excepted, that the temporal resolution was tested for timesteps from 5 min to 60 min, using a grid resolution of 1000 m. Particles dispersal were compared with the highest resolution case which was 5 min in this case.

Figure 3.14 shows that a coarser temporal resolution impacts exponentially the difference of the final position of the particles on average ($R^2 = 0.99$) (i.e. increased the error). The results are approximately ten times higher for the temporal resolution than for spatial resolution, with on average 664 m to 4,493 m difference observed for the simulations ran with a 10 min resolution and 60 min resolution, respectively (Figure 3.14.B). The same observation is made for temporal resolution with an increase of the extreme error observed representing 0.78% and 14.5% for 10 min resolution and 60 min resolution respectively. However, the range of RE for the temporal resolution remained constant with a value of 30.81 km ± 3 km. Also, the RE varied spatially as shown on figure 3.18. The temporal resolution tests showed that RE is related to the velocity range (difference between the highest and lowest velocity observed through the period of simulation) (Figure 3.18). Indeed, particles released where the velocity range is higher than 1 m/s showed a higher relative error (> 2 km, in red) and particles released area where velocity range is below 0.5 m/s show a relative error < 500 m (Figure 3.18).

As observed for spatial resolution tests, results showed that the relative error (RE) decreased for particles released from South to North, which was correlated with a decrease of the northwards velocity (time averaged velocity among Y axis) (green curve) (Figure 3.19). Further, the relative error also declined from west to east following the reduction of eastwards velocity (time averaged velocity among X axis) (orange curve) (Figure 3.19).

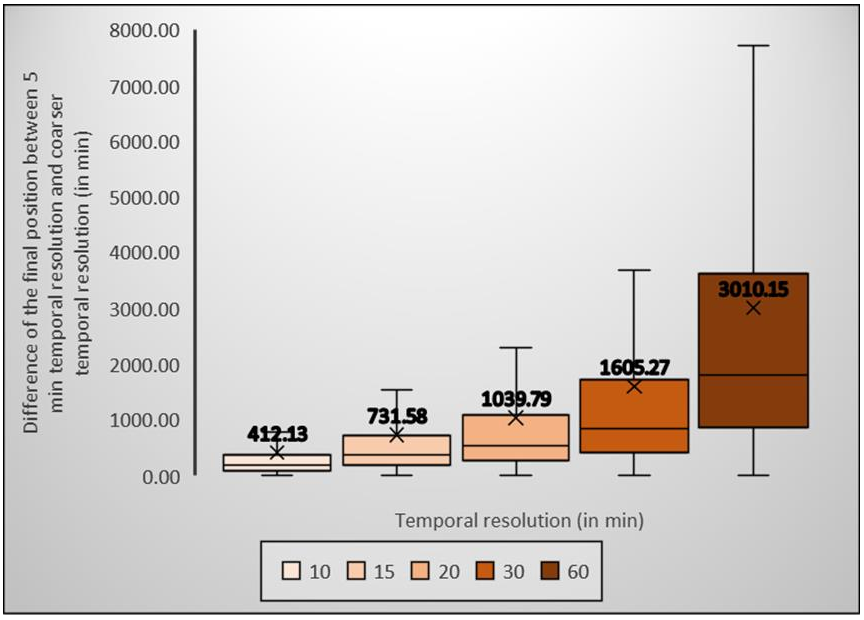

Figure 3.17: Box plot showing the distance of the final position between the finest resolution and coarser resolutions for temporal variation resolution. Darker are the box plots and coarser was the resolution. Results are based on 10,000 particles – showing maximum, minimum, median (crossbar) and average (cross) values.

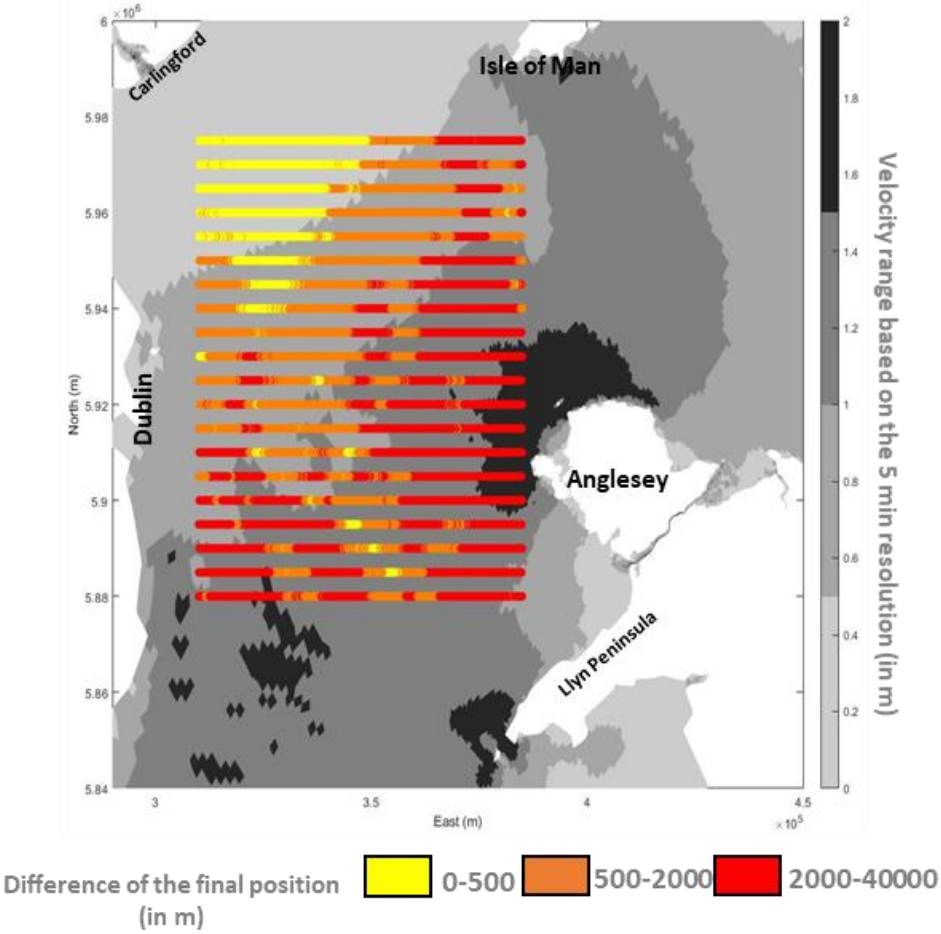

Figure 3.18: Distance of the final position for 10,000 particles depending on the release position between the finest resolution and the coarsest resolution for temporal variation resolution. Particles are ranked with: 1) in yellow error from 0 km to 0.5 km; 2) in orange error from 0.5 km to 2 km; and 3) error from 2 km to 40 km.

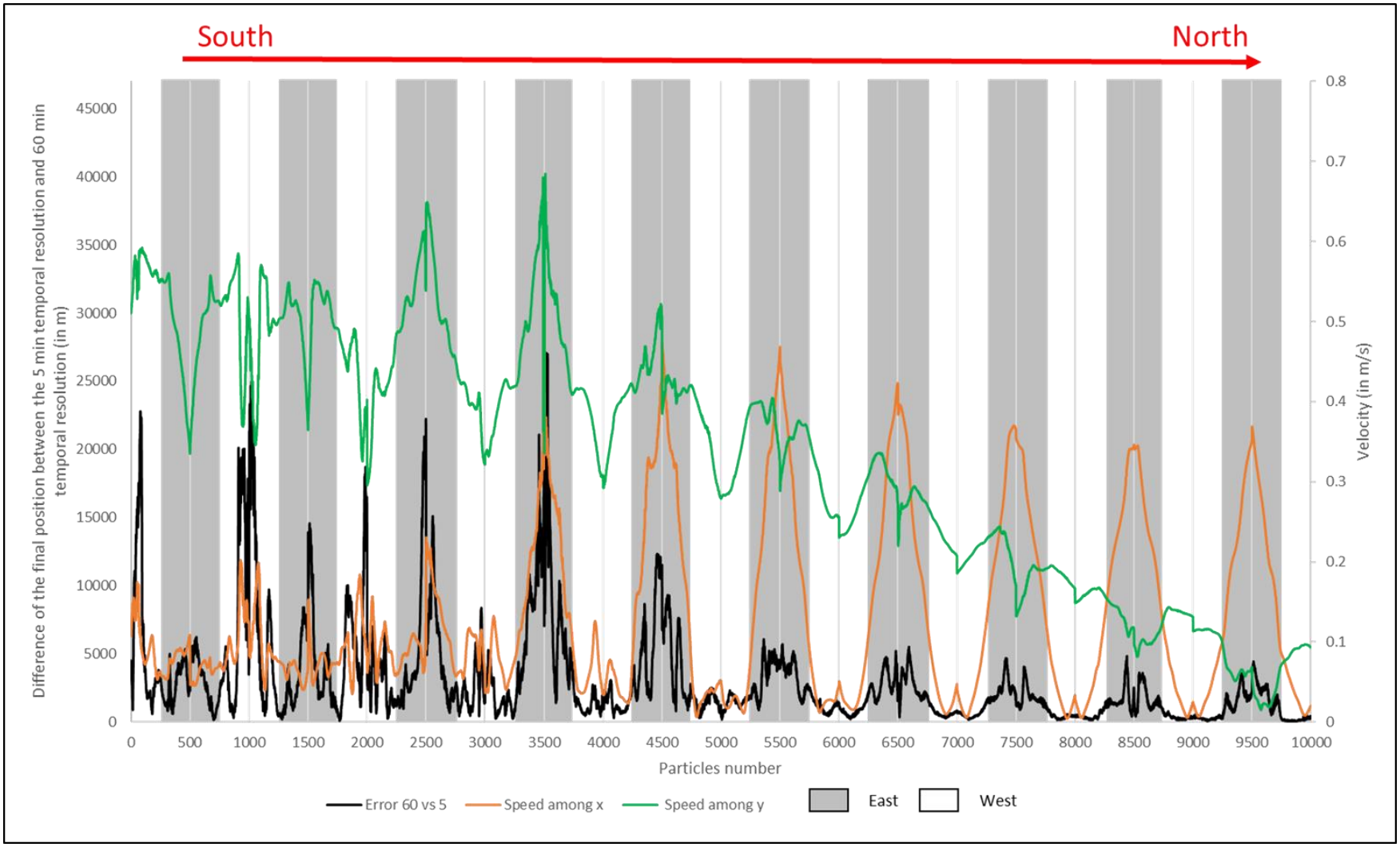

Figure 3.19: Impact of velocity on final position difference between the simulation using 5 min resolution and 60 min resolution with: 1) in black the difference of the final position between 5 min resolution and 60 min resolution (in m); 2) in orange speed among x ($*10^4$ m/s); and 3) in green speed among y ($*10^4$ m/s). The spatial distribution of particles is represented by 1) the red arrow for South-North direction; and 2) grey and white stripes for east and west position respectively.

3.5 Number of particles

3.5.1 Computational efficiency

Mussels are reported to release several billions of gametes during the spawning period, resulting in several millions of larvae in the water column (Sprung, 1983). However, it is computationally impractical to simulate millions of particles. Therefore, the number of particles simulated per PTM was varied in the range 50 to 100,000 to understand how this affects the PTM runtime. This was repeated for different grid resolutions (30 m to 100 m) (Figure 3.20). The test was performed for a short simulation of 25 hours (typical tidal conditions) with 30 min output using the Menai Strait model. The particles were released from the north of Anglesey within an area of 0.04 km^2 (coordinates (in UTM): x = $4.3*10^5$ and y = $5.91*10^6$).

Figure 3.20 shows that 88% of the increase PTM runtime is explained by the number of released particles (R^2 = 0.88 on average for all grid resolution tested). However, no significant difference was observed for the simulations with 50 particles to 2,000 particles. Also, the run-time of the PTM is linearly affected by the grid resolution (R^2 = 0.98) – meaning that the finer the grid the longer the run-time. Nevertheless, the results show that the main parameter to reduce the run-time is the number of particles released per simulation. Indeed, the correlation coefficient values increase when the resolution get coarser. The run-time seemed most efficient for less than 10,000 particles (solid line portion of the curves). However, it is necessary to test whether the number of particles affects the overall particle dispersal distribution.

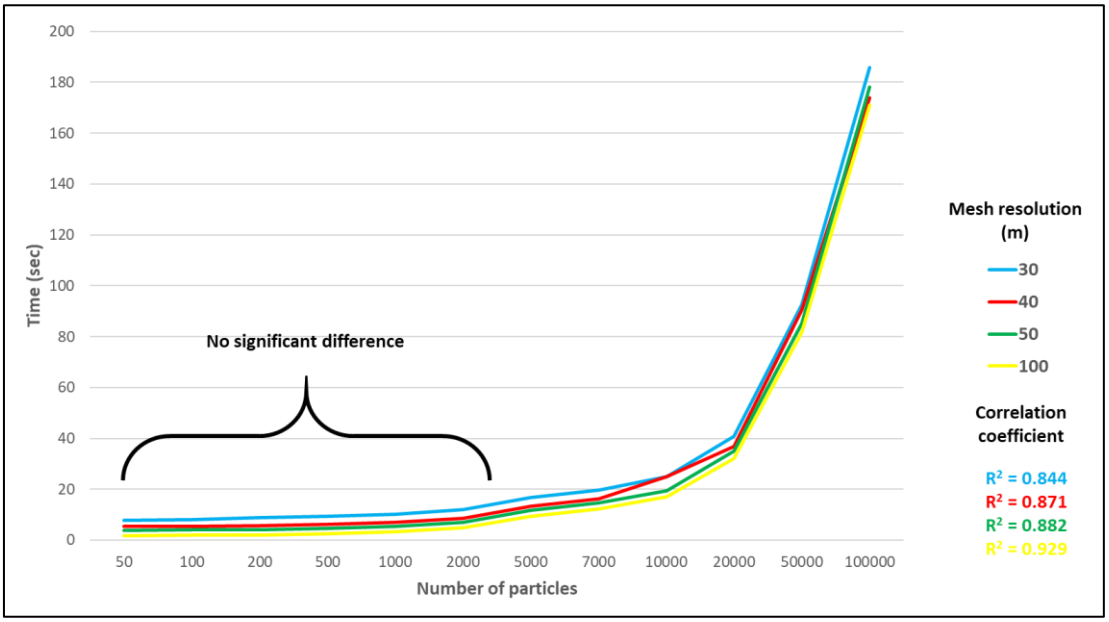

Figure 3.20: Time to run a PTM depending on 1) the number of particles; and 2) the scale of the grid with in blue 30 m, in red 40 m, in white 50 m and in yellow 100 m.

3.5.2 Number of particles limit in the PTM

The first step recommended by Simons *et al.* (2013) was to conduct a sensitivity test to determine the minimum number of particles required to avoid an under-sampling error (Robins *et al.*, 2012). A convergence test was performed to study the optimal number of particles to be used in the PTMs. For all tests, PTMs were simulated for two weeks to capture a spring-neap tidal cycle. Particles were released from northeast entrance of the Menai Strait (coordinates (in UTM): $x = 4.25*10^5$ and $y = 5.9*10^6$) with a random position within an area of 0.04 km^2 (Figure 3.21). For each test, the number of particles was increased from 50 to 15,000 particles, totalling 14 separate simulations. At the end of each two-week simulation, the concentration of particles occurring in the 5 areas surrounding the release site were calculated: 1) southwest Menai Strait; 2) Caernarfon area; 3) the Swellies; 4) Bangor area; and 5) northeast Menai Strait (Figure 3.21). I assumed that the simulation with the most particles (15,000) best represented the dispersal distribution, consequently each simulation was compared to the one with 15,000 particles (Figure 3.22). When the percentage difference in all areas 1-5 fell within 10% difference of the 15,000 particles simulation, I was confident that the simulation statistically represented the dispersal distribution.

The results varied depending on the area. Area 1 showed a convergence of the results from 7,000 particles (5.65% difference) while Area 3 showed a convergence from 200 particles released (9.22% difference) (Figure 3.22). Those results might be the consequence of both the distance from the releasing position and the narrow shape of the Menai Strait, where particles are trapped, especially in the Swellies (47% of the particles released in average for all simulations). Area2, Area 4 and Area 5 showed a good convergence from 1,500 particles, 700 particles and 2,000 particles respectively. Overall, it was assumed that 7,000 particles were needed to statistically represent dispersal within the Menai Strait.

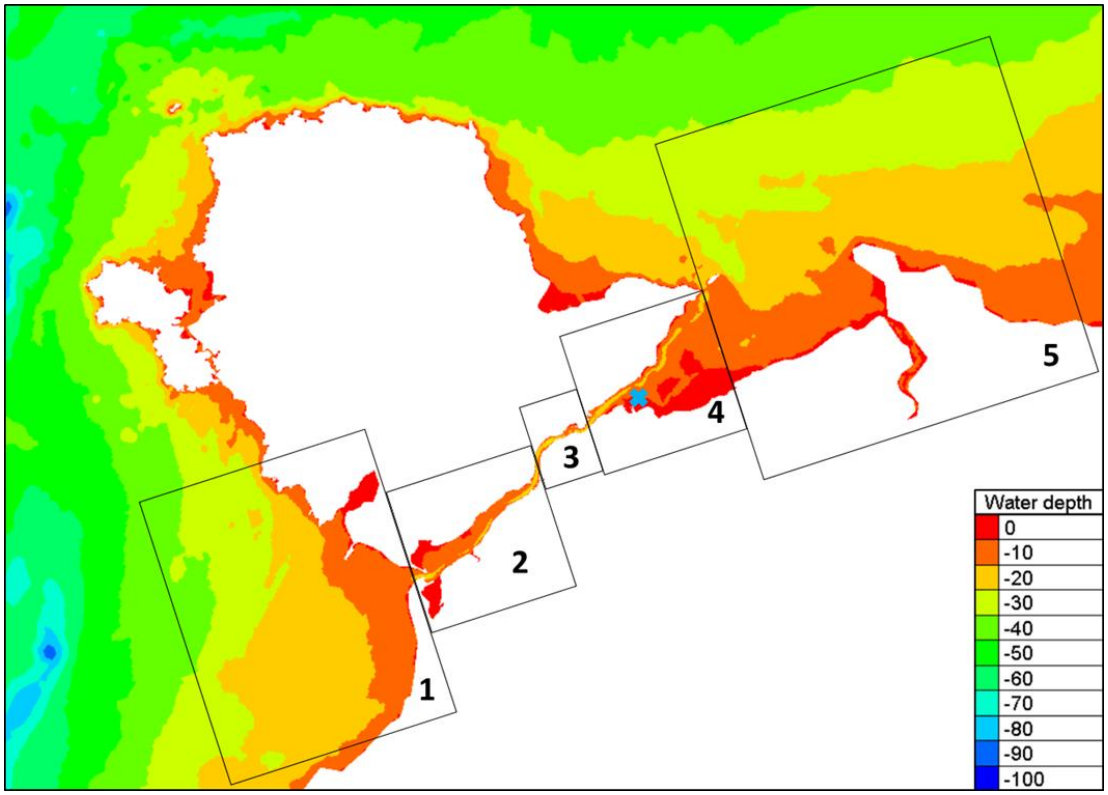

Figure 3.21: Map of the Menai Strait with the limit of five areas of interest for the convergence test with the blue cross corresponding to the release position.

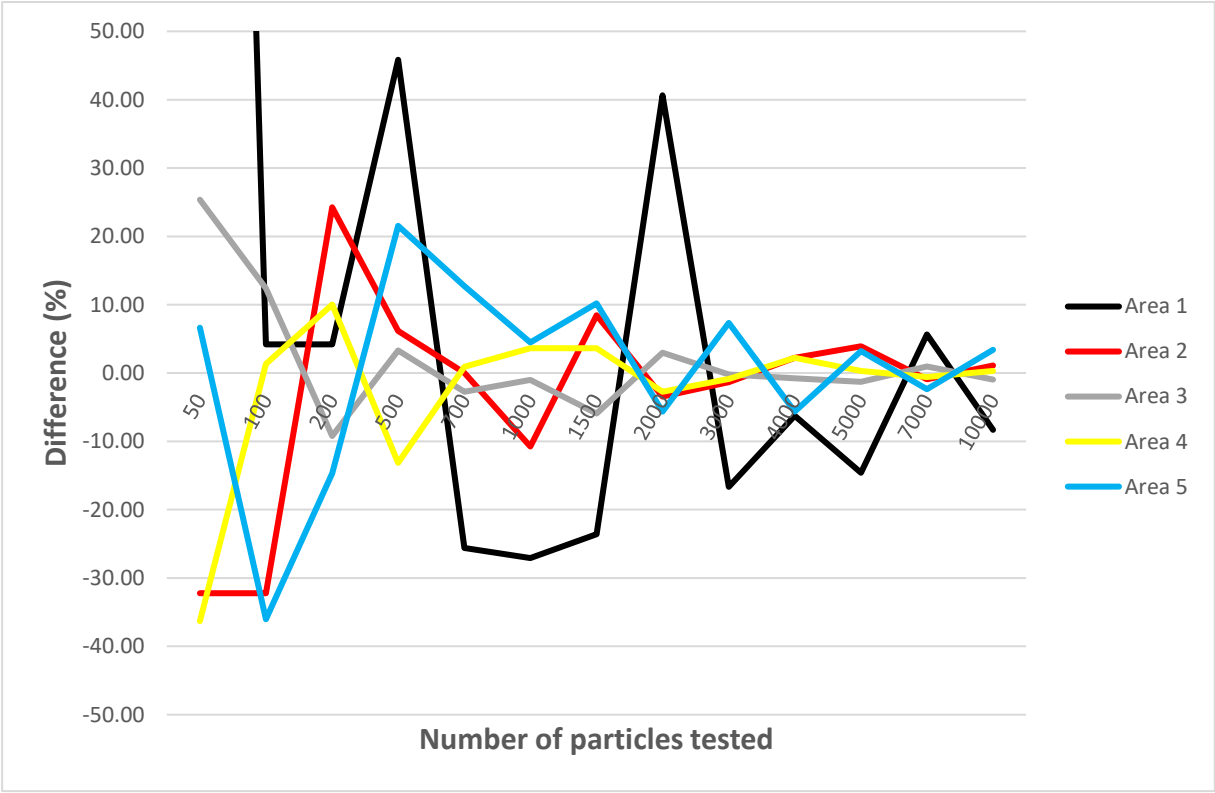

Figure 3.22: Difference of the particles distribution (in %) per area depending on the number of particles tested with areas represented 1) in black for area 1; 2) in red for area 2; 3) in grey for area 3; 4) in yellow for area 4; and 5) in blue for area 5.

3.6 Released area

Litterature showed the importance of released site on larval dispersal at a regional or country scale as the hydrodynamics currents are different, however no previous study show the importance of release area at a mussel bed scale (Hill, 1990; Salomon, 1990; Ellien *et al.*, 2000). Mussel beds size varied from few m^2 to several km^2 (e.g. commercial Bangor mussel bed), which might have an impact on mussel larvae dispersal (e.g. variation of current strength and direction among a single mussel bed). For example, the mussel bed in Bangor expand in length from Beaumaris to Menai Bridge and the width of the Strait, which represents approximately 8.31 km^2. In addition, the residual currents varies greatly among the Bangor mussel bed (Figure 3.23). Consequently, two tests were performed to study: 1) the importance of released location at a mussel bed scale and 2) the importance of size of the released patch.

3.6.1 Release position from a single mussel bed

Sensitivity test was performed to study the variation of particles dispersal from a single mussel bed (e.g. commercial Bangor mussel bed). Particles were released from three locations from northeast entrance of the Menai Strait with a random position within an area of 0.04 km^2: A) Beaumaris (x: $4.266e^5$ and y: $5.9008e^6$ in UTM); B) Bangor harbour (x: $4.26e^5$ and y: $5.8996e^6$ in UTM); and C) Bangor pier (x: $4.245e^5$ and y: $5.8993e^6$ in UTM) (Figure 3.24). At the end of each one-week simulation, the concentration of particles occurring in the 5 areas surrounding the release site were calculated: 1) southwest Menai Strait; 2) Caernarfon area; 3) the Swellies; 4) Bangor area; and 5) northeast Menai Strait (Figure 3.21).

Table 3.2 shows that particles released from Bangor pier (B) and Bangor harbour (C) have the similar particles distribution among the five areas with: 26.4% for area 1, 21% for area 2, 3.9% for area 3, 22.7% for area 4 and 25.2% for area 5. Particles release from Beaumaris (A) are mostly found after ine week in area 5 (40.5%) and less found in area 1 (11.8%).

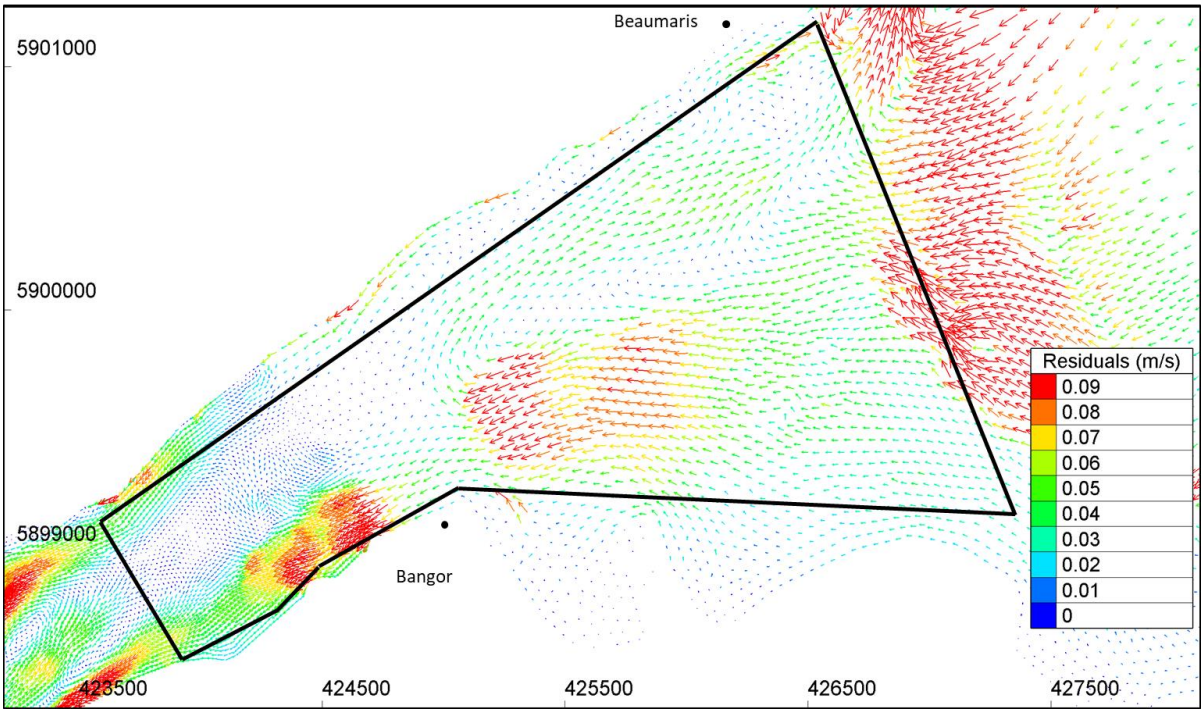

Figure 3.23: Map of the residual currents of the northeastern entrance of the Menai Strait. The black area corresponds to the limit of the commercial Bangor mussel bed.

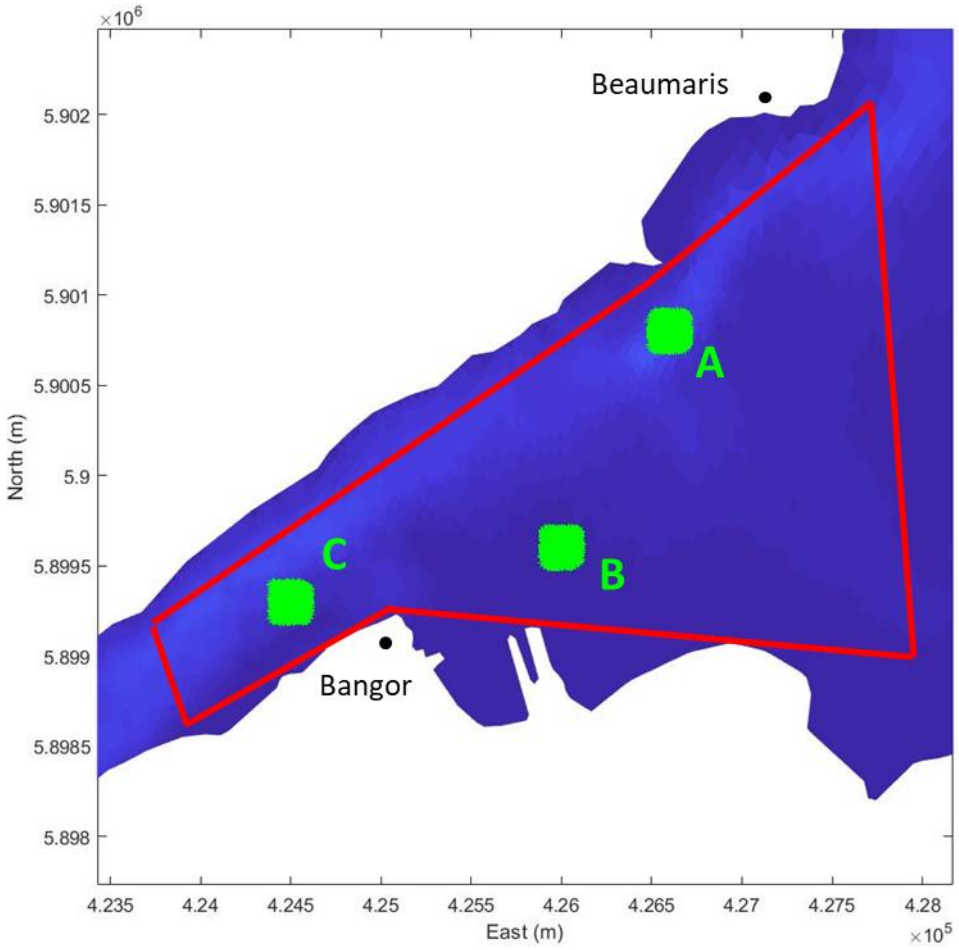

Figure 3.24: Map of the northeastern entrance of the Menai Strait with in green the release positions: Beaumaris (A), Bangor harbour (B) and Bangor pier (C). The red area corresponds to the limit of the commercial Bangor mussel bed.

Table3.2: Sensitivity on the release location at the scale of a mussel bed in the Menai Strait. Results show the distribution (%) of 7,000 particles released from three locations (A,B,C) per area after one week simulation.

	Particles per areas (%)				
Sites of release	1	2	3	4	5
A	11.8	15.4	4.3	28.0	40.5
B	27.7	21.7	3.9	19.7	27.0
C	25.1	22.2	3.8	25.6	23.3

3.6.2 Size of released patch

Sensitivity test was performed to study the impact of the size of released patch on particles dispersal. Particles were released from Bangor harbour (e.g. northeast entrance of the Menai Strait, x: $4.26e^5$ and y: $5.8996e^6$ in UTM) with a random position within an area of: 1) $4e^{-5}$ km^2; 2) $1.6e^{-3}$ km^2; 3) $1e^{-2}$ km^2; 4) $4e^{-2}$ km^2; 5) $1.6e^{-1}$ km^2; and 5) 1 km^2 (Figure 3.25). At the end of each one-week simulation, the concentration of particles occurring in the 5 areas surrounding the release site were calculated: 1) southwest Menai Strait; 2) Caernarfon area; 3) the Swellies; 4) Bangor area; and 5) northeast Menai Strait (Figure 3.21).

No significant difference was observed among the simulations with 12% ± 3% for area 1 , 19% ± 1% for area 2, 5% ± 2% for area 3, 28% ± 1% for area 4 and 37% ± 2% for area 5.

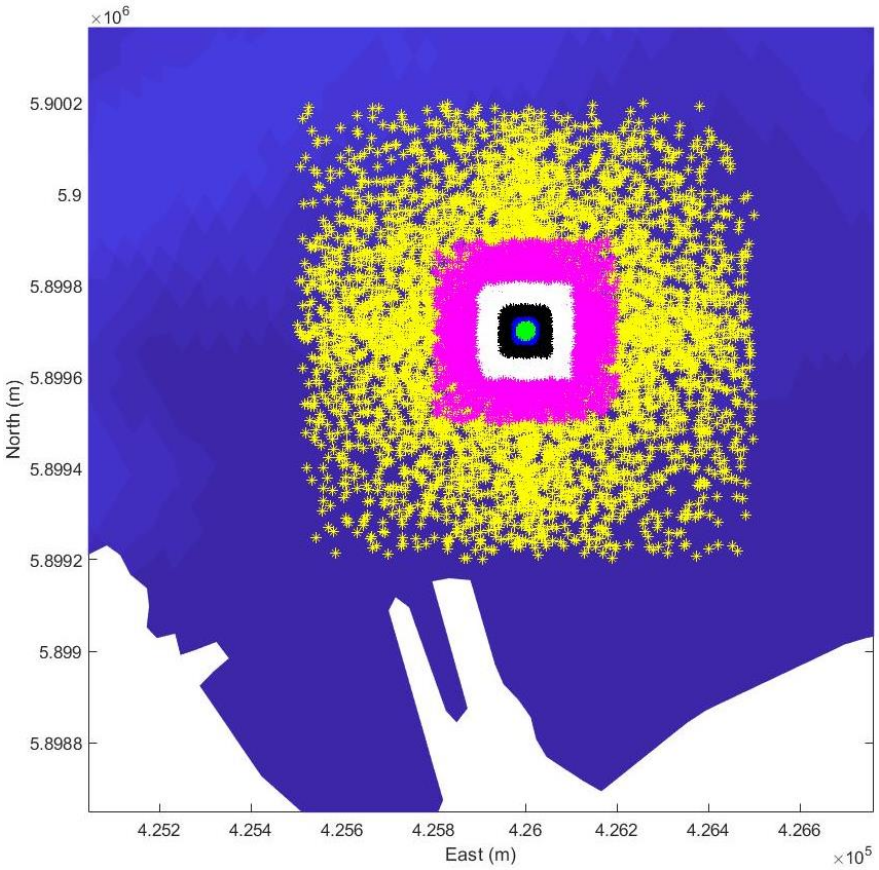

Figure 3.25: Map of the northeastern entrance of the Menai Strait at Bangor harbour representing the size of released patches: 1) $4e^{-5}$ km^2 (green); 2) $1.6e^{-3}$ km^2 (blue); 3) $1e^{-2}$ km^2 (black); 4) $4e^{-2}$ km^2 (white); 5) $1.6e^{-1}$ km^2 (magenta); and 5) 1 km^2 (yellow).

3.7 Validation of PTM via observed drifter trajectories

The results obtained in the previous sections should be verified against existing observations (Kozalka *et al.*, 2010; Sebille *et al.*, 2018). One way to validate PTMs is to compare modelled particles trajectories with observed drifter trajectories (Edwards *et al.*, 2006; De Dominicis *et al.*, 2012).

3.7.1 Materials and methods

For this project, two drifters were released from different locations at the surface in the eastern Irish Sea, close to the Bangor mussel bed but outside the constriction of the Menai Strait. They were set at a depth 1.5 m below the surface and their positions were recorded every 10 min as they were transported with the tidal currents, as described below (Figure 3.26):

- **Drifter 1** was released on 27/04/2018 at 9:30 am from the east of Puffin Island (53.31 and -3.99 in latitude and longitude respectively). The drifter was taken out of the water

on 29/04/2018 at 12:30 to the west of Puffin Island (53.32 and -4.04 in latitude and longitude respectively) (Figure 3.26.B).

- **Drifter 2** was released on 14/05/2019 at 12:00 am from north of Llandudno (53.39 and -3.94 in latitude and longitude respectively). The signal of the drifter was lost on 17/05/2019 at 3:00 when the drifter was north of Anglesey (53.62 and -4.42 in latitude and longitude respectively) (Figure 3.26.A). However, the buoy was recovered on Seascale beach (North west coast of England) around June. Unfortunately, it was not possible to use this last position to validate the particle tracking model as the exact date and position of landing on beach are not known.

The Lagrangian PTM described in section 3.1.1 was used here to retrace the drifter trajectory (see Appendix C). Velocity fields output from the ocean model were linearly interpolated in time from 30 min to 5 min, according to the results obtained in section 4 (Figure 3.17), then bi-linearly interpolated in space to the position of each particle. The Menai Strait hydrodynamic model was used to test the PTM on Drifter 1 while the Irish Sea model was used for Drifter 2. In both cases, 7,000 particles were released from the released position of both drifters. The velocity data used in the PTM was depth-averaged, interpolated onto a 20 m resolution grid. However, the drifters were released near the surface, where velocities are potentially stronger than the depth averaged values (because less frictional influence near the surface), and subjected to wind-driven forces and waves effects (Weber, 1981; Weber, 1983; Prandle, 1982; Wu, 1983; Proctor *et al.*, 1994; Chang *et al.*, 2012; Genç *et al.*, 2015; Afenyo *et al.*, 2016). Consequently, an approximation of the surface current was calculated based on literature. The surface wind-driven current is generally between 1.9% and 3.5% of the wind speed (Proctor *et al.*, 1994; Chang *et al.*, 2012). The equations given by Proctor *et al.* (1992) and Chang *et al.* (2012) were tested on both drifters (Equation 3.1). Wind speed data were downloaded from Centre for Environmental Data Analysis website (https://www.ceda.ac.uk/) for the stations Valley on Anglesey (53.25 and -4.53 in latitude and longitude respectively) used for Drifter 1 and for Rhyl (53.31 and -3.50 in latitude and longitude respectively) used for Drifter 2 (Figure 3.26.A). Hourly wind data were linearly interpolated to 5 min to fit the PTM temporal resolution. The surface velocity is typically between 7% to 15% higher than the depth-averaged velocity for shallow water and deeper water, respectively (Prandle, 1982). Consequently, the depth-averaged velocity computed from the hydrodynamic model was increased by 7% and 15% to study the drifter 1 and drifter 2, respectively (Equation 3.2). Finally, a stochastic term that represents sub-grid-scale mixing was added to the particles displacement to simulate diffusion in the environment that is not accounted for the hydrodynamic model (Okubo, 1971; Hunter *et al.*, 2012; Proctor *et al.*, 1994; La Case & Boyer, 2000; Chung & Duyen, 2012; Robins *et al.*,

2012; Kosalka *et al.*, 2013; Robins *et al.*, 2013; Sayol *et al.*, 2014; Afenyo *et al.*, 2016; Sebille *et al.*, 2018). Here, the equation used by Proctor *et al.* (1994), Ross & Sharples (2004) and Robins *et al.* (2013) was used but with a constant coefficient of diffusion, K (Equation 3.3). In summary, the particles displacement in time were calculated as the sum of: 1) advection from surface tidal current; 2) advection from surface wind-driven currents; and 3) sub-grid-scale turbulent diffusion (Equation 3.4).

Three PTM tests were performed on both Drifter 1 and Drifter 2. Test 1 simulated particle advection only using the depth-averaged velocity computed by TELEMAC. Test 2 simulated particle advection only using the approximation of tide-driven and wind-driven surface flows as described above. The method which gave the best result (the smallest difference between last particles position and last recorded drifter position on average for all particles) in Test 2 will be used in the Test 3. In Test 3, particle dispersal was simulated but this time included sub-grid-scale turbulent mixing. The test was repeated varying the diffusion coefficient K from 0 to 10 m^2/s. For each case, three PTM simulations were performed, since the mixing process is random and will generate different particle trajectories. Two metrics were calculated to validate the PTM: 1) the difference between PTM trajectories and the drifters were calculated at each time step (10 min) enabling the root mean squared error (RMSE) to be calculated; and 2) the difference between last positions of the particles and drifters (RE) (Figure 3.11).

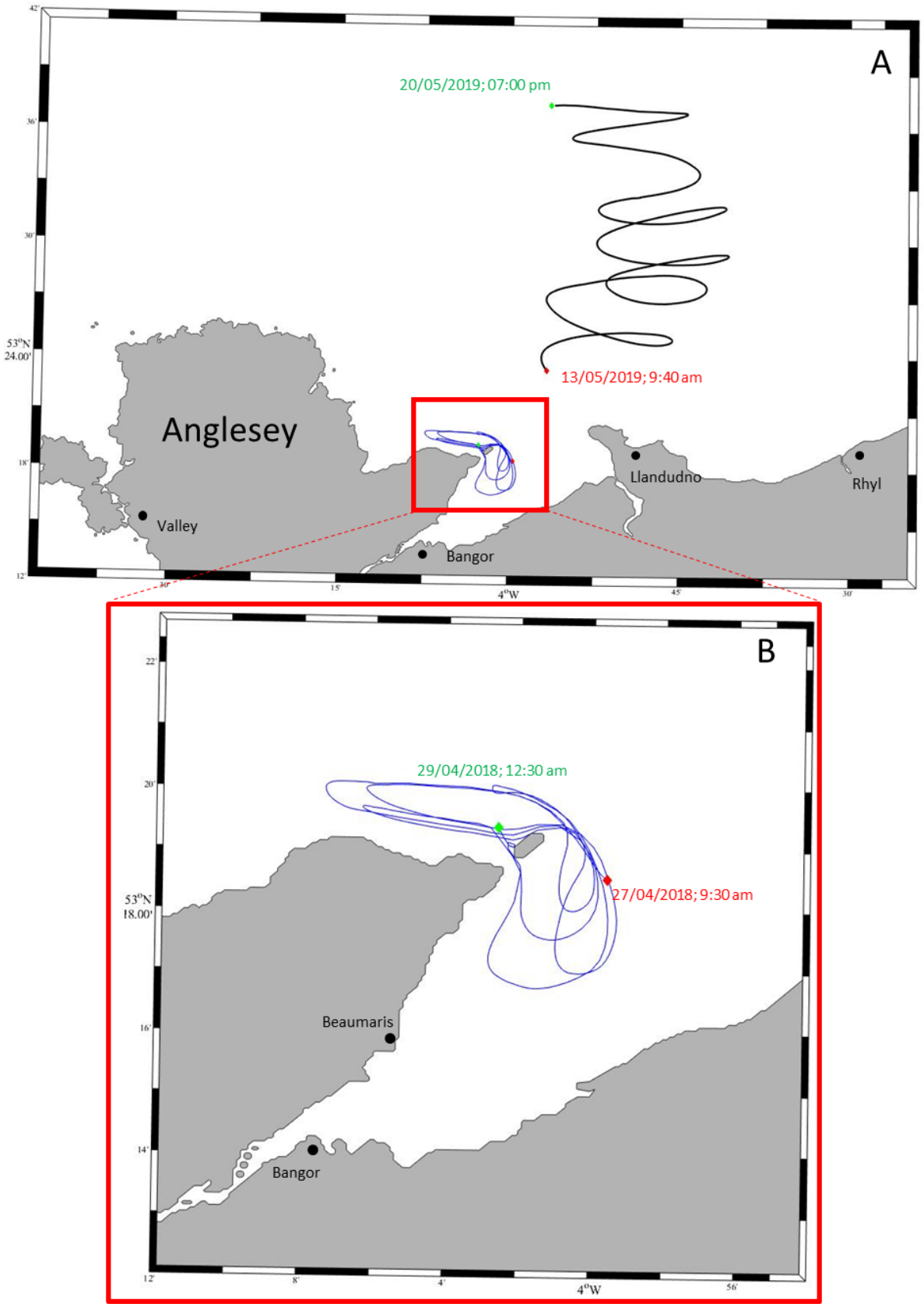

Figure 3.26: Drifters trajectories with: 1) in blue Drifter_1 (released in 2018); and 2) in black Drifter_2 (released in 2019). First and last position are represented by red and green respectively.

$$U_{windimpact} = U_{wind} * 0.035$$
$$V_{windimpact} = V_{wind} * 0.035$$

(1) Proctor *et al.* (1992)

$$U_{windimpact} = U_{wind} * 0.019 + 0.06$$
$$V_{windimpact} = V_{wind} * 0.019 + 0.06$$

(2) Chang *et al.* (2012)

Equation 3.1: Approximation of the wind impact on surface current tested with U_{wind} and V_{wind} which are the x any wind component respectively downloade from Ceda.

$$U_{surface} = U_{model} * 1.07$$
$$V_{surface} = V_{model} * 1.07$$

Drifter 1

$$U_{surface} = U_{model} * 1.15$$
$$V_{surface} = V_{model} * 1.15$$

Drifter 2

Equation 3.2: Approximation of the surface velocity with U_{model} and V_{model} velocity from Telemac hydrodynamic model.

$$x_{diffusivity} = \frac{A}{r} * \cos(2\pi A) * \sqrt{(2K\Delta t)}$$
$$y_{diffusivity} = \frac{A}{r} * \sin(2\pi A) * \sqrt{(2K\Delta t)}$$

Equation 3.3: Random displacement model for longitudinal and lateral diffusion (x and y respectively) with 1) Δt is the time step (in s); 2) A is a random in the range [0,1]; 3) r is the standard deviation of Acos(2πA) with a value of $1/\sqrt{6}$; and 4) K is the coefficient diffusion (m^2/s).

$$x(it+1, ip) = x(it, ip) + (U_{surface} + U_{windimpact}) * \Delta t + x_{diffusivity}$$
$$y(it+1, ip) = y(it, ip) + (V_{surface} + V_{windimpact}) * \Delta t + y_{diffusivity}$$

Equation 3.4: Particle position at t+1 depending on 1) particle position at t; 2) surface velocity ($U_{surface}$ and $V_{surface}$); 3) wind impact velocity ($U_{windimpact}$ and $V_{windimpact}$); and 4) diffusivity ($x_{diffusivity}$ and $y_{diffusivity}$).

3.7.2 Results

Comparison of results from Test 1 and Test 2 showed:

(1) for Drifter 1: An improvement of RE of 27% when wind-driven currents were included from Proctor *et al.* (1992), but a deterioration of 96% when wind-driven currents were included from Chang *et al.* (2012) (Table 3.3).

(2) for Drifter 2: Inclusion of both wind-driven approximations reduced the relative error for the last position, by 36% and 79% for Proctor *et al.* (1992) and Chang *et al.* (2012), respectively (Table 3.3).

The simulation using the equation from Proctor *et al.* (1992) gave best results for Drifter 1, while the equation from Chang *et al.* (2012) gave best results for Drifter 2 with RMSE values of 2,643 m and 6,523 m, respectively, on average for all particles (Table 3.3). The minimum relative error for the last position of particles was 639 m and 5,997 m for Drifter 1 and Drifter 2, respectively (Table 3.3). Consequently, the equations from Proctor *et al.* (1992) and Chang *et al.* (2012) were used in Test 3 for Drifter 1 and Drifter 2 respectively.

The test 3, where sub-grid-scale mixing was included, showed significant improvements for the relative error on the last position for drifter 2 only (Table 3.4). The best results for Drifter 2 was 39 m obtained with K = 4 m^2/s. However, results using diffusivity of 8 m^2/s and 9 m^2/s gave similar answers. The improvement observed varied from 99% and 79% for K = 4 m^2/s and K = 1 m^2/s respectively. Results were not improved significantly for the relative error of the last position for Drifter 1 with a value of 739 m ± 90 m for all diffusivity values tested (Table 3.4). Indeed, results highlighted a decline of the RE between 2% and 23% for K = 6 m^2/s and K = 9 m^2/s respectively. RE on average for all particles did not vary among the different simulations for Drifter 1. However, the closest particle to the drifter was 653 m obtained with K = 6 m^2/s. An increase of the diffusivity coefficient led to an increase of the range of RE simulated, as expected, but the average RE of the last position remained similar for both drifters (Table 3.4). Figure 3.27 showed that particle with the closest trajectory to the drifter is different to the particle with the closest last position for both drifters.

Table 3.3: Sensitivity test on: 1) advection only (Test 1); and 2) wind approximation using two different equations (Test 2) for Drifter 1 and Drifter 2. RMSE are presented for both Test 1 and Test 2 with in red the best values highlighted for both drifters.

		Drifter 1			**Drifter 2**		
		Test 1	***Test 2***		***Test 1***	***Test 2***	
			Proctor *et al.* (1992)	Chang *et al.* (2012)		Proctor *et al.* (1992)	Chang *et al.* (2012)
Distance (in m)	Average	3621.99	**2634.27**	7134.44	30996.58	19976.23	**6523.52**
	Minimum	3268.40	**639.44**	6890.11	29825.53	19208.18	**5997.14**
	Maximum	3952.77	9400.57	7255.23	32071.50	20895.78	7092.91
	Range	684.37	8761.13	365.11	2245.97	1687.61	1095.77

Table 3.4: Sensitivity test on coefficient diffusivity (in m^2/s) for Drifter 1 and Drifter 2. Results show the relative error (RE) for 7000 particles simulated for: 1) the average; 2) the minimum; 3) the maximum; and 4) the range.

Drifter id	**Distance**	**Diffusivity K (in m^2/s)**									
		1	*2*	*3*	*4*	*5*	*6*	*7*	*8*	*9*	*10*
Drifter 1	Average	1834.94	1925.68	1995.36	2062.50	2109.28	2160.59	2202.47	2237.65	2259.88	2295.53
	Minimum	766.39	744.52	744.49	767.07	719.51	**653.28**	673.76	706.54	834.52	778.53
	Maximum	5113.60	5504.74	5090.26	5458.58	5066.74	5398.98	5835.45	5716.25	5317.10	5655.24
	Range	4347.20	4760.22	4345.77	4691.51	4347.23	4745.70	5161.69	5009.70	4482.57	4876.72
Drifter 2	Average	6699.88	6881.51	7107.35	7241.25	7522.80	7724.39	7845.19	7491.40	8420.09	6037.896
	Minimum	1241.19	714.67	248.75	**39.32**	183.74	202.78	69.45	39.83	43.17	108.03
	Maximum	12523.93	15718.06	16995.66	18445.62	20152.61	21122.25	22342.34	21250.82	23718.96	20227.64
	Range	11282.74	15003.39	16746.91	18406.3	19968.87	20919.47	22272.89	21210.98	23675.79	20119.61

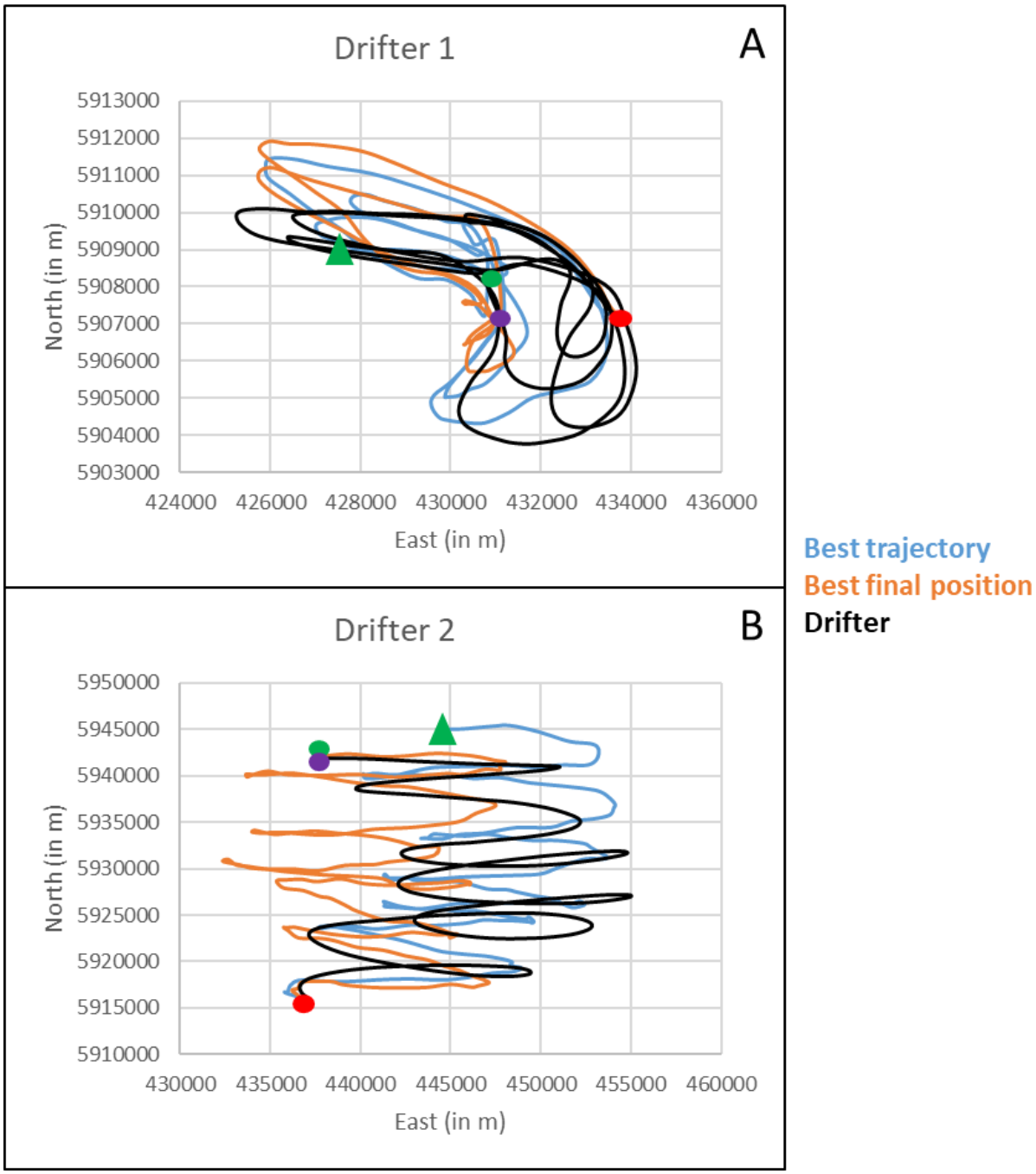

Figure 3.27: Best particle trajectory (in blue) and best finale position (in orange) of 7,000 particles simulated compared to Drifter 1 (A) and Drifter 2 (B) (both in black). The starting position is representing by a red dot. Final positions are indicated by: 1) by a green triangle for the best trajectory; 2) by a green dot for the best final position; and 3) by a purple dot for the drifter.

3.8 Conclusions from Chapter 3

Testing and optimising the computational runtime of the particle tracking model is an important step for research sensitivity studies that use large data sets. A practical compromise needs to be met between increasing the spatial and temporal resolution of the model and the computational runtime. The PTM developed for this study comprises three parts: 1) creation of an orthogonal mesh from a triangular mesh, e.g. limit of the domain and velocity interpolation; 2) input parameterisation, e.g. number and location of particles; and 3) determination of the particles motion through space and time. Parts 1 and 2 impact the PTM computational time (Figure 3.1), hence, sensitivity tests were done on these parts as shown in table 3.1.

The PTM runtime to create an orthogonal mesh of interpolated velocities was function of the size of the domain and the spatial grid resolution (Figure 3.7). The runtime increased linearly with the domain size, whereas the spatial grid resolution influenced the runtime exponentially (Test-1, Figure 3.7). The upper limit of grid resolution was established for this study (10 m) for both Irish Sea and Menai Strait model, due to the storage memory within Matlab. However, working with a smaller domain would enable a finer mesh resolution (< 10 m) to be created. The velocity interpolation from the TELEMAC unstructured mesh to an orthogonal grid was exponentially influenced by the number of velocity files generated (R^2 = 0.98), i.e., the interpolation process slowed down over time due to reduced storage memory (Figure 3.8). Test-2 (which tested the number of velocity files interpolated according to the grid resolution for the Menai Strait model) also showed that grid resolution also influenced the runtime for velocity interpolation but linearly (R^2 = 0.88). Using these results, it is possible to pre-determine the time required for the first part of the PTM to run. For example, to simulate 2 months (2,928 time steps of 30 min), it will take approximately 3 days and 6.5 days for the Menai Strait and the Irish Sea models respectively.

The third part of the PTM contains the equation for the motion of the particles through space and time. As one would expect, increasing the number of time steps increased the PTM runtime linearly. Results showed that grid resolution impacted the PTM runtime linearly (R^2 = 0.98). Indeed, for the same domain, a grid resolution of 50 m took twice as long as a 100 m grid resolution. Further, this study showed that PTM runtime increased exponentially according to the number of particles released (R^2 = 0.88) (Figure 3.20). However, the runtime was markedly reduced for simulations containing less than 10,000 particles. Sprung (1983) showed that *Mytilus edulis* release several billions of gametes during the spawning period. However, in this study, it was computationally impractical to simulate millions of particles. According to the

results, a simulation of 10,000 particles for a period of 2 months with a grid resolution of 20 m will take approximately 2 hours using the Menai Strait model and 6 hours using the Irish Sea model.

The tests undertaken on the computational efficiency of the PTM showed that the least efficient part of the PTM is the interpolation of velocity (part 1). However, once the velocity has been interpolated it can be reused for several simulations that cover the same time period. The runtime can be reduced by reducing the resolution of the mesh (e.g. create a coarser mesh) or reducing the number of particles simulated. Therefore, these two parameters must be studied to assess their impact on model accuracy.

Firstly, the number of particles released from a source location must be evaluated; too few particles may misrepresent the realistic range of dispersal, whereas too many will result a PTM runtime that is inefficient (Macdonalds *et al.*, 2006). For this study, the minimum number of particles to be simulated was established as 7,000, above which the dispersal range did not vary markedly (Figure 3.22). However, the minimum number could be reduce in area with weaker and less complex current than the Menai Strait (Simons *et al.*, 2013). Secondly, the spatial and temporal resolution of the Menai Strait is major importance to simulate accurately the particle dispersal within the channel. The Strait with a minimum width of 300 m in the Swellies (Kratzer *et al.*, 2003). Results here showed that the grid resolution required to resolve particle dispersal through the Swellies is < 100 m (Figure 3.13). Above this limit, the coastline and islands are poorly resolved (200 m). Because of the narrow width of the Menai Strait, the future sensitivity tests on spatial and temporal resolution were performed in the western part of the Irish Sea to avoid particles interacting with the coast.

According to the literature, higher spatial and temporal resolution improves model performance and so particle trajectory accuracy (Vadivieso Da Costa & Blanke, 2004; Andrejev *et al.*, 2011; Qin *et al.*, 2014; Putman & He, 2013; Kvile *et al.*, 2018; Dauhajre *et al.*, 2019). Consequently, two tests were performed to study the impact of spatial and temporal resolution on the model accuracy. The relative error (RE) is defined as the distance between last position of particles from simulation with different resolution (spatial and temporal). RE decreased exponentially as the spatial or temporal resolution was refined (Figures 3.14 and 3.17). Further, RE > 5 km were observed when the resolution was coarser than 1,000 m and 30 min for spatial and temporal resolution tested. These high RE values may misrepresent larvae dispersal and connectivity especially in area of strong velocity such as the Menai Strait. Indeed, RE varied spatially for both tests performed (Figures 3.15 and 3.18). Results showed that velocity was an important factor to consider defining the spatial and temporal resolution of the PTM. In particular, where velocity is high (> 0.5 m/s), decreasing the temporal and spatial resolution increased relative

error. Also, results showed a clear correlation between the increase of velocity and increase of RE (Figures 3.16 and 3.19). Consequently, the grid resolution must be adapted according to the velocity of the area of interest. In this study, particles encountered both areas with strong velocities (e.g. the Menai strait with peak flows exceeding 1 m/s) and areas with low velocities (e.g. Eastern Irish Sea). Future simulations will be done separately using the Menai Strait model and the Irish Sea model with grid resolutions of 20 m and 50 m, respectively. Furthermore, temporal resolution of the PTM had a significant impact on model accuracy (Figure 3.28). However, fine temporal resolution models are often impractical computationally. For example, 5 min output resolution for six weeks simulation generated storage limitation problems in this study.

Ocean models use discretized spatial grids and instantaneous velocity data are output at the specified output frequency. Consequently, it is important that the PTM reconstructs the continuous velocity field at the spatial/temporal resolution of the dispersed particles (Griffies *et al.*, 2000). Linear and bilinear interpolation were used to represent the continuous velocity field for temporal and spatial resolution respectively. Both spatial and temporal interpolation (downscaling from 1,000 m to 50 m and from 60 min to 5 min) reduced the RE by 35 % (Figure 3.12). Spatial interpolation was not needed when the resolution of the mesh was 50 m, however it remains essential for coarser resolutions (e.g. > 50 m).

The results obtained previously are theoretical and need to be tested among data collected from field observations (Kozalka *et al.*, 2010; Sebille *et al.*, 2018). One way to validate PTMs is to compare modelled particles trajectories with observed drifter trajectories (Edwards *et al.*, 2006; De Dominicis *et al.*, 2012). As most drifters are released at the surface, they are subjected to wind-driven forces, waves effects and potentially stronger currents than the depth averaged values (Weber, 1981; Weber, 1983; Prandle, 1982; Wu, 1983; Proctor *et al.*, 1994; Chang *et al.*, 2012; Genç *et al.*, 2015; Afenyo *et al.*, 2016). Two drifters were released: 1) Drifter 1 in April 2018 for 2 days near Puffin Island; and 2) Drifter 2 in May 2019 for 4 days near Llandudno (Figure 3.26). The results showed good agreements of the model with the two drifter experiments. Accounting for wind-driven and surface velocities improved the model validation by 27% and 80% for the drifter 1 and the drifter 2, respectively (Table 3.3). The improvement observed for drifter 1 is explained by the presence of land where simulated particles landed (around 50% for all simulations). Consequently, the improvement on average for all particles was reduced as half of them were trapped on land. These results show the complexity to validate PTM in coastal areas and the importance of release site to observed drifter trajectories. However, the improvement of the results using wind and surface velocity approximation show the importance to consider these parameters to study larval dispersal. Indeed, larvae can migrate

vertically in the water column (Lane *et al.*, 1985; Gaylord *et al.*, 2002; Criales *et al.*, 2007; Harnett *et al.*, 2007; Robins *et al.*, 2012; Robins *et al.*, 2013; Rhörs *et al.*, 2014; Weidberg *et al.*, 2015; Daigle *et al.*, 2016). Consequently, mussel larvae are subject to tidal advection only in the middle of the water column and higher velocity at the surface coupled with wind driven current during their PLD.

Diffusivity is usually added in the PTM in order to simulate the unresolved physics and/or larval behaviour uncertainties (Proctor *et al.*, 1992; Griffa, 1996; Berloff & McWilliams, 2003; Ross & Sharples, 2004; Robins *et al.*, 2013). Sensitivity test 3 (sub-grid-scale mixing was included) showed that diffusivity improved the results obtained for the Drifter 2 (e.g. decrease of RE from 6,523 m to 290 m, on average for all particles for all diffusion coefficient tested), with the best results obtained for K = 4 m^2/s (RE = 39 m). However, RE increased with diffusivity when looking at Drifter 1 results (decline between 2% to 23% for K = 6 m^2/s and K = 9 m^2/s, respectively). In TELEMAC 2D, artificial diffusion was previously defined with a value of 1 m^2/s, which corresponds to an intermediate value chosen by the users (pers. com. on TELEMAC forum). As the artificial diffusivity in TELEMAC 2D is a function of the grid scale, a coarse resolution (> 500 m) will not see any effect of diffusivity. The Drifter 1 was released in an area where the grid resolution was 100 m while the Drifter 2 was released in an area of 1,000 m resolution (see Chapter 2, Figures 2.2 and 2.5). This explained the need for diffusion for particles simulated offshore and not for particles simulated near the coast. Further, results showed that for both drifters, particles with the closest trajectory to the drifter (smallest RMSE) were different to the particles with closest final position (smallest RE) (Figure 3.27). Consequently, the number of particles simulated is a crucial parameter to take into account in order to represent accurately the mussel larvae travel during their pelagic phase. Therefore, larvae dispersal in the Irish Sea will be simulated with K = 4 m^2/s because: 1) the best results were observed for this value; and 2) the majority of the Irish sea grid has a spatial resolution > 500 m. However, simulations in the Menai Strait will not take into account any diffusivity as results increased RE.

The results of the 2D simulations created in this study were compared with those from a 3D baroclinic model, which showed similar results (in terms of RE) (data not shown as they will be published by the owner of the 3D simulation). A difference was expected as during the period of drifter released (e.g. May and June), the Irish Sea is thermally stratified in 3 regions which results in the creation of frontal systems (e.g. Liverpool bay, Western Irish Sea and St Georges channel) (Figure 1.21) (Golding *et al.*, 2004; Howarth, 2005). However, stratification in the eastern Irish Sea (area of interest) are negligible as waters are well mixed by storms and tides (Howarth, 2005). This explains the similarity of the 2D and 3D results. Further, the future

simulations created to predict larval dispersal from north Wales were done during March and April when the water is well mixed in the entire Irish Sea (Simpson, 1971; Gowen *et al.*, 1995; Howarth, 2005). Data from the AMM 15 model (Graham *et al.*, 2018) simulated daily-average temperature of bottom and surface in the Irish sea, from 1990 to 2014, showed that temperature difference between bottom and surface varied from 0ºC to 0.15ºC for the period of interest (e.g. March to April) (Figure 3.29). Therefore, the facts that the 2D model reproduced well the drifter trajectories, produced similar flows to a 3D model and the water was well mixed during March-April, suggests that 3D modelling is not necessary to simulate larval dispersal in the northeast Irish Sea during March and April. Further, high spatial and temporal resolution is essential to resolve accurately coastal areas (< 50m) therefore a 3D model is computationally impractical. Indeed, most of the time 3D model showed a spatial resolution > 1 km or a temporal resolution > 3 hours or reduce the pelagic larvae duration or a small domain of study (Davies & Gerritsen, 1992; Aldridge & Davies, 1993; North *et al.*, 2008; Ayata *et al.*, 2009; Moreno Navas *et al.*, 2011; Sundelof & Jonsson, 2011; Nicolle *et al.*, 2013; Hoyer *et al.*, 2014; Sebille *et al.*, 2018). For the first time, these results quantify the relative error induced for a 'high' spatial-temporal-resolution PTMs under different conditions. The future simulations developed in Chapters 4 and 5 to study mussel larvae dispersal in the Irish Sea will be based on the previous conclusions:

- The Menai Strait model will be used to study larval dispersal within the channel for a short period (e.g. one week) with: 1) 7,000 particles per site of interest; 2) with temporal linear interpolation from 30 min to 5 min; 3) bilinear spatial interpolation; and 4) without additional sub-grid-scale mixing.
- The Irish Sea model will be used to simulate larval dispersal outside of the Menai Strait and the connectivity among the principal mussel beds in the region (e.g. commercial or scientific interests) over a longer period (e.g. 6 weeks PLD) with: 1) 7,000 particles per site of interest; 2) with temporal linear interpolation from 30 min to 5 min; 3) bilinear spatial interpolation; and 4) with sub-grid-scale mixing (i.e. diffusivity) with $K = 4\ m^2/s$.

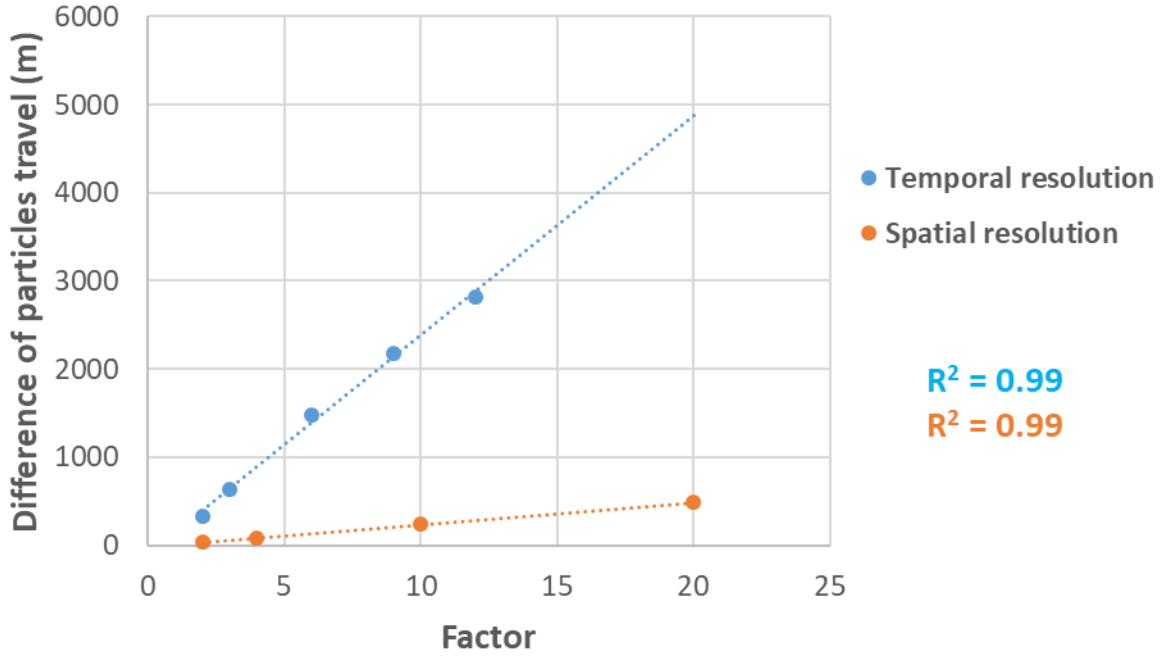

Figure 3.28: Plot showing RE of distance travelled by particles (10,000) released on the Irish Sea grid between the finest resolution and coarser resolutions with: 1) in orange, the results for temporal resolution; and 2) in blue, results for spatial resolution.

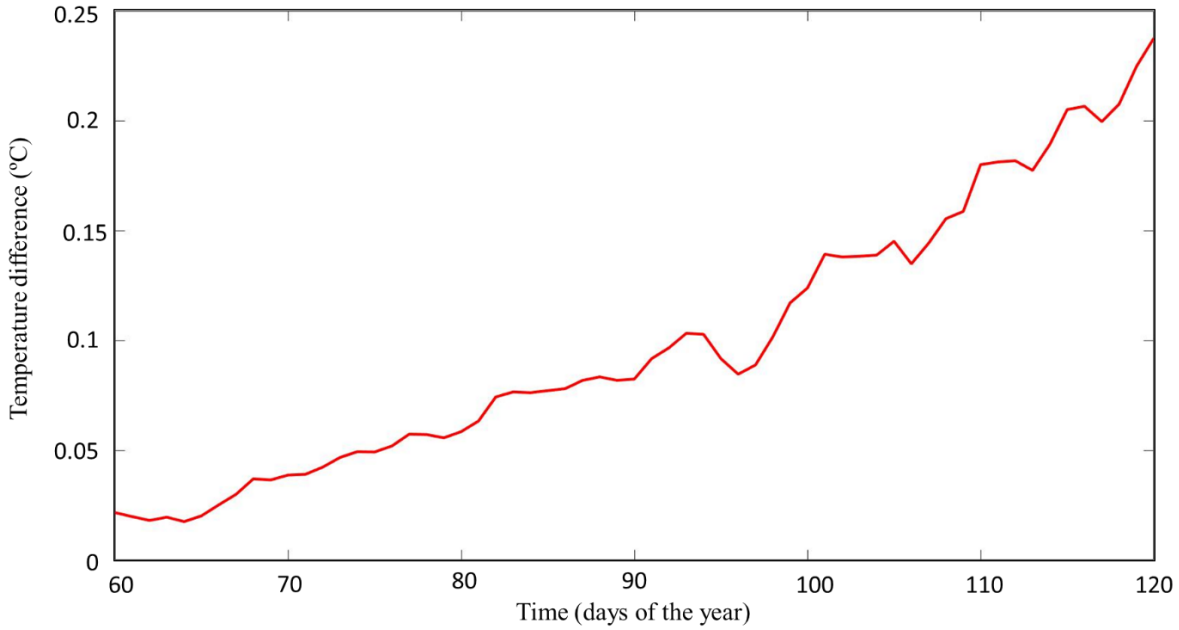

Figure 3.29: Graph showing the temperature difference between the surface and the bottom in the Irish Sea during March and April average for 24 years (1990 to 2014).

Chapter 4: Menai Strait mussels

Mytilus edulis in the Menai Strait have been exploited for over 50 years because the strong tidal currents that promote the transport of nutrients and water renewal (Ewins & Spencer, 1967; Simpson *et al.*, 2007). The two commercial mussel beds are located in the south (Brynsiencyn) and in the North (Bangor) of the Menai Strait (see Chapter 1, Figure 1.4). Mussel production is based on bottom culture, which uses wild spat collected throughout the Irish Sea and relaid on plots in the Menai Strait (Aldon, 1998; Asokan & Mohamed, 2009). The location of wild seed beds is crucial to the commercial viability of the mussel companies who manage the relaid mussel seed beds over 3 years period before selling for human consumption.

The study will focus firstly on larval dispersal from the Menai Strait where the most important commercial mussel bed is located. To do so, spawning events of the mussel bed during spring and summer 2018 was studied to understand when spawning events occur using Condition Index (CI) and commercial Meat Yield (MY), which both relate the amount of bivalve meat to the quantity of shell (e.g. represent the evaluation of merchantable trait in blue mussel) (Filgueira *et al.*, 2013). Indeed, it was previously shown that a drop of these indexes corresponds to a spawning event (Dare, 1976; Slabyj *et al.*, 1978; Knights *et al.*, 2006; McQuaid & Phillips, 2006; Duinker *et al.*, 2008). Literature has shown that spawning events of *Mytilus edulis* depend on environmental factors (e.g. air temperature, sea temperature, lunar phase, tidal currents, season and geographic distribution) and biological factors (e.g. size, age and conspecific spawning) (Chipperfield, 1953; Seed, 1969; Slabyj *et al.*, 1978; Lutz *et al.*, 1980; Lowe *et al.*, 1982; King *et al.*, 1989; Gardener and Skibinski, 1990; Newel *et al.*, 1991; Toro *et al.*, 2002; Duinker *et al.*, 2008; Doherty *et al.*, 2009; Klibansky and McCartney, 2014; Fernandez *et al*., 2015). In addition, in the laboratory, mussel spawning is induced by thermal shock, which consists of an increase of the seawater temperature (Pronker *et al.*, 2008; Mestre *et al.*, 2009; Hennebicq *et al.*, 2013). Consequently, it is important to study the correlation between environmental factors variation (e.g. air temperature, sea surface temperature, moon phases, water elevation and wind) and CI and/or MY variation. Then, to qualify and quantify larval dispersal in the Menai Strait, a PTM approach has been used. The flow regime in the Menai Strait has previously been studied using observational techniques, such as tracking drifters (Harvey, 1968) and deploying current meters (Simpson *et al.*, 1971), but also using numerical modelling (Davies & Robins, 2017). However, no previous studies used particles tracking model to represent the impact of tide on particle dispersal in the Menai Strait.

These experiments will help to plan efficiently the mussel collection in time (e.g. if the period of spawning is known, the time of harvest can be deduced) in area defined by the PTM.

This study addresses an important scientific question on what are the principal factors influencing gamete release and how larvae travel within a tidal channel with strong and complex

circulation. In addition, it is important for the project partner to know where the larvae from Bangor travel to understand their contribution and possibly define new areas of wild spat to harvest.

These experiments will answer several questions:

- When do mussel spawns in the Menai Strait?
- What are the environmental factors inducing spawning?
- How does the tide (neap vs spring; flood vs ebb) influence mussel larval dispersal?
- What proportions of mussels are likely exported out of the Menai Strait?
- Can mussels potentially settle in the Strait despite the strong currents?
- Are the two commercial mussel beds connected?

4.1 Spawning period

Previous studies on *Mytilus edulis* spawning events have shown that the phenomena usually happens during spring and summer with geographical and interannual variability (Chipperfield, 1953; Seed, 1969; Bayne, 1976; Lutz *et al.*, 1980; Lowe *et al.*, 1982; Sprung, 1983; King *et al.*, 1989; Newell *et al.*, 1991; Lemaire *et al.*, 2006; Nahrgang *et al.*, 2013; Fernandez *et al*., 2015). These authors showed that spawning events were impacted by local environmental factors (e.g. air temperature, sea temperature, lunar phasing, salinity, tidal currents, season and geographic distribution) and biological factors (e.g. size, age and conspecific spawning). Spawning has been shown to be strongly influenced by the condition index (CI) and the commercial meat yield (MY) (Equation 4.1). Understanding the periodicity of spawning is important for the management of the mussel industry. Further, the timing of spawning is required so that realistic weather conditions encountered during the pelagic phase such as wind data can be incorporated into the larval dispersal simulations.

4.1.1 Materials and methods

Mytilus edulis were sampled daily over spring and summer 2018 (23rd of March to 28th of September), from the intertidal area of the commercial mussel bed located near Bangor in the Menai Strait (53.2348 and -4.13045) (Figure 4.1). Sampling did not occur on the following dates due to either poor weather conditions or neap tides (when the bed where submerged): 1) 5th to 21th May; 2) 22nd July to 13th August; and 3) 14th to 20th September. Mussels were

collected and transported to the laboratory, then scrubbed to remove all epibionts and drained before processing.

The protocol to calculate the condition index was based on the one used by Duinker *et al.* (2008). The total meat weight was first calculated. The length and width of mussels were measured using a calliper to mm accuracy (Figure 4.2). Based on the methods used by Slabyj *et al.* (1978), the shelf measurements were separated into two distinct size classes: 1) Sample_1 with length of 51 mm and width of 23 mm and 2) Sample_2 with length of 60 mm and width of 26.6 mm on average. For each sample, 1 kg of live mussels were placed in boiling water for 9 minutes. The cooked meat was then separated from the shells. The cooked meat and shells were then dried and weighed separately to calculate the condition index (CI) as described in Equation 4.1 (Duinker *et al.*, 2008). The commercial meat yield (MY) was also considered for comparison (Equation 4.1) using a correlation analysis against CI.

A T-test was performed on the shell length and width of Sample_1 and Sample_2. Environmental factors were analysed against the timings of potential spawning. These factors were: 1) sea surface temperature (SST) which were recorded every 10 mins with a logger located on Bangor Pier (53.240623 and -4.125929) deployed by CEFAS (the logger did not record data from 26th March to 31st April); 2) air temperature (AT) from Valley, Anglesey (53.2524 and -4.53524) downloaded from CEDA (https://catalogue.ceda.ac.uk); 3) the difference between AT and SST (AT - SST) to study thermal shock; 4) wind data (W) from Valley, Anglesey (53.2524 and -4.53524) downloaded from CEDA (https://catalogue.ceda.ac.uk); 5) the phase of the lunar cycle recorded daily from https://moonphases.co.uk; and 6) water elevation (WE) from the Menai Strait TELEMAC model created and validated previously (see chapter 2).

Equation 4.1: Equations used to calculate the commercial meat yield (MY) and the condition index (CI), from Duinker *et al.* (2008).

$$MY = (\text{Cooked meat weight}/(\text{empty shell weight} + \text{cooked meat weight})) * 100$$

$$CI = (\text{Cooked meat weight}/(\text{whole live weight} - \text{shell weight})) * 100$$

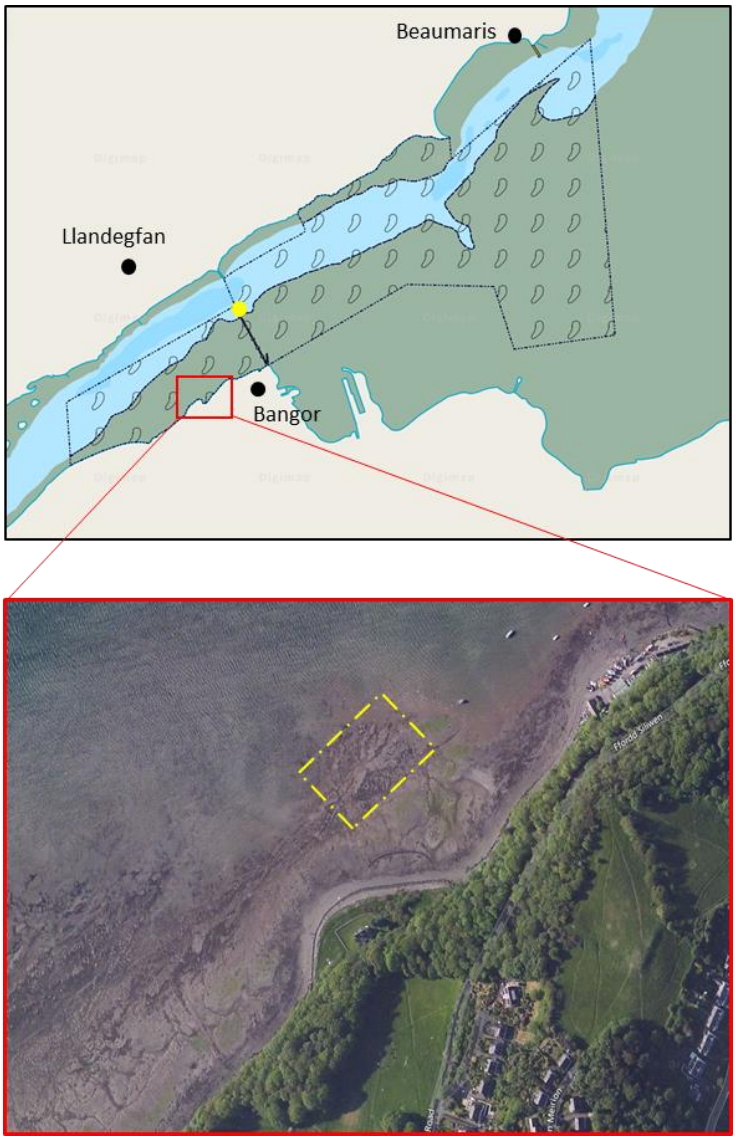

Figure 4.1: Area of the sample collection (yellow dotted square) in the Menai Strait. The logger location is represented by a yellow dot.

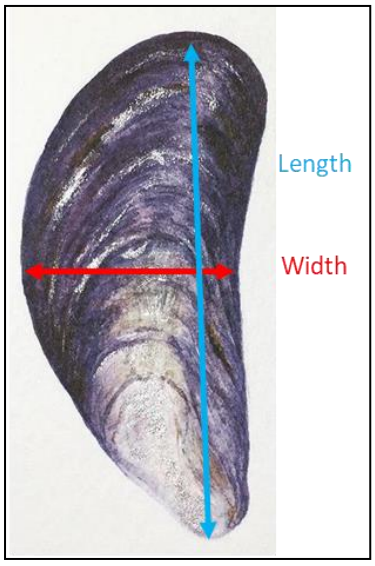

Figure 4.2: Method of mussel measurement.

4.1.2 Results

Sample_1 (smaller mussels) had an average shell length of 50.9 mm and shell width of 23.1 mm while Sample_2 (larger mussels) had an average shell length of 59.9 mm and width of 26.6 mm (Table 4.1 and Figure 4.3). The T-test results showed that the observed difference between the sampled means was significant for both width and length. Therefore, Sample_1 and Sample_2 can be studied independently.

Figure 4.4 showed the variation of CI and MY through spring and summer 2018. The comparison of the two curves showed higher values using CI (time-averaged value of 23.26%) than MY (time-averaged value of 17.98%) for both samples (Figure 4.4). There was a high correlation index of 0.98 (sample 1) and 0.92 (sample 2) when comparing MY and CI. As the two curves are well correlated for both samples, the further comparisons of potential spawning (e.g. variation of CI curve) with environmental factors were made using CI calculated.

The average values for the CI for the Bangor mussels over the spring and summer of 2018 was 24.34% and 22.17% for Sample_1 and Sample_2, respectively. Further, the variation of CI among the period of study showed a correlation of 0.94 between samples. Indeed, Figure 4.5 shows that CI followed three clear trends for both samples: 1) a decrease in CI from the end of March to the start of May to reach minimum values of 17.28% (Sample_1) and 16.40 % (Sample_2) (R^2 = 0.37); 2) an increase in CI from the start of May to the start of July with maximum values of 32.31% (Sample_1) and 27.33% (Sample_2) (R^2 = 0.85); and 3) a decrease in CI from July to the end of summer (R^2 = 0.35). Further, the CI of Sample_1 was 9.30% higher than Sample_2 on average (Figure 4.5). CI variation trough spring/summer is correlated (R^2 = 0.80) to the variation of SST and AT (Figure 4.5). Indeed, the maximum temperature is reached during July with values of 18.57°C and 22.55°C for SST and AT, respectively.

Three biggest drops in CI were noticeable for both samples through the period of study (Figure 4.5 and Table 4.2):

- 26th - 27th March with a drop of CI of 4.21% and 5.55% for Sample_1 and Sample_2 respectively.
- 22nd - 23rd April with a drop of CI of 3.28% and 3.73% for Sample_1 and Sample_2 respectively.
- 20th - 21st September with a drop of CI of 4.07% and 3.40% for Sample_1 and Sample_2 respectively.

Results showed that every decrease in CI happened 1 or 2 days after an increase of SST and AT of 2.4°C ± 0.2°C and 2.18°C ± 0.47°C respectively (Table 4.2). Furthermore, the spawning events occurred when AT was lower than SST by 3°C on average (Table 4.2).

Several events with small fluctuation of CI were observed during spring and summer of 2018 (Table 4.3). There were 9 events for Sample_1 and 8 for Sample_2. However, both samples had a small fluctuation of CI at the same time for 6 events: 31st March; 1st May; 24th May; 3rd July; 11th July and 24th August (Table 4.3). In most cases, these fluctuations happened when a difference between AT and SST was greater than at 1°C, except for 12th June and the 11th July. However, for these events the AT dropped by 1.62°C and 2°C. Results also showed that for all small fluctuations events, SST increased by 0.52°C on average (Table 4.3).

The three biggest drops of CI happened when the moon phase is around 60% (third-quarter neap tide) while all the small fluctuations events happened when the moon phase is close to full moon (> 80%) or new moon (< 15%) (Figure 4.6.A). Furthermore, Figure 4.6.B highlighted that the biggest drop of CI happened when the water elevation never exceeded 2.5 m above the mussel bed, which was related to the moon phase's results. The opposite observation was made for small fluctuation of CI events, which happened during bigger tide. No correlation was observed when drop of CI were compared with the wind data (strength and direction) (Figure 4.6.C).

Table 4.1: Details of sample collection for the meat yield experiment per sample with in the red the total of mussels and weight sampled cumulated.

Sample name	Average size		Average	
	Length (mm)	Width (mm)	Mussels per sample	Weight of the sample (g)
Sample_1	50.9 ± 5	23.1 ± 3	61 ± 20	1009 ± 10
Sample_2	59.9 ± 7	26.6 ± 5	40 ± 7	1011 ± 11
		Total	8398	$168*10^3$

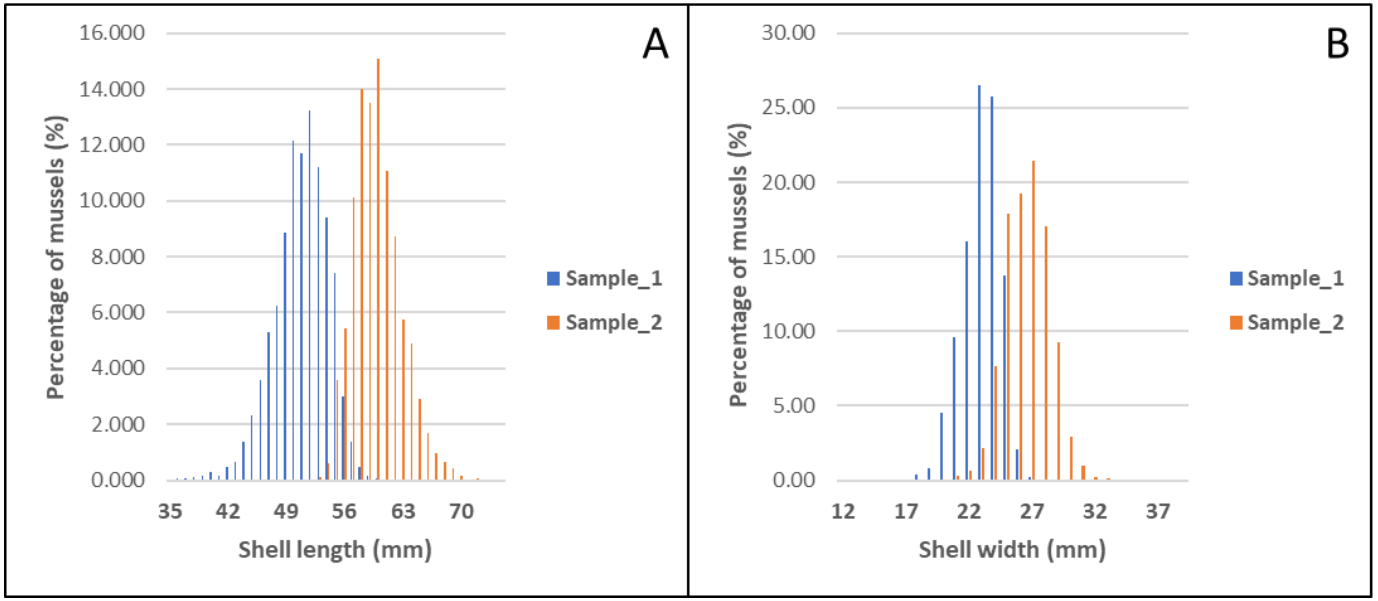

Figure 4.3: Mussel distribution among Sample_1 (in blue) and Sample_2 (in orange) depending on: A) shell length and B) shell width.

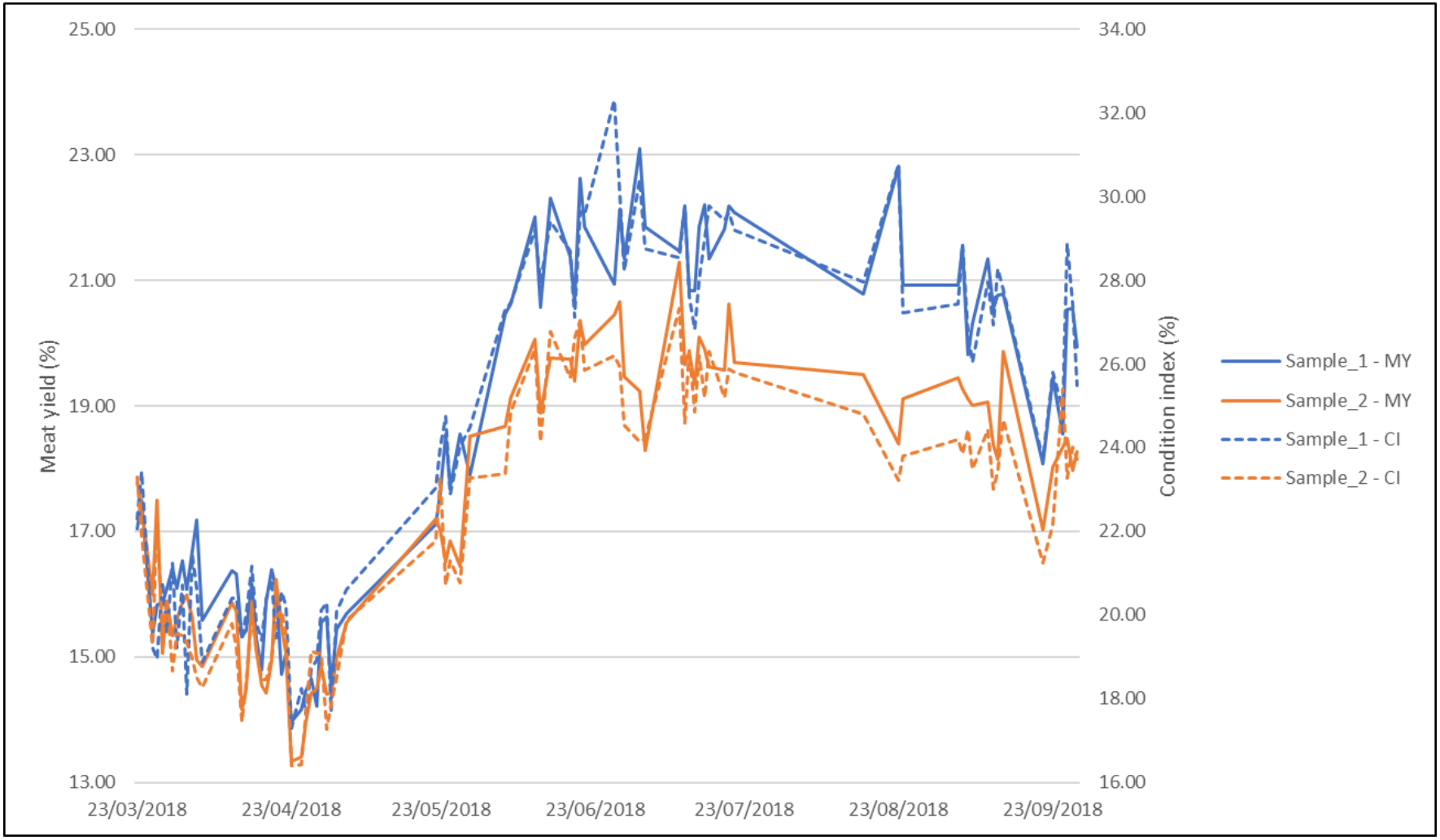

Figure 4.4: Evolution of meat yield (MY, solid line) and condition index (CI, dotted line) for Sample_1 (in blue) and Sample_2 (in orange).

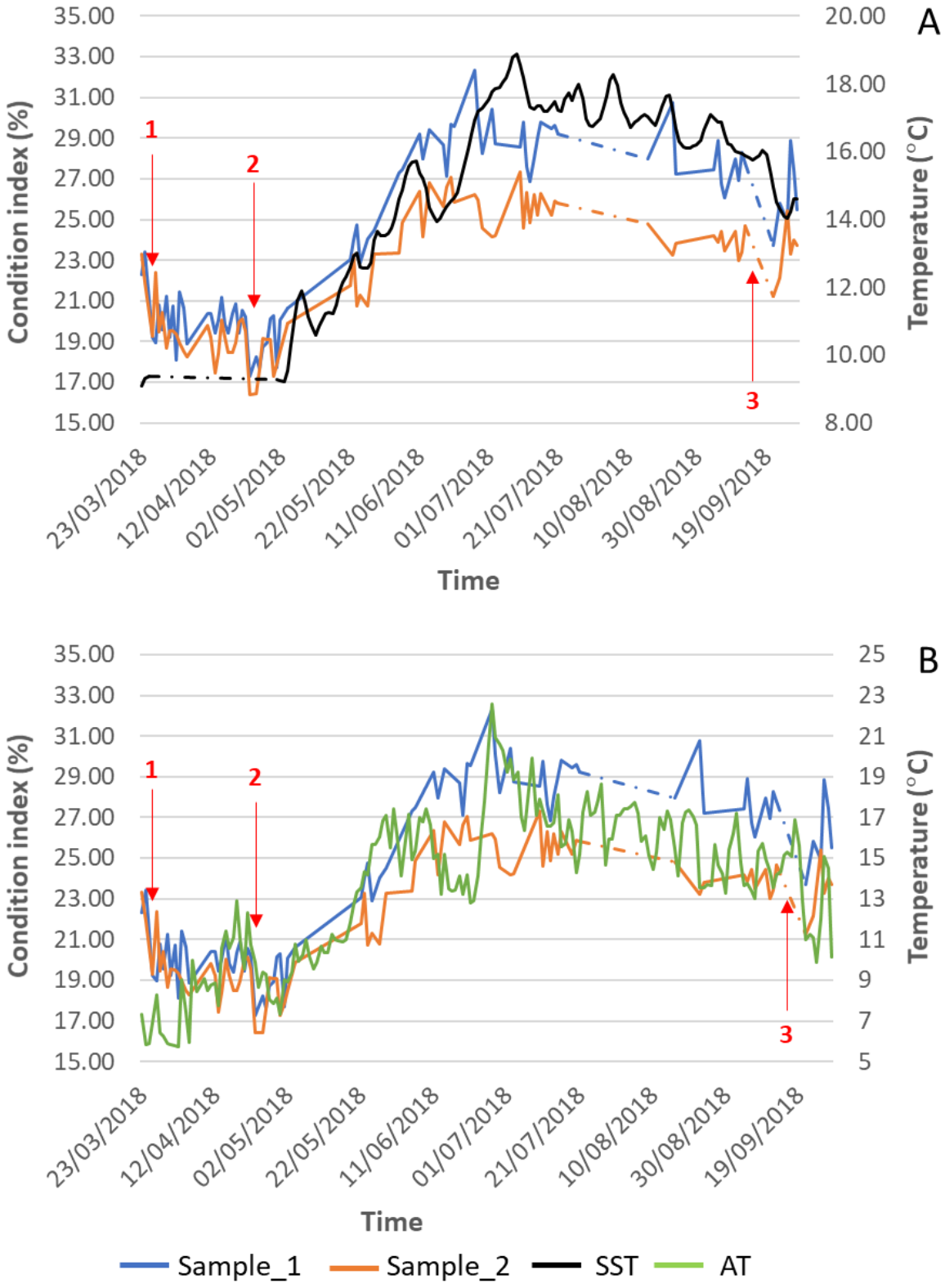

Figure 4.5: Evolution of 1) Meat yield for sample_1 (in blue) and sample_2 (in orange) over spring/summer 2018 on both figures A and B; 2) Sea surface temperature (SST) in green on figure A; and 3) Air temperature (AT) in yellow on figure B. The portion of the curves in dashed line corresponds to period when data were not collected. Red arrows point days of massive spawning events.

Table 4.2: Biggest drop of CI with the corresponding: 1) Date; 2) MY variation in % for both samples; 3) CI variation in % for both samples; 4) SST difference between the day of spawning and the day before in ºC; 5) AT difference between the day of spawning and the day before in ºC; and 6) Difference between AT and SST in ºC.

Spawning events	Date	MY variation (%)		CI variation (%)		SST variation (ºC)	AT variation (ºC)	AT – SST (ºC)
		Sample 1	*Sample 2*	*Sample 1*	*Sample 2*			
1	*26/27 March*	-2.14	-2.34	-4.21	-5.55	0.26	2.00	-3.49
2	*22/23 April*	-2.12	-2.89	-3.28	-3.73	N/A	2.75	N/A
3	*20/21 September*	-2.72	-2.86	-4.07	-3.40	0.22	1.80	-2.56

Table 4.3: Small fluctuation of CI in red with the corresponding: 1) Date; 2) MY variation in % for both samples; 3) CI variation in % for both samples; 4) SST difference between the day of spawning and the day before in ºC; 5) AT difference between the day of spawning and the day before in ºC; and 6) Difference between AT and SST in ºC.

Date	MY variation (%)		CI variation (%)		SST difference (ºC)	AT difference (ºC)	AT – SST (ºC)
	Sample 1	*Sample 2*	*Sample 1*	*Sample 2*			
31-Mar	-0.32	-0.54	-2.03	-1.74	N/A	-0.4	N/A
05-Apr	-1.6	-0.11	-1.76	-0.24	N/A	-1.57	N/A
13-Apr	-1.04	-1.69	-0.98	-2.35	N/A	0.37	N/A
01-May	-1.12	0.02	-2.59	-1.82	N/A	1.7	N/A
24-May	-0.84	-0.52	-1.87	-2.55	0.43	0.8	1.44
12-Jun	-1.45	-1.18	-1.25	-2.21	0.44	-1.62	-0.03
28-Jun	-0.92	-0.37	-2.25	-1.38	0.86	0.94	3.74
03-Jul	-1.18	-1.66	-1.99	-2.06	0.67	0.625	5.61
11-Jul	-1.36	-1.64	-2.17	-2.72	0.43	-2	-0.87
24-Aug	-1.89	-1.1	-3.55	-1.57	0.36	-3.05	3.69
06-Sep	-1.72	-0.15	-2.14	-0.58	0.45	-3.475	-3.49

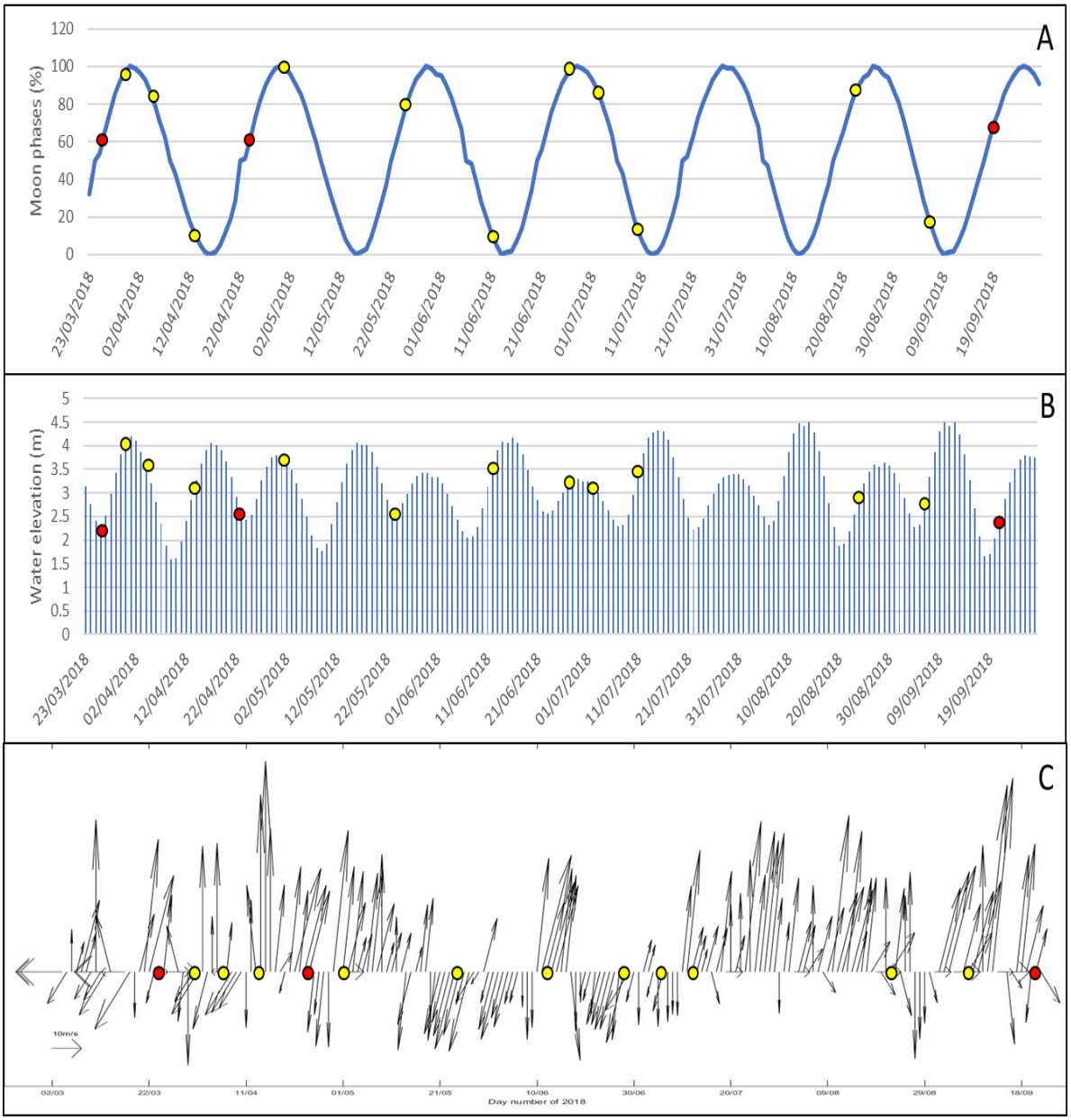

Figure 4.6: Evolution of: A) Moon phases in % with full moon represented by 100 % and new moon represented by 0 %; B) Water elevation in m; and C) Wind strength and direction by arrows. Red dots represent the massive spawning events and yellow dots represent the trickle spawning events.

4.1.3 Discussion

In this study, major spawning events were defined depending on two criteria: 1) synchronous drop of CI for both Sample_1 and Sample_2; and 2) CI decreases > 2.5% between two sampling days. Trickle spawning events were defined as a small fluctuation of CI between 1.5% to 2.5% (Knights *et al.*, 2006; McQuaid & Phillips, 2006). Indeed, a significant drop in MY and CI are known to correspond to a spawning event (Dare, 1976; Slabyj *et al.*, 1978; Duinker *et al.*, 2008). Processing more than two samples in the same day required too much time for a daily basis experiment even if samples were located on the same mussel bed (e.g. two samples took

3h30min to process), also only one mussel bed was selected as it would have been impossible to collect at different sites during a low tide (mussel beds of interest too far from each other). Furthermore, blue mussels sampled could only be used once, which means that everyday new mussels were sampled and processed. This could lead to uncertainties on spawning interpretation. However, blue mussels spawn synchronously (e.g. gametes are released at the same time for all individuals in the water column) to increase fertilization success, which means (Toro *et al.*, 2002; Mestre *et al.*, 2009). Larval spawning events were observed throughout the spring and summer of 2018 in the Menai Strait. This result correlates with the extensive literature on the spawning patterns of *Mytilus edulis* from distinct geographical location (Chipperfield, 1953; Seed, 1969; Bayne, 1976; Lutz *et al.*, 1980; Lowe *et al.*, 1982; Sprung, 1983; King *et al.*, 1989; Newell *et al.*, 1991; Lemaire *et al.*, 2006; Nahrgang *et al.*, 2013; Fernandez *et al*., 2015). Chipperfield (1953) showed that *Mytilus edulis* first spawned in late April, from six distinct sites within the Irish Sea. For their study, sea temperatures had risen from 10ºC to 13ºC. In this study, the first major spawning event occurred at the end of March. The earlier spawning could be explained by a temperature anomaly, which happened at the beginning of March 2018, with air temperature reaching 25ºC for 2 days. This temperature rise could have induced an earlier spawning. However, the second and the third major spawning events occurred in late April and late September, which is the spawning period observed previously in literature (Wilson & Seed, 1974; Slabyj *et al.*, 1978; Duinker *et al.*, 2008).

These spawning events occurred during a rise of air temperature of 2/3ºC. Further, these spawning events occurred simultaneously for both Sample_1 and Sample_2. In the laboratory, larval spawning can be induced by a thermal shock on the mussels, which consists of an increase of the seawater temperature (Pronker *et al.*, 2008; Mestre *et al.*, 2009; Hennebicq *et al.*, 2013). In nature, mussels in the intertidal area can be subjected to a thermal shock if the AT and SST differ. The observations here showed that the main spawning events occurred when the SST was 3ºC higher than the AT on average for two main spawning events (26th March and 20th September). Also apparent in literature, larval spawning is described in terms of weeks (Chipperfield, 1953; Doherty *et al.*, 2009) rather than day-to-day, as described here. Some of the trickle spawning events observed could be the continuation of main spawning events within that week such as the trickle events on 31st March and 1st May that followed shortly after the first and second major spawning events respectively. No correlation can be made between the trickle spawning and the difference between AT and SST. However, in every case, an increase of SST (> 0.35ºC) was observed when trickle spawning occurred. These results highlight the importance of temperature (SST and AT-SST) on larval spawning events for the first time at a daily observation. Literature has shown that spawning events of *Mytilus edulis* depend on

environmental factors (e.g. air temperature, sea temperature, lunar phase, tidal currents, season and geographic distribution) and biological factors (e.g. size, age and conspecific spawning) (Chipperfield, 1953; Seed, 1969; Slabyj *et al.*, 1978; Lutz *et al.*, 1980; Lowe *et al.*, 1982; King *et al.*, 1989; Gardener and Skibinski, 1990; Newel *et al.*, 1991; Toro *et al.*, 2002; Duinker *et al.*, 2008; Doherty *et al.*, 2009; Klibansky and McCartney, 2014; Fernandez *et al*., 2015). In this study, mussels of different sizes were collected from a single intertidal mussel bed located in the Menai Strait near Bangor. The samples were divided in two statistically significant groups depending on shell length and shell width with Sample_1 representing the "small" mussels and Sample_2 representing the "big" mussels. Consequently, the impact of environmental parameters (e.g. air temperature, moon phases, sea surface temperature, food availability and geographic distribution) were the same for both samples. Daily, sample-averaged, estimates of condition index (CI) and meat yield (MY) showed similar patterns throughout the period of study, with three clear trends observed for both samples. The first period (March to May 2018) showed decreases in meat yield (R^2 = 0.37), followed by and increase until the beginning of July (R^2 = 0.85), and finally a decrease until end of September (R^2 = 0.35). This trend is correlated with the variation of SST and AT, when both temperatures increased until the first week of July then decreased. During March to May 2018 the decrease of CI is the consequence of two main spawning event during this period (26th March and 22nd April 2018). Then, the second period (e.g. increase of CI from May to July 2018) can be explain by the presence of phytoplankton. *Mytilus edulis* feed from phytoplankton to build their own biomass (Fernandez *et al.*, 2015). According to the literature, a phytoplankton bloom in the Irish Sea usually occurs between March and May with a low summer biomass (Foster *et al.*, 1982; Gowen *et al.*, 1995; Kennington *et al.*, 1998; Hartnoll *et al.*, 2002; Gowen & Stewart, 2005). This might explain the increase of CI and MY from late April to the beginning of July when food availability is maximum (Newell *et al.*, 1982).

The results showed that sample-averaged CI were higher for Sample_1 than Sample_2 by almost 10% (and by 5.80% for MY) throughout spring and summer of 2018. Similar observations were made previously for *Mytilus edulis* MY by Slabyj *et al.* (1978) in Maine (USA) and Dare & Edwards (1976) in the Menai Strait (UK). Mussel growth has been shown to vary spatially and temporally depending on environmental parameters (e.g. temperature, salinity and food availability) (Bergstrom *et al.*, 2015; Bergstrom & Lindegarth, 2016). The CI was calculated for a single mussel bed where mussels encounter similar environmental factors. Consequently, the mussel growth rate in this area must be approximately the same for the mussels sampled. So, the relative size between samples gave an idea of the relative age between them, which means mussels from Sample_1 were younger (because smaller) than mussels from

Sample_2. Consequently, CI and MY of younger mussels are higher during spring and summer in the Menai Strait. This result matches with observations made in Norway by Duinker *et al.* (2008), except that the difference here between the samples was greater (almost 10%) than observed in Norway (5%). This difference could be due to the difference of temperature of the water between Norway and North Wales and its impacts on food availability for *Mytilus edulis* (Bayne & Worrall, 1980; Page & Humbard, 1987). Further, the difference of CI between Sample_1 (younger mussel) and Sample_2 (older mussel) increased linearly (R^2 = 0.35) through spring and summer. This difference could result from a lower fecundity in younger mussels (Sample_1) with more energy allocated to the development of storage reserve than the gametogenesis (Bayne, 1976; Lowe *et al.*, 1982; Sprung, 1983). Indeed, the estimated CI showed higher values with a difference of 9.41% on average between Sample_2 and Sample_1 for the three main spawning events.

Studies in North America showed that larval spawning events for *Mytilus edulis* occurred during a period between spring tide (Battle, 1931; Newell *et al.*, 1991). Here in the Menai Strait, the results showed that the main spawning events occurred during the third-quarter moon phase, approaching neap tides. In North Wales during neap tides, low water occurs during night (from 10 pm to 4 am) and mid-day (from 10 am to 3 pm). At these times of low water, therefore, mussels are exposed to minimal (midnight) and maximal (noon) air temperatures. Consequently, the maximum difference between AT and SST is observed during these two times of the day. This helps explain the previous result, which considers that a thermal shock induced larval spawning. The trickle spawning events occurred especially during the spring tide period. The difference between the AT and SST cannot explain these events as no patterns were observed with values varying greatly from -3.49ºC to 5.61ºC. However, Battle (1931) proposed the idea that hydrostatic pressure (e.g. pressure exerted by the water column on mussel) might influence spawning in *Mytilus edulis*. Also, Famme *et al.* (1986) showed that the pumping rate, equivalent to feeding rate, decreases linearly with an increasing hydrostatic pressure. This could lead to a trickle spawning as a result of a stress on *Mytilus edulis*.

Improved the knowledge of timing of larval spawning is important for the Mussel industry in North Wales as the culture technique relies on wild spat collection. The ability to predict mussel spawning events will be an economical advantage to either harvest spat from designated area or to place collector ropes at the right time. This first study has provided a temporal answer in terms of the date of spawning and the environmental factors that can induce spawning events in the Menai Strait. In the next section, a particle-tracking model has been used to help to understand the spatial distribution of mussel larvae through time after spawning events.

4.2 Menai Strait PTM simulations

The first attempt to study the dispersal of material in the Menai Strait was performed by Harvey (1967). Drifting wood was released at both the north and south extremities of the Strait and Harvey's results showed the presence of a southwest residual current of 13 million m^3 to 35 million m^3 during a semi-diurnal tidal condition for neap tide and spring tide respectively. However, some of the drifters managed to travel north-eastwards through the Strait, presumably trapped near the banks during each ebbing tide. Indeed, drifters released at the south entrance of the Strait were found near Plas Newydd after two days. However, this is the first study to quantify the effect of the release period (e.g. influence of the tide) and the release location on the dispersal of material in the Menai Strait.

4.2.1 Materials and methods

A hydrodynamic model of the Menai Strait was created using TELEMAC-2D (see Chapter 2, Section 2.1.2.). The mesh resolution was 20 m within the Strait. A month-long simulation was computed for the period 1st March 2018 to 31st March 2018. The model was validated using tide gauge data and current data as presented in Chapter 2, Section 2.5. The depth-averaged currents computed by the model were ouput every 30 minutes and used as inputs for a Lagrangian particle tracking model (PTM) created using MATLAB. The PTM considered both advective and diffusive processes as presented in Chapter 3 (section 3.6.1). No swimming behaviour was considering since the strong tidal currents in Menai Strait (> 2 $m.s^{-1}$) are vertically homogenous meaning that any vertical migration behaviour of the larvae would have minimal impact on their dispersal (Pernet *et al.*, 2003). Further, no mortality was considered as this would reduce the number of samples for the statistical analysis, and because there is insufficient information of mortality rates during PLD (Horvath & Crane, 2010). Six particles release sites were chosen where there are mussel beds present (Bangor, Plas Menai and Brynsiencyn) and in regions of geographic interest (the Swellies, Plas Newydd and Abermenai Point) (Figure 4.7.A). 7,000 particles were released from each site scattered randomly within an area of 0.1 km^2 (Figure 4.7.B). Simulated velocities were linearly interpolated from 30 min to 5 min and particle positions were spatially bilinearly interpolated within the PTM to accurately represent the evolving velocity field. Furthermore, if particles were advected onto land, they were reflected back to their previous position (North *et al.*, 2008; Coscia *et al.*, 2013). Every particle position was recorded until the end of the simulation. Eight simulations were performed, with the release time shifted according to the tide (Figure 4.8). Four simulations

started during spring tides when water elevation was: 1) high; 2) low; 3) mid-ebb; and 4) mid-flood (Figure 4.8). The same method was applied during neap tides (Figure 4.8). As spawning period was previously studied on mussel bed located at Bangor, the time of released was based from there (Figure 4.8).

At the end of each simulation, a total of 56,000 particles where present in the domain which represented 336,000 particles across all simulations. The Menai strait was divided into 6 areas as presented in Figure 4.7 to estimate the proportion of larvae located in each area depending on: 1) the site of release; and 2) the tidal phase during release. The effect of the tidal phase on particle dispersal was studied in four ways: 1) comparison of all simulations one by one; 2) comparison of neap vs spring (4 simulations per tide); 3) comparison of ebb vs flood (2 simulations per tide); and 4) comparison of HW vs LW (2 simulations per tide). Area 1 covered particles that exited the Menai Strait from the south. Areas 2, 3, 4 and 5 are located inside the Menai Strait and represent the areas of Caernarfon, Plas Newydd, the Swellies and Bangor, respectively. Area 6 covered particles that exited the Menai Strait from the North. Finally, the residual currents were calculated within Blue Kenue package.

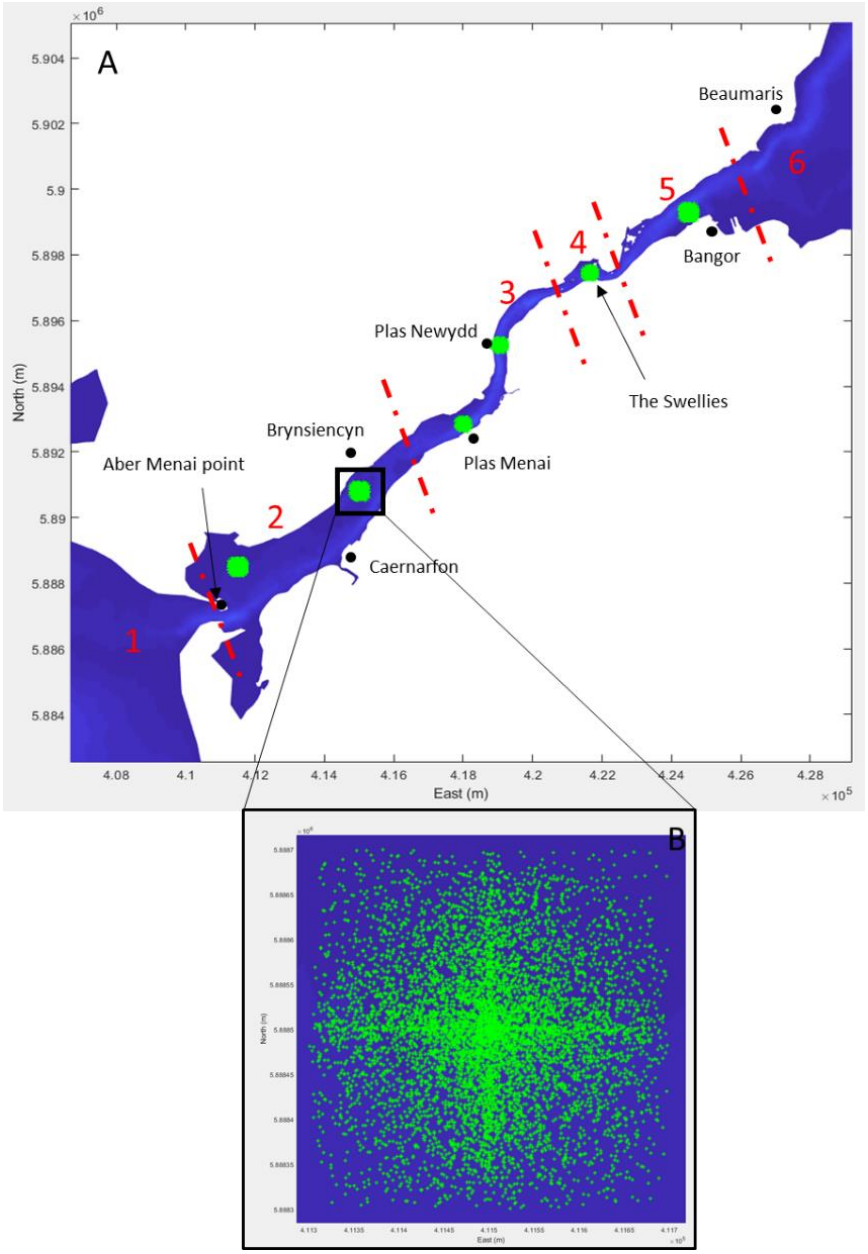

Figure 4.7: Particle release position in the Menai Strait (green patches) and areas of interest delimited by red dotted lines. Example of particles scattered in an area of 0.1 km2 from Brynsiencyn are presented in the sub-figure B.

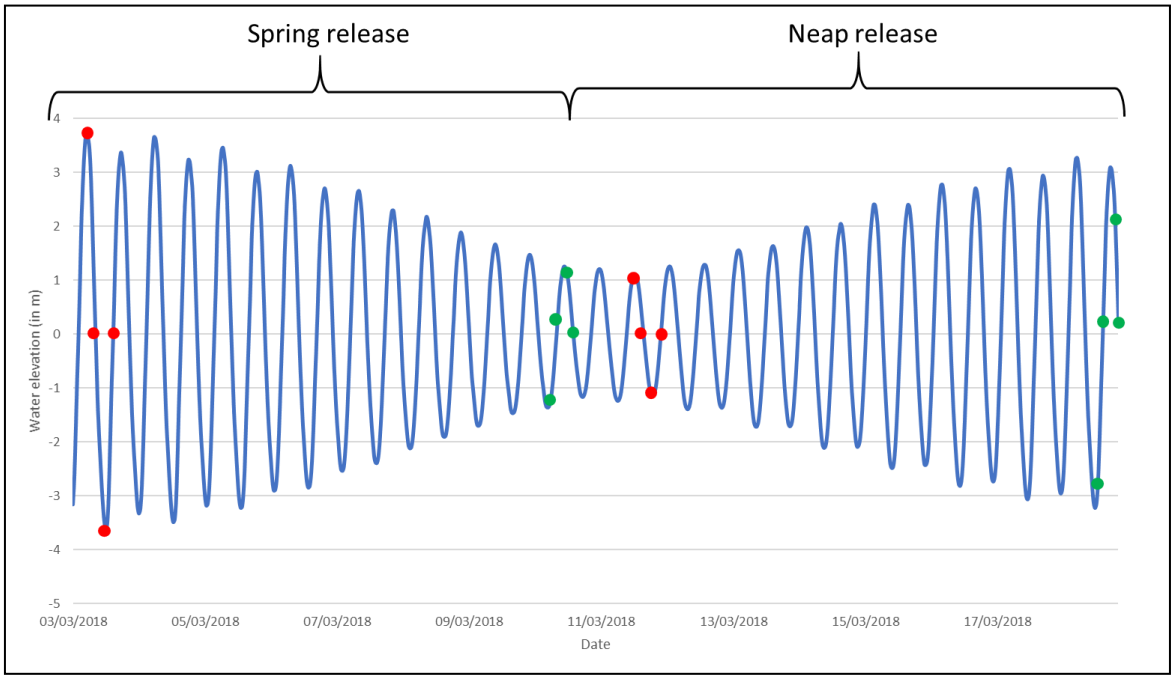

Figure 4.8: Bangor water elevation from the 3rd of March 2018 to the 19th of March 2018. Released time of particles for the eight simulations are represented in red for starting time and in green for the ending time.

4.2.2 Results

Here the results focus on the patterns of larval dispersal over one week, from selected release sites within the Menai Strait, in particular their ability to exit the strait from either the north or south and, hence, be exposed to wider dispersal around the Irish Sea during the later stage of their larval phase. All simulations together showed that 48% of the particles dispersed out of the Menai Strait within one week. The majority of the particles (45%) exited from the south of the Strait (Area 1), due to the strong and persistent southwest residual current. Only 3% of the particles dispersed north into Area 6. The remaining 52% of the particles were retained within the Menai Strait within one week (39% in the Swellies (Area 3), 7% in Plas Newydd (Area 4), 5% in Caernarfon (Area 2) and 1% in Bangor (Area 5)). This final result is interesting because it implies that there is a very low retention of larvae at Bangor mussel bed.

Different larval dispersal patterns were observed depending on the release site within the Strait, although a common result was that the Swellies acted as a trapping region for larvae dispersing north and south (Figures 4.9 and 4.10). For particles released from the Bangor mussel bed, 8% exited from the south while 12% exited from the north (Figure 4.9.A). Further, most of these particles were trapped in the Swellies, 73%. For particles released from Abermenai Point, 94% exited from the south and no particles dispersed further north than the Swellies (Figures 4.9.F). Similar results were simulated for particles released from Brynsiencyn (72% exited the south)

and < 0.5% dispersed north of the Swellies (Figure 4.9.E). For particles released from the Swellies, 68% remained in the same area within one week (Figure 4.9.B). Similarly, 40% of the particles released from Plas Newydd and Plas Menai were trapped in the Swellies, while 2% exited from the north and 40% from the south (Figures 4.9.C and 4.9.D). For all the particles that exited from the north of the Strait after one week, approximately 55% were released from Bangor and 25% from the Swellies (Figure 4.10). On the other hand, release sites south of the Swellies (Abermenai Point, Brynsiencyn, Plas Menai and Plas Newydd) contributed to 90% of particles that exited the south of the Strait (Figure 4.10). Plas Newydd acted as a tipping point, where particles were distributed equally within Areas 2, 3, 4 and 5 (~ 20% for each) and ~11% for Areas 1 and 6 (Figure 4.10).

The simulations showed different particles dispersal patterns within one week due to the tidal phase, although a clear correlation between the tidal phase and dispersal was not detected (Figure 4.11). 75% of particles released during neap ebb tide exited from the south of the Strait while < 1% exited form the north (Figure 4.11.A). However, 56% ± 3% of particles released during spring HW or neap LW exited from the south of the Strait and 2% ± 1% exited from the north (Figures 4.11.G and 4.11.D). Other scenarios showed similar results with 34% ± 7% and 5 % ± 1.5% of particles exiting from the south and north respectively (Figures 4.11.B; 4.11.C; 4.11.E; 4.11.F and 4.11.H). Three different groups were observed when focusing on particles that were retained in the Swellies. The first groups comprised particles released during neap flood tide, neap HW, spring flood and spring LW, showing 50% ± 3% retention in the Swellies (Figures 4.11.B; 4.11.C; 4.11.F and 4.11.H). The second group comprised particles released during neap LW, spring ebb tide and spring HW, showing 31% ± 1% retention in the Swellies (Figures 4.11.D; 4.11.E and 4.11.G). The third group comprised particles released during neap ebb tide with 18% retention in the Swellies. Two groups were apparent when focusing on particles retained in Area 2 (Caernarfon): 1) 8% ± 0.5% for release during neap HW and spring flood tide; and 2) 4 % ± 1% for all other scenarios (Figure 4.11). Results showed particles released during neap LW and spring ebb tide led to 12% ± 1% retention in Area 3, while releasing during neap flood tide and spring flood tide led to 7% ± 0.2% retention in Area 3 and other scenarios led to 5% ± 1.5% retention in Area 3 (Figure 4.11).

The comparison between neap and spring tides showed no difference among areas except for Bangor (Area 5) (Figure 4.12.A). Indeed, the spring tide release contributed to 81% of the particles found in Bangor area after one week. Further, Figure 4.11 shows that when particles were released during neap tide, they were found further south, along the Llyn peninsula (Area 1). Equal proportions of particles released during ebb or flood tides dispersal to Plas Newydd and Bangor (Areas 3 and 5) (Figure 4.12.B). However, particles released during ebb tide were

more likely to exit from the south of the Strait (65%) than particles released during flood (Figure 4.12.B). Particles released during HW or LW showed no significant difference in dispersal patterns (Figure 4.12.C). Particles released at LW contributed mostly (65% ± 5%) to the particles found in Areas 3, 5 and 6 (Figure 4.12.C).

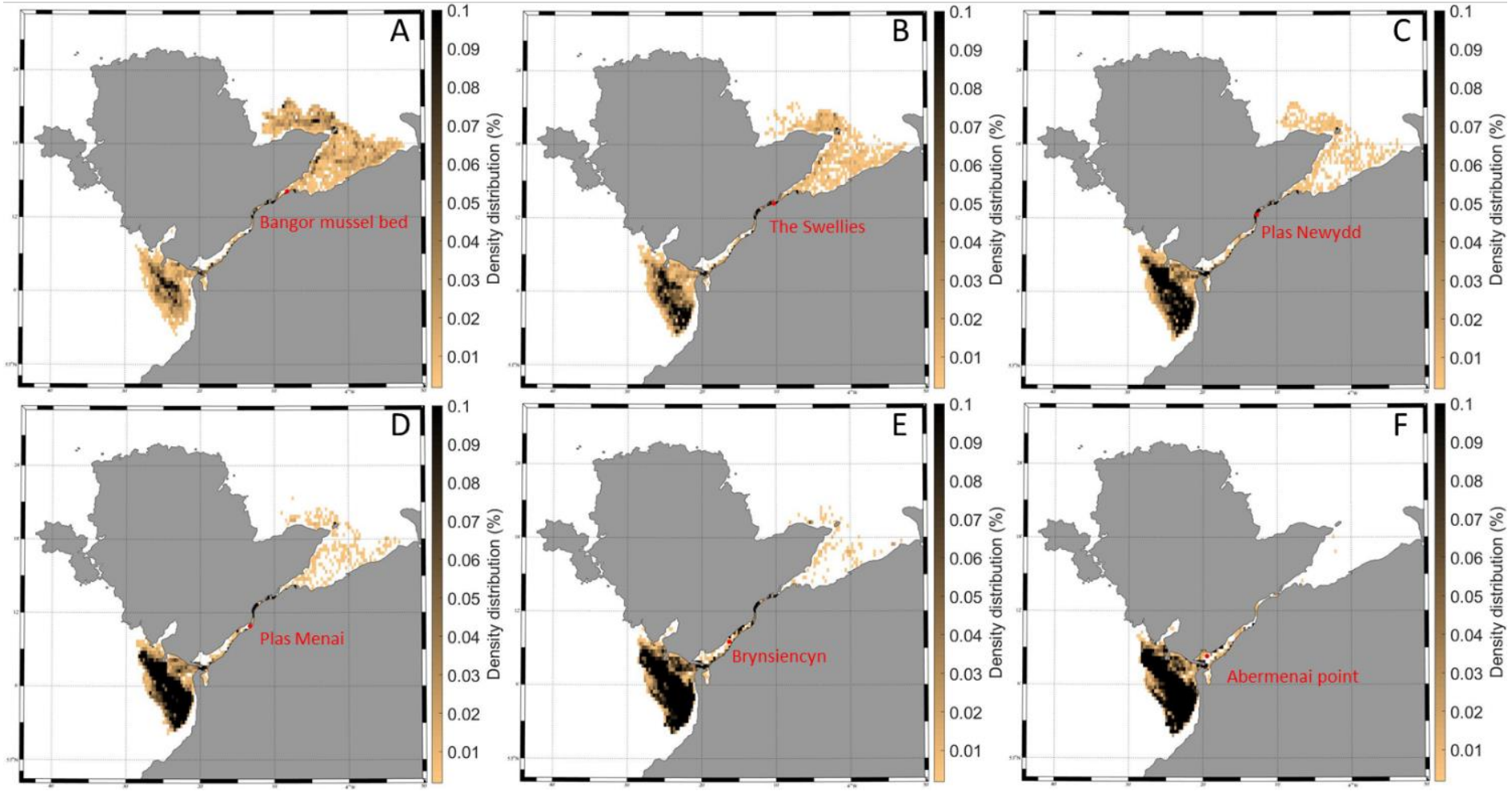

Figure 4.9: Density distribution of mussel larvae after one week with released area represented by a red dot: (A) Bangor mussel bed; (B) the Swellies; (C) Plas Newydd; (D) Plas Menai; (E) Brynsiencyn; and (F) Abermenai point.

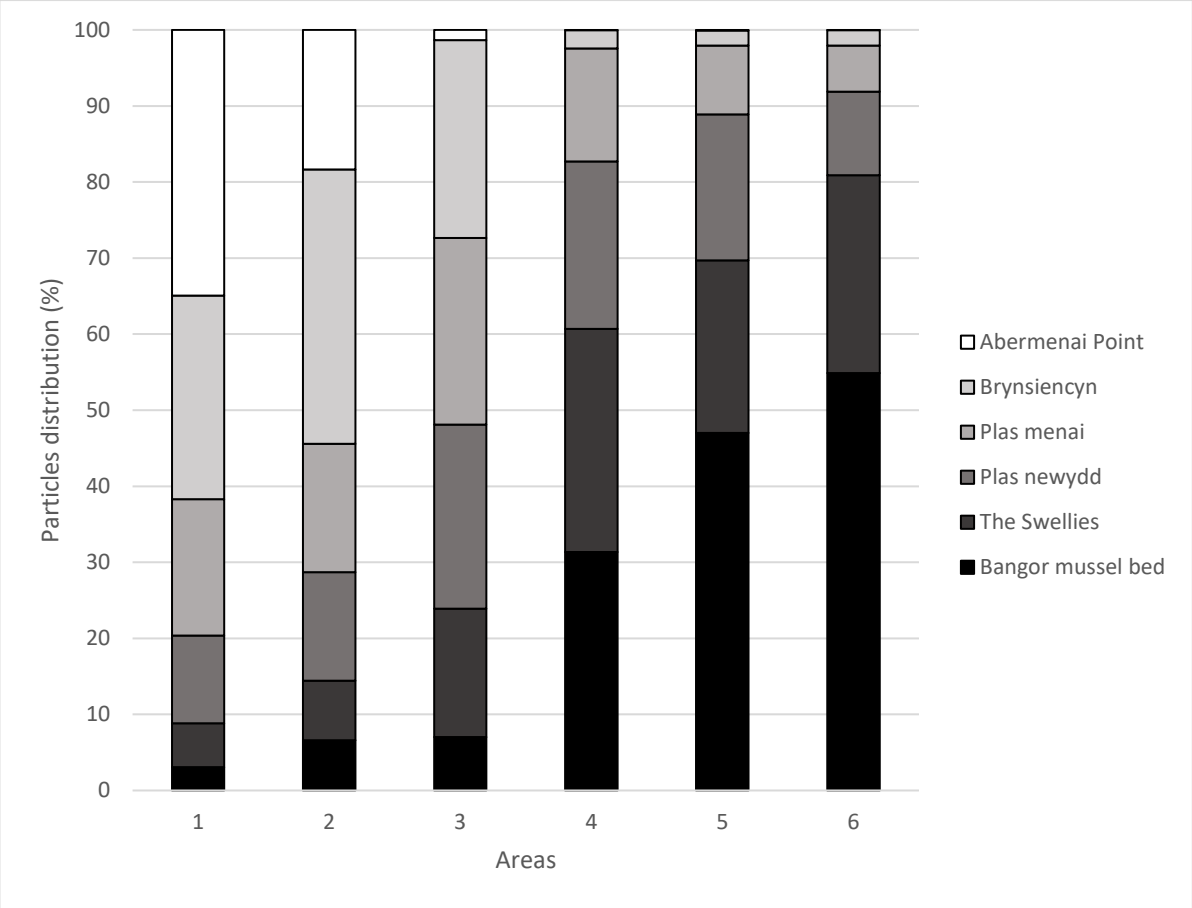

Figure 4.10: Particles distribution in % for 6 areas of interest depending on the release site: The areas of interest are : 1) South of the menai Strait; 2) Caernarfon; 3) Plas newydd; 4) the Swellies; 5) Bangor; 6) North of the Menai Strait. The sites of released are represented in: 1) black for Bangor mussel bed; 2) light black for the Swellies; 3) dark grey for Plas Newydd; 4) medium grey for Plas menai; 5) light grey for Brynsiencyn; and 6) white for Abermenai point.

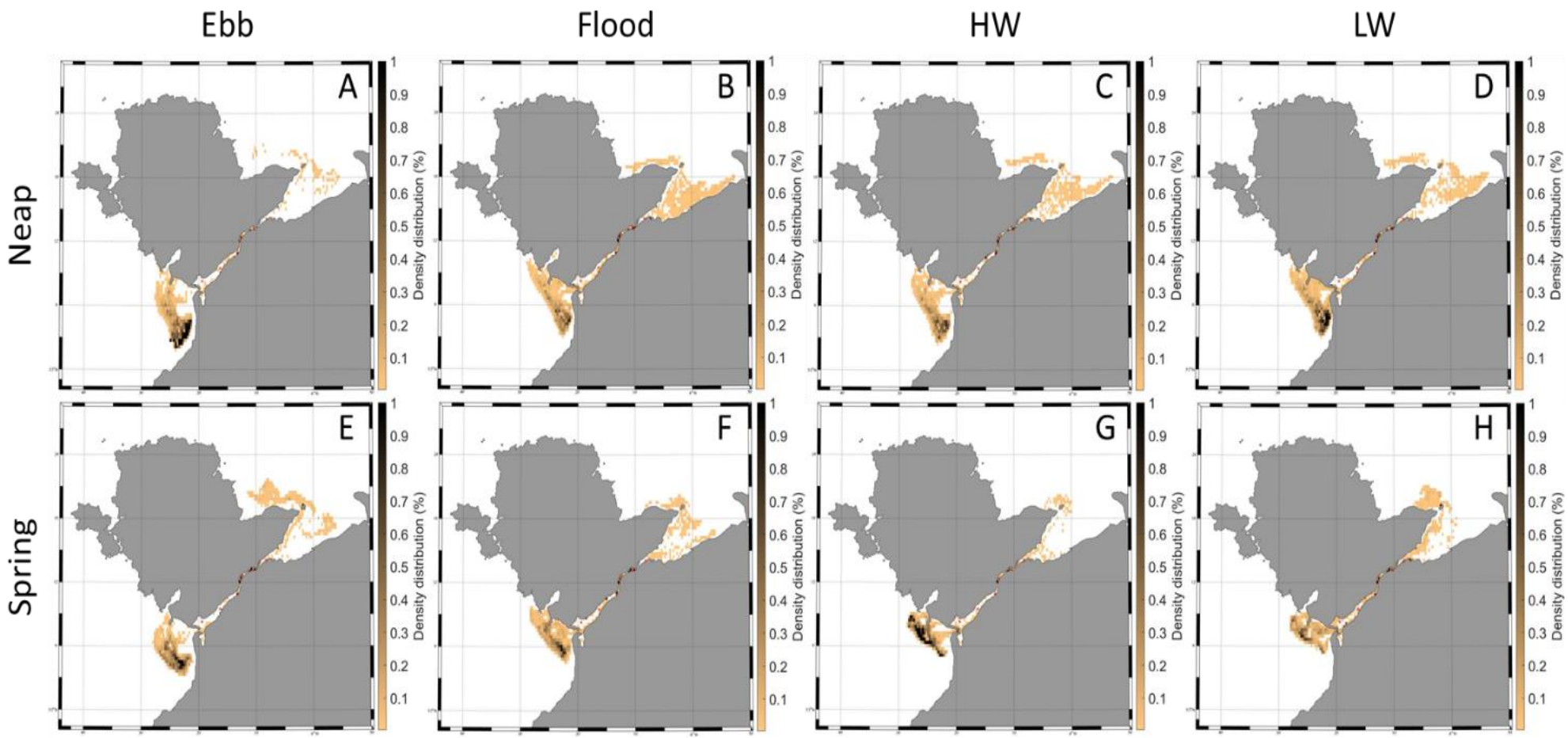

Figure 4.11: Density distribution of mussel larvae after one week depending on the tidal phase during particle release: (A) neap ebb; (B) neap flood; (C) neap HW; (D) neap LW; (E) spring ebb; (F) spring flood; (G) spring HW; and (H) spring LW.

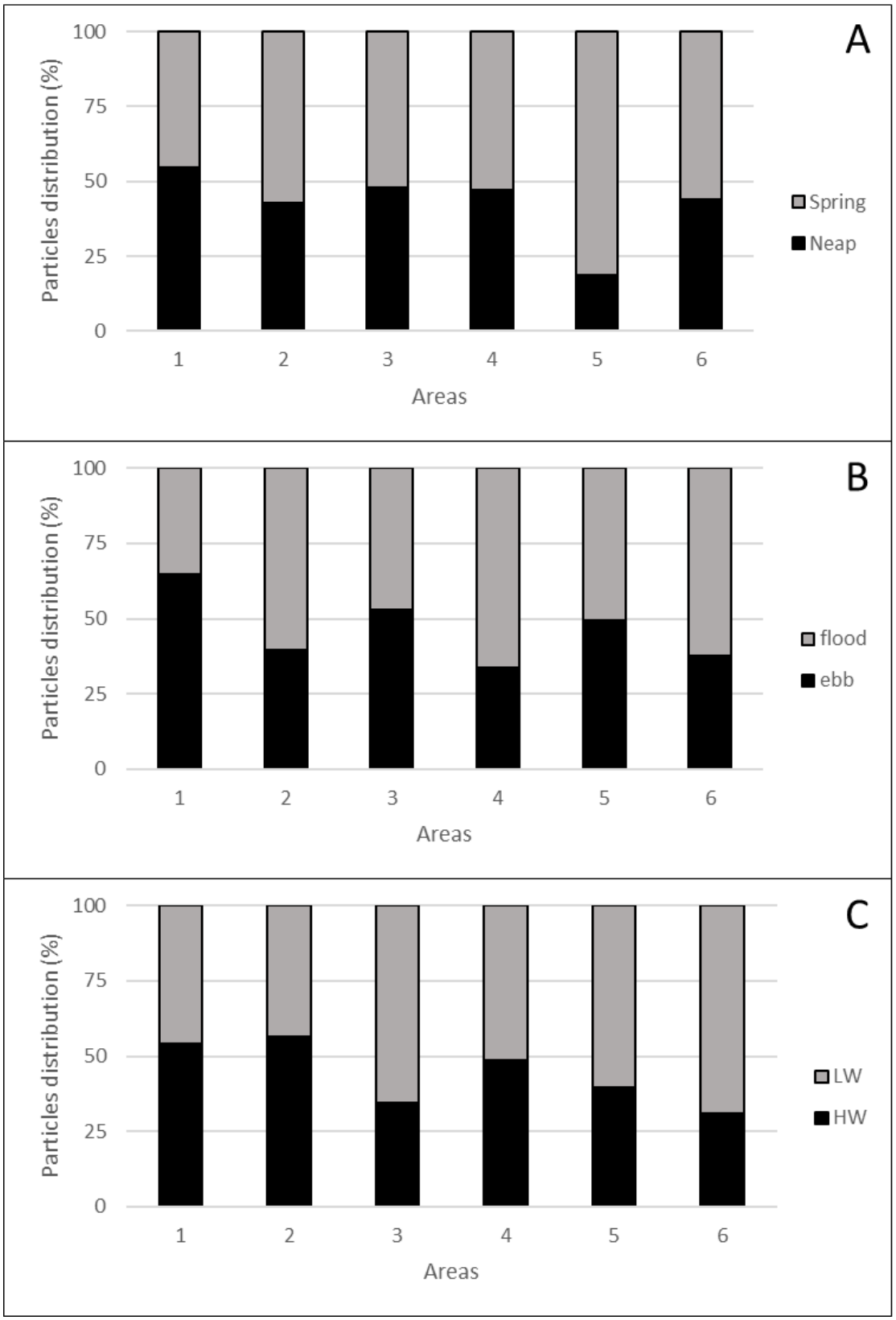

Figure 4.12: Particles distribution in % for 6 areas of interest depending on the release tide. The areas of interest are : 1) South of the Menai Strait; 2) Caernarfon; 3) Plas Newydd; 4) the Swellies; 5) Bangor; and 6) North of the Menai Strait. Particles were released during: (A) spring tide in grey and neap tide in black; (B) flood tide in grey and ebb tide in black; and (C) LW in grey and HW in black.

4.2.3 Discussion

Considering all PTM simulations within the Menai Strait, 95% of particles were present south of the Swellies after one week, meaning only 5% were present in the northern part of the Strait. Further, approximately half of these particles managed to exit the Strait after one week, the vast majority exiting from the southern end. These results are consistent with the literature, which confirmed a persistent south-west residual current through the Strait (Harvey, 1967; Simpson *et al.*, 1971; Sherwin *et al.*, 1997; Rippeth *et al.*, 2002; Tweddle *et al.*, 2005; Simpson *et al.*, 2007; Davies & Robins, 2017). For the particles that remained within the Menai strait after one week (52%), the majority of them were trapped in the Swellies (39%) especially in the north part of the Swellies. Further, 68% of particles released from the Swellies remained there. These results are different from those presented by Harvey (1967), whereby drifters located in the Swellies after one week represented 1.7% of all the drifters released. However, the comparison was not exact as the drifters were released from different locations and during different dates. Nevertheless, the PTM may over-predict particles retention within this very energetic and narrow (250 m) part of the channel. Although the model was configured to maximise spatial and temporal resolution of the flow field (PTM timestep of 5 min and 20 m mesh) whilst being computationally practical.

Particles released from Abermenai Point did not go further north than the Swellies. Harvey (1967) made the same observations with drifters released at the south entrance of the Menai Strait. Despite the SW residual current, particles can travel north in the Menai Strait over one week. This phenomenon could be caused by strong southwest winds that reverse the surface flow (Simpson *et al.*, 1971), or by transvers flow on the ebb tide trapping particles close to the banks of the channel (Robins *et al.*, 2012). Also, the results in this study suggested that approximately 10% of particles released from the Bangor mussel bed reached both north and south exit of the Menai Strait. Again, these results are correlated with Harvey (1967) in which approximately 10% and 3% of particles were found at both south and north exit when drifters were released from Bangor. The similar results observed for Plas Newydd and Plas Menai is explained by the proximity of the two sites where particles encounter similar tidal flows. Results showed that 80% of the particles reaching the north exit of the Menai Strait came from the Bangor mussel bed and the Swellies, while 90% of the particles found in the south came from Abermenai Point, Brynsiencyn, Plas Menai and Plas newydd. The Swellies, because of the strong and complex currents, acts as a barrier that reduce connectivity between the mussel beds located in the south and the north of the Menai Strait. Genetic studies could address this new hypothesis by studying the genetic difference among several broadcast spawning species (e.g.

mussels, limpets and barnacles) at different location along the Menai Strait (Berumen *et al.*, 2012; Pusack *et al.*, 2014; Harrison *et al.*, 2014).

The comparison between particles released during neap and spring tide showed no significant difference on their contribution to the particles found in Areas 1, 2, 3, 4 and 6 after one week. The difference calculated between the residual current shows that the components U and V and direction are mostly similar within the Menai Strait, which never exceed 0.05 m/s, 0.04 m/s and 80 degrees respectively (Figures 4.13.A; 4.13.B and 4.13.C). However, within Area 5 (Bangor), the spring tide simulation showed a difference of residual current direction of 80 degrees compared with the neap tide release (Figures 4.13.C). The difference caused the particles to remain in Area 5 by pushing them on the coast. Figure 4.11 showed that particles were found more south along the Llyn Peninsula when release during neap tide. The strongest magnitude is observed for a spring tide release simulation with values above 0.015 m/s within the Menai Strait. However, the residuals of U and V components seem to be higher when particles were released during neap tide at the south exit of the Menai Strait with maximum values of 0.5 m/s for both (Figures 4.13.A, 4.13.B and 4.13.D). A previous study performed by Campbell *et al.* (1998) showed that the ebb flow southwards was 10% to 15% stronger than the flood flow northwards. The results above confirmed this when 65% of the particles found in the south exit of the Menai Strait came from a release during ebb tide. The flood tide pushed the particles northward where they were trapped in the Swellies especially those released from Plas Newydd. This explains why the flood contributed to 66% of the particles found in the Swellies after one week. Furthermore, for the particles released from the Bangor mussel bed during flood, they had more chance exiting the Menai Strait where the residuals currents are northward (Figure 4.14). The same observations were made for simulations releasing particles at HW and LW. Indeed, for particles released at LW, the flood tide transported the particles northward which explains why LW released particles promotes northward travel.

The results presented here have shown that the tidal period and the area of release markedly impacted the particle dispersal patterns. The fieldwork to establish the mussel (spawning timings) showed that the larger spawning events occurred during neap tide and smaller trickle spawning events occurred during spring tide. As the mussel were located in the high intertidal area, they are submerged only at HW. Consequently, for the year 2018, the dispersal of particles after one week are more likely to be represented by the results shown in Figures 4.9.A; 4.11.C and 4.11.G. These results highlight the possibility for mussel larvae to settle in the Menai Strait after one week. However, this settlement might not be definitive as it was previously shown that mussel could have several settlement stages with the first settlement on filamentous algae and the second on already established mussel bed (Maas Geesteranus, 1942; Bayne, 1964;

Petersen, 1984; McGrath & Gosling, 1988; Grizzle *et al.*, 1996; Dobretsov & Wahl, 2001). Further, it is established that *Mytilus edulis* PLD can reach six weeks according to different environmental factors (e.g. temperature, ability to find a substrate) (Bayne, 1965; Seed, 1969). Consequently, mussel larvae from the Menai Strait can possibly connect with other mussel beds located along the north welsh coast.

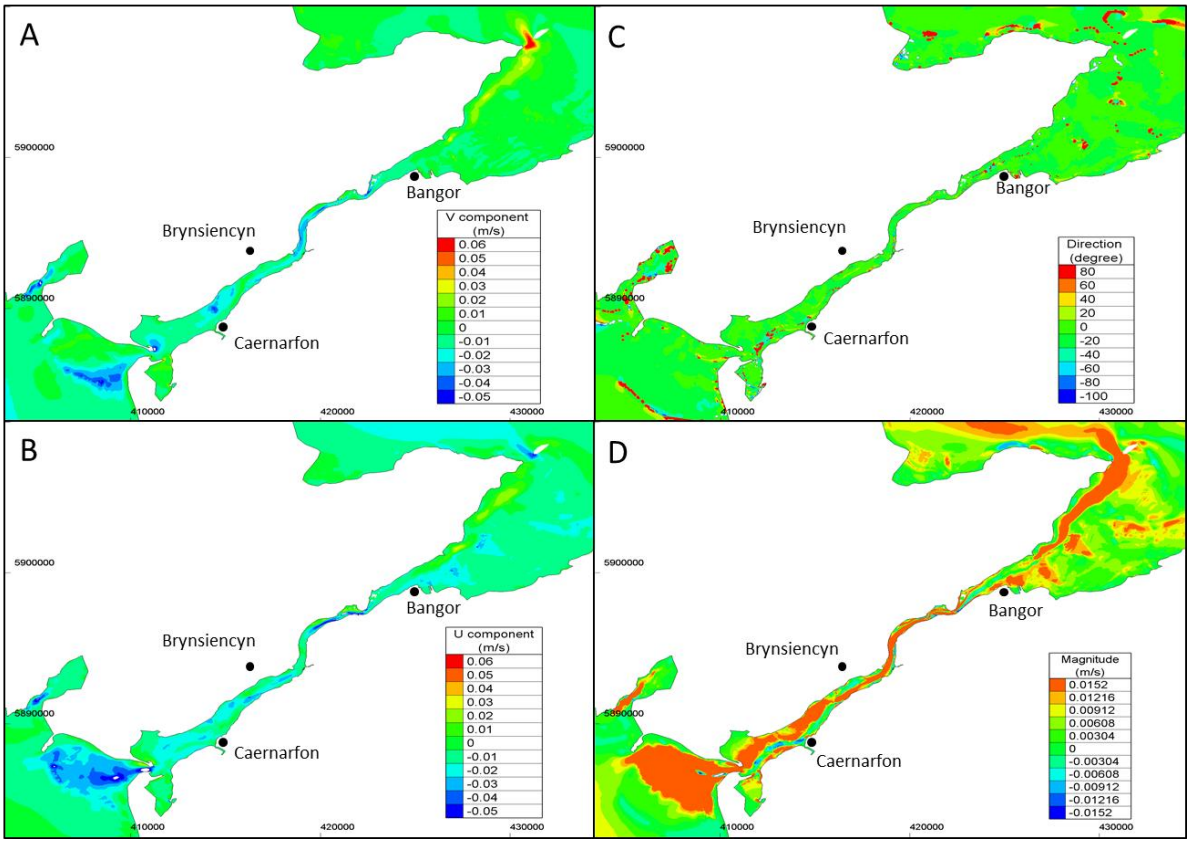

Figure 4.13: Difference of the residual current between simulations starting during spring tide and simulation starting during neap tide. Results present the difference for: A) V component in m/s; B) U component in m/s; C) direction in degrees; and D) magnitude in m/s. Warm colours (red to yellow) show a positive difference when spring is higher than neap. Green colours show when both residuals are equal. Cold colours (Light blue to dark blue) show when neap is higher than spring.

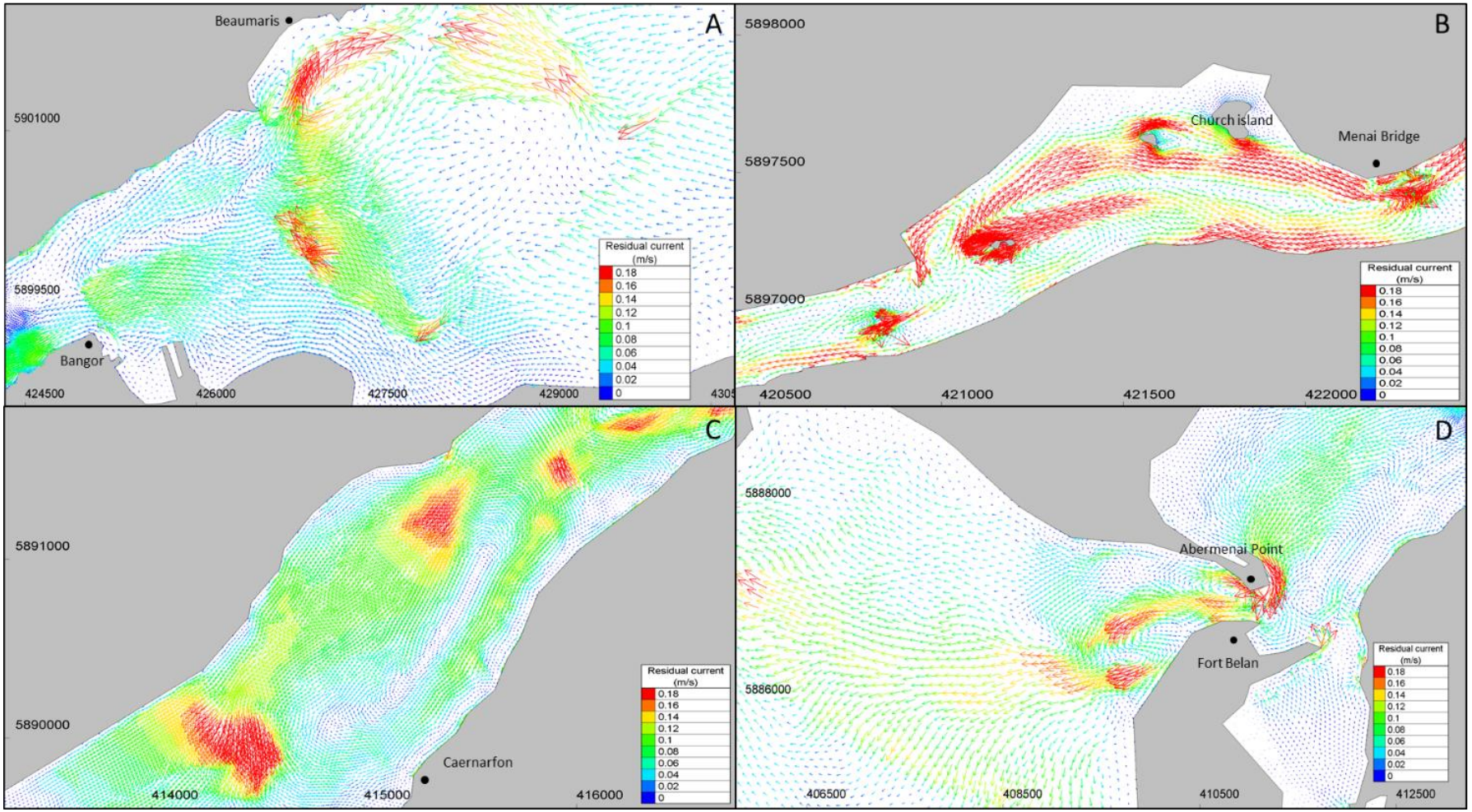

Figure 4.14: Residual current in the Menai Strait for a week of simulation starting during ebb: A) North of the Menai Strait; B) The Swellies; C) Caernarfon; and D) South of the Menai Strait. Residual currents are represented by arrows for the direction and colours for the strength.

Chapter 5: Mussel beds dispersal and connectivity in North Wales

Mytilus edulis are present at geographically distinct mussel beds throughout the Irish Sea, with the highest densities found in the north of Ireland, North Wales and Pembrokeshire (Gosling *et al.*, 2008) (Figure 1.11). The mussel industry in North Wales represents one third of the UK production (valued at 15.10 £m), which made shellfisheries aquaculture the third most important and lucrative activity (Hambrey & Evans, 2016). During the past 10 years, Morecambe Bay has been one of the main sources of recruitment of wild mussel spat and has been an area where wild mussel spat has been harvested to be seeded in the Menai Strait; although this resource has varied interannually (pers. com. with farmer). One of the main questions of this study is to understand if mussel larvae from North Wales settle in Morecambe Bay and if not, where can they be found in the Irish Sea. A key aim of this chapter is to use modelling to quantify and qualify the mussel larval dispersal from selected North Wales mussel populations. Previous attempt was made by Robins *et al.* (2013) who showed the importance of larvae behaviour on dispersal (e.g. swimming behaviour tidally or diel synchronized). However, the PLD last for 28 days when larvae can spend up to 40 days in the water column, plus physical parameters such as wind driven current were not considered. This study will focus exclusively on selected mussel bed in north Wales for the economic and environmental interest. Furthermore, the PLD will be extend to 6 weeks in order to simulate larvae dispersal until they reach a critical stage when settlement is compulsory. Further, two behaviours were considered if larvae travel at the surface and if the travel at mid-depth. Consequently, for larvae positioned at the surface the wind driven were considered as it has been shown to influence larvae dispersal, however larvae at mid-depth were tidally advected only (Lane *et al.*, 1985; Gaylord *et al.*, 2002; Criales *et al.*, 2007; Harnett *et al.*, 2007; Robins *et al.*, 2012; Robins *et al.*, 2013; Rhörs *et al.*, 2014; Weidberg *et al.*, 2015; Daigle *et al.*, 2016).

The connectivity between distinct shellfish populations within the Irish Sea has been studied by Robins *et al.* (2013), who showed variable connectivity according to the site of release and larvae behaviour (e.g. passive, tidally synchronized swimming and diel-synchronized swimming). Robins *et al.* (2013) studied larval dispersal for a pelagic larval duration (PLD) limited to 26-30 days. However, several authors demonstrated that mussel PLD are between 20 to 45 days in North Wales, where sea temperatures range from 8ºC to 15ºC and salinities from 30‰ to 35‰ (Brenko & Calabrese, 1969; Bayne, 1976; Beaumont & Budd, 1982; Sprung, 1984; Pechenik *et al.*, 1990; Lecorre *et al.* 2013; Filgueira *et al.*, 2015; Dinh & Fotedar, 2016). Beyond this limit of 45 days mussel reach a critical stage (e.g. pediveliger) when they must find a substratum to attach (Brinkman *et al.*, 2003). Previous study by Harnett *et al.* (2007) showed the importance of wind-driven currents on scallop larval dispersal in the Irish Sea. The aim of

this chapter was to investigate the wider dispersal of mussel larvae throughout the northern Irish Sea to understand how the larvae from the Menai Strait connect with sites of interest (e.g. Morecambe Bay).

Model simulations were undertaken to: 1) study the dispersal of mussel larvae from 10 different sites according to two plausible larval behaviours (i.e. larvae remain at the surface or larvae travel in the mid-water column); 2) quantify the distance that mussel larvae travel according to their release site and behaviour; and 3) qualify and quantify the connectivity between the 10 release sites (and other sink mussel bed sites in the Irish Sea) during spring and summer 2018 for a PLD between 20 and 45 days.

5.1 Materials and methods

The hydrodynamic model of the Irish Sea (Grid 1: see Chapter 2, Section 2.1.1.) was used as the basis for these simulations. The unstructured mesh has a resolution varying from 30 m within the Menai Strait to 2,000 m further offshore. Two simulations, each two months long, were computed for the periods of: 1) March to April 2014; and 2) March to April 2018. These simulations were validated using tide gauge data and current data as presented in Chapter 2 (Section 2.4.5.). The depth-averaged currents computed by the model were output every 30 minutes, then interpolated to a constant spatial resolution of 50 m and used for the subsequent Lagrangian particle tracking model (PTM) simulations. The same parameters and assumptions used for study of larvae dispersal in the Menai Strait (Chapter 4, Section 4.2) were used here:

- Simulate dispersal using both advective and diffusive processes.
- No larval swimming behaviour was simulated.
- The Irish Sea is considered well mixed during the period of study
- No mortality was considered.
- Linear temporal interpolation of velocity from 30 min (Telemac output) to 5 min (PTM output).
- Bi-linear interpolation of velocity data to individual particle positions.
- Particles advected onto land are reflected back to their previous position, maintaining the maximum number of particles throughout the simulated period of dispersal.

Ten larvae release sites were chosen where there are commercial mussel beds (Bangor, Brynsiencyn, Holyhead Mostyn and Conwy), natural mussel beds (Llandudno and Red Wharf Bay) and mussel beds established due to human infrastructure (Offshore wind farms: Rhyl Flat, Gwynt Y Mor and North Hoyle) (Figure 5.1). From each site, 7,000 particles were released, distributed randomly within an area of 0.2 km^2. Each PTM simulation lasted 45 days (e.g. 2,160

time steps) to match the maximum recorded mussel PLD (Figure 5.1). Every particle position was recorded until the end of the simulation. Eight simulations in total were performed. Two simulations were performed for particles which travelled in the middle of the water column (i.e. 2D advection subjected to tidal currents only) during March-April 2014 and March-April 2018. Three simulations were performed for particles released at the surface during 2014 and three were performed during 2018 where both tidal and wind-driven currents were taken into account using the method presented in Chapter 3 Section 3.6., to parameterise surface-driven flows (Equations 3.1 and 3.2). Each three simulations were performed using wind data from different meteorological stations. Then results of each simulation were added in order to represent more accurately the wind field during 2014 and 2018. The stations for wind data were chosen due to their proximity to the 10 release sites. Wind speed data were downloaded for March and April 2014 and 2018, from Centre for Environmental Data Analysis website for the stations: 1) Valley on Anglesey (53.25 latitude and -4.53 longitude); 2) Rhyl (53.31 latitude and -3.50 longitude); and 3) Crosby (53.497 latitude and -3.0563 longitude) (Figure 4.15) (from CEDA website). The years simulated were chosen to study the influence of the wind-driven currents on larval dispersal based on: 1) the field work conducted in this study and observations from mussel farms for 2018 when no settlement was observed in Morecambe Bay (Chapter 4, Section 4.1) (Trevor Jones, pers. comm.); and 2) observations form mussel farms of settlement in 2014 when massive recruitment was observed in Morecambe Bay (1,100 tonnes harvested by the mussel farms) (Trevor Jones, pers. comm.). The timings of particle releases were defined by the period of spawning observed in 2018 during the field work conducted in this study, i.e. simulation from 26th of March 2018 to 10th of April 2018 (Chapter 4, Section 4.1). For the simulation in 2014, the period of release was based on the results obtained in Section 4.1.1., indeed main spawning events appeared when the difference between air temperature (AT) and sea surface temperature (SST) was between 3.5ºC and 2.5ºC. The difference between AT and SST from March 2014 to September 2014 was calculated. Appendix D showed a difference of 2.55ºC the 12th March 2014 which might have make the mussel spawn according to the field work results obtained in this study. Consequently, particles simulated during 2014 were released from the 12th March 2014 to 23rd April 2014.

The spatial density distribution of dispersed particles (or 'heat maps') was calculated every week (i.e. weekly cumulative dispersal) as the percentage of all released particles per 25 km^2 grid cell. This procedure was repeated for both larval behaviours. Additionally, the cumulative distance (CD) (e.g. sum of the distance made for each time step) and the net transport (NT) (e.g. from starting position to final position) for each particle from their release position to their weekly final position was calculated (Figure 5.2). The normality of the data distribution was

first studied for all sites. Then an Anova test was performed to study the statistical difference of the distance travelled by larvae depending on: 1) the site of release and 2) the weekly PLD. Further, a correlation test was used to compare the weekly CD according to the different released sites.

Connectivity and self-recruitment were calculated (cumulative weekly values) for the weeks 3, 4, 5 and 6 (e.g. 21 days to 42 days) for all simulations. Connectivity matrices describe the exchange between distinct populations as the percentage of particles reaching a settlement area from a released site (Ayata *et al.*, 2010). In this study, 10 release sites and 5 settlement sites were used where mussel settlement was previously observed (pers. comm. with Trevor Jones (Extramussels Ltd) and Nicolas Chopin (BIM in Ireland)) (Figure 5.1). The settlement sites are located on the eastern Irish Coast (e.g. Dublin, Dundalk and Drogheba) and the western British coast (e.g. Morcambe Bay and Solway Firth) (Figure 5.1, orange dots). Particles were counted as settlers when they were present within an area of 25 km^2 of one of the 15 sites of interest at the end of each week. Results of each connectivity matrix are presented in percentages, which means that values close to 100% indicate a high connectivity or self-recruitment, whereas values close to zero indicate low connectivity or self-recruitment.

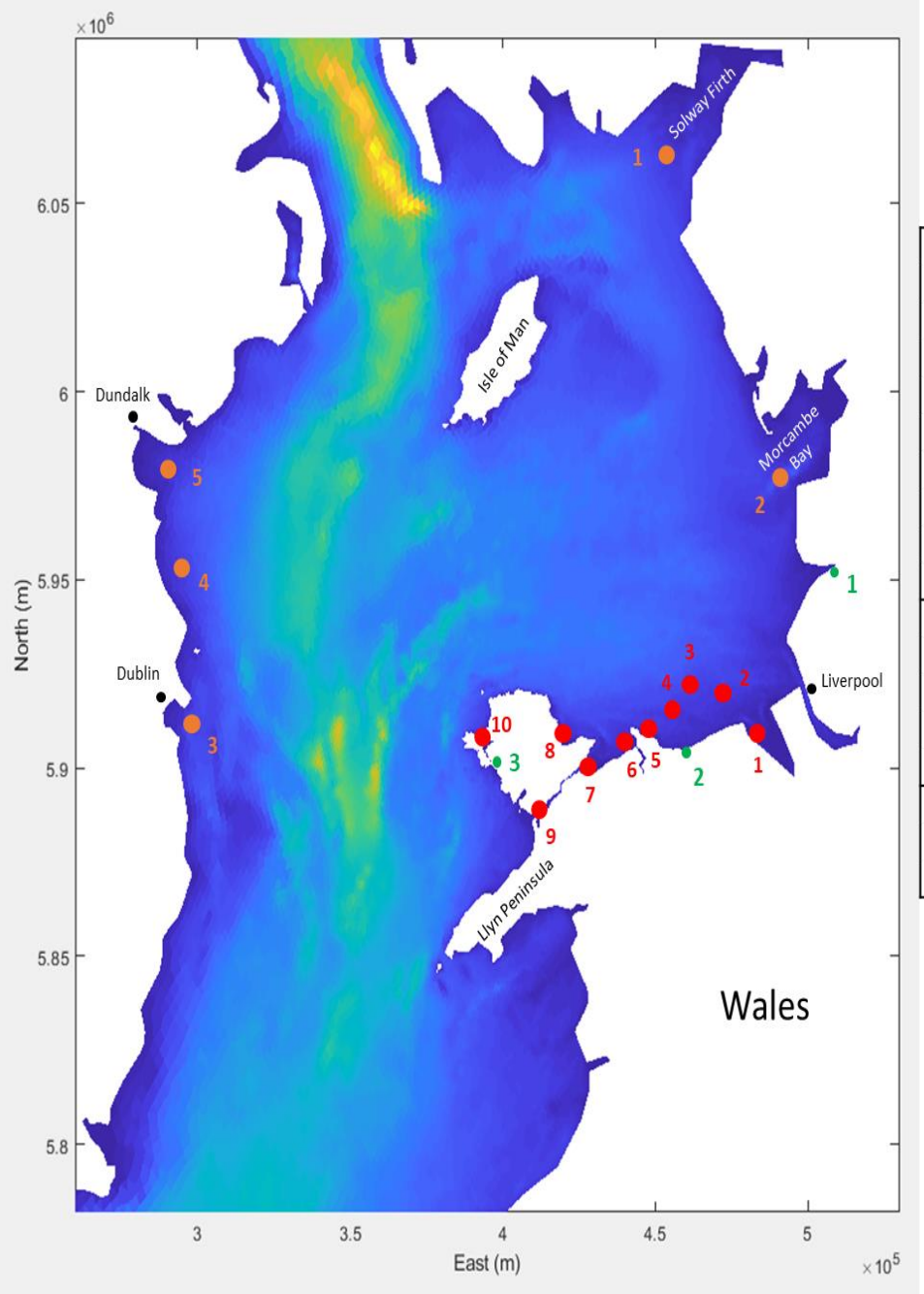

Figure 5.1: Location of particle release/settlement sites (red dots), settlement sites only (orange dots) and wind station data (green dots).

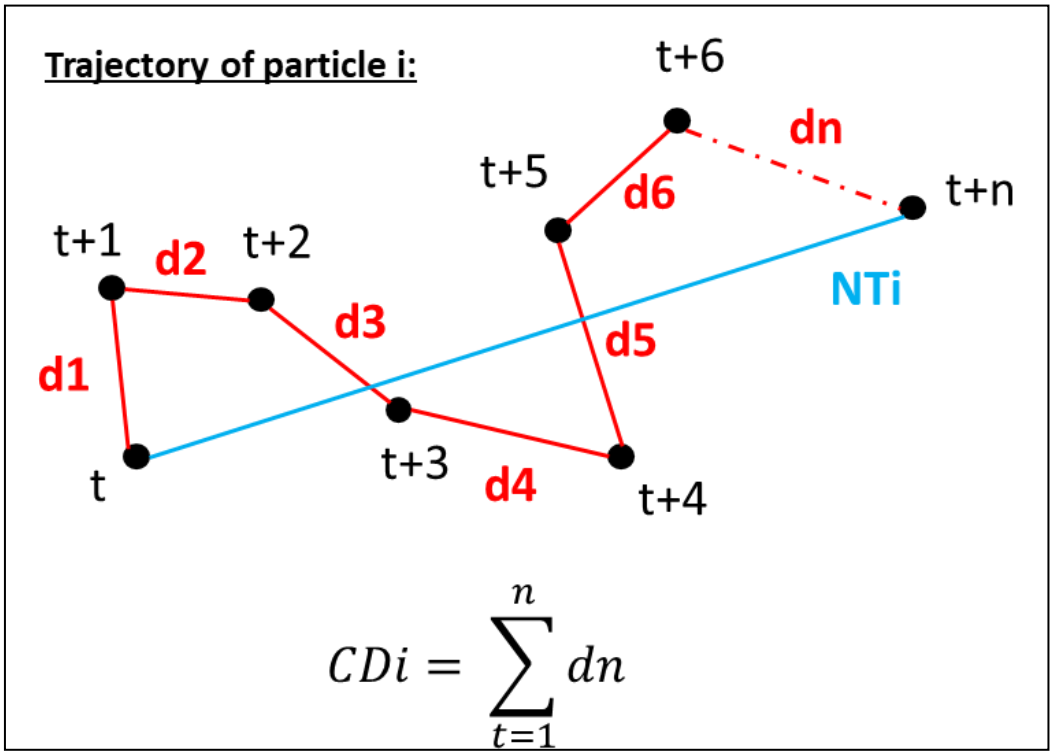

Figure 5.2: Cumulative distance (CD) and net transport (NT) calculated for particle i during n timestep with black dot representing particle position at each time step (t) and red line representing the distance (d) travelled by particle during two time steps.

5.2 Results: Simulated larvae distribution

5.2.1 Simulation representing larvae released at mid-water depth

5.2.1.1 Larval distribution

The simulated distribution of larvae, when released at mid water depth, were studied during March and April in 2014 and 2018. The results were very similar for both years. Therefore, only the distribution of particles for 2018 are presented in this section. However, results of particles simulated at mid-waters in 2014 can be found in Appendix E. Figure 5.3 shows the cumulative weekly particle distribution for all 70,000 particles (7,000 per 10 released sites). Considering all release sites together, the northern limit of particle distribution was the approximate latitude of the Isle of Man, and the southern limit was southern Cardigan Bay (Figure 5.3.F). Particles dispersed west to the middle of the Irish Sea, but no particles reached the eastern Irish coast. Particles were capable of dispersing east to the coast around Liverpool – but not as far north as Morecambe Bay. During, the first two weeks simulated, the particle distribution was highest at the southwestern approach to the Menai Strait (2.5%) and near

Llandudno (2%) (Figures 5.3.A and 5.3.B). After three weeks simulation, particles were found mostly near Llandudno (1.5%) and along the Llyn Peninsula (1%) (Figure 5.3.C). For the last three weeks of simulation, particles were more distributed near Llandudno (1.5%) (Figures 5.3.D; 5.3.E and 5.3.F).

Figure 5.4 shows larvae distribution per site after 6 weeks simulated. Larvae released from Bangor and Brynsiencyn showed the same patterns, namely a southward particle dispersal (Figures 5.4.G and 5.4.I). Particles released from Llandudno and Conwy showed both a westward dispersal along the north coast of Anglesey and a southward dispersal when reaching the north entrance of the Menai Strait (Figure 5.4.E). Red Wharf Bay and Holyhead sites show also the same patterns with a westward dispersal of the particles (Figures 5.4.H and 5.4.J). Particles released from the offshore wind farms (North Hoyle, Gwynt Y Mor and Rhyl flat) show similar larval dispersal with a majority of particles remaining in the same area (Figures 5.4.B; 5.4.C and 5.4.D). Mostyn showed a particle dispersal both westwards along the north welsh coast and northward along the English coast to Southport (Figure 5.4.A).

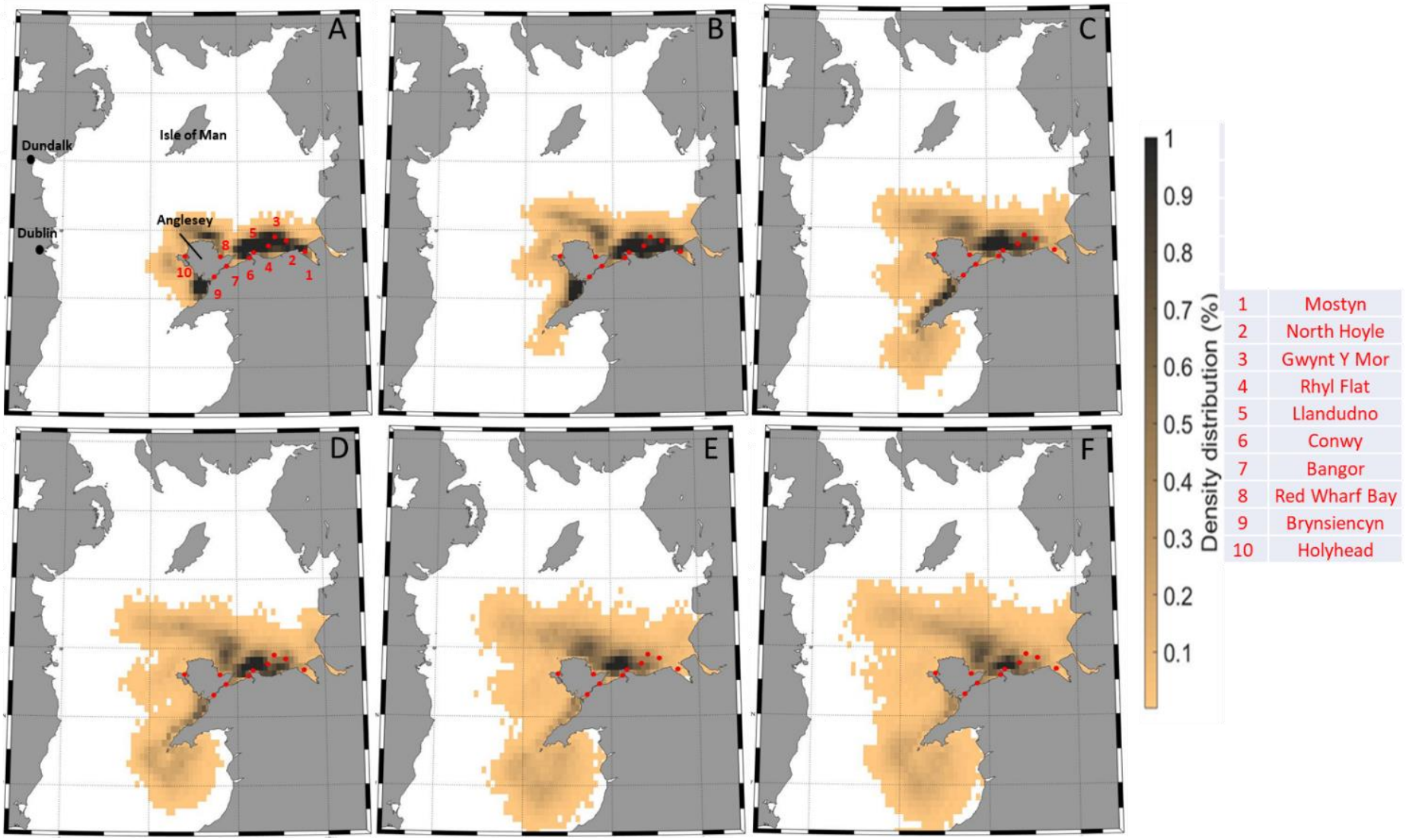

Figure 5.3: Maps showing the density distribution of mussel larvae released at the midwater column in March-April 2018 (advected by tide only) from 10 released areas (red dots) during: (A) week 1; (B) week 2; (C) week 3; (D) week 4; (E) week 5; and (F) week 6.

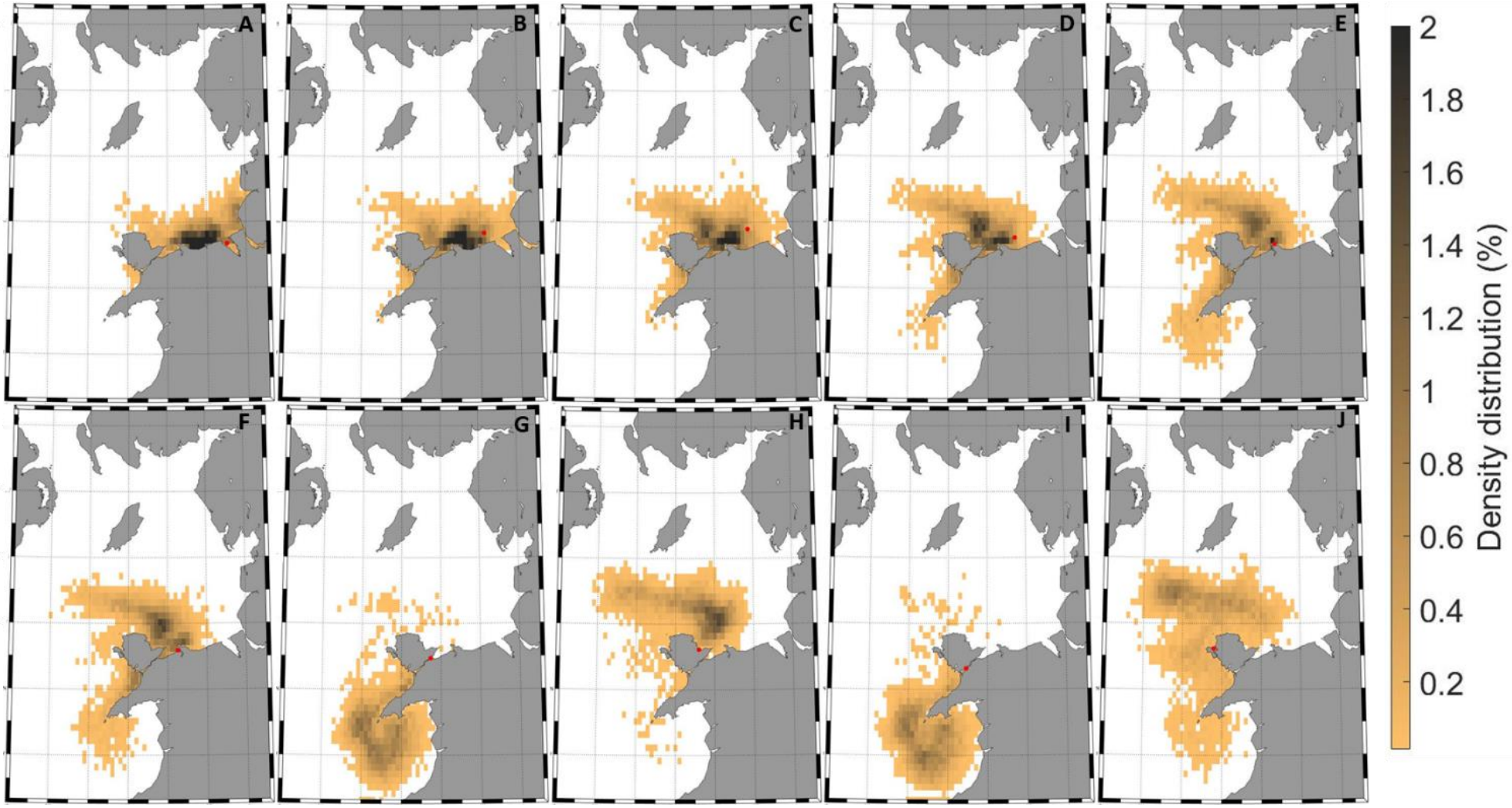

Figure 5.4: Maps showing the density distribution of mussel larvae released at the midwater column (advected by tide only) after 6 weeks simulation in March-April 2018 from 10 released areas (red dots): (A) Mostyn; (B) North Hoyle; (C) Gwynt Y Mor; (D) Rhyl Flat; (E) Llandudno; (F) Conwy; (G) Bangor; (H) Red Wharf Bay; (I) Brynsiencyn; and (J) Holyhead.

5.2.1.2 Distance travelled

For all released particles across all sites, the average cumulative distance (CD) after 6 weeks was 2,315 km (Figure 5.5). Particles released from Anglesey (Red Wharf Bay and Holyhead) dispersed furthest from week 1 to week 6, indeed cohort average CD varied from 301 km to 2,161 km for Red Wharf Bay and from 435 km to 2,884 km for Holyhead (Figure 5.5). In contrast, particles released from Mostyn dispersed least from week 1 to week 6 (cohort average CD from 288 km to 1,992 km) (Figure 5.5). Particles from the Menai Strait (Bangor and Brynsiencyn) showed a low CD on cohort average compare to the other sites with CD varying from 326 km to 2,155 km for Bangor and from 302 km to 2,161 km for Brynsiencyn for week 1 and week 6 respectively (Figure 5.5). Particles released from Offshore wind farms (North Hoyle, Gwynt Y Mor and Rhyl Flat) showed intermediate cohort average CD from week 1 to week 3, with CD varying from 340 km to 1,075 km on average for the three sites (Figures 5.5.A; 5.5.B and 5.5.C). Cohort average CD remained intermediate compare to the other sites from week 4 to week 6 for Gwynt Y Mor (from 1,479 km to 2,240 km) and for Rhyl flat (from 1,498 km to 2,293 km), whereas North Hoyle showed a low cohort average CD low from week 4 to week 6 compare to the other sites (from 1,431 km to 2,144 km) (Figures 5.5.D; 5.5.E and 5.5.F). During week 1, Llandudno and Conwy showed a low cohort average CD compare to the other sites (317 km and 314 km, respectively) (Figure 5.5.A). Cohort average CD of Llandudno remained low during week 2 and week 3 (659 km and 1,042 km, respectively), whereas Conwy showed an intermediate cohort average CD (671 km and 1,069 km, respectively) (Figures 5.5.B and 5.5.C). From week 4 to week 6, Conwy showed a high cohort average CD compare to the other sites (from 1,502 km to 2,308 km), whereas Llandudno showed an intermediate cohort average compare to the other sites from week 4 to week 6 (from 1,456 km to 2,224 km) (Figures 5.5.D; 5.5.E and 5.5.F). Each week, the cohort-averaged CD were significantly different among the 10 release sites (p-value < 0.0001). For all 70,000 particles, the CD values increased linearly during the 6 weeks ($R^2 = 0.99$) (Figure 5.5). This evolution of CD between each week showed strong correlation among the sites ($R^2 = 0.93$, on average), excepted for Holyhead and Red Wharf Bay which were correlated together ($R^2 = 0.99$) but not with the 8 other sites ($R^2 = 0.055$, on average). The net transport (NT) of particles also showed a linear increase ($R^2 = 0.95$) over the six weeks to reach 43km, on average for all sites (Figure 5.6.A).

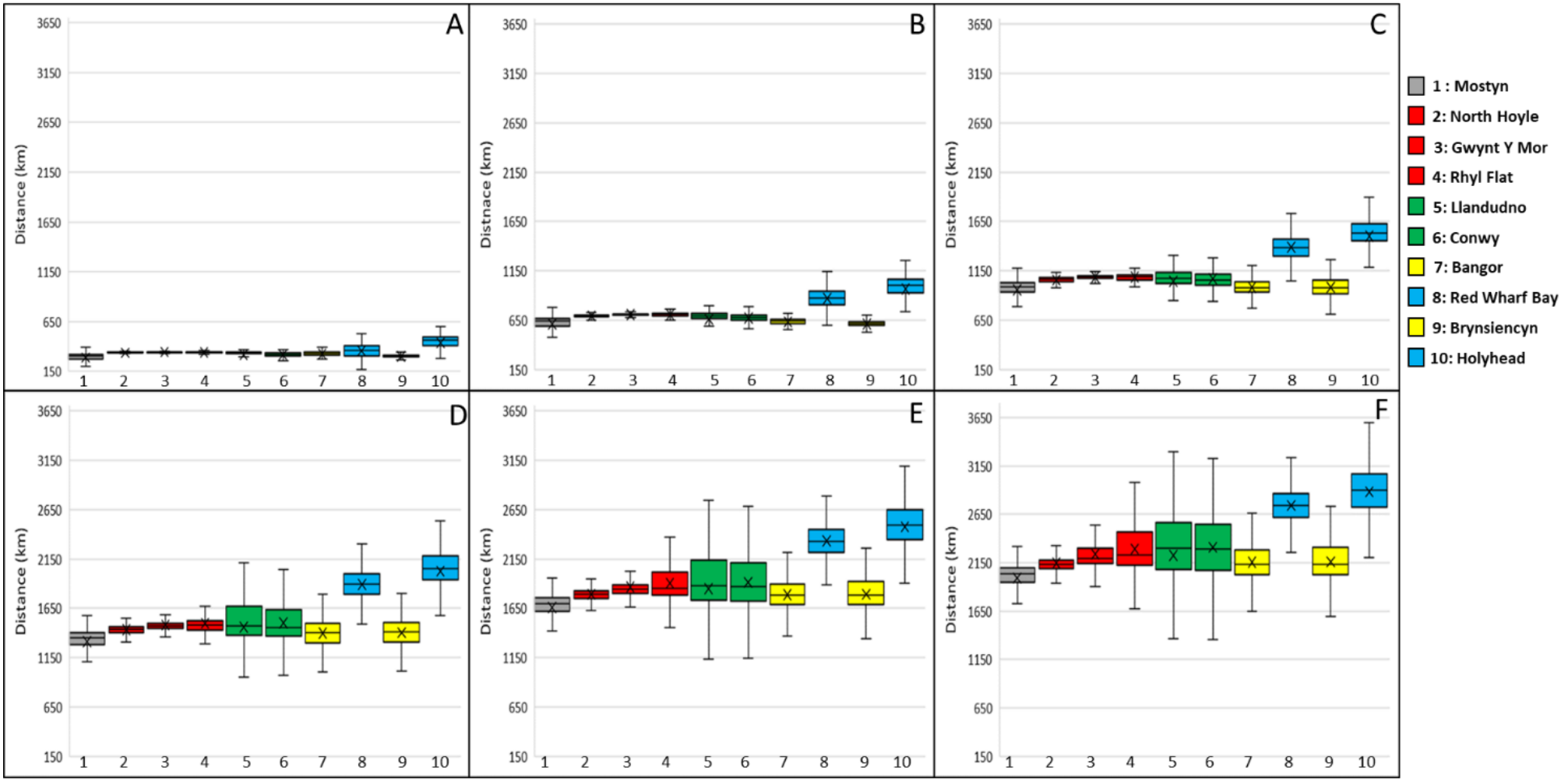

Figure 5.5: Cumulative distances travelled by cohort of 7,000 particles when release at the mid-water in March-April 2018 column during week 1 (A), week 2 (B), week 3 (C), week 4 (D), week 5 (E); and week 6(F). Sites are coloured according to their location: Mostyn (grey), Offshore wind farms (red), Great Orme (green), Menai Strait (yellow), Anglesey (blue). Results are based on 7,000 particles – showing maximum, minimum, median (crossbar) and average (cross) values.

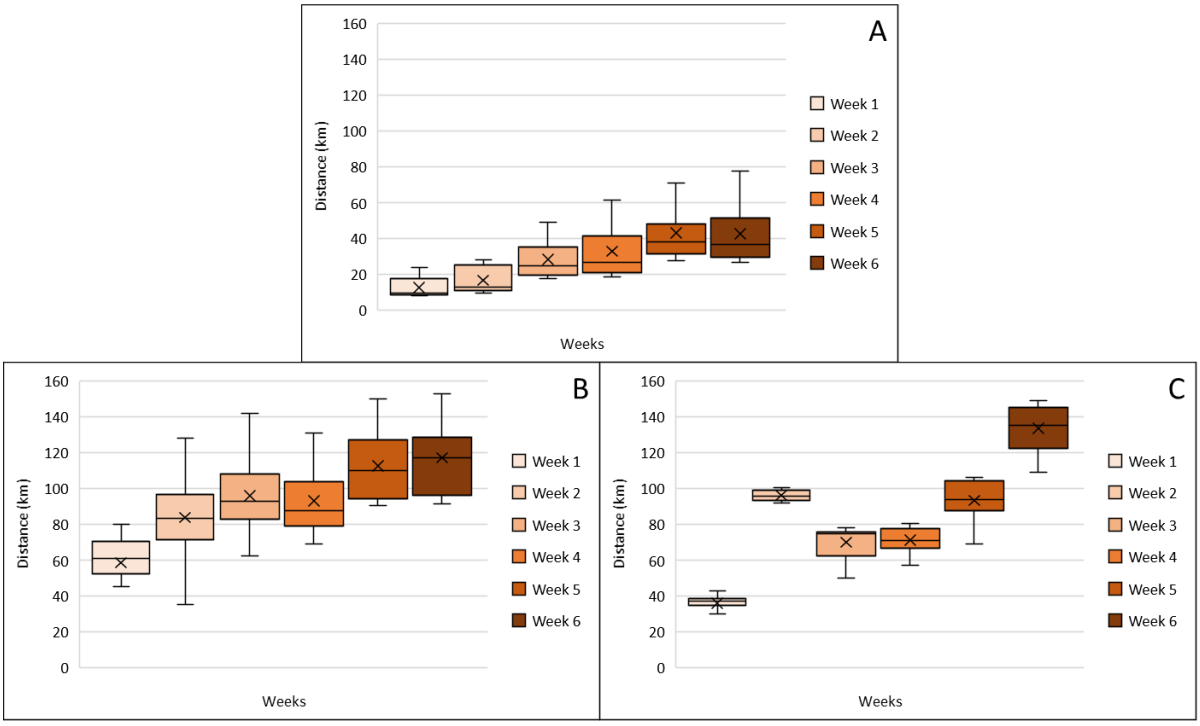

Figure 5.6: Net transport (NT) distances of particles per week when released at mid-water depth (A); at the surface in 2014 (B); and at the surface in 2018 (C). Results are based on: 70,000 particles (A) and 210,000 particles (B and C) – showing maximum, minimum, median (crossbar) and average (cross) value.

5.2.1.3 Connectivity

The estimated connectivity between the 10 released sites, and five settlement only sites is presented in Table 5.1 and Figure 5.7. Results showed decreased connectivity through time for 9 sites (maximum decrease for Bangor (90%) and minimum decrease for North Hoyle (39%), between week 3 and week 6) (Table 5.1). On the other hand, increased connectivity of 17% between week 3 and week 6 was simulated from Red Wharf Bay (site 8) (Table 5.1).

Mostyn was connected mostly with North Hoyle at week 3 and week 4 (18.2% on average) (Figures 5.7.a and 5.7.b), and more connected with Rhyl Flat at week 5 and 6 (11.8%) (Figures 5.7.c and 5.7.d). Larvae released from North Hoyle showed the highest connectivity with Rhyl Flat (site 4) through time with value varying from 19.2% (week 3) to 9.5% (week 6) (Figure 4.21). Results highlighted that Gwynt Y Mor was mostly connected with Rhyl Flat at week 3 and week 4 (11.84% on average) (Figures 5.7.a and 5.7.b), then connectivity was highest with Llandudno for week 5 and week 6 (6.4%) (Figures 5.7.c and 5.7.d). Particles released from Llandudno showed higher self-recruitment than connectivity with other sites for all weeks (10.7% on average) (Figure 5.7). Conwy was simulated to be mostly connected with Llandudno for all weeks, with connectivity values varying from 10.7% (week 3) to 3.2% (week 6) (Figure 5.7). Bangor showed highest connectivity with Brynsiencyn for all weeks simulated (0.6% on

average) (Figure 5.7). Red Wharf Bay was simulated to be mostly connected with Holyhead at week 3 (0.12%) (Figure 5.7.a), and self-recruitment was more important for weeks 4, 5 and 6 (0.23% on average) (Figures 5.7.b, 5.7.c and 5.7.d). Particles released from Brynsiencyn showed higher self-recruitment than connectivity with other sites for all weeks (0.4% on average) (Figure 5.7). The same result was observed for Holyhead where self-recruitment showed the highest results for all weeks (0.78%) (Figure 5.7).

Table 5.1: Cumulative percentage (= sum of the connectivity percentage) of particles (representing mussel larvae dispersing in mid-waters in 2018) per release site which were simulated to connect with settlement site, for different PLD: week 3, week 4, week 5, and week 6.

Release site number	1	2	3	4	5	6	7	8	9	10
Release site name	Mostyn	North Hoyle	Gwynt Y Mor	Rhyl Flat	Llandudno	Conwy	Bangor	Red Wharf Bay	Brynsiencyn	Holyhead
Week 3	45.9	51.6	32.1	26.4	33.6	26.7	1.6	0.5	1.1	1.8
Week 4	43.5	42.9	26.6	22.9	27.2	19.3	0.7	0.4	0.5	0.9
Week 5	40.3	34.4	21.3	17.6	21.2	12.4	0.3	0.5	0.2	0.4
Week 6	37.4	31.5	19.3	14.2	18.5	9.7	0.2	0.6	0.1	0.3

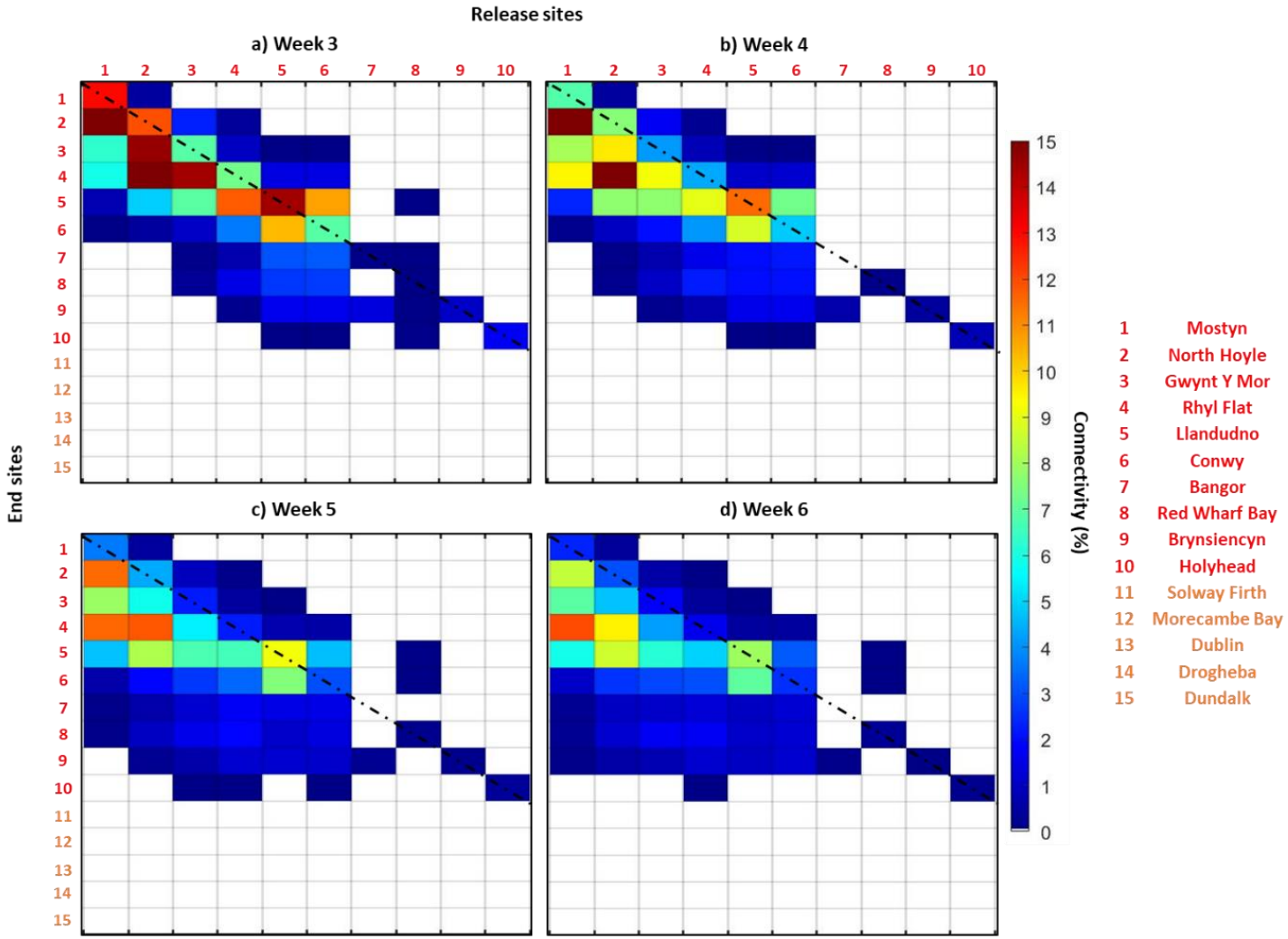

Figure 5.7: Connectivity matrices for larvae release in the mid-water column in March-April 2018 during (a) week 3; (b) week 4; (c) week 5; and (d) week 6. Connectivity between larvae from a source (column) with a sink (row) is highlighted by colour scale with high connectivity in red, low connectivity in blue and no connectivity in white. Self-recruitment (e.g. retention within the release site) is indicated by cells that cross the diagonal dashed line. Sites are colour coded as: red = source and sink sites and orange = sink sites only.

5.2.2 Simulations representing larvae released at the surface in 2014

5.2.2.1 Larval distribution

Larval dispersal was simulated during March and April 2014, parameterised for particles positioned near the sea surface. Results show weekly distributions (up to 6 weeks PLD) of 210,000 particles (three wind scenarios x 7,000 particles per site x 10 sites). Figure 5.8 shows that particles dispersed north as far as the North Channel within 5 weeks but did not disperse further south than the Llyn Peninsula (Figures 5.8.D and 5.8.E). The majority of particles dispersed northeast towards the England/Scotland coasts (Figure 5.8). The maximal concentration of particles simulated during March-April 2014 was:

- During week 1: at the entrance of Morecambe Bay (1.5%) (Figure 5.8.A)
- During week 2: 13% of particles were found in the south area of Morecambe Bay (Figure 5.8.B).
- During week 3: the highest percentage of larvae was observed in Morecambe Bay (12%) and in the Ribble estuary (10%) (Figure 5.8.C).
- During week 4: 10% of larvae were encountered in Morecambe Bay and 5% in the middle of the eastern Irish Sea (Figures 5.8.D).
- During weeks 5 and 6: larvae can be found mostly in Morecambe Bay (13%) (Figures 5.8.E and 5.8.F).

For all sites after 6 weeks simulated, the highest density of particles was in Morecambe Bay (Figure 5.9). However, the value of density varied among the sites with a maximum observed for particles released from Llandudno (35%) and Rhyl (31%) and minimum observed for Bangor (6%) (Figure 5.9). The other sites showed the same density in Morecambe Bay with on average 21% ± 2% (Figure 5.9).

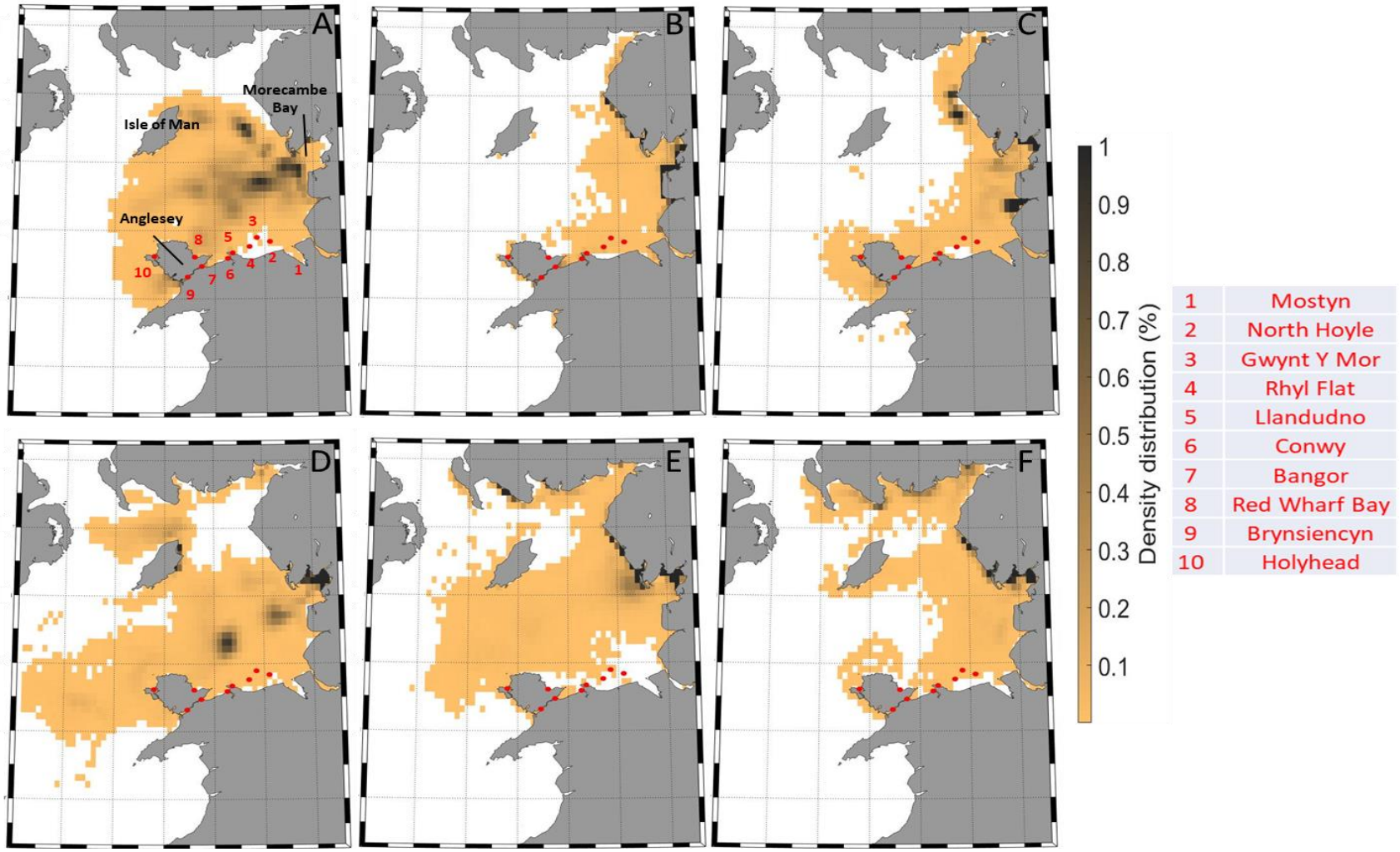

Figure 5.8: Maps showing the density distribution (%) of particles (representing mussel larvae dispersing near the surface) when released during March and April 2014 from 10 released areas (red dots) during: (A) week 1; (B) week 2; (C) week 3 (D) week 4; (E) week 5; and (F) week 6.

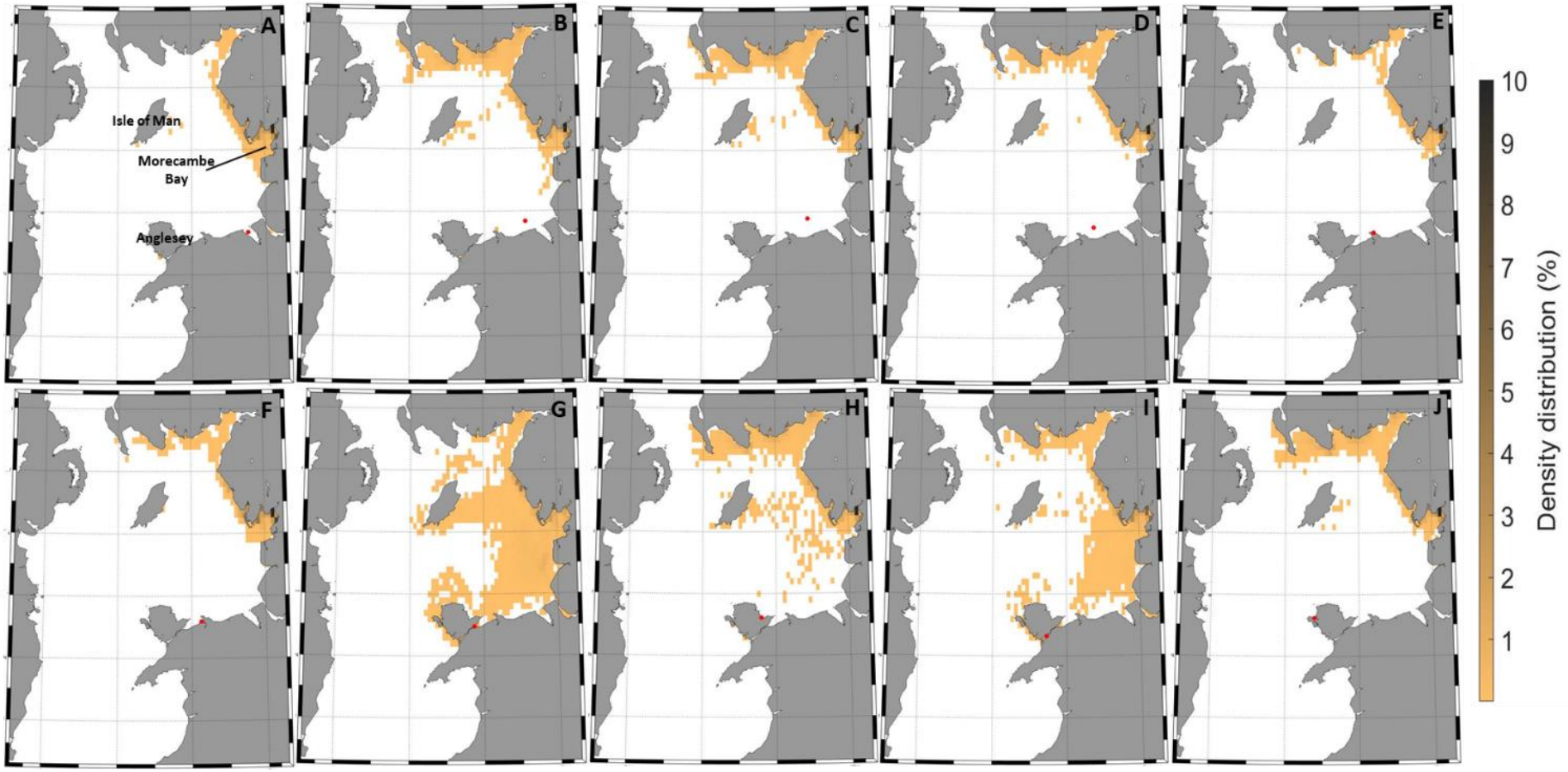

Figure 5.9: Maps showing the density distribution of mussel larvae released at the surface (advected by tide and wind-driven current) during March-April 2014 after 6 weeks simulation from 10 released areas (red dots): (A) Mostyn; (B) North Hoyle; (C) Gwynt Y Mor; (D) Rhyl Flat; (E) Llandudno; (F) Conwy; (G) Bangor; (H) Red Wharf Bay; (I) Brynsiencyn; and (J) Holyhead.

5.2.2.2 Distance travelled

Cumulative distance (CD) travelled by the particles after 6 weeks PLD was 1,386 km, on average for all 210,000 particles (three wind scenarios x 7,000 particles per 10 sites). The sites located in the Menai Strait (Bangor and Brynsiencyn) showed a low CD compare to the other sites during week 1 on average for all particles (207 km for Brynsiencyn and 323 km for Bangor) (Figure 5.10.A). Brynsiencyn CD remained low compared to the other sites during week 2 (439 km) and week 3 (631 km), whereas Bangor CD was the third highest compare to the other sites during week 2 (622 km) and week 3 (791km) (Figures 5.10.B and 5.10.C). During week 4, Bangor (1,116 km) remained the third highest CD, whereas Brynsiencyn (1,031 km) showed an intermediate CD compare to the other sites (Figure 5.10.D). During week 5 and week 6, Bangor (from 1,426 km to 1,496 km) and Brynsiencyn (from 1,435 km to 1,692 km) showed the highest CD compare to the other sites (Figure 5.10.E and 5.10.F). The sites located on Anglesey (Holyhead and Red Wharf Bay) showed the highest CD from week 1 to week 4, with CD varying: 1) from 440 km to 1,212 km for Holyhead; and 2) from 410 km to 1,143 km for Red Wharf Bay (Figures 5.10.A; 5.10.B; 5.10.C and 5.10.D). During week 5 and week 6, Holyhead (from 1,419 km to 1,556 km) and Red Wharf Bay (from 1,352 km to 1,496 km) showed a high CD compare to the other sites (Figure 5.10.E and 5.10.F). Llandudno (from 368 km to 1,442 km) and Conwy (from 335 km to 1,426 km) showed intermediate CD during all weeks compared to the other sites (Figure 5.10). Mostyn (from 295 km to 1,259 km) showed a low CD during all simulation (from week 1 to week 6) compare to the other sites, with the lowest CD during week 3 (624 km) (Figure 5.10). The sites representing the offshore wind farms (Rhyl Flat, Gwynt Y Mor and North Hoyle) showed different patterns during week 1, when Rhyl Flat (359 km) and Gwynt Y Mor (348 km) exhibited an intermediate CD, whereas North Hoyle (334 km) showed a low CD compare to the other sites (Figure 5.10.A). Rhyl Flat maintained an intermediate CD during week 2 and week 3 (from 594 km to 753 km), whereas Gwynt Y Mor (from 570 km to 706 km) and North Hoyle (from 546 km to 675 km) showed a low CD compare to the other sites (Figures 5.10.B and 5.10.C). From week 4 to week 5, North Hoyle showed the lowest CD (from 840 km to 1,006 km), followed by Gwynt Y Mor (from 881 km to 1,076 km) and Rhyl Flat (from 990 km to 1,318 km). During each week, cohort averaged CD was highly significantly different among the 10 released sites (p-value < 0.0001). Also, a linear increase of CD was simulated, averaged for all particles ($R^2 = 0.98$) (Figure 5.10). The evolution of CD through time (6 weeks) showed a high correlation among the sites ($R^2 = 0.82$, on average for all sites), except for Brynsiencyn which exhibited low correlation with

North Hoyle (R^2 = 0.06), Gwynt Y Mor (R^2 = 0.06), Rhyl Flat (R^2 = 0.45), Red Wharf Bay (R^2 = 0.27) and Holyhead (R^2 = 0.07). The net transport (NT) of particles simulated at the surface during March and April 2014 showed an increase from week 1 to week 3 (from 59 km to 96 km, on average for all sites) (Figure 5.6.B). Then, NT decreased between week 3 and week 4 from 96 km to 93 km, on average for all sites (Figure 5.6.B). Finally, NT increased until week 6 from 93 km to 117 km, on average for all sites (Figure 5.6.B).

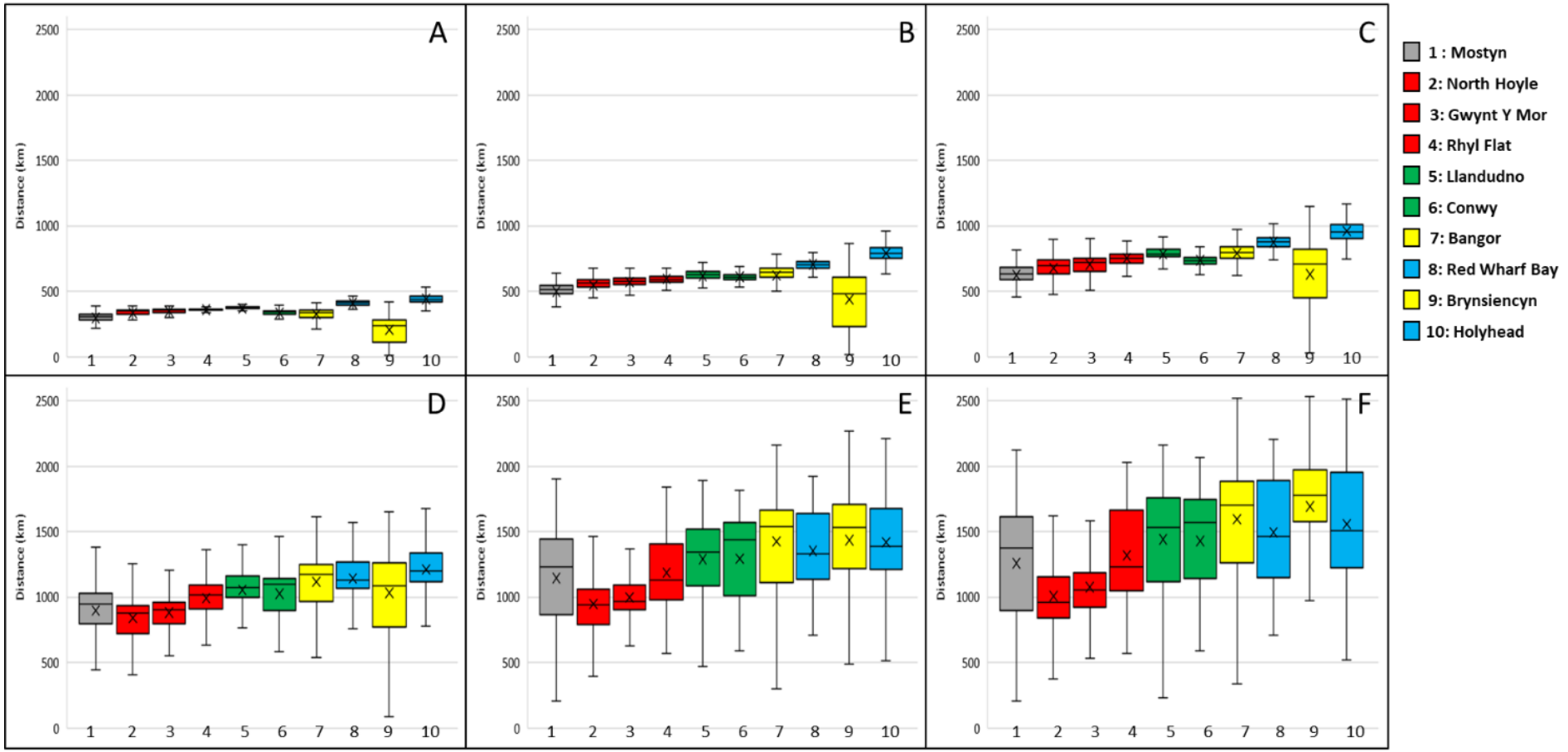

Figure 5.10: Cumulative distance (CD) travelled by particles (representing mussel larvae dispersing near the surface) when released during March and April in 2014 during week 1 (A), week 2 (B), week 3 (C), week 4 (D), week 5 (E) and week 6 (F). Sites are coloured according to their location: Mostyn (grey), Offshore wind farms (red), Great Orme (green), Menai Strait (yellow), Anglesey (blue). Results are based on 21,000 particles – showing maximum, minimum, median (crossbar) and average (cross) valu

5.2.2.3 Connectivity

The simulated connectivity between the 10 sites based on all three scenarios, showed a significant differentiation among sites and through time (Table 5.2 and Figure 5.11). Table 4.5 represents the total percentage of particles found in settlement sites selected per released site. Results showed an increase of the total connectivity with other sites from week 3 to week 6 for Mostyn (from 2% to 4%) and Conwy (from 1.5% to 5.1%) (Table 5.2). On the other hand, the other sites showed a decrease in total connectivity, from week 3 to week 6, with the maximum decrease from Brynsiencyn (-450%) and minimum from Llandudno (-32%) (Table 5.2).
Results showed that sites located in the Menai Strait (Bangor and Brynsiencyn) are mostly connected with Brynsiencyn during week 3, with 3.9% for particles released from Bangor and 14.3% for particles released from Brynsiencyn (Figure 5.11.a). The same results are observed during week 4 with 1.6% for particles released from Bangor and 4.7% for particles released from Brynsiencyn are connected with Brynsiencyn (Figure 5.11.b). During week 5, Bangor showed a highest connectivity with Morecambe Bay (1%), whereas Brynsiencyn showed highest connectivity with itself (1.5%) (Figure 5.11.c). During week 6, both Bangor and Brynsiencyn are mostly connected with Morecambe Bay (3.8% and 2.3%, respectively) (Figure 5.11.d). The sites located on Anglesey (Red Wharf Bay and Holyhead) are mostly connected with Morecambe Bay from week 3 to week 6, varying from 4.1% to 1% for Red Wharf Bay and from 3.6% to 1.2% for Holyhead. Mostyn and Conwy are mostly connected with Morecambe Bay from week 3 to week 6 with connectivity varying from 1) 1.8% to 4% for Mostyn; and 2) 1.5% to 5.1% for Conwy (Figure 5.11). The other sites (North Hoyle, Gwynt Y Mor, Rhyl Flat and Llandudno) are all mostly connected with Morecambe Bay from week 3 to week 6, with connectivity varying from: 1) 2.5% to 0.7% for North Hoyle; 2) 2.2% to 0.4% for Gwynt Y Mor; 3) 3.5% to 1.4% for Rhyl Flat; and 4) 3.8% to 1.9% for Llandudno (Figure 5.11).

Table 5.2: Cumulative percentage (= sum of the connectivity percentage) of particles (representing mussel larvae dispersing near the surface in 2014) per release site which were simulated to connect with settlement site, for different PLD: week 3, week 4, week 5 and week 6.

Release site number	1	2	3	4	5	6	7	8	9	10
Release site name	Mostyn	North Hoyle	Gwynt Y Mor	Rhyl Flat	Llandudno	Conwy	Bangor	Red Wharf Bay	Brynsiencyn	Holyhead
Week 3	1.99	2.47	2.23	3.51	5.53	1.50	13.25	4.38	33.59	4.01
Week 4	1.57	0.74	0.61	1.12	3.06	0.79	5.64	1.67	12.09	1.48
Week 5	1.68	2.19	1.89	1.79	3.44	1.21	2.57	2.28	3.64	2.06
Week 6	4.07	0.68	0.55	2.01	4.21	5.10	5.56	1.55	5.99	1.87

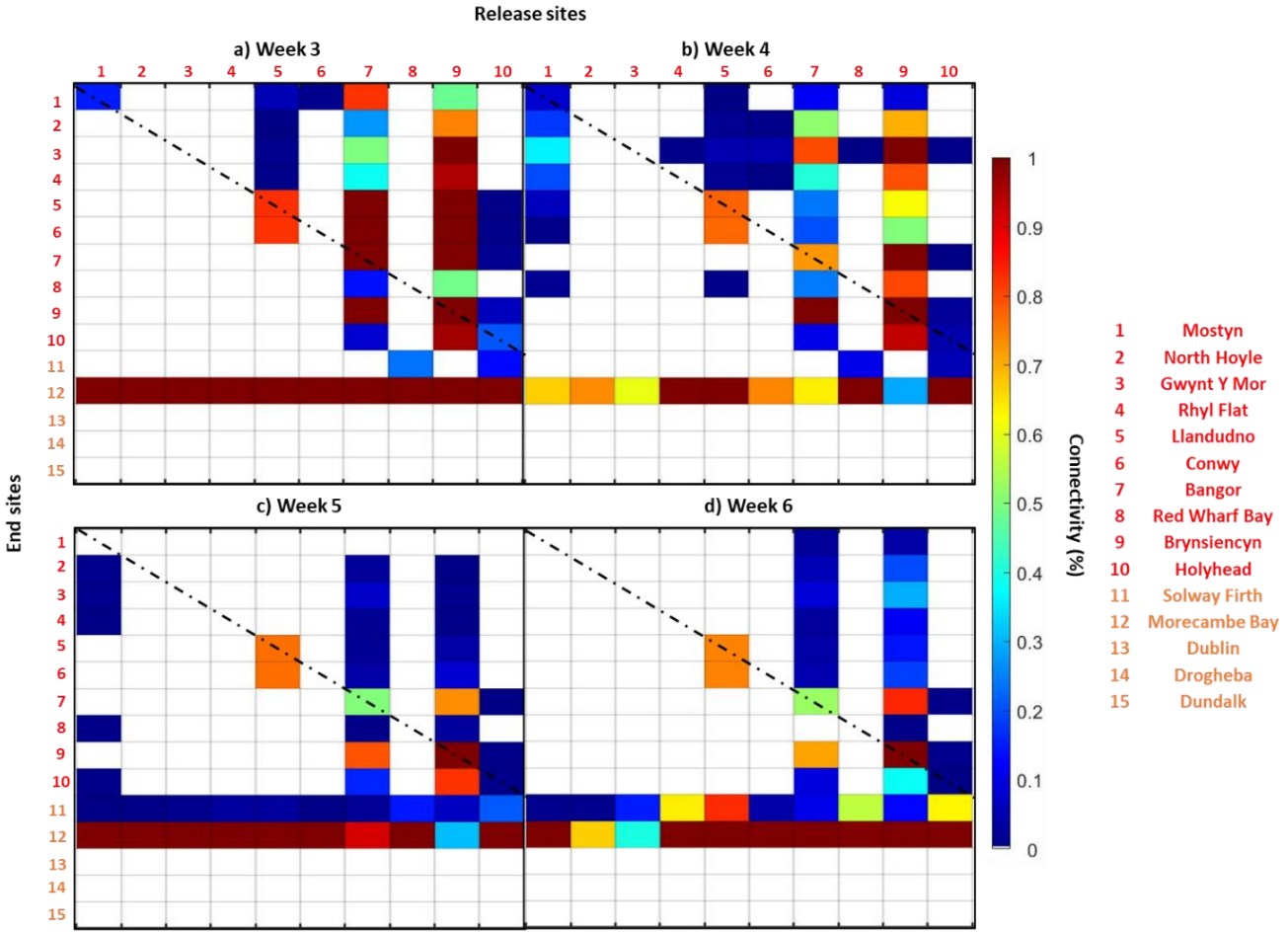

Figure 5.11: Connectivity matrices for particles (representing mussel larvae dispersing near the surface) when released from 10 sources site (1-10) during March and April in 2014, during (a) week 3, (b) week 4, (c) week 5 and (d) week 6. Connectivity between larvae from a source (column) with a sink (row) is highlighted by colour scale with high connectivity in red, low connectivity in blue and no connectivity in white. Self-recruitment (e.g. retention within the release site) is indicated by cells that cross the diagonal dashed line. Sites are colour coded as: red = source and sink sites and orange = sink sites only.

5.2.3 Simulations representing larvae released at the surface in 2018

5.2.3.1 Larval distribution

Results are presented the distribution of particles 210,000 particles (three wind scenarios x 7,000 particles per site x 10 sites) within 6 weeks PLD when released in March-April 2018 (and parameterised based on tide and wind-driven) are presented on Figure 5.12. By week 6, results showed that particles reached as far north as the North Channel and as far south as Cardigan Bay (northern region around the Llyn Peninsula) (Figure 5.12.E). A proportion of particles were also transported west to the east coasts of Ireland and Northern Ireland (Figure 4.26). High concentrations of larvae were simulated:

- During week 1: at the south entrance of the Menai Strait (1.5%) and in the middle of the eastern Irish Sea (1.5%) (Figure 5.12.A)
- During week 2: south of Dublin (1.2%) and in the middle of the western Irish Sea (1%) (Figure 5.12.B).
- During week 3: between Anglesey and the Isle of man (0.7%) (Figure 5.12.C).
- During week 4: between Anglesey and the Isle of man (0.5%) (Figure 5.12.D).
- During week 5: the south coast of the Isle of Man (0.6%) (Figure 5.12.E).
- During week 6: north of Dundalk (2.5%) (Figure 5.12.F).

Looking at the dispersal results per site in 2018 after 6 weeks simulated, results showed that particles density distribution varied according to the sites of release (Figure 5.13). Indeed, particles released from Bangor (6.5%) and Brynsiencyn (11.2%) showed a similar pattern, with particles mostly found near Dublin (Irish coast) (Figure 5.13). The highest distribution of particles was observed in the western Irish Sea for North Hoyle (2.2%), Gwynt Y Mor (1.7%), Rhyl Flat (1.5%) and Mostyn (3.3%) (Figure 5.13). Particles released from Llandudno (4.2%), Conwy (2.8%), Red Wharf Bay (6.5%) and Holyhead (6%) were mostly found near Dundalk (Irish coast) after 6 weeks (Figure 5.13).

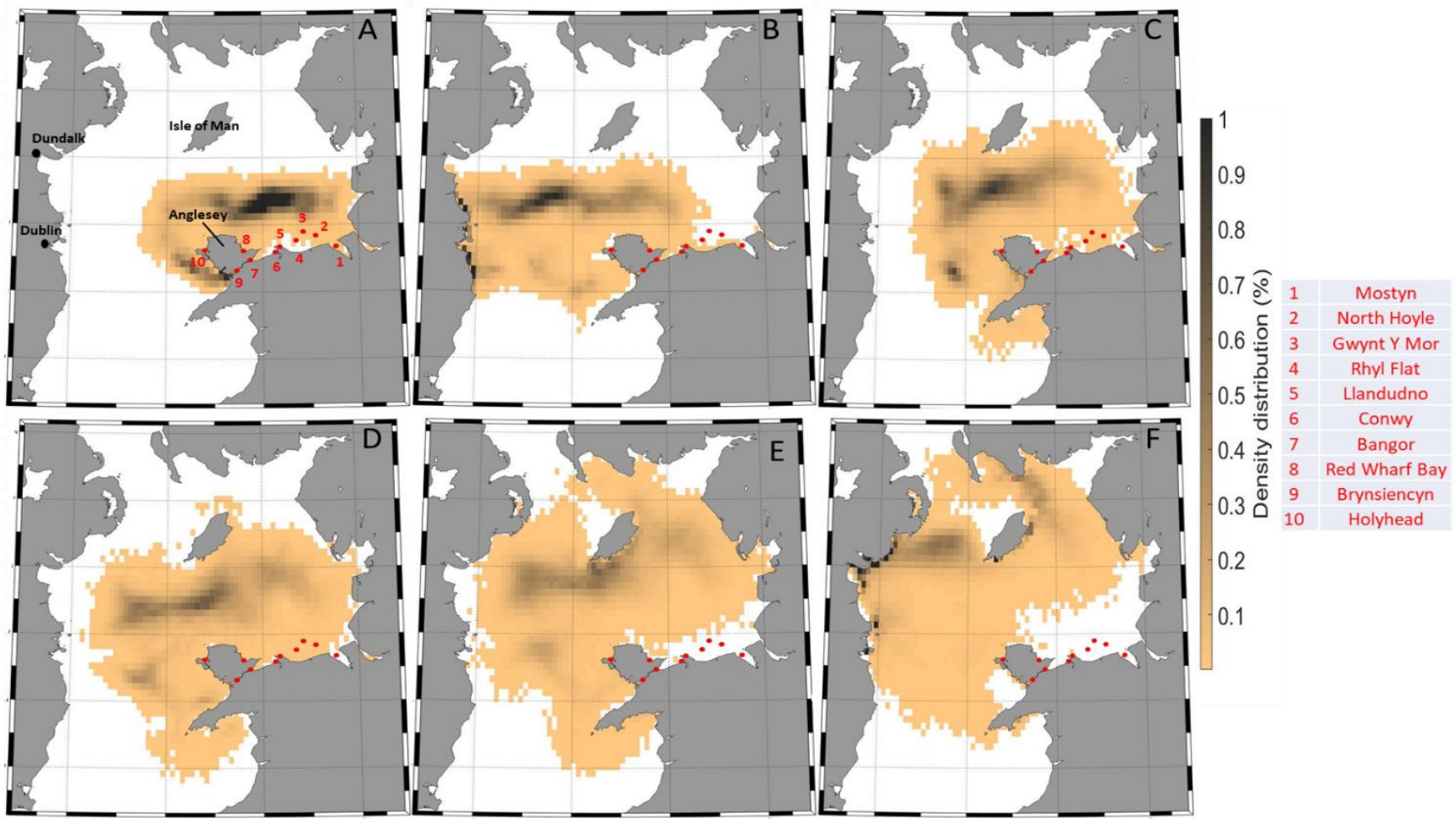

Figure 5.12: Maps showing the density distribution (%) of particles (representing mussel larvae dispersing near the sea surface) released from 10 sites (red dots) during March to April 2018 during: (A) week 1; (B) week 2; (C) week 3; (D) week 4; (E) week 5; and (F) week 6.

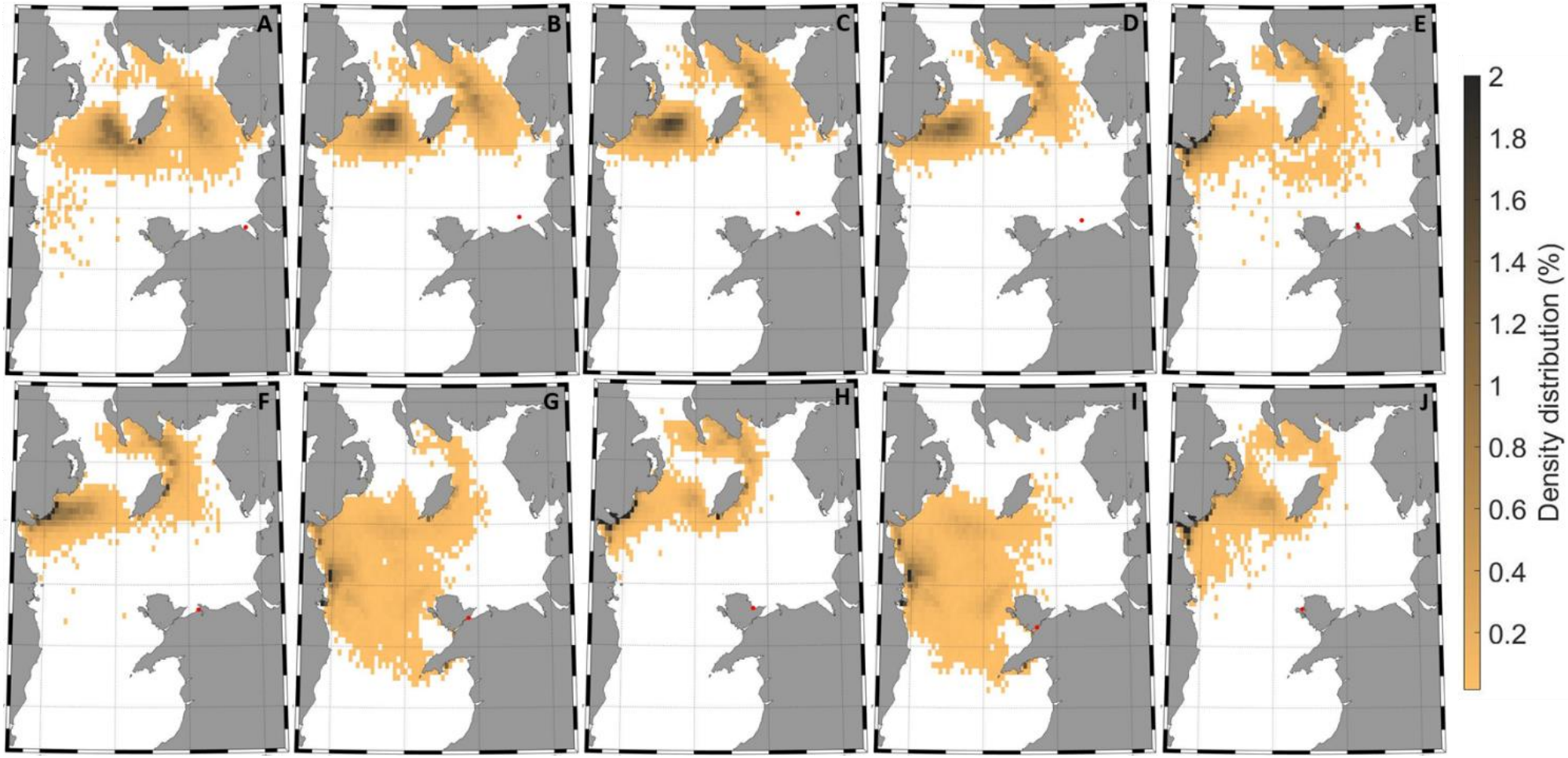

Figure 5.13: Maps showing the density distribution of mussel larvae released at the surface (advected by tide and wind-driven current) during March-April 2018 after 6 weeks simulation from 10 released areas (red dots): (A) Mostyn; (B) North Hoyle; (C) Gwynt Y Mor; (D) Rhyl Flat; (E) Llandudno; (F) Conwy; (G) Bangor; (H) Red Wharf Bay; (I) Brynsiencyn; and (J) Holyhead.

5.2.3.2 Distance travelled

On average for all sites, the cumulative distance (CD) travelled by particles after 6 weeks was 2,514 km (Figure 5.14). The sites located in the Menai Strait (Bangor and Brynsiencyn) showed the lowest cohort average CD during week 1 and week 2, with CD varying: 1) from 309 km to 770 km for Bangor; and 2) from 270 km to 697 km for Brynsiencyn (Figures 5.14.A and 5.14.B). During week 3, Brynsiencyn cohort average CD remained the lowest among the 10 sites (1,224 km), whereas Bangor showed the highest cohort average CD (1,311 km) (Figure 5.14.C). Cohort average CD for Bangor remained the highest from week 4 to week 6 (from 1,874 km to 2,724 km, respectively), same results is observed for Brynsiencyn with high cohort average CD compare to the other sites from week 4 to week 6 (from 1,784 km to 2,641 km, respectively) (Figures 514.D; 5.14.E and 5.14.F). Sites located on Anglesey (Holyhead and Red Wharf Bay) showed high cohort average CD during week 1 and week 2, with CD varying: 1) from 528 km to 934 km for Holyhead; and 2) from 406 km to 845 km for Red Wharf Bay (Figures 5.14.A and 5.14.B). Cohort average CD remained high for Holyhead compare to the other sites during week 3 (1,304 km), whereas Red wharf Bay cohort average CD was low compare to the other sites during week 3 (12,588 km) (Figure 5.14.C). Sites located on Anglesey showed high cohort average CD compare to the other sites during week 4 and week 6, varying: 1) from 1,721 km to 2,402 km for Red Wharf Bay; and 2) from 1,742 km to 2,385 km for Holyhead (Figures 5.14.D; 5.14.E and 5.14.F). Cohort average CD showed intermediate values compare to the other sites during week 1 and week 2 for particles released from Llandudno (from 358 km to 811 km) and Conwy (from 364 km to 827 km) (Figures 5.14.A and 5.14.B). Llandudno cohort averaged CD remained intermediate during week 3 (1,272 km) and week 4 (1,755 km), whereas Conwy showed high cohort average CD simulated during week 3 (1,307 km) and week 4 (1,803 km) (Figures 5.14.C and 5.14.D). Finally, cohort average CD simulated for Conwy was intermediate during week 5 (2,133 km) and week 6 (2,530 km), whereas Llandudno showed low cohort average CD compare to the other sites (2,133 km during week 5 and 2,459 km during week 6) (Figures 5.14.E and 5.14.F). Rhyl Flat showed an intermediate value of cohort average CD compare to the other sites from week 1 (370 km) to week 6 (2,500 km) (Figure 5.14). North Hoyle and Gwynt Y Mor showed intermediate cohort average CD during week 1 and week 2, with CD varying: 1) from 358 km to 790 km for North Hoyle; and 2) from 363 km to 798 km for Gwynt Y Mor (Figures 5.14.A and 5.14.B). Cohort average CD was low during week 3 and week 4 for North Hoyle (from 1,266 km to 1,732 km) and for Gwynt Y Mor (from 1,254 km to 1,722 km) (Figures 5.14.C and 5.14.D). During week

5 and week 6. Cohort average CD was intermediate compare to the other sites during week 5 and week 6 for North Hoyle (from 2,155 km to 2,488 km) and for Gwynt Y Mor (from 2,137 km to 2,468 km) (Figures 5.14.E and 5.14.F). Mostyn cohort average CD showed intermediate values during week 1 (342 km) and week 2 (778 km) (Figures 5.14.A and 5.14.B). Then, cohort average CD for Mostyn was intermediate compare to the other sites from week 3 (1,297 km) to week 6 (2,541 km) (Figures 5.14.C; 5.14.D; 5.14.E and 5.14.F). CD was significantly different among the sites for each week (p-value < 0.0001). Weekly results showed a linear increase of CD for all sites ($R^2 = 0.99$) (Figure 5.14). The comparison of CD between each week showed strong correlation among all the sites ($R^2 = 0.88$, on average).

The net transport (NT) of particles for larvae behaviour travel at the surface showed an increase between week 1 and 2 (from 36 km to 96 km, on average for all sites) (Figure 5.6.C). Then, NT decreased between week 2 and week 3 from 96 km to 70 km, on average for all sites (Figure 5.6.C). NT remained constant between week 3 and week 4 (Figure 5.6.C). Finally, NT increased between week 4 to week 6 from 71 km to 134 km, on average for all sites (Figure 5.6.C).

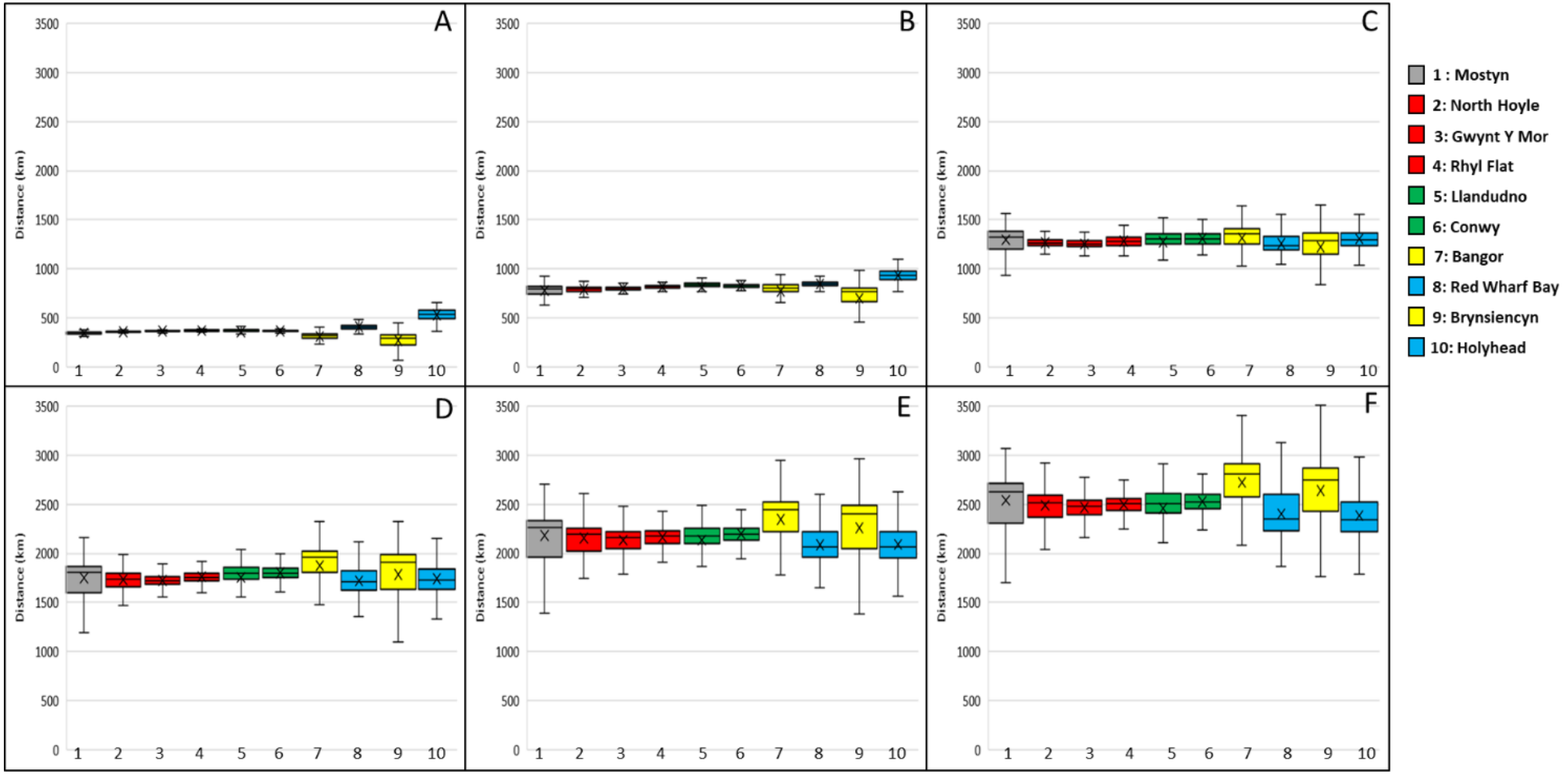

Figure 5.14: Cumulative distance (CD) travelled by particles (representing mussel larvae dispersing near the sea surface) during March-April 2018 during week 1 (A), week 2 (B), week 3 (C), week 4 (D), week 5 (5) and week 6 (F). Sites are coloured according to their location: Mostyn (grey), Offshore wind farms (red), Great Orme (green), Menai Strait (yellow), Anglesey (blue). Results are based on 21,000 particles – showing maximum, minimum, median (crossbar) and average (cross) value.

5.2.3.3 Connectivity

Connectivity between sites is presented in Table 5.3 and Figure 5.15. Results showed reduced connectivity for Mostyn between week 3 and week 6 (from 0.55% to 0.05% respectively), Llandudno (from 5.16% to 3.42% respectively) and Conwy (from 0.02% to 0% respectively) (Table 5.3). North Hoyle, Gwynt Y Mor, Bangor and Brynsiencyn showed an increase of connectivity (0.05%, 0.01%, 2.05% and 2.91% respectively) between week 3 and week 4. Then, connectivity decreased for these four sites until week 6 (Table 5.3).

Results showed that sites located in the Menai Strait (Bangor and Brynsiencyn) are mostly connected with Brynsiencyn during week 3, with 0.3% for particles released from Bangor and 0.3% for particles released from Brynsiencyn (Figure 5.15.a). The same results are observed during week 4 with 1.3% for particles released from Bangor and 2% for particles released from Brynsiencyn are connected with Brynsiencyn (Figure 5.15.b). During week 5 and week 6, Brynsiencyn is mostly self-connected (0.2% and 0.1%, respectively), whereas Bangor is mostly connected with Brynsiencyn during week 5 (0.1%) and week 6 (0.07%) (Figures 5.15.c and 5.15.d). The sites located on Anglesey (Holyhead and Red Wharf Bay) showed no connectivity with the selected sites for during all weeks simulated, excepted for Holyhead which appeared to be self-seeded during week 3 (0.04%) and week 4 (0.001%) (Figure 5.15). Llandudno is mostly self-connected (2%, on average for all week) and connected with Conwy (2%, on average for all week) from week 3 to week 6 (Figure 5.15). Conwy showed connectivity with Holyhead only during week 3 (0.02%), then no connectivity was observed between Conwy and other selected sites from week 4 to week 6 (Figure 5.15). Offshore wind farms sites (North Hoyle, Gwynt Y Mor and Rhyl Flat) showed no connectivity with the selected sites during week 3 (Figure 5.15.a). From week 4 to week 6, Rhyl Flat maintained no connectivity with the other sites, whereas North Hoyle (0.04%, on average for all weeks) and Gwynt Y Mor (0.01%, on average for all weeks) showed connectivity with Morecambe Bay (Figures 5.15.b; 5.15.c and 5.15.d). Mostyn is mostly connected with Llandudno (0.1%) and Holyhead (0.1%) during week 3 (Figure 5.15.a). Then, Mostyn is mostly connected with Morecambe Bay from week 4 to week 6 (0.1%, on average for all the week) (Figures 5.15.b; 5.15.c and 5.15.d).

Table 5.3: Cumulative percentage (= sum of the connectivity percentage) of particles (representing mussel larvae dispersing near the surface in 2018) per release site which were simulated to connect with settlement site, for different PLD: week 3, week 4, week 5 and week 6.

Release site number	1	2	3	4	5	6	7	8	9	10
Release site name	Mostyn	North Hoyle	Gwynt Y Mor	Rhyl Flat	Llandudno	Conwy	Bangor	Red Wharf Bay	Brynsiencyn	Holyhead
Week 3	0.55	0	0	0	5.16	0.02	0.53	0	0.60	0.04
Week 4	0.43	0.05	0.01	0	4.06	0.01	2.05	0	2.91	0
Week 5	0.16	0.04	0.02	0	3.64	0	0.23	0	0.34	0
Week 6	0.05	0.02	0	0	3.42	0	0.10	0	0.12	0

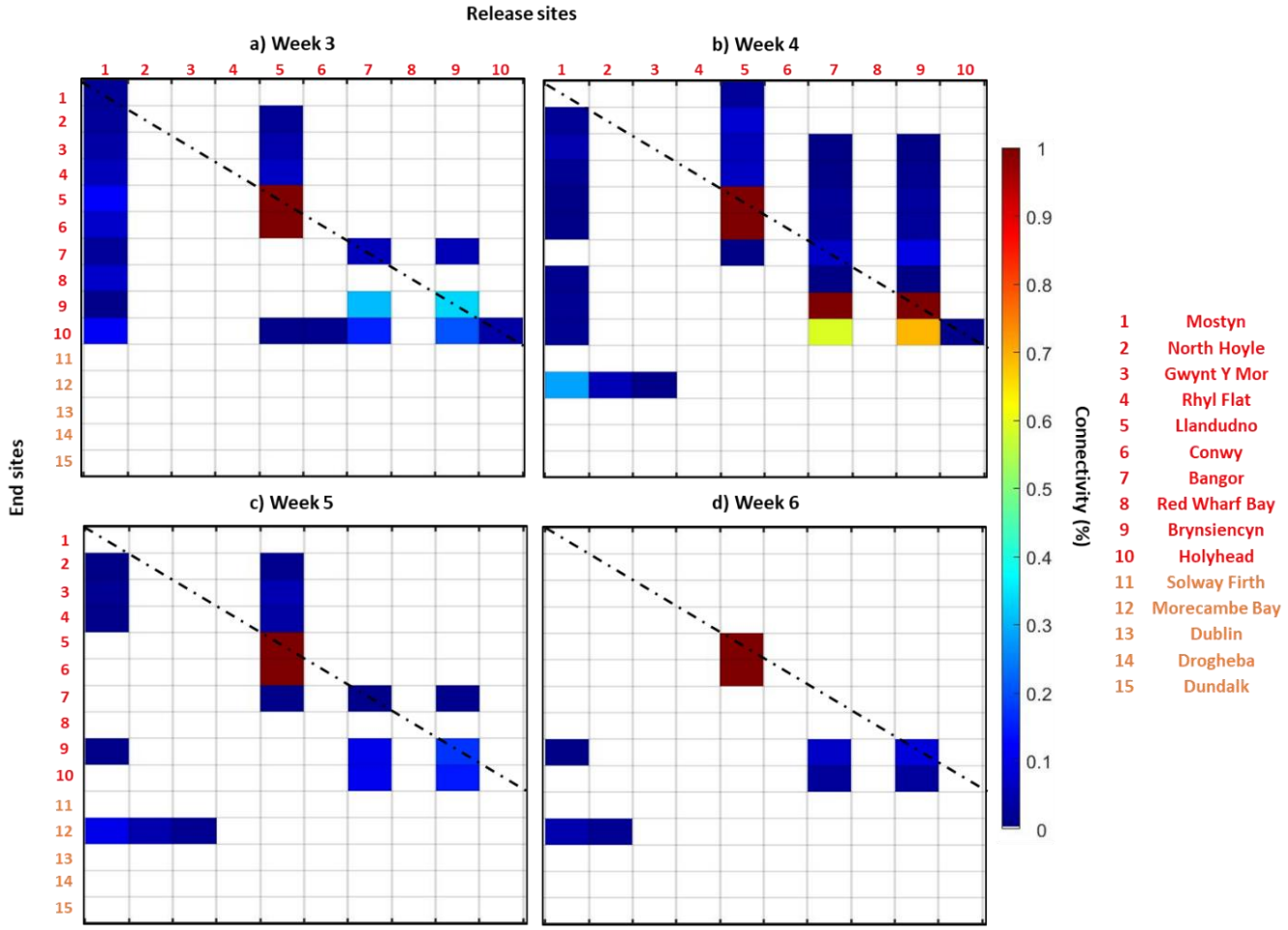

Figure 5.15: Connectivity matrices for particles (representing mussel larvae dispersing near the surface) when released from 10 sources site (1-10) during March and April in 2018, during (a) week 3, (b) week 4, (c) week 5 and (d) week 6. Connectivity between larvae from a source (column) with a sink (row) is highlighted by colour scale with high connectivity in red, low connectivity in blue and no connectivity in white. Self-recruitment (e.g. retention within the release site) is indicated by cells that cross the diagonal dashed line. Sites are colour coded as: red = source and sink sites and orange = sink sites only.

5.2.4 Comparison of the results

The difference (in %) of CD between the simulations was calculated per site and per week. Results showed that CD is less important when larvae are released at the surface in 2014 than larvae released at mid-water depth (-25.7%). No significant difference is observed among the 10 sites (p-value = 0.7). However, results showed a significant difference between the week (p-value < 0.0001). Indeed, the first week CD are approximately similar between the two larvae behaviour (1%), then CD is 15% higher when larvae are released at the surface on average for all sites at week 2. Then, from week 3 to week 6, the difference in CD remains constant to 35% in favour of larvae released at mid water depth. In 2018, larvae released at the surface showed a CD 13.5% higher than larvae release at mid-water depth on average for all weeks and sites. No significance difference was observed among the week with p-value = 0.73. However, results showed a significant difference (p-value < 0.0001) among the 10 sites. Indeed, particles released from Red Wharf Bay and Holyhead at the surface showed a CD 6% lower than particles released at mid-water depth. The other sites (e.g. Mostyn, North Hoyle, Gwynt Y Mor, Rhyl Flat, Llandudno, Conwy, Bangor and Brynsiencyn) showed that CD was 18.5% higher when particles were released at the surface than mid-water depth. The comparison between larvae released at the surface in 2014 and 2018 showed that CD 34% higher for the year 2018 on average for all sites and weeks. Results highlighted that no significant difference was observed among the 10 sites (p-value = 0.55). However, a significant difference was observed between the week (p-value < 0.0001). Indeed, after one week, CD was 6% higher for the year 2018, then increased to 26% at week 2 on average for all sites. Then, from week 3 to week 6, the difference in CD remains constant to 43% in favour of year 2018.

The difference (in %) of NT between the simulations was calculated per site and per week. Results showed that NT is higher when larvae are released at the surface in 2014 than larvae released at mid-water depth (300%, on average for all sites and all weeks). Results showed a sites effect (p-value = 0.0002). Indeed, results showed that NT was increased by 68% when larvae are released at the surface from Bangor and Brynsiencyn, whereas NT increased by 355% when release from the other sites (e.g. Mostyn, North Hoyle, Gwynt Y Mor, Rhyl Flat, Llandudno, Conwy, Red Wharf Bay and Holyhead). Also, results highlight a significant difference among the week simulated (p-value < 0.0001). The first two weeks showed a difference of 450%, on average for both weeks, between the two larval behaviour in favour of larvae released at the surface in 2014, then the difference decreased to 221% on average for the last 4 weeks. In 2018, larvae released at the surface showed a NT 250% higher than larvae

release at mid-water depth on average for all weeks and sites. Significance difference was observed among the 10 sites with p-value = 0.003. Indeed, results showed that NT was increased by 70% when larvae are released at the surface from Bangor and Brynsiencyn, whereas NT increased by 300% when release from the other sites (e.g. Mostyn, North Hoyle, Gwynt Y Mor, Rhyl Flat, Llandudno, Conwy, Red Wharf Bay and Holyhead). Also, results showed a significant difference (p-value < 0.0001) among the weeks. Week 2 showed that NT is 570% higher when particles are released at the surface, whereas the other weeks showed a difference of 195% in favour of larvae released at the surface. The comparison between larvae released at the surface in 2014 and 2018 showed that NT 21% higher for the year 2018 on average for all sites and weeks. A significant difference was observed between the week (p-value < 0.0001). Indeed, results showed that NT is higher during week 1, 3, 4 and 5 for the year 2014 (37% on average), whereas NT is higher in 2018 for week 2 and week 6 (12%, on average). Also, results highlighted that sites have a significant effect on NT difference between larvae released at the surface during 2014 and 2018 (p = 0.02). Indeed, Holyhead showed a NT higher by 70% in 2018, whereas the other sites showed that NT increased by 16% in 2018.

5.3 Discussion

Several mussel beds are well established in North Wales: 1) commercial mussel beds (Bangor, Brynsiencyn, Holyhead, Mostyn); 2) natural mussel beds (Llandudno and Red Wharf Bay); 3) both natural and commercial mussel bed (Conwy); and 4) mussel beds established due to humans' infrastructures (Offshore wind farm (OWF): Rhyl Flat, Gwynt Y Mor and North Hoyle), therefore larval dispersal was studied from these 10 sites. Larvae are considered to behave as passive particles because of the lack of knowledge about mussel larvae behaviour in details (Roberts, 1997; Knights *et al.*, 2006). However, previous studies have shown that the vertical position of larvae in the water column can varied through time (Conway *et al.*, 1997; Dobretsov & Miron, 2001; Knights *et al.*, 2006; Criales *et al.*, 2007; Weidberg *et al.*, 2015).
The simulated larvae behaviours were chosen to represent two extreme cases of larvae behaviour (e.g. larvae travelled at the surface and larvae travelled in mid-waters with no vertical swimming) and, hence, capture a wide range of potential dispersal distributions. In particular, the PTM was parameterised to represent larvae that remain in the surface layer and larvae that are present in the mid-waters. Indeed, if particles stay at mid-water depth, they are only submitted to tidal advection, whereas when larvae are at the surface, they encountered stronger currents (e.g. wind driven currents) which increase their dispersal (Lane *et al.*, 1985; McQuaid & Phillips, 2000; Larghier, 2003; Sundelof & Jonsson, 2011; Weidberg *et al.*, 2015). In

addition, previous studies showed the importance of circulation patterns on interannual variability of larvae recruitment and eggs/larvae dispersal (Van der Veer *et al.*, 1998; Larghier, 2003; Palatella *et al.*, 2014). In order to capture some interannual variability in mussel larvae dispersal, simulations occurred during two contrasting years (e.g. 2014 and 2018). Indeed, Figures 5.16 and 5.17, showed that the wind during March and April 2014 and 2018 were different in strength and direction and consequently have a different impact on surface currents. These years were also chosen according to mussel farms harvest data which showed that in 2014, 1,100 tonnes of seed were harvested in Morecambe Bay, whereas recruitment in 2018 was too small to be harvested (Trevor Jones, pers. comm.). Simulations were conducted during March and April for both years. These periods simulated were chosen according to the first main spawning event that was observed in 2018 (end of March, Chapter 4, Section 4.1). The period chosen has a consequence on the hydrodynamic current in the Irish Sea (e.g. water column remained well mix until May) (Simpson, 1971; Gowen *et al.*, 1995; Golding *et al.*, 2004; Howarth, 2005).

Assuming mussel larvae are distributed throughout the water column, e.g. developing weak vertical migration, then their dispersal will be controlled by tidal currents and in particular tidal residuals (Raby *et al.*, 1994). These tidal residuals can be represented by the monthly-averaged velocities output from the model (Figure 5.18). The residual patterns presented in Figure 5.18 do not change markedly from one month to another or from a year to another as demonstrated by Harvey (1968). The same results are observed when the strength and the residual currents are compared between simulation in 2014 and 2018 (Figure 5.19), which explain why the mussel larvae distribution is the same when release in mid-waters. These patterns can be used to explain the variability in the larvae dispersal simulated from the mid-water scenarios here (Figures 5.3 and 5.4). Particles released from Bangor and Brynsiencyn dispersed south-westwards through the Menai Strait, along the Llyn Peninsula and into Cardigan Bay – in accordance with the residual tidal currents (Figure 5.18) (Campbell *et al.*, 1998). These results are correlated with observations made using: 1) tracking drifters by Harvey (1968); and 2) currents meters in the Menai Strait by Simpson *et al.* (1971). The dispersal of particles from Llandudno and Conwy was westwards due to residual current westwards along the north Wales and Anglesey coasts and south-westwards towards the Menai Strait (Figure 5.18). Particles from Red Wharf Bay and Holyhead dispersed westwards then offshore and northwards in accordance with the residual currents (Figure 5.18). The same residual currents were observed by Ward *et al.* (2015) and Robins *et al.* (2015) around Anglesey, especially near Holyhead were strong tidal currents occur. Particles released from the offshore wind farms (North Hoyle, Gwynt Y Mor and Rhyl flat) remained in the same area because of the weak residual currents

(between 0.009 m/s and 0.007 m/s) (Aldridge, 1993) (Figure 5.18). Mostyn showed a different pattern compared to the other release sites as particles travelled both westwards along the north welsh coast and northwards along the English coast to Southport (Aldridge, 1993) (Figure 5.18). For the four sites (North Hoyle, Gwynt Y Mor, Rhyl flat and Mostyn) located in the eastern Irish Sea, previous studies observed the same patterns (Heaps, 1972; Heaps & Jones, 1977; Aldridge, 1993; Aldridge & Davies, 1993). The larvae dispersal varied in direction and distance travelled between the 10 released sites, which is the consequence of wide variability of tidal current velocities which can reach 2 m/s in certain localised regions such as headlands (e.g. Llyn Peninsula and northwest Anglesey) and tidal channel (e.g. Menai Strait) (Campbell *et al.*, 1998; Rippeth *et al.*, 2002; Serhadliglu *et al.*, 2013; Neill *et al.*, 2014; Neill *et al.*, 2016). The site of larval release is a major of importance as previously demonstrated for other area and other species (Hill, 1990; Salomon, 1990; Ellien *et al.*, 2000).

However, the comparison of CD per sites between mid-waters simulations and near surface simulations showed that sites effect is significant when larvae released at mid-waters and at the surface in 2018 (p-value < 0.0001), whereas in 2014, when wind is strong and consistent in a specific direction, sites have less impact on dispersal (p-value = 0.7) (Ellien *et al.*, 2000). For the 2014 simulations, results showed that particles from all sites mostly concentrated near Morecambe Bay. This is the consequence of a persistent westerly wind during March and April which reduced the influence of residual tidal currents shown in Figure 5.18. These results are correlated with previous studies (Harvey, 1968; Simpson *et al.*, 1971; Campbell *et al.*, 1998) which showed that southwards residual currents in the Menai Strait can be reversed to northwards flow at the surface during strong and consistent wind events. For the 2018 simulations, the wind in March and April was generally weaker than March-April 2014 and the wind direction varied (Figures 5.16 and 5.17). Consequently, particles were influenced by both wind-driven and tidal residuals, and the local release locations remained an important factor on dispersal. For the first time, this study showed that sites effect on dispersal could be remove if PLD occurs during strong and consistent wind event like in March-April 2014.

Consequently, the potential dispersal of mussel larvae is greatly affected if they are released at the surface or at mid-waters. This was previously explained as the different currents strength and direction encountered by larvae which influence dispersal (Gaylord *et al.*, 2002; Harnett *et al.*, 2007; Sundelof & Jonsson, 2011; Coscia *et al.*, 2012; Robins *et al.*, 2012; Robins *et al.*, 2013; Rhörs *et al.*, 2014; Phelps *et al.*, 2015; Daigle *et al.*, 2016). Assuming mussel larvae are distributed near the surface of the water column (Maximovitch *et al.*, 1996; Dobretsov & Miron, 2001), e.g. developing strong upwards vertical migration, then their dispersal will be controlled by both tidal residuals and wind-driven surface flows. Previous studies showed the potential

importance of wind driven current on invertebrate's dispersal (Johnson & Hess, 1990; McQuaid & Phillips, 2000; Harii & Kayanne, 2003; Guizien *et al.*, 2006; Gaonkar *et al.*, 2012). Results showed that the distribution of larvae varied greatly if they were released at the surface or at mid water-depth per sites and per weeks (Figures 5.3; 5.4; 5.8; 5.9; 5.12 and 5.13). These results highlighted the importance of the vertical position of larvae in water column for future simulations. Indeed, for the simulations computed here representing larvae in the surface layer, larvae distribution for year 2014 and 2018 were primally controlled by the wind driven currents. For the 2014 simulations, the population-average cumulative distance (CD) travelled by particles in surface waters was 26% less than for particles in mid-waters. This is because of the persistent westerly wind transported the particles towards the UK coast where they remained until the end of simulation. This result could influence positively mussel recruitment in UK by maintaining mussel larvae on the coast. On the other hand, for the 2018 simulations, the population-average CD travelled by particles in surface waters was 14% greater than for particles in mid-waters. However, a large proportion of larvae remained offshore during the 6 weeks PLD (Figures 5.12 and 5.13). This could induce decreased mussel recruitment during 2018, as shown previously by McQuaid (1996), a greater PLD (e.g. possible increase of CD) does not mean effective dispersal or effective connectivity. These results are also supported by observations made by mussel farmers which noticed no recruitment in 2018 and abundant recruitment in 2014 on the UK coast. The match between observations and simulations support the hypothesis of mussel larvae dispersion mostly at the surface, as demonstrated by Dobretsov & Miron (2001) who showed that the majority of *M.edulis* larvae were collected between 1.5 m and 3 m depth. The interannual variation of CD travelled by larvae was also showed by McQuaid & Philipps (2000) in South Africa and its importance on recruitment.

The population-average net transport (NT) was higher for particles in surface waters than mid-waters, by > 100 km for both years. This result suggests that, if larvae were distributed near the surface, the possible area of settlement is higher than for larvae in mid-waters. Similar observations were made by Molen *et al.* (2007) on fish eggs during spring spawning. Consequently, all mussel larvae released from North Wales have the potential to be connected within a metapopulation when released in mid-waters (North wales mussel beds) and at the surface (Irish coast, Isle of Man coast and northern UK coast) (i.e. group of spatially separated populations of the same species, which interact at some level) (Levins, 1969; Sale *et al.*, 2006; Carson *et al.*, 2011; Gimenez *et al.*, 2019). Consequently, this result has both negative and positive impact: 1) reduce the chance of extinction of *M.edulis* in the Irish Sea by increasing connection among the mussel beds (e.g. positive impact) (Hanski, 1982, 1985; Fahrig &

Merriam, 1985); and 2) increase contact among mussel beds could enhance the spread of disease (Hess, 1996; Robins *et al.*, 2019).

The variation of NT (interannually and behaviourally) influences the connectivity among the different mussel beds. The results highlighted that the vertical position of mussel larvae in the water column has a strong influence on larval dispersal and consequently the connectivity among the mussel beds (Sheltema, 1986; Knights *et al.*, 2006; Van der Molen *et al.*, 2007). Mussel farmers data showed an important mussel larvae recruitment in Morecambe Bay in 2014 which allowed them to harvest several tonnes of mussel seed, whereas in 2018 no seed where harvested in Morecambe Bay (Trevor Jones pers. comm.). The simulations produced for 2014 and 2018 show the same patterns. Indeed, the connectivity matrices showed that when the larvae were ready to settle in 2014 (e.g. from week 3 to week 6), all the released sites were mostly connected with Morecambe Bay (2% on average for all sites). Further, for the period simulated in 2018 only 3 sites (e.g. Mostyn, North Hoyle and Gwynt Y Mor) were connected with Morecambe Bay after week 4 at very low level (0.06%). These results coupled with mussel farmers observations confirmed that: 1) the PTM created represented accurately mussel larval dispersal in the Irish Sea; and 2) *M.edulis* are mostly distributed in the upper water column and influenced by wind-driven currents (McQuaid & Phillips, 2000; Gilg & Hilbish, 2003; Weidberg *et al.*, 2015). In addition, results showed an interannual difference for connectivity among the sites of release when larvae travelled at the surface (Figures 5.11 and 5.15). Understanding interannual variation of mussel settlement and the possibility to predict where to collect mussel seeds is a major of importance for mussel farmers. Despite the good correlation between particle tracking model and farmer observations, uncertainties about settlement remain. Indeed, no field experiments were carried out to study where the larvae come from and when they exactly settle. However, it's complex to observe with accuracy the time of settlement as larvae can measured less than 1 mm. In addition, to study where the larvae come from, other scientific tools (e.g. genetic and/or microchemistry) than modelling must be used in the future.

The overall results suggest that mussel travel will mostly influenced by surface current, consequently spat should be collected on ropes at the surface (from 0 m to 5 m) . In addition, it seems that no matter the year or the depth simulated mussel larvae can be found between Anglesey and the Isle of Man, which might be a future spot to collect mussel larvae using long lines. In addition, the south of the Menai Strait (i.e. near Brynsiencyn) showed good results for a settlement area, it used to be an important source of spat (Pers. Comm Trevor Jones) but it appears that mussel larvae don't settle there anymore. Further studies should investigate the reasons (unsuitable sea bed, predators, competition inter-specific…).

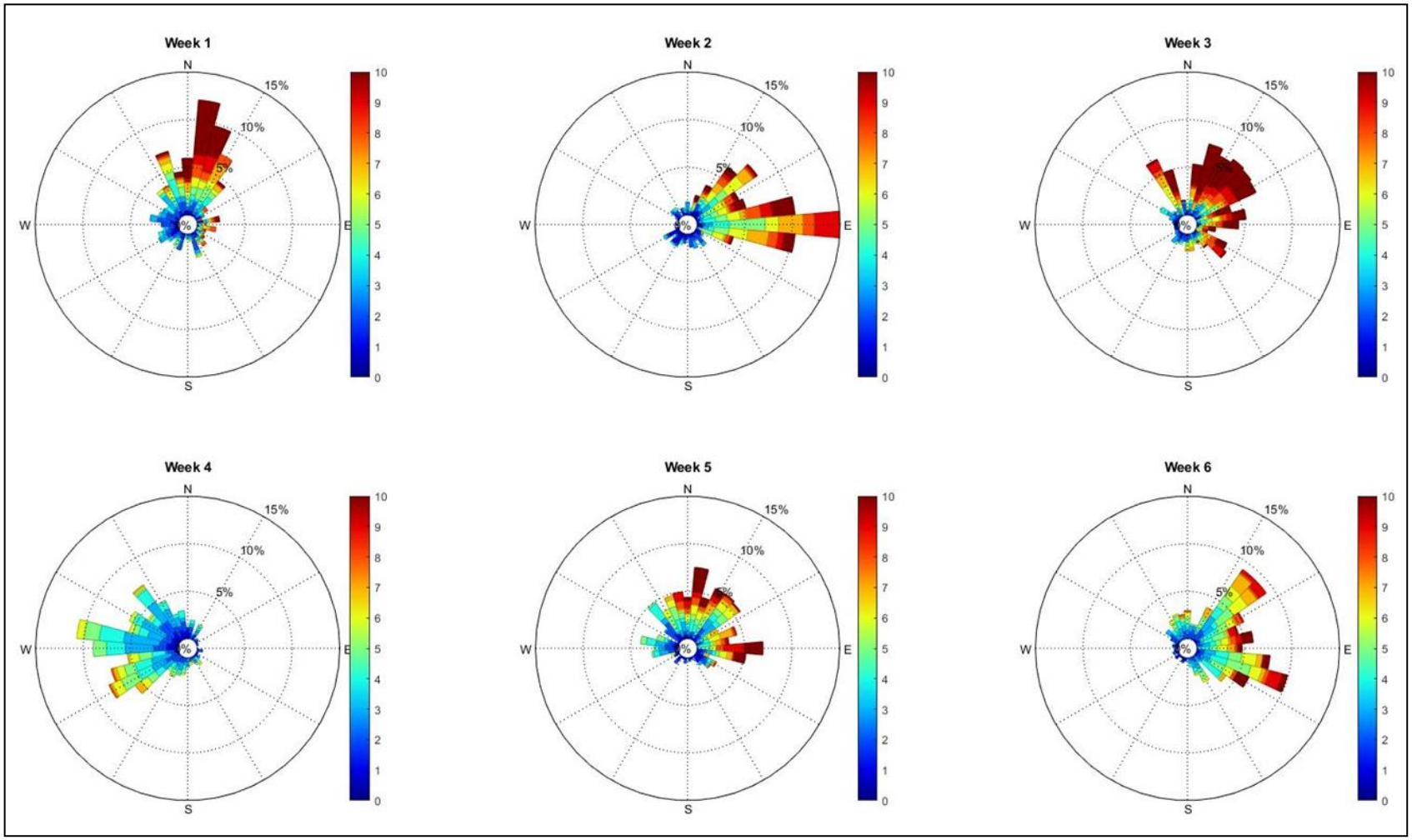

Figure 5.16: Wind rose corresponding to the PLD of larvae during March and April 2014 from 3 wind stations (Valley, Rhyl and Crosby). The direction is based on where the wind blow to. The wind strength (m/s) is represented by colour scale. The frequency is represented by the inner circle.

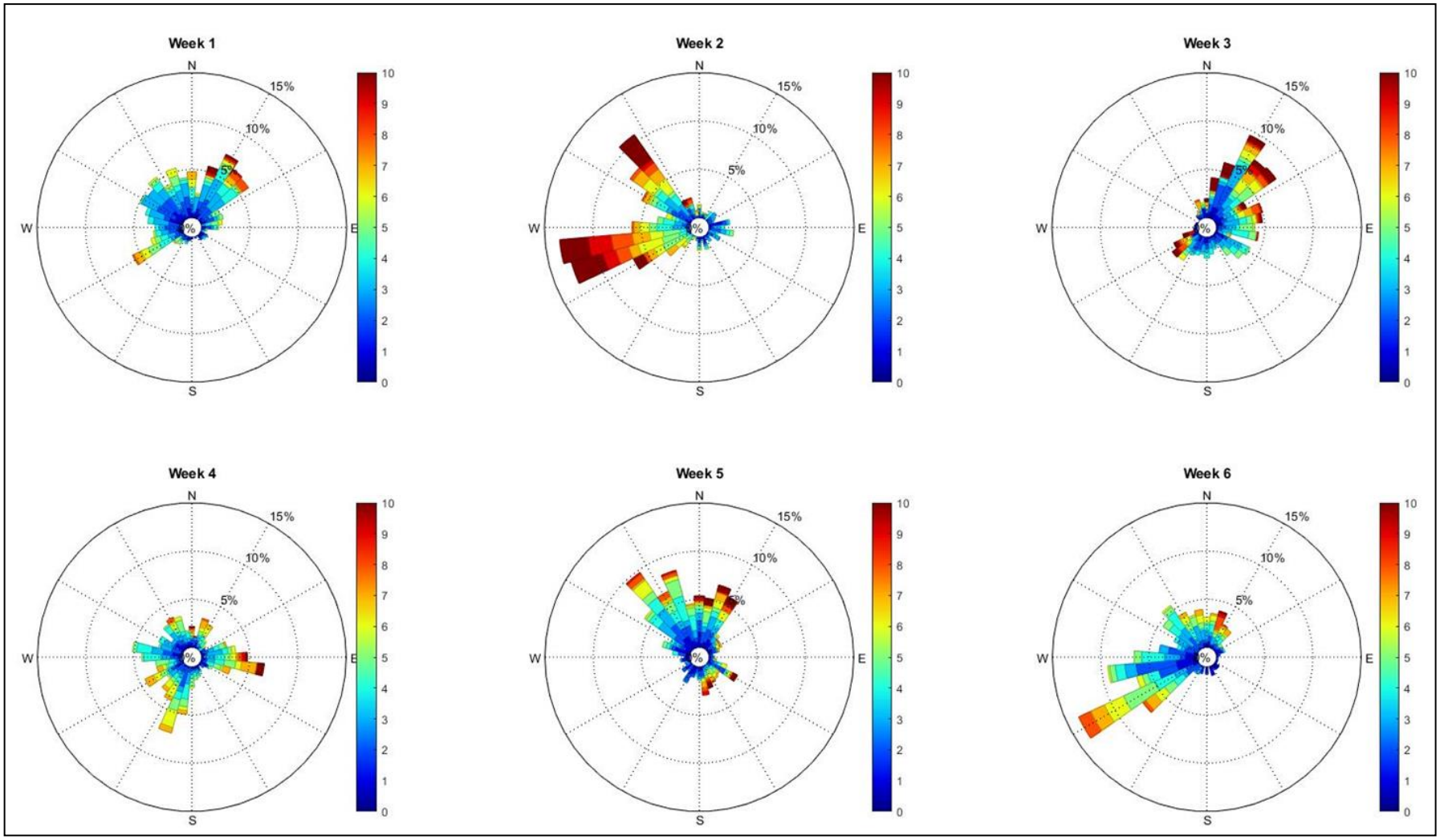

Figure 5.17: Wind rose corresponding to the PLD of larvae during March and April 2018 from 3 wind stations (Valley, Rhyl and Crosby). The direction is based on where the wind blow to. The wind strength (m/s) is represented by colour scale. The frequency is represented by the inner circle.

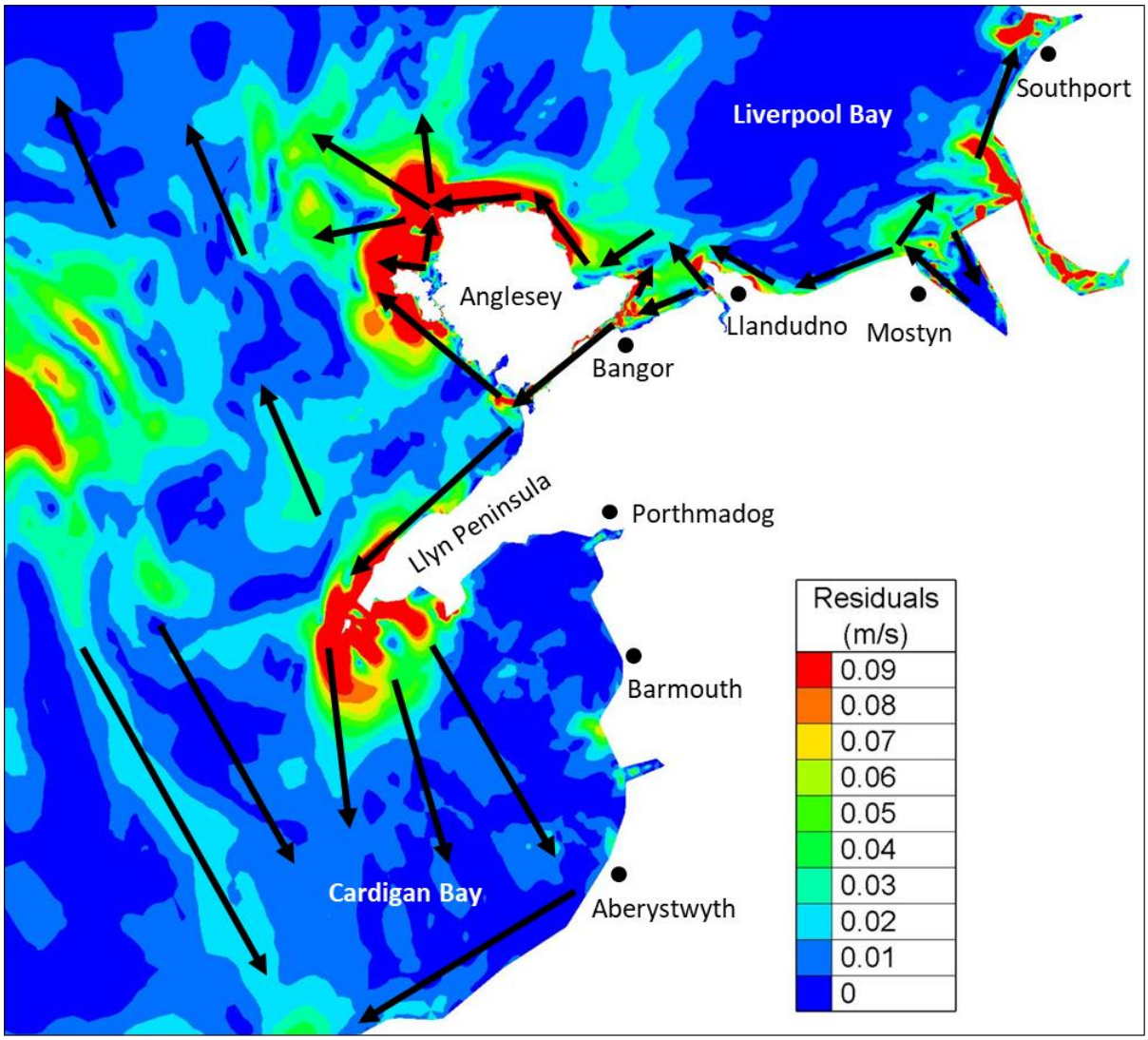

Figure 5.18: Residual currents from March to April 2018 in Cardigan Bay. Direction of the residual currents are presented by black arrows and strength (m/s) by colour scale.

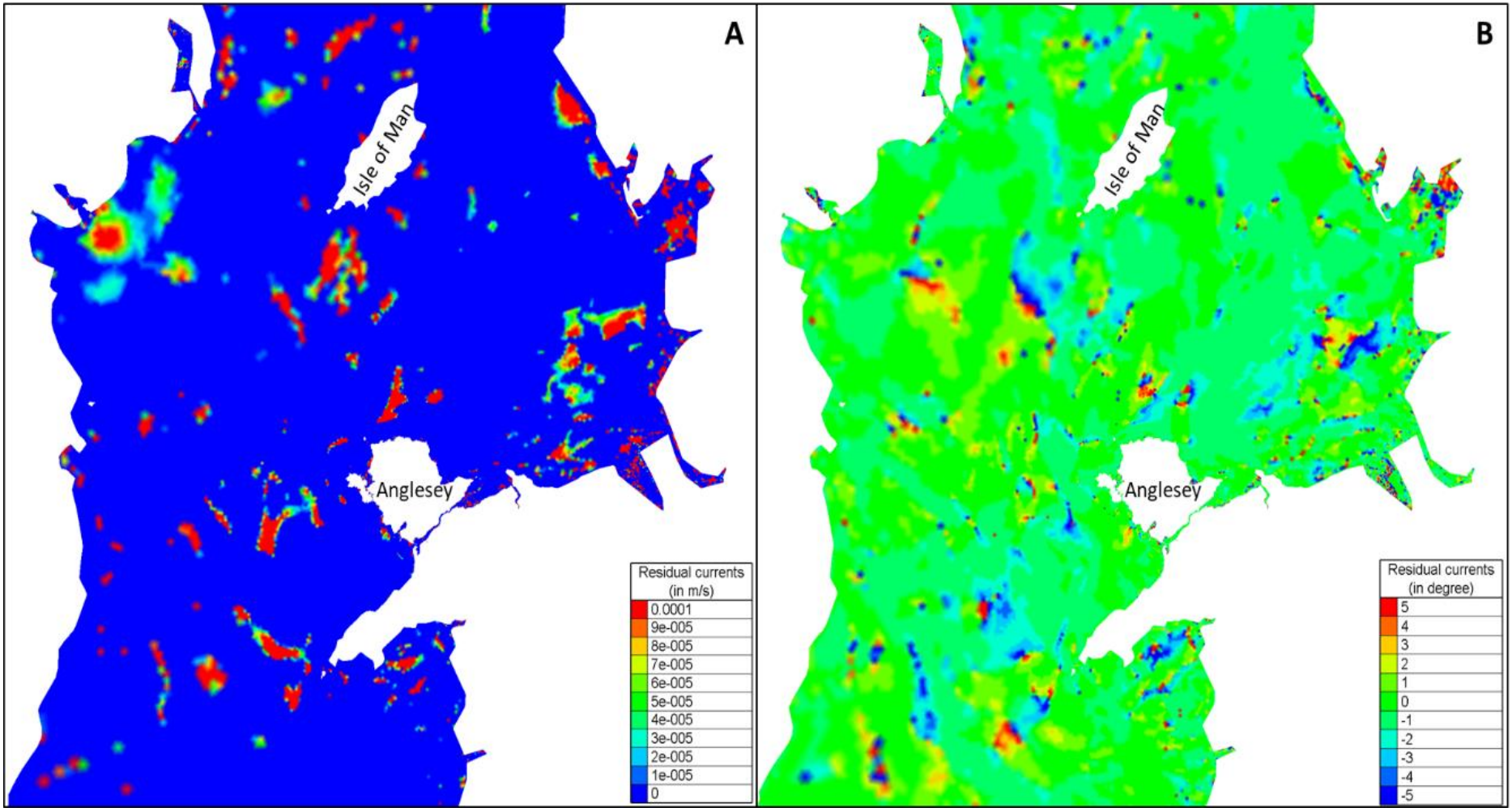

Figure 5.19: Map showing the difference of the residual currents for magnitude (A) and direction (B) between the hydrodynamics model created to simulate larval dispersal in 2014 and 2018.

Chapter 6: General conclusion

Throughout the previous chapters presented in this thesis, a robust method to simulate larval dispersal in well-mixed coastal regions has been developed. This method has been applied to the North Wales mussel populations – simulating the temporal and spatial variability in larval dispersal and population connectivity according to key drivers such as spawning time and location, larval duration and behaviour, and oceanic currents. The key findings highlighted in this study have broader implications for: 1) future modelling studies of larval dispersal applied to a range of marine species; 2) understanding larval transport and population dynamics; and 3) the impacts and management of commercial shellfisheries.

6.1 Particle tracking model (PTM) assessment

An extensive range of sensitivity tests were performed with the PTM in Chapter 3 in order to optimise the modelling experiments performed in Chapters 4 and 5 and to provide guidelines for future larval dispersal model studies. It is particularly important to accurately resolve the hydrodynamics for larval dispersal modelling, because there is often a lack of evidence on larval behaviour, and so many experiments have simply parameterised larval transport as neutrally-buoyant passive particles (McQuaid & Phillips, 200; Dobretsov & Miron, 2001). The results here showed the importance of fine spatial and temporal model resolution in regions with strong ocean currents and complex circulation patterns, such as undulating coastlines comprising headlands, islands, estuaries and tidal straits. Consequently, the spatial and temporal resolution of the ocean model should be determined according to the maximum velocity of the area of interest, but within the practical constraints of computational efficiency and data storage.

This study has demonstrated that, for larval dispersal studies, depth-averaged ocean models configured on an unstructured grid can accurately represent the flow field for well-mixed coastal environments – and therefore are a good alternative to 3D structured models that require considerably more computational effort. Indeed, 3D models used to simulate larval transport typically have a spatial resolution that exceeds 1 km and temporal resolution greater than 1 hour, which would not resolve coastal circulation patterns that are important for larval transport (Wing *et al.*, 1998a; 1998b). For the well-mixed northeast Irish Sea, results here showed that a 2D model accurately reproduced the hydrodynamics during spring and summer periods, based on a good quality observational data from velocity moorings and drifter deployments. Where 3D models are required for larval dispersal modelling, for example to resolve seasonally stratified flows, tidal mixing fronts and upwelling (Davies & Gerritsen, 1992; Aldridge & Davies, 1993; North *et al.*, 2008; Ayata *et al.*, 2009; Moreno Navas *et al.*, 2011; Sundelof & Jonsson, 2011; Nicolle *et al.*, 2013; Hoyer *et al.*, 2014; Sebille *et al.*, 2018), it is recommended

that the coastal zone is also well resolved. This may require the coupling of fine resolutions unstructured coastal 2D models with coarser resolution structured 3D models, and also possibly accounting for wave energy at the coastal boundary. Future studies should be done using drifters at different places (around Anglesey, eastern irish Sea, Menai Strait), under different tides and wind conditions to measure accurately the flow in the Irish Sea and so validate the hydrodynamics model more accurately.

6.2 Larval dispersal and population dynamics

Larval dispersal is function of three main parameters: 1) spawning time and location; 2) larval transport; and 3) settlement success (Pineda *et al.*, 2007). In the thesis, these parameters were studied in Chapter 4 and Chapter 5 based on: 1) field work that evaluated the Condition Index, which is a proxy for the timing of *Mytilus edulis* spawning events; 2) numerical modelling that evaluated *M. edulis* dispersal and connectivity under different potential behavioural and physical parameters (specifically mid-water larvae transported by the tide vs. surface larvae transported by tidal and wind-driven currents); and 3) settlement data observed by mussel farmers (Extramussel Limited) and presented in the scientific literature (Dare & Davies, 1975; Dare, 1976; Edwards, 1977). Through a successful field campaign, this study has established the timing of spawning for the Menai Strait mussel population based on the relevant environmental factors. The dispersal results showed good agreement with observations when particles travelled at the surface. This novel and important result suggests that *M.edulis* larvae are to some extent influenced by surface currents in the Irish Sea. This may maybe because the larvae behave passively and a proportion will inevitably be distributed near the surface – especially in shallow waters, or due to vertical migration behaviour. This key result builds on growing body of evidence for the need for new research, that investigates in situ vertical larval behaviour, for several species.

This study demonstrates the importance of local circulation patterns in controlling larval dispersal and population connectivity. The results showed a clear structure within the connectivity of the North Wales mussel populations that are distributed in close proximity to one another. This result confirms the need for fine resolution coastal models, since this structure would not be resolved by typical 3D/coarse-grid methods. However, for periods of strong winds, this spatial population structure was overridden, and all larvae were transported in the direction of the prevailing wind. This raises an interesting question regarding population spread: are populations able to spread, given long enough time, via ‘normal’ environmental conditions, or is spread controlled by extreme events such as strong winds? Given the wide geographic

spread and high abundance of *M.edulis* in the Irish Sea (Gosling *et al.*, 2008; Michalek *et al.*, 2016), and the large natural variability in oceanographic and atmospheric conditions (Simpson *et al.*, 1971; Heaps, 1972; Simpson *et al.*,1978; Heaps & Jones, 1977; Simpson & Bowers, 1981; Geos, 2001; Bush, 2015; Howarth, 2015), there is possibility of connectivity among all the mussel beds within the Irish Sea. Consequently, for the first time this study highlights the possibility of a *Mytilus edulis* metapopulation in the Irish Sea. These new findings open the way for genetics studies in the Irish Sea on *Mitylus edulis* to study family relationship among the mussel beds in North Wales or use microchemistry tools for future research. In addition, future research should be done on settlement onshore and offshore to either validate particle tracking model and to shoe the connectivity among the mussel beds in north Wales. Also, a good way to study population dynamics will be to create a map of the North Wales mussel bed and their size to quantify their contribution to connectivity.

6.3 Management of commercial shellfisheries

This thesis provides a robust and computationally efficient tool to aid mussel farmers in planning the harvest of mussel seed in the Irish Sea, based on local tide and temperature conditions that induce spawning, and on wind and tidal conditions that control larval dispersal. Predicting the spawning events based on air/sea temperature will help to plan the optimum time to harvest seeds (e.g. between 3 to 6 weeks after spawning). Then, according to the wind forecast, mussel farmers can predict the locations to collect mussel seed, e.g. via roped collection or harvest seed from designated areas such as Morecambe bay. Crucially the model simulations here have shown the maximal larval dispersal potential and the likely spatial variability in settlement. Based on these results, collecting ropes should be deployed near the surface to maximize the catch probability. Further, this study provides evidence for Menai Strait mussel farmers that their *Mytilus edulis* larvae can readily disperse beyond the Menai Strait and so contribute to the replenishment of others mussel beds located along the Irish Sea coast. However, results also highlight that Bangor mussel beds do not recrtuit enough to be self-sustainable, in contrary to the eastern Irish Sea (Morcambe Bay and Offshore wind farms). In this thesis, areas to collect mussel were defined as: 1) those previously known by the mussel farmers such as Morecambe Bay, Solway Firth, Brynsiencyn and Conwy and 2) new areas discovered such as the middle part of the eastern Irish Sea either in Liverpool Bay or between the Isle of Man and Anglesey.

This thesis showed the importance of human infrastructures (e.g. wind farms) on *Mytilus edulis* recruitment and dispersal. In the near future, the number of offshore wind farms will increase

in the Irish Sea and consequently there is a possibility for new settlement location for mussel larvae. This new insight opens the way to study the benefit or disadvantage of such structures on the recruitment and dispersal of mussel larvae.

6.4 Final remarks

In conclusion, this thesis has developed a practical modelling methodology to characterise the key spatial and temporal control on *Mytilus edulis* larval dispersal. New observations of larval spawning patterns within the Menai Strait have helped constrain the model simulations. The spatial extent of larval dispersal from the North Wales mussel populations has been established for the first time. These findings have raised new exciting scientific questions in different research areas such as: 1) genetic studies of fine scale population structure; 2) vertical larval migration behaviour of different species; 3) coastal management and the impact of human structure on larvae dispersal; 4) climate change impact on spawning events; and 5) management of mussel beds. The method developed in this study will be an efficient tool to help mussel shellfisheries predict spatial and temporal larvae recruitment every year and hopefully lead to a more sustainable management. Also, the tool created could be used for other purposes such as for other marine species, drifting microplastics or other pollutants or the spread of invasive species.

References

Aagaard, A.; Warman, C.D. & Depledge, M.H. (1995). Tidal and seasonal changes in the littoral zone of Keterminde Fjord, Denmark. *Marine Ecology Progress Series*, 122: 165-172.

Afenyo, M.; Veitchi, B. & Khan, F. (2016). A state-of-the-art review of fate and transport of oil spills in open and ice-covered water. *Ocean Engineering*, 119: 233-248.

Aldon, E.T. (1998). The different ways to grow oysters and mussels. *SEAFDEC Asian Aquaculture*, 20(4): 14-15.

Allen, J.S. & Newberger, P.A. (1996). Downwelling circulation on the Oregon continental shelf. Part I: response to idealized forcing. *Journal of Physical Oceanography*, 26: 2011-2035.

Allen, J.S. & Newberger, P.A. (1998). On symmetric instabilities in oceanic bottom boundary layers. *American meteorological Society*, 28: 1131-1151.

Andrejev, O; Soomere, T.; Sokolov, A. & Myrberg, K. (2011). The role of the spatial resolution of a three-dimensional hydrodynamic model for marine transport risk assessment. *Oceanologia*, 53: 309-334.

Asokan, P.K. & Mohamed, K.S. (2011). Mussel farming methods. Calicut research of central marine fisheries research institute.

Ata, R.; Goeury, C. & Hervouet, J.M. (2014). Telemac modeling system: TELEMAC-2d software (release 7.0), user manual. Paris: EDF-R&D.

Ayata, S.D.; Ellien, C.; Dumas, F.; Dubois, S. & Thiebaut, E. (2009). Modelling larval dispersal and settlement of the reef-building polychaete *Sabellaria alveolate*: role of hydroclimatic processes on the sustainability of biogenic reefs. *Continental Shelf Research*, 29(13): 1605-1623.

Aypa, S.M. (1990). Mussel culture. In: Regional seafarming development and demonstration project (RAS), selected papers on mollusc culture. National Inland Fisheries Institute, Kasetsart University Campus Bangkhen, Bangkok.

Bayne, B.L. (1964). Primary and secondary settlement in *Mytilus edulis L*. (mollusca). *Journal of Animal Ecology*, 33: 513-523.

Bayne, B.L. (1965). Growth and the delay of metamorphosis of the larvae *Mytilus edulis*. *Ophelia*, 2: 1-47.

Bayne, B.L. (1976). Marine mussels: their ecology and physiology. Cambridge: University Press.

Beaumont, A.R. & Budd, M.D. (1982). Delayed growth of mussel (*Mytilus edulis*) and scallop (*Pecten maximus*) veligers at low temperatures. *Marine Biology*, 71: 97-100.

Becker, B.J.; Levin, L.A.; Fodrie, F.J. & McMillan, P.A. (2007). Complex larval connectivity patterns among marine invertebrate populations. *Ecology*, 104: 3267-3272.

Beguer-Pon, M.; Shan, S.; Thompson, K.R.; Castonguay, M.; Sheng, J. & Dodson, J.J. (2016). Exploring the role of the physical marine environment in silver eel migrations using a biophysical particle tracking model. *ICES Journal of Marine Science*, 73: 57-74.

Berumen, M.L.; Almany, G.R.; Planes, S.; Jones, G.P.; Saenz-Agudelo, P. & Thorrold, S.R. (2012). Persistence of self-recruitment and patterns of larval connectivity in a marine protected area network. Ecology and Evolution, 2(2): 444-452.

Block, J.W. & Geelen, H.J.F.M. (1958). The substratum required for settling of mussels (*Mytilus edulis L.*). *Archives Néerlandaises de Zoologie*, 13: 446-460.

Boromthanarat, S.; Deslous-Paoli, J.M. & Heral, M. (1987). Reproduction and recruitment of *Mytilus edulis* reared on the crawls in the Bay of Marennes-Oleron. *Haliotis*, 16: 317-326.

Bourban, S.E.; Couch, S.J.; Baldock, A. & Cheeseman, S. (2014). Coastal shelf model of northern European waters to inform tidal power industry decisions: SMARTtide. *Underwater technology*, 32(1): 15-26.

Bowden, K.F. (1980). Chapter 12 Physical and dynamical oceanography of the Irish Sea. *Elsevier Oceanography Series*, 24(B): 391-413.

Bowers, D.G.; Macdonald, R.G.; McKee, D.; Nimmo-Smith, W.A.M. & Graham, G.W. (2013). On the formation of tide-produced seiches and double high waters in coastal seas. *Estuarine, Coastal and Shelf Science*, 134: 108-116.

Brenko, M.H. & Calabrese, A. (1969). The combined effect of salinity and temperature on larvae of the mussel *Mytilus edulis*. *Marine Biology*, 4: 224-226.

British oceanographic Data Centre, 1969,National Oceanographic Centre, accessed 1 January 2020, https://www.bodc.ac.uk/.

Buchan, S.; Floodgate, G.D. & Crisp, D.J. (1973). Studies of the seasonal variation of the suspended matter of the Menai Straits II. Mid-stream data. *Deutsche Hydrografische Zeitschrift*, 26: 74:83.

Buschbaum, C. (2002). Predation on barnacles of intertidal and subtidal mussel beds in the Wadden Sea. *Helgoland Marine Research*, 56: 37-43.

Bush, L.E.; Balestrini, S.J.; Robins, P.E. & Davies, A.J. (2015). The reproduction and connectivity of *Sabellaria alveolata* reefs in Wales. NRW Evidence report No 049 - MAR4REF Bangor University.

Campbell, A.R.; Simpson, J.H. & Allen, G.L. (1998). The Dynamical balance of flow in the Menai Strait. *Estuarine, Coastal and Shelf Science*, 46: 449-455.

Centre for Environmental Data Analysis, 23 May 2018, accessed 1 January 2020, https://www.ceda.ac.uk/.

Chang, Y.C., Chen, G.Y., Tseng, R.S., Centurioni, L.R. & Chu, P.C. (2012). Observed near-surface currents under high wind speeds. *Journal of Geophysical Research*, 117, C11026.

Chen, C. & Liu, H. (2003). An unstructured grid, finite-volume, three-dimensional, primitive equations ocean model: Application to coastal ocean and estuaries. *American meteorological Society*, 20: 159-186.

Chen, C.; Huang, H.; Beardsley, R.C.; Liu, H.; Xu, Q. & Cowles, G. (2007). A finite volume numerical approach for coastal ocean circulation studies: comparisons with finite difference models. *Journal of Geophysical Research Oceans*, 112(C3).

Chia, F.S.; Buckland-Nicks, J. & Young, C.M. (1984). Locomotion of marine invertebrate larvae: a review. *Canadian Journal of Zoology*, 62(7): 1205-1222.

Chipperfield, P.N.J. (1953). Observations on the breeding and settlement of *Mytilus edulis (L.)* in british waters. *Journal of the marine biology Association of the United Kingdom* 32: 449-476.

Chung, D.H. & Duyen, N.T.K. (2012). Sensitivity of lagrangian particle tracking based on a 3D numerical model. *Journal of Modern Physics*, 3: 1972-1978.

Cockrell, M.L.; Bernhardt, J.R. & Leslie, H.M. (2015). Recruitment, abundance and predation on the blue mussel (*Mytilus edulis*) on northeastern estuarine rocky shores. *Ecosphere*, 6(1): 1-24.

Commito, J.A.; Commito, A.E.; Platt, R.V.; Grupe, B.M.; Dow Piniak, W.E.; Gownaris, N.J.; Reeves, K.A. & Vissichelli, A.M. (2014). Recruitment facilitation and spatial pattern formation in soft-bottom mussel beds. *Ecosphere*, 5(12): 160.

Condie, S. & Condie, R. (2016). Retention of plankton within ocean eddies. *Global Ecology and Biogeography*, 25: 1264-1277.

Conway, D.V.P.; Coombs, S.H. & Smith, C. (1997). Vertical distribution of fish eggs and larvae in the Irish Sea and southern North Sea. *ICES Journal of Marine Science*, 54(1): 136-147.

Coscia, I.; Robines, P.E.; Porter, J.S.; Malham, S.K. & Ironside, J.E. (2012). Modelled larval dispersal and measured gene flow: seascape genetics of the common cockle Cerastoderma edule in the southern Irish Sea. *Conservation Genetics*, 14: 451-466.

Cote, I.M. (1995). Effect of predatory crab effluent on byssus production in mussels. *Journal of experimental Marine Biology and Ecology*, 188(2): 233-241.

Cowen, R.K.; Paris, C.B. & Srinivasan, A. (2006). Scaling of connectivity in marine populations. *Science*, 311(5760): 522-527.

Criales, M.M.; Browder, J.A.; Mooers, C.N.K.; Robblee, M.B.; Cardenas, H. & Jackson, T.L. (2007). Cross-shelf transport of pink shrimp larvae: interactions of tidal currents, larval vertical migrations and internal tides. *Marine Ecology progress Series*, 345: 167-184.

Dabrowski, T.; Hartnett, M. & Berry, A. (2003). Modelling hydrodynamics of Irish Sea. *Computational Fluid and Solid mechanics 2003*; Proceedings second MIT conference on computational fluid and solid mechanics, 877-881.

Dabrowski, T. 2005. A flushing study analysis of selected Irish waterbodies. Ph.D. Thesis, Civil Engineering Department, National University of Ireland, Galway.

Dabrowski, T. & Hartnett, M. (2008). Modelling travel and residence times in the eastern Irish Sea. *Marine pollution bulletin*, 57: 41-46.

Dabrowski, T.; Hartnett, M. & Olbert, A.I. (2010). Influence of seasonal circulation on flushing of the Irish Sea. *Marine pollution bulletin*, 60(5): 748-758.

Daigle, R.M.; Chasse, J. & Metaxas, A. (2016). The relative effect of behaviour in larval dispersal in a low energy embayment. *Progress in Oceanography*, 144: 93-117.

Dame, R.F. (1993). The role of bivalve filter feeder material fluxes in estuarine ecosystems. In: Dame R.F. (eds) Bivalve filter feeders. Nato ASI Series (Series G: Ecological sciences), vol 33. Springer, Berlin, Heidelberg.

Dame, R.F.; Bushek, D. & Prins, T.C. (1998). Benthic suspension feeders as determinants of ecosystem structure and function in shallow coastal waters. *Ecological Comparisons of Sedimentary Shores*, 151: 11-37.

Dare, P.J. (1976). Settlement, growth and production of the mussel, *Mytilus edulis L.*, in Morecambe Bay, England. *Fishery Investigations, Ministry of Agriculture, Fisheries and Food, Series II*, 28.

Dare, P.J. (1982). Notes on the swarming behaviour and population density of *Asterias rubens L.* (Echinodermata: Asteroidea) feeding on the mussel *Mytilus edulis*. *Journal du Conseil Permanent International pour l'Exploration de la Mer*, 40: 112-118.

Dare, P.J. & Edwards, D.B. (1976). Experiments on the survival, growth and yield of relaid seed mussels (*Mytilus edulis L.*) in the Menai Strait, north Wales. *ICES Journal of Marine Science*. 37(1): 16-28.

Dauhajre, D.P.; McWilliams, J.C. & Renault, L. (2019). Nearshore lagrangian connectivity: submesoscale influence and resolution sensitivity. *Journal of Geophysical research: Oceans*, 24(7): 5180-5204.

Davies, A.M. & Gerritsen, H. (1992). An intercomparison of three-dimensional tidal hydrodynamic models of the Irish Sea. *Tellu*s, 46(A): 200-221.

Davies, A.M. & Aldridge, J.N. (1993). A numerical model study of parameters influencing tidal currents in the Irish Sea. *Journal of Geophysical. Research Oceans*, 98 (C4): 7049-7067.

Davies, A.M. & Hall, P. (2000). A three-dimensional model of diurnal and semidiurnal tides and tidal mixing in the North Channel of the Irish Sea. *Journal of Geophysical research*, 105: 17079-17104.

Davies, A.M. & Robins, P.E. (2017). Residual flow, bedforms and sediment transport in a tidal channel modelled with variable bed roughness. *Geomorphology*, 295: 855-872.

De Dominicis, M.; Leuzzi, G.; Monti, P.; Pinardi, N. & Poulain, P.M. (2012). Eddy diffusivity derived from drifter data for dispersion model applications. *Ocean Dynamics*, 62: 1381-1398.

De Vooys, C.G.N. (1999). Numbers of larvae and primary plantigrades of the mussel *Mytilus edulis* in the western Dutch Wadden Sea. *Journal of Sea Research*, 41: 189-201.

Dickey-Collas, M.; Gowen, R.J. & Fox, C.J. (1996). Distribution of larval and juvenile fish in the western Irish Sea: relationship to phytoplankton, zooplankton biomass and recurrent physical features. *Marine and Freshwater Research*, 47(2): 169-181.

DIGIMAP, 2000, accessed 1 January 2020, https://digimap.edina.ac.uk/.

Dimou, K.N. & Adams, E.E. (1993). A random-walk, particle tracking model for well-mixed estuaries and coastal waters. *Estuarine, Coastal and Shelf Science*, 37: 99-110.

Dinh, H.Q. & Fotedar, R. (2016). Early development of the blue mussel Mytilus edulis (Linnaeus, 1758) cultured in potassium-fortified inland saline water. *Aquaculture*, 452: 373-379.

Dobretsov, S.V. & Miron, G. (2001). Larval and post-larval vertical distribution of the mussel *Mytilus edulis* in the White Sea. *Marine Ecology Progress Series*, 218; 179-187.

Dobretsov, S.V. & Wahl, M. (2001). Recruitment preferences of blue mussel spat (*Mytilus edulis*) for different substrata and microhabitats in the White Sea (Russia). *Hydrobiologia*, 445: 27-35.

Dobson, M.R.; Evans, W.E. & James, K.H. (1970). The sediment on the floor of the southern Irish Sea. *Marine Geology*, 11(1): 27-69.

Duinker, A.; Haland, L.; Hovgaard, P. & Mortensen, S. (2008). Gonad development and spawning in one and two-year-old mussels (*Mytilus edulis*) from Western Norway. *Journal of the marine biology Association of the United Kingdom* 88: 1465-1473.

Durst, F.; Miloievic, D. & Schonung, B. (1984). Eulerian and lagrangian predictions of particulate two-phase flows: a numerical study. *Applied Mathematical Modelling*, 8(2): 101-115.

Edwards, R.T. (1987). Sestonic bacteria as a food source for filtering invertebrates in two southeastern blackwater rivers. *Limnology and Oceanography*, 32(1): 221-234.

Edwards, K.P.; Hare, J.A.; Werner, F.E. & Blanton, B.O. (2006). Lagrangian circulation on the southeast US continental shelf: implications for larval dispersal and retention. *Continental Shelf Research*, 26: 1375-1394.

Ellien, C.; Thiebaut, E.; Barnay, A.S.; Dauvin, J.C.; Gentil, F. & Salomon, J.C. (2000). The influence of variability in larval dispersal on the dynamics of a marine metapopulation in the eastern Channel. *Oceanologica Acta*, 23(4): 423-442.

Elliott, A.J. (1991). EUROSPILL: oceanographic processes and NW European shelf databases. *Marine Pollution Bulletin*, 22(11): 548-553.

Embleton, C. (1964). The deglaciation of Arfon and southern Anglesey, and the origin of the Menai Straits. *Proceeding of the Geologists' Association*, 75(4): 407-429.

Ewins, P.A. & Spencer, C.P. (1967). The annual cycle of nutrients in the Menai Straits. *Journal of the Marine Biology Association of the United Kingdom* 47: 533-542.

Fahrig, L. & Merriam, G. (1985). Conservation of fragmented populations. *Conservation Biology*, 8: 50-59.

Fenoglio-marc, L.E.; Garcia, M.J. & Kjaer, N. (2005). Inter-annual to decadal sea level change in south-western Europe from satellite altimetry and in-situ measurements. *International Association of geodesy Symposia*, 129: 242-247.

Fernandes, E.H.; Dyer, K.R. & Niencheski, L.F.H. (2001). Calibration and validation of the TELEMAC-2D model to the Patos lagoon (Brazil). *Journal of Coastal Research*, 34: 470-488.

Ferrarin, C.; Umgiesser, G.; Cucco, A.; Hsu, T.; Roland, A. & Amos, C.L. (2008). Development and validation of a finite element morphological model for shallow water basins. *Coastal Engineering*, 55: 716-731.

Filgueira, R.; Comeau, L.A.; Landry, T.; Grant, J.; Guyondet, T. & Mallet, A. (2013). Bivalve condition index as an indicator of aquaculture intensity: a meta-analysis. *Ecological Indicators*, 25: 215-229.

Filgueira, R.; Brown, M.S.; Comeau, L.A. & Grant, J. (2015). Predicting the timing of the pediveliger stage of *Mytilus edulis* based on ocean temperature. *Journal of Molluscan Studies*, 81: 269-273.

Fugro GEOS (2001). Wind and wave frequency distributions for sites around the British Isles. Health and Safety Executive.

Gaitan-Espitia, J.; Quintero-Galvis, J.F.; Mesas, A. & D'Elia, G. (2016). Mitogenomics of southern hemisphere blue mussels (Bivalvia: pteriomorphia): insights into the evolutionary characteristics of the *Mytilus edulis* complex. *Scientific reports*, 6: 26853.

Gaonkar, C.A.; Samiksha, S.V.; Grinson, G.; Aboobacker, V.M.; Vethamony, P. & Anil, A.C. (2012). Numerical simulations of barnacle larval dispersion coupled with field observations on larval abundance, settlement and recruitment in a tropical monsoon influenced coastal marine environment. *Journal of Marine Systems*, 94: 218-231.

Garcia-Garcia, L.M.; Ruiz-Villareal, M. & Bernal, M. (2016). A biophysical model for simulating early life stages of sardine in the Iberian Atlantic stock. *Fisheries research*, 173(3): 250-272.

Gaylord, B.; Reed, D.C.; Raimondi, P.T.; Washburn, L. & McLean, S.R. (2002). A physically based model of macroalgal spore dispersal in the wave and current-dominated nearshore. *Ecology*, 83(5): 1239-1251.

Geller, J.B.; Walton, E.D.; Grosholz, E.D. & Ruiz, G.M. (1997). Cryptic invasions of the crab *Carcinus* detected by molecular phylogeography. *Molecular Ecology*, 6(10): 901-906.

Genc, O., Ardiclioglu, M. & Agiralioglu, N. (2015). Calculation of mean velocity and discharge using water surface velocity in small streams. *Flow Measurement and Instrumentation*, 41: 115-120.

Gibbson, W. (1987). Menai strait fault system: an early Caledonian terrane boundary in North Wales. *Geology*, 15(8): 744-747.

Gilg, M.R. & Hilbish, T.J. (2003). Patterns of larval dispersal and their effect on the maintenance of a blue mussel hybrid zone in southwestern England. *Evolution*, 57: 1061-1077.

Gimenez L.; Robins, P. & Jenkins, S.R. (2019). Role of trait combinations, habitat matrix, and network topology in metapopulation recovery from regional extinction. *Limnology and Oceanography*, 9999: 1-15.

Golding, N., Vincent, M. & Connor, D.W. (2004). The Irish Sea Pilot. Report on the development of a marine landscape classification for the Irish Sea. JNCC and online at www.jncc.gov.uk/irishseapilot. DEFRA 2004.

Goode, D.J. (1990). Particle velocity interpolation in block-centered finite difference groundwater flow models. *Water Resources research*, 26(5): 925-940.

Gosling. E.M. (1992). Systematic and geographic distribution of Mytilus. In: E.M. Gosling, editor. The mussel *Mytilus*: ecology, physiology, genetics and culture, New York: Elsevier. pp. 1-17.

Gosling, E.; Doherty, S. & Howley, N. (2008). Genetic characterization of hybrid musel (*Mytilus*) populations on Irish coasts. *Journal of the Marine Biological Association of the United Kingdom*, 88(2): 341-346.

Gouesbet, G. & Berlemont, A. (1999). Eularian and lagrangian approaches for predicting the behaviour of discrete particles in turbulent flows. *Progress in Energy and Combustion Science*, 25:133-159.

Gowen, R.J., Stewart, B.W., Mills, D.K. & Elliott, P. (1995). Regional differences I stratification and its effect on phytoplankton production and biomass in the north western Irish Sea. *Journal of Plankton Research*, 17(4): 753-769.

Graham, J.A.; O'Dea, E.; Holt, J.; Polton, J.; Hewitt, H.T.; Furner. R.; Guihou, K.; Brereton, A.; Arnold, A.; Wakelin, S.; Castillo Sanchez, J.M. & Mayorga Adame, C.G. (2018). AMM15: a new high-resolution NEMO configuration for operational of the European north-west shelf. *Geoscientific Model Development*, 11: 681-696.

Green, M. & McCave, I.N. (1995). Seabed drag coefficient under tidal currents in the eastern Irish Sea. *Journal of Geophysical Research Atmospheres*, 100 (C8): 16057-16069.

Griffies, S.M.; Boning, C.; Bryan, F.O.; Chassignet, E.P.; Gerdes, R.; Hasumi, H.; Hirst, A.; Treguier, A.M. & Webb, D. (2000). Developments in ocean climate modelling. *Ocean Modelling*, 2: 123-192.

Grizzle, R.E.; Short, F.T.; Neweel, C.R.; Hoven, H. & Kindblom, L. (1996). Hydrodynamically induced synchronous waving of seagrasses: 'monami' and its possible effects on larval mussel settlement. *Journal of Experimental Marine Biology and Ecology*, 206: 165-177.

Guizien, K.; Brochier, T.; Duchene, J.C.; Koh. B.S. & Marsaleix, P. (2006). Dispersal of *Owenia fusiformis* larvae by wind-driven currents: turbulence, swimming behaviour and mortality in a three-dimensional stochastic model. *Marine Ecology Progress Series*, 311: 47-66.

Hadziabdic, P. & Rickards, L.J. (1999). Review of the Irish Sea (area 6) oceanography.

Hambrey, J. & Evans, S. (2016). Strathpeffer, Scotland. Aquaculture in England, Wales and Northern Ireland: an analyse of the economic contribution and value of the major sub-sectors and the most important farmed species.

Hamilton, D.J.; Nudds, T.D. & Neate, J. (1999). Size-selective predation of blue mussels (*Mytilus edulis*) by common eiders (*Somatera mollissima*) under controlled field conditions. *The Auk*, 116(2); 403-416.

Hanski, I. (1982). Dynamics of regional distribution: the core satellite hypothesis. *Oikos*, 38: 210-221.

Hanski, I. (1985). Single-species spatial dynamics may contribute to long-term rarity and commonness. *Ecology*, 66: 335:343.

Harii S. & Kayanne H. (2003). Larval dispersal, recruitment, and adult distribution of the brooding stony octocoral *Heliopora coerulea* on Ishigaki Island, southwest Japan. *Coral Reefs*, 22: 188-196.

Harnett, M.; Berry, A.; Tully, O. & Dabrowski, T. (2007). Investigations into the transport and pathways of scallop larvae – the use of numerical models for managing fish stocks. *Journal of Environmental Monitoring*, 9: 403-410.

Harrison, K.A.; Pavlova, A.; Telonis-Scott, M. & Sunnucks, P. (2014). Using genomics to characterize evolutionary potential for conservation of wild populations. *Evolutionary Applications*, 7(9): 1008-1025.

Harvey, J.G. (1968). The flow of water through the Menai Straits. *Geophysical Journal of the Royal Astronomical Society*, 15: 517-528.

Harvey, J.G. (1972). Water temperatures at Menai Bridge pier, 1955-1968. *Deutsche Hydrografische Zeitschrift*, 25(5): 202-215.

Heaps, N.S. (1972). Estimation of density currents in the Liverpool Bay area of the Irish Sea. *Geophysical Journal of the Royal Astronomical Society*, 30: 415-432.

Heaps, N.S. & Jones, J.E. (1977). Density currents in the Irish Sea. *Geophysical Journal International*, 51(2): 393-429.

Herlyn, M., Millat, G. & Petersen, B. (2008). Documentation of sites of intertidal blue mussel (*Mytilus edulis L.*) beds of the Lower Saxonian Wadden Sea, southern North Sea (as of 2003) and the role of their structure for spatfall settlement. *Helgoland Marine Research*, 62: 177-188.

Herman, P.J.P. (1993). A set of models to investigate the role of benthic suspension feeders in estuarine ecosystems. In: R.F. Dame (Ed.), *Bivalve Filter Feeder in Estuarine and Coastal Ecosystem Processes*. Springer Verlag, Berlin: 421-454.

Hervouet, J.M. (2000). TELEMAC modelling system: an overview. *Hydrological processes*, 14(13): 2209-2210.

Hess, G. (1996). Disease in metapopulation models: implications for conservation. *Ecology*, 77(5): 1617-1632.

Hilbish, T.J.; Mullinax, A.; Dolven, S.I.; Meyer, A.; Koehn, R.K. & Rawson, P.D. (2000). Origin of the antitropical distribution pattern in marine mussels (*Mytilus spp.*): routes and timing of transequatorial migration. *Marine Biology*, 136(1): 69-77.

Hill, A.E. (1990). Pelagic dispersal of Norway *Nephrops norvegicus* larvae examined using an advection-diffusion-mortality model. *Marine Ecology Progress Series*, 64: 217-226.

Hill, A.E. (1993). Seasonal gyres in shelf seas. *Annales Geophysicae*, 11: 1130-1137.

Hill, A.E.; Brown, J. & Fernand, L. (1997). The summer gyre in the western Irish Sea: shelf sea paradigms and management implications. *Estuarine, Coastal and Shelf Science*, 44(1): 83-95.

Hjort, J. (1914). Fluctuations in the great fisheries of northern Europe reviewed in the light of biological research. *Rapports et Proces-Verbaux des reunions du Conseil permanent International pour l'Exploration de la Mer*, 20:1-228.

Hjort, J. (1926). Fluctuations in the year classes of important food fishes. *Journal du Conseil*, 1(1): 5-38.

Holt, J.T., Proctor, R., Blackford, J.C., Allen, J.I. & Ashworth, M. (2004). Advective controls on primary production in the stratified western Irish Sea: an eddy-resolving model study. *Journal of Geophysical Research*, 109 (C05024).

Horsburgh, K.J. & Hill, A.E. (2003). A three-dimensional model of density-driven circulation in the Irish Sea. *Journal of Physical Oceanography*, 33: 343-365.

Horvath, T. & Crane, L. (2010). Hydrodynamics forces affect alrval zebra mussel (*Dreissena polymorpha*) mortality in a laboratory setting. *Aquatic invasions*: 5(4): 379-385.

Howarth, M.J. (2005). Hydrography of the Irish Sea. Tech. rep., SEA6 Technical report, Department of Trade and Industry offshore energy Strategic Assessment programme, UK.

Hoyer, A.B.; Wittmann, M.E.; Chandra, S.; Schladow, S.G. & Rueda, F.J. (2014). A 3D individual-based aquatic transport model for the assessment of the potential dispersal of planktonic larvae of an invasive bivalve. *Journal of Environmental Management*, 145: 330-340.

Hunt, H.L. & Scheibling, R.E. (1996). Physical and biological factors influencing mussel (*Mytilus trossulus, M. edulis*) settlement on a wave-exposed rocky shore. *Marine Ecology Progress Series*, 142: 135-145.

Hunter, J.R.; Craig, P.D. & Phillips, H.E. (1993). On the use of random walk models with spatially variable diffusivity. *Journal of Computational Physics*, 106: 366-376.

Huntley, M. & Zhou, M. (2004). Influence of animals on turbulence in the sea. *Marine Ecology Progress Series*, 273: 65-79.

James, M.K.; Polton, J.A.; Brerreton, A.R.; Howell, K.L.; Nimmo-Smith, W.A.M. & Knights, A.M. (2019). Reverse engineering field-derived vertical distribution profiles to infer larval swimming behaviours. *Proceedings of the national academy of Sciences of the United States of America*, 116(24): 11818-11823.

Johnson, D.F. & Hess K.W. (1990). Numerical simulations of blue crab larval dispersal and recruitment. *Bulletin of Marine Science*, 46(1): 195-213.

Jones, J.E. & Davies, A.M. (2005). An intercomparison between finite difference and finite element (TELEMAC) approaches to modelling west cost of Britain tides. *Ocean Dynamics*, 55: 178-198.

Jones, J.E. & Davies, A.M. (2006). Application of a finite element model (TELEMAC) to computing the wind induced response of the Irish Sea. *Continental Shelf Research*, 26: 1519-1541.

Jones, J.E. & Davies, A.M. (2010). Application of a finite element model to the computation of tides in the Mersey Estuary and Eastern Irish Sea. *Continental Shelf Research*, 30: 491-514.

Katz, C.H.; Cobb, J.S. & Spaulding, M. (1994). Larval behaviour, hydrodynamic transport, and potential offshore-to-inshore recruitment in the American lobster *Homarus americanus*. *Marine Ecology Progress Series*, 103(3): 265-273.

Keen, E.M. (2015). Net savvy: a practical guide to zooplankton sampler design. NOAA Technical Memorandum NMFS.

Keough, M.J. & Downes, B.J. (1982). Recruitment of marine invertebrates: the role of active larval choices and early mortality. *Oecologica*, 54: 348-352.

Kim, T,H., Shibuya, K., Doi, K., Aoyama, Y. & Hayakawa, H. (2011). *Polar Science*, 5(1): 21-39.

Kinlan, B.P.; Gaines, S.D. & Lester, S.E. (2005). Propagule dispersal and the scales of marine community process. *Diversity and Distribution*, 11: 139-148.

Knights, A.M.; Crowe, T.P. & Burnell, G. (2006). Mechanisms of larval transport: vertical distribution of bivalve larvae varies with tidal conditions. *Marine Ecology Progress Series*, 326: 167-174.

Koszalka, I.; LaCasce, J.H. & Orvik, K.A. (2009). Relative dispersion in the Nordic Seas. *Journal of Marine Research*, 67: 411-433.

Koszalka, I. & LaCasce, J.H. (2010). Lagrangian analysis by clustering. *Ocean Dynamics*, 60(4): 957-972.

Koszalka, I.; LaCasce, J.H. & Mauritzen, C. (2013). In pursuit of anomalies – analysing the poleward transport of Atlantic water with surfaces drifters. *Deep-Sea Research II*, 85: 96-108.

Kratzer, S.; Bowers, D. & Tett, P.B. (2000). Seasonal changes in colour ratos and optically active constituents in the optical Case-2 waters of the Menai Strait, North Wales. *International Journal of Remote Sensing*, 21: 2225-2246.

Kratzer, S.; Buchan, S. & Bowers, D.G. (2003). Testing long-term trends in turbidity in the Menai Strait, North Wales. *Estuarine, Coastal and Shelf Science*, 56: 221-226.

Kratzer, S.; Bowers, D. & Tett, P.B. (2000). Seasonal changes on colour ratios and optically active constituents in the optical Case-2 waters of the Menai Strait, North Wales. *International Journal of Remote Sensing*, 21(11): 2225-2246.

Kvile, K.O.; Romagnoni, G.; Dagestad, K.F.; Langangen, O. & Kristiansen, T. (2018). Sensitivity of modelled North Sea cod larvae transport to vertical behaviour, ocean model resolution and interannual variation in ocean dynamics. *ICES Journal of Marine Science*, 75(7): 2413-2425.

LaCasce J.H. & Bower, A. (2000). Relative dispersion in the subsurface North Atlantic. *Journal of Marine Research*, 58: 863-894.

Lapointe, L. & Bourget, E. (1999). Influence of substratum heterogeneity scales and complexity on a temperate epibenthic marine community. *Marine Ecology progress Series*, 189: 159-170.

Lane, D.J.W.; Beaumont, A.R. & Hunter, J.R. (1985). Byssus drifting and the drifting threads of the young post-larval mussel *Mytilus edulis*. *Marine Biology*, 84(3): 301-308.

Langendoen, E.J.; Mendoza, A.; Abad, J.D.; Tassi, P.; Wamg, D.; Ata, R.; Abdarrezzak, K.E.K.; Hervouet, J.M. (2016). Improved numerical modelling of morphodynamics of rivers with steep banks. *Advances in Water Resources*, 93: 4-14.

Larghier, J.L. (2003). Considerations in estimating larval dispersal distances from oceanographic data. Ecological Application, 13 supplement: S71-S89.

Lee, A.J. & Ramster, J.W. (1981). 1981: Atlas of the seas around the British Isles. Ministry of Agriculture, Fisheries and Food.

Lett, C.; Verley, P.; Mullon, C.; Parada, C.; Brochier, T.; Penven, P. & Blanke, B. (2008). A lagrangian tool for modelling ichthyoplankton dynamics. *Environmental Modelling & Software*, 23(9): 1210-1214.

Levin, L.A. (1990). A review of methods for labelling and tracking marine invertebrate larvae. *Ophelia*, 32: 115-144.

Levin, L.A. (2006). Recent progress in understanding larval dispersal: new directions and digressions. *Integrative and Comparative Biology*, 46: 282-297.

Levins, R. (1969). Some demographic and genetic consequences of environmental heterogeneity for biological control. *Bulletin of the Entomological Society of America*, 15: 237-240.

Lewis, M.; Neill, S.; Robins, P.; Hashemi, M.R. & Ward, S. (2017). Characteristics of the velocity profile at tidal-stream energy sites. *Renewable energy*, 114: 258-272.

Liu, P.L.F. & Losada, I.J. (2002). Wave propagation modelling in coastal engineering. *Journal of Hydraulic Research*, 40(3): 229-240.

Lowe, D.M.; Moore, M.N. & Bayne, B.L. (1982). Aspects of gametogenesis in the marine mussel *Mytilus edulis L.*. *Journal of the marine biology Association of the United Kingdom*, 62: 133-145.

Lubchenco, J. & Menge, B.A. (1978). Community development and persistence in a low rocky intertidal zone. *Ecological Monographs*, 59: 67:94.

Maas Gesteranus, R.A. (1942). On the formation of banks by *Mytilus edulis*. *Archives Néerlandaises de Zoologie*, 6: 283-326.

Mackie, A.S.Y. (1990). Offshore benthic communities of the Irish Sea. In O'Connor, F.B. (Ed.), The Irish Sea: an environmental review. Part 1. Nature conservation. Liverpool University Press, Liverpool, pp. 169-218.

Mahdavimanesh, M.; Noghrehabadi, A.R.; Behbahaninejad, M.; Ahmadi, G. & Dehghanian, M. (2013). Lagrangian Particle tracking: Model development. *Life Science Journal*, 10:34-41.

Martinez, J.; Robledo, J.A.F. & Figueras, A. (1994). Settlement and post-larvae behaviour of *Mytilus galloprovincialis*: field and laboratory experiments. *Marine Ecology Progress Series*, 112: 107-117.

Maxomovich, S.A.; Sukhotin, A.A. & Minichev, Y.S. (1996). Long-term dynamics of blue mussel (*Mytilus edulis L.*) culture settlements (the White Sea). *Aquaculture*, 147: 191:204.

McDonald, J.H.; Seed, R. & Koehn, R.K. (1991). Allozyme and morphometric characters of three species of *Mytilus* in the northern and southern hemispheres. *Marine Biology*, 111: 323-335.

McDonald, N.J.; Davies, M.H.; Zundel, A.K.; Howlett, J.D.; Demirbilek, Z.; Gailani, J.Z.; Lackey, T.C. & Smith, J. (2006). PTM: particle tracking model. Report 1: Model theory, implementation, and example applications. Technical Report ERDC/CHL TR-06-20, US Army Corps of Engineers.

McKay, W.A. & Pattenden, N.J. (1993). The behaviour of plutonium and americium in the shoreline waters of the irish Sea: a review of harwell studies in the 1990s. *Journal of Environmental Radioactivity*, 18(2): 99-132.

McGrath, D.; King, P.A. & Gosling, E.M. (1988). Evidence for the direct settlement of *Mytilus edulis* larvae on adult mussel beds. *Marine Ecology Progress Series*, 47: 103-106.

McQuaid, C.D. (1996). Biology of the gastropod family Littorinidae. I. Evolutionary aspects. *Oceanography Marine Biology Annual Review*, 34: 233-262.

McQuaid, C.D. & Philips, T.E. (2000). Limited wind-driven dispersal of intertidal mussel larvae: in situ evidence from the plankton and the spread of the invasive species *Mytilus Galloprovincialis* in South Africa. *Marine Ecology Progress Series*, 201: 211-220.

McShane, P.E.; Black, K.P. & Smith, M.G. (1988). Recruitment processes in *Haliotis rubra* (Mollusca: Gastropada) and regional hydrodynamics in southeastern Australia imply localized dispersal of larvae. *Journal of Experimental Marine Biology and Ecology*, 124: 175-203.

Meire, P.M. (1993). The impact of bird predation on marine and estuarine bivalve populations: a selective review of patterns and underlying causes. *Bivalve Filter Feeders*, 197-243.

Metaxas, A. (2001). Behaviour in flow: perspectives on the distribution and dispersion of meroplanktonic larvae in the water column. *Canadian Journal of Fisheries and Aquatic Sciences*, 58: 86-98.

Morello, S.L. & Yund, P.O. (2016). Response of competent blue mussel (*Mytilus edulis*) larvae to positive and negative cues. *Journal of Experimental Marine Biology and Ecology*, 480: 8-16.

Moreno Navas, J.; Telfer, T.C. & Ross, L.G. (2011). Application of 3D hydrodynamic and particles tracking models for better environmental management of finish culture. *Continental Shelf Research*, 31: 675-684.

Myrand, B.; Guderley, H. & Himmelman, J.H. (2000). Reproduction and summer mortality of blue mussel *Mytilus edulis* in the Magdalen Islands, southern Gulf of St. Lawrence. *Marine Ecology Progress Series*, 197: 193-207.

Nanninga, G.B. & Berumen, M.L. (2014). The role of individual variation in marine larval dispersal. *Frontiers in marine Science*, 1(71): 1-17.

Neil, C.; Cunningham, A.; McKee, D. & Polton, J.A. (2012). Remote sensing of seasonal stratification dynamics in the southern Irish Sea. *Remote Sensing of Environment*, 127: 288-297.

Neill, S.P. & Hashemi, M.R. (2018). Fundamentals of ocean renewable energy: generating electricity from the sea. Elsevier, London.

Newell, R.I.E.; Hilbish, T.J.; Koehn, R.K.; Newell, C.J. (1982). Temporal variation in the reproductive cycle of *Mytilus edulis L.* (bivalvia, mytilidae) from localities on the east coast of the United States. *The Biological Bulletin*, 162(3): 229-310.

Nicolle, A.; Dumas, F.; Foveau, A.; Foucher, E. & Thiebaut, E. (2013). Modelling larval dispersal of the king scallop (*Pecten maximus*) I nthe English Cahnnel: examples from the bay of Saint-Brieuc and the bay of Seine. *Ocean dynamics*, 63: 661-678.

Noonburg, E.G.; Chen, A.; Shima, J.S. & Swearer, S.E. (2015). Demographic heterogeneity and the dynamics of open populations. *Ecology*, 96(5): 1159-1165.

North, E.W.; Schlag, Z.; Hood, R.R.; Li, M.; Zhong, L.; Gross, T. & Kennedy, V.S. (2008). Vertical swimming behaviour influence the dispersal of simulated oyster larvae in a coupled particle-tracking and hydrodynamic model of Chesapeake Bay. *Marine Ecology Progress Series*, 359: 99-115.

Nystrom, E.; Rehmann, C. & Oberg, K.A. (2007). Evaluation of mean velocity and turbulence measurements with ADCPs. *Journal of Hydraulic Engineering*, 33(12): 1310-1318.

Okubo, A. (1971). Oceanic diffusion diagrams. *Deep Sea Research and Oceanographic Abstracts*, 18(8): 789-802.

Ompi, M. (2010). Settlement behaviour and size of mussel larvae from the family mytilidae *Brachidontes erosus* (Lamarck, 1819), *Brachidontes rostratus* (Dunker, 1857), *Trichomya hirsutus* (Lamarck, 1819), and *Mytilus galloprovincialis* Lamarck, 1819. *Journal of Coastal Development*, 13(3): 215-227.

O'Neill, S.M.; Sutterlin, A.M. & Aggett, D. (1983). The effect of size-selective feeding by starfish (*Asterias vulgaris*) on the production of mussels (*Mytilus edulis*) cultured on nets. *Aquaculture*, 35: 211-220.

O'Sullivan, D.; Lordan, C.; Doyle, J.; Berry, A. & Lyons, K. (2015). Metapopulation connectivity via larval transport of the Norway lobster *Nephrops norvegicus* in waters around Ireland: a modelled approach. *Marine Ecology Progress Series*, 534: 95-106.

Osuna, P. & Wolf, J. (2005). A numerical study on the effect of wave-current interaction processes in the hydrodynamics of the Irish Sea. In proceeding of the 5th International Conference on Ocean wave measurement and analysis: WAVES2005, 3rd to 7th of July, Madrid, Spain.

Paine, R.T. (1974). Intertidal community structure. *Oecologia*, 15(2): 93-120.

Palatella, L.; Bignami, F.; Falcini, F.; Lacorata, G.; Lanotte, A.S. & Santoleri, R. (2014). Lagrangian simulations and interannual variability of anchovy egg and larva dispersal in the Sicily Channel. *Journal of Geophysical Research: Oceans*, 119(2): 1306-1323.

Paris, C.B.; Helgers, J.; van Sebille, E. & Srinivasan, A. (2013). Connectivity modelling system: A probabilistic modelling tool for the multi-scale tracking of biotic and abiotic variability in the ocean. *Environmental Modelling & Software*, 42: 47-54.

Parker-Humphreys, (2004). Distribution and relative abundance of demersal fishes from beam trawl surveys in the irish Sea (ICES division VIIa) 1993-2001. Centre for Environment, Fisheries and Aquaculture Science, Sciences Series Technical Report, number 120.

Pechenik, J.A.; Eyster, L.S.; Widdos, J. & Bayne, B.L. (1990). The influence of food concentration and temperature on growth and morphological differenciation of blue mussel *Mytilus edulis L.* larvae. *Journal of Experimental Marine Biology and Ecology*, 136: 47-64.

Pernet, F.; Tremblay, R. & Bourget, E. (2003). Settlement success, spatial pattern and behaviour of mussel larvae *Mytilus* spp. In experimental 'down-welling' systems of varying velocity and turbulence. *Marine Ecology Progress Series*, 260: 125-140.

Petersen, J.H. (1984). Larval settlement behaviour in competing species*: Mytilus californianus Conrad* and *M. edulis L.*. *Journal of Experimental Marine Biology and Ecology*, 82: 147-159.

Petraitis, P.S. (1995). The role of growth in maintaining spatial dominance by mussels (*Mytilus edulis*). *Ecology*, 76: 1337-1346.

Phelps, J.J.C.; Polton, J.A.; Souza, A. J. & Robinson, L.A. (2015). Behaviour influences larval dispersal in shelf sea gyres: *Nephrops norvegicus* in the Irish Sea. *Marine Ecology Progress Series*, 518: 177-191.

Piano, M.; Ward, S.; Robins, P.; Neill, S.; Lewis, M.; Davies, A.; Powell, B.; Owen, A.W. & Hashemi, R. (2015). Characterizing the tidal energy resource of the west Anglesey demonstration zone (UK), using TELEMAC-2D and field observations. In: Moulinec, Charles; Emerson, David (Hg.): Proceedings of the XXII TELEMAC-MASCARET Technical User Conference October 15-16, 2042. Warrington: STFC Daresbury Laboratory. S. 195-203.

Piano, M.; Neill, S.P.; Lewis, M.J., Robins, P.E., Hashemi, M.R., Davies, A.G., Ward, S.L. & Roberts, M.J. (2017). Tidal stream resource assessment uncertainty due to flow asymmetry and turbine yaw misalignment. *Renewable Energy*, 114(B): 1363-1375.

Pineda, J. (2000). Linking larval settlement to larval transport: assumptions, potentials and pitfalls. *Oceanography of the Eastern Pacific*, 1: 84-105.

Pineda, J.; Hare, J.A. & Sponangule, S. (2007). Larval transport and dispersal in the coastal ocean and consequences for population connectivity. *Oceanography*, 20(3): 22-39.

Plag, H.P. & Tsimplis (1999). Temporal variability of the seasonal sea-level cycle in the North Sea and the Baltic Sea in relation to climate variability. *Global Planet*, 20: 173-203.

Porri, F.; McQuaid, C.D.; & Radloff, S. (2006). Spatio-temporal variability of larval abundance and settlement of *Perna perna*: differential delivery of mussels. *Marine Ecology Progress Series*, 315: 141-150.

Porri, F.; Jordaan, T. & McQuaid, C.D. (2008). Does cannibalism of larvae by adults affect settlement and connectivity of mussel populations? *Estuarine, Coastal and Shelf Science*, 79: 687-693.

Power, J.H. (1996). Simulations of the effect of advective-diffusive processes on observations of plankton abundance and population rates. *Journal of Plankton Research*, 18(10): 1881-1896.

Prandle, D. (1982). The vertical structure of tidal currents and other oscillatory flows. *Continental Shelf Research*, 1(2): 191-207.

Prandle, D. (1987). The fine structure of nearshore tidal and residual circulations revealed by H.F. radar surface current measurements. *Journal of Physical Oceanography*, 17: 231-245.

Prandle, D. (1991). A new view of near-shore dynamics based on observations from HF radar. *Progress in Oceanography*, 27: 403-438.

Prandle, D. (1997). Tidal currents in shelf seas – their nature and impacts. *Progress in Oceanography*, 40: 245-261.

Prandle, D. & Matthews J. (1990). The dynamics of nearshore surface currents generated by tides, wind and horizontal density gradients. *Continental Shelf Research*, 10(7): 665-681.

Proctor, R.; Flather, R.A. & Elliott, A.J. (1994). Modelling tides and surface drift in the Arabian Gulf – applications to the gulf oil spill. *Continental Shelf Research*, 14(5): 531-545.

Pugh, D.T. (1996). Tides, surges and mean sea-level (reprinted with corrections), John Willey, Chichester, UK.

Putman, N.F. & He, R. (2013). Tracking the long-distance dispersal of marine organisms: sensitivity to ocean model resolution. *Journal of the Royal Society Interface*, 10(81).

Pusack, (2014). Spatial and temporal patterns of larval dispersal in a coral-reef fish metapopulation: evidence of variable reproductive success. *Molecular Ecology*, 23(14): 3396-3408.

Qin, X.; Sebille, E. & Gupta, A.S. (2014). Quantification of errors induced by temporal resolution on lagrangian particles in an eddy-resolving model. *Ocean Modelling*, 76: 20-30.

Raby, D.; Lagadeuc, Y.; Dodson, J.J. & Mingelbier, M. (1994). Relationship between feeding and vertical distribution of bivalve larvae in stratified and mixed waters. *Marine Ecology Progress Series*, 103(3): 275-284.

Reaugh, K.E. (2006). Recruitment patterns and processes and the connectivity of rocky shores in southern Africa. University of Cape Town.

Reusch, T.B.H. & Chapman, A.R.O. (1997). Persistence and space occupancy by subtidal blue mussel patches. *Ecological Monographs*. 67: 65-87.

Rhors, J.; Christensen, K.H.; Vikebo, F.; Sundby, S.; Saetra, O. & Brostrom, G. (2014). Wave induced transport and vertical mixing of pelagic eggs and larvae. *Limnology and Oceanography*, 59(4): 1213-1227.

Richards, M.G.; Huxham, M. & Bryant, A. (1999). Predation: a causal mechanism for variability in intertidal bivalve populations. *Journal of Experimental Marin Biology and Ecology*. 241(2): 159-177.

Riginos, C. & Cunningham, C.W. (2005). Local adaptation and species segregation in two mussel (*Mytilus edulis* x *Mytilus trossulus*) hybrid zones. *Molecular Ecology*, 14(2): 381-400.

Rippeth, T.R.; Williams, E. & Simpson, J.H. (2001). Reynolds stress and turbulent energy production in a tidal channel. *Journal of Physical Oceanography*, 32: 1242-1251.

Robins, P.E.; Neill, S. & Gimenez Noya, J. (2012). A numerical study of marine larval dispersal in the presence of an axial convergent front. *Esturaine, Coastal and Shelf Science*, 100: 172-185.

Robins, P.E.; Neill, S.P.; Gimenez, L.; Jenkins, S.R. & Malham, S.K. (2013). Physical and biological controls on larval dispersal and connectivity in a highly energetic shelf sea. *Limnology and Oceanography*, 58(2): 505-524.

Robins, P.E.; Lewis, M.J.; Freer, J.; Cooper, D.M.; Skinner, C.J. & Coulthard, T.J. (2018). Improving estuary models by reducing uncertainties associated with river flows. *Estuarine, Coastal and Shelf Science*, 207: 63-73.

Robins, P.E.; Farkas, K.; Cooper, D.; Malham, S. & Jones, D.L. (2019). Viral dispersal in the coastal zone: a method to quantify water quality risk. *Environment International*, 126:430-442.

Ross, O.N. & Sharples, J. (2004). Recipe for 1-D lagrangian particle tracking models in space-varying diffusivity. *Limnology and Oceanography*, 2(9): 289-302.

Rodhouse, P.G.; Roden, C.M.; Burnell, G.M.; Hensey, M.P.; McMahon, T.; Ottway, B. & Ryan, T.H. (1984). Food ressourse, gametogenesis and growth of *Mytilus edulis* on the shore and in suspended culture: Killary harbour, Ireland. *Journal of the marine biology Association of the United Kingdom* 64: 513-529.

Rowe, M.D.; Anerson, E.J.; Wynne, T.T.; Stumpf, R.P.; Fanslow, D.L.; Kijanka, K., Vanderploeg, H.A.; Strickler, J.R. & Davis, W. (2016). Vertical distribution of buoyant Microcystis blooms in a lagrangian particle tracking model for short-term forecasts in Lake Erie. *Journal of Geophysical Research: Oceans*, 121: 5296-5314.

Salomon, J.C. (1990). Role of instantaneous and long-term water movements on the recruitment and life of benthic fauna in the English Channel. *La mer*, 28: 211-217.

Sayol, J.M.; Orfila, A.; Simarro, G.; Conti, D.; Renault, L. & Molcard, A. (2014). A lagrangian model for tracking surface spills and SaR operations in the ocean. *Environmental Modelling & Software*, 52: 74-82.

Scheltema, R.S. (1986). On dispersal and planktonic larvae of benthic invertebrates: an eclectic overview and summary of problems. *Bulletin of Marine Science*, 39(2): 290-32.

Schiavina, M.; Marino, I.A.M.; Zane, L. & Melia, P. (2014). Matching oceanography and genetics at the basin scale. Seascape connectivity of the Mediterranean shore crap on the Adriatic Sea. *Molecular Ecology*, 23: 5496-5507.

Sebille, E.; Griffies, S.M.; Abernathey, A.; Adams, T.P.; Berloff, P.; Biastoc, A.;Blanke, B.; Chassignet, E.P.; Cheng, Y.; Cotter, C.J.; Deleersnijder, E.; Doos, K.; Drake, H.F.; Drijfhout, S.; Gary, S.F.; Heemink, A.W.; Kjellson, J.; Koszalka, I.M.; Lange, M.; Lique, C.; MacGilchrist, G.A.; Marsh, R.; Adame,C.G.M.; McAdam, R.; Nencioli, F.; Paris, C.B.; Piggott, M.D.; Polton, J.A.; Ruhs, S.; Shah, S.H.A.M.; Thomas, M.D.; Wang, J.; Wolfram. P.J.; Zanna, L. & Zika, J.D. (2018). Lagrangian ocean analysis: fundamentals and practices. *Ocean Modelling*, 121: 49-75.

Seed, R. (1969). The ecology of *Mytilus edulis L.* (lamellibranchiate) on exposed rocky shore. *Oecologia*, 3: 277-316.

Seed, R. (1976). Ecology. In: Bayne, B.L., Ed., Marine Mussels: Their Ecology and Physiology, Cambridge University Press, Cambridge, 13-65.

Seed, R. & Brown, R.A. (1977). A comparison of the reproductive cycles of *Modiolus modiolus (L.), Cerastoderma (=Cardium) edule (L.)* and *Mytilus edulis L.* in Strangford Lough, Northern Ireland. *Oecologia*, 30: 173-188.

Seed, R. & Suchanek, T. (1992). Population and community ecology of *Mytilus*. In: Developments in aquaculture and fisheries science: The mussel *Mytilus*: ecology, physiology, genetics and culture. *Elsavier Science*, 87-169.

Sheaves, M. (2009). Consequences of ecological connectivity: the coastal ecosystem mosaic. *Marine Ecological Progress Series*, 391: 107-115.

Sheltema, R.S. (1986). On dispersal and planktonic larvae of benthic invertebrates: an eclectic overview and summary of problems. *Bulletin of Marine Science*, 39(2): 290-322.

Shima, J.S.; Noonburg, E.G. & Swearer, S.E. (2015). Consequences of variable larval dispersal pathways and resulting phenotypic mistures to the dynamics of marine metapopulations. *Biology Letters*, 11, 20140778.

Schouten, M.W.; Matano, R.P. & Scrub, T.P. (2005). A description of the seasonal cycle of the equatorial Atlantic from altimeter data, *Deep Sea Research*, 52: 477-493.

Siegfried, W.R.; Hockey, P.A.R. & Branch, G.M. (1994). The exploitation of intertidal and subtidal biotic resources of rocky shores in Chile and South Africa – an overview. In: Siegfried R.S. (ed.) Rocky shores: exploitation In Chile and South Africa. Springer-Verlag, Berlin, pp. 1-13.

Simons, R.D.; Siegel, D.A. & Brown, K.S. (2013). Model sensitivity and robustness in the estimation of larval transport: a study of particles tracking parameters. *Journal of Marine Systems*, 119-120: 19-29.

Simpson, J.H. (1971). Density stratification and microstructure in the western Irish Sea. *Deep Sea Research and Oceanographic Abstracts*, 18(3): 309-319.

Simpson, J.H.; Forbes, A.M.G. & Gould, W.J. (1971). Electromagnetic Observations of water flow in the Menai Straits. *Geophysical Journal of the Royal Astronomical Society*, 24: 245-253.

Simpson, J.H.; Allen, C.M. & Morris, N.C.G. (1978). Fronts on the continental shelf. *Journal of Geophysical Research*, 83: 4607-4614.

Simpson, J.H. & Bowers, D. (1981). Models of stratification and frontal movement in shelf seas. *Deep Sea Research*, 28(A): 727-738.

Simpson, J.H. & Nunes, R.A. (1981). The tidal intrusion front: an estuarine convergence zone. *Estuarine, Coastal and Shelf Science*, 13(3): 257-266.

Simpson, J.H.; Berx, B.; Gascoigne, J. & Saurel, C. (2007). The interaction of tidal advection, diffusion and mussel filtration in a tidal channel. *Journal of Marine Systems*, 68(3): 556-568.

Smaal, A.C. (2002). European mussel cultivation along the Atlantic coast: production status, problems and perspectives. In: Vadstein O., Olsen Y. (eds) Sustainable Increase of Marine Harvesting: Fundamental Mechanisms and New Concepts. Developments in Hydrobiology, vol. 167. Springer, Dordrecht.

Snodden, L.M. & Roberts D. (1997). Reproductive patterns and tidal effects on spat settlement of *Mytilus edulis* populations in Dundrum bay, Northern Ireland. *Journal of the marine biology Association of the United Kingdom* 77: 229-243.

Soulsby, R. L.; Hamm, L.; Klopman, G.; Myrhaug, D.; Simons, R. R. & Thomas, G. P. (1993). Wave-current interaction within and outside the bottom boundary layer. *Coastal Engineering*, 21: 41-69.

Sprung, M. (1983). Reproduction and fecundity of the mussel *Mytilus edulis* at Helgoland (North Sea). *Helgolander Meeresunters*, 36: 243-255.

Sprung, M. (1984). Physiological energetics of musse lalrvae (*Mytilus edulis*). I. Shell growth and biomass. *Marine Ecology Progress Series*, 17: 283-293.

Suchanek, T.H. (1978). The ecology of *Mytilus edulis L.* in exposed rocky intertidal communities. *Journal of Experimental Marine Biology and Ecology*, 31: 105-120.

Suchanek, T.H. (1985). Mussels and their role structuring rocky shore communities. In: The ecology of rocky coasts (ed. P.G. Moore and R. Seed), pp. 70-96. London: Hodder & Stoughton.

Sundelof, A. & Jonsson, P.R. (2011). Larval dispersal and vertical migration behaviour – a simulation study for short dispersal times. *Marine Ecology*, 33(2): 183-193.

Swearer, S.E.; Shima, J.S.; Hellberg, M.E.; Thorrold, S.R.; Jones, G.P.; Robertson, D.R.; Morgan, S.G.; Selkoe, K.A.; Ruiz, G.M. & Warner, R.R. (2002). Evidence of self-recruitment in demersal marine populations. *Bulletin of marine Science*, 70: 251-271.

Swearer, S.E.; Treml, E.A. & Shima, J.S. (2019). A review of biophysical models of marine larval dispersal. Marine biology, an annual review, 57: 325-357.

TELEMAC-MASCARET, 1987, accessed 1 January 2020, http://www.opentelemac.org/

Thiel, M. & Ullrich, N. (2002). Hard rock versus soft bottom: the fauna associated with intertidal mussel beds on hard bottoms along the coast of Chile, and considerations on the functional role of the mussel beds. *Helgoland Marine Research*, 56: 21-30.

Thorarinsdóttir, G.G. & Gunnarsson, K. (2003). Reproductive cycles of *Mytilus edulis L.* on the west and east coast of Iceland. *Polar Research*, 22: 217-223.

Thorarinsdóttir, G.G.; Gudfinnsson, H.G.; Egilsdóttir, S. & Pálsson, J.O. (2013). The gametogenic cycle and spawning in *Mytilus edulis* in two fjords in north-western Iceland. *Journal of the marine biology Association of the United Kingdom*, 93: 1609-1615.

Thorson, G. (1950). Reproductive and larval ecology of marine bottom invertebrates. *Biological Reviews*, 25(1): 1-45.

Toro, J.E.; Thompson, R.J. & Innes, D.J. (2002). Reproductive isolation and reproductive output in two sympatric mussel species (*Mytilus edulis*, *Mytilus trossulus*) and their hybrids from Newfoundland. *Marine Biology*, 141: 897-909.

Troost, K.; Veldhuizen, R.; Stamhuis, E.J. & Wolff, W.J. (2008). Can bivalve veligers escape feeding currents of adult bivalves? *Journal of Experimental marine Biology and Ecology*, 358(2): 185-196.

Tsimplis, M.N. & Woodworth, P.L. (1994). The global distribution of the seasonal sea level cycle calculated from coastal tide gauge data. *Journal of Geophysical Research*, 99: 16,031-16,039.

Tweddle, J.F.; Simpson, J.H. & Janzen, C.D. (2005). Physical controls of food supply to benthic filter feeders in the menai Strait, UK. *Marine Ecology Progress Series*, 289: 79-88.

Vainola, R. & Streklov, P. (2011). *Mytilus trossulus* in northern Europe. *Marine Biology*, 158(4): 817-833.

Valdivieso Da Costa, M. & Blanke, B. (2004). Lagrangian methods for flow climatologies and trajectory error assessment. *Ocean Modelling*, 6(3): 335-358.

Van der Molen, J.; Rogers, S.I., Ellis, J.R., Fox, C.J. & McCloghrie, P. (2007). Dispersal patterns of the eggs and larvae of spring-spawning fish in the Irish Sea, UK. *Journal of Sea Research*, 58(4): 313-330.

Van der Schatte, A.O.; Jones, L.; Le Vay, L.; Christie. M.; Wilson, J. & Malham, S.K. (2018). A global review of the ecosystem services provided by bivalve aquaculture. *Reviews in Aquaculture*, 1-23.

Van der Veer, H.W.; Ruardij, P.; Van den Berg, A.J. & Ridderinkhof, H. (1998). Impact of interannual variability in hydrodynamic circulation on egg and larval transport of plaice *Pleuronectes platessa L.* in the southern North Sea. *Journal of Sea Research*, 39(1): 29-40

Van de Koppel, J.; Rietkerk, M.; Dankers, N. & Herman, P.M.J. (2005). Scale-dependent feedback and regular spatial patterns in young mussel beds. *American Naturalist*, 165: 66-77.

Villaret, C.; Hervouet, J.M.; Kopmann, R.; Merkel, U. & Davies, A.G. (2013). Morphodynamic modelling using the TELEMAC finite-element system. *Computers & Geosciences*, 53: 105-113.

Vincent, M.A.; Atkins, S.M.; Lumb, C.M.; Golding, N.; Lieberknecht, L.M. & Webster, M. (2004). Marine nature conservation and sustainable development - the Irish Sea Pilot., Report to Defra by the Joint Nature Conservation Committee, Peter-borough.

Walters R.A. (2005). Coastal ocean models: two useful finite element methods. *Continental Shelf Research*, 25: 775-793.

Walters, R.A. (2006). Design considerations for a finite element coastal ocean model. *Ocean Modelling*, 15:90-100.

Ward, S.L.; Green, J.A.M. & Pelling, H.E. (2012). Tides, sea-level rise and tidal power extraction o nthe European shelf. *Ocean Dynamics*: 62(8): 1153-1167.

Weber, J.E. (1981). Ekman currents and mixing due to surface gravity waves. *Journal of Physical Oceanography*, 11: 1431-1435.

Weber, J.E. (1983). Steady wind and wave induced currents in the open ocean. *Journal of Physical Oceanography*, 13: 524-530.

Weidberg, N.; Porri, F.; Von der Meden, C.E.O.; Jackson, J.M.; Goschen, W. & McQuaid, C.D. (2015). Mechanisms of nearshore retention and offshore export of mussel larvae over the Alghus Bank. *Journal of Marine Systems*, 144: 70-80.

Widdows, J.; Fieth, P. & Worrall, C.M. (1979). Relationships between seston, available food and feeding activity in the common mussel *Mytilus edulis*. *Marine Biology*, 50(3): 195-207.

Widdows, J.; Pope, N.D.; Brinsley, M.D.; Gascoigne, J. & Kaiser, M.J. (2009). Influnence of self-organised structures on near-bed hydrodynamics and sediment dynamocs within a mussel (Mytilus edulis) bed in the Menai Strait. *Journal of Experimental Marine Biology and Ecology*, 379: 92-100.

Wiebe, P.H. & Benfield, M.C. (2003). From the Hensen net toward four-dimensional biological oceanography. *Progress in Oceanography*, 56(1): 7-136.

Wilson, J.H. & Seed, R. (1974). Reproduction in Mytilus edulis L. (Mollusca: bivalvia) in Carlingford Lough, Northern Ireland. Irish Fisheries Investigations Series B., 15.

Wing, S.R., Botsford, L.W. & Quinn, J.F. (1998a). The impact of coastal circulation on the spatial distribution of invertebrate recruitment, with implications for management. In: Jamieson G.S., Campbell A. (eds). Proceedings of the North Pacific symposium on invertebrate stock assessment and management. Canadian Special Publications in Fisheries and Aquatic Sciences, vol. 125. National Research Council of Canada, Ottawa, Ontario, Canada.

Wing, S.R.; Botsford, L.W.; Ralston, S.V. & Largier, J.L. (1998b). Meroplanktonic distribution and circulation in a coastal retention zone of the northern California upwelling system. *Limnology and Oceanography*, 43: 1710-1721.

Witman, J.D.; Genovese, S.J.; Bruno, J.F., McLaughlin, J.W. & Pavlin, B.I. (2003). Massive prey recruitment and the control of rocky subtidal communities on large spatial scales. *Ecological Monographs*, 73(3): 441-462.

Wu, J. (1983). Sea-surface drift currents induced by wind and waves. *Journal of Physical Oceanography*, 13: 1441-1451.

Xing, J. & Davies, A.M. (2001). A three-dimensional baroclinic model of the Irish Sea: formation of the thermal fronts and associated circulation. *Journal of Physical Oceanography*, 31: 94-114.

Xu, J; Qi, H.; Fang, X.; Lu, L.; Ge, W.; Wang, X.; Xu, M.; Chen, F.; He, X. & Li, J. (2011). Quasi-real-time simulation of rotating drum using discrete element method with parallel GPU computing. *Particuology*, 9: 446-450.

Yang, Z. & Khangaonkar, T. (2009). Modeling tidal circulation and stratification in Skagit river estuary using an unstructured grid ocean model. *Ocean Modelling*, 28: 34-49.

Young, R.T. (1946). Spawning and settling season of the mussel, *Mytilus californicus*. *Ecology*, 27: 354-363.

Young, C.M. (1983). Functional significance of larval behaviour in an intertidal population of the ascidian *Pyura haustor*. *American Zoologist*, 30(2): 131-140.

Appendix

Appendix A: Tidal range in the Irish Sea.

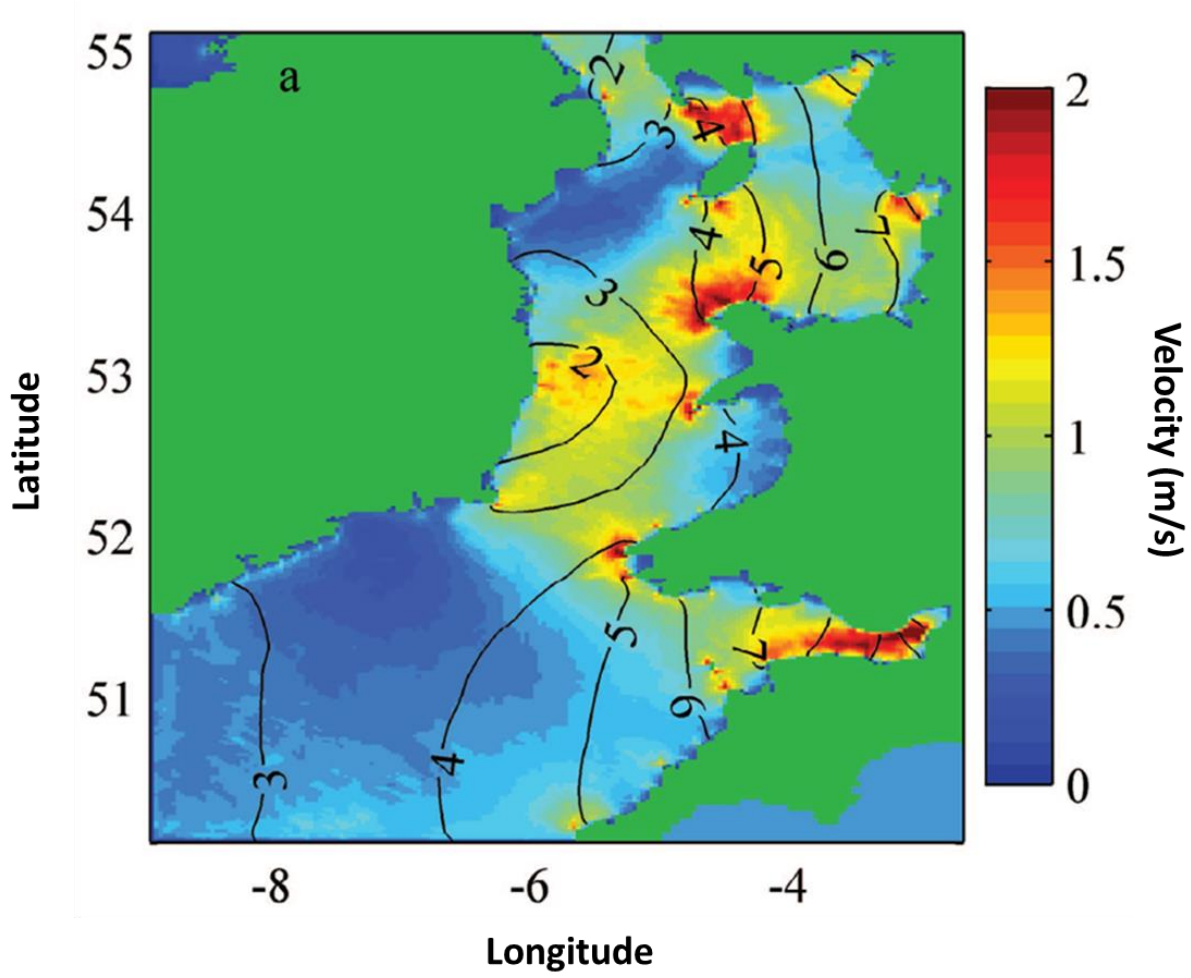

Figure A.1: Map showing the cotidal contours of maximum tidal range (m), superimposed on coloured contours of maximum depth-averaged scalar velocity (m/s) in the Irish Sea from Robins *et al.* (2013).

Appendix B: Example of steering file used to create hydrodynamic model using TELEMAC-2D of the Irish Sea.

```
/*************************************************************
*******/
/                  TELEMAC STEERING FILE                      /
/                                                             /
/                                                             /
/*************************************************************
*******/
/*************************************************************
*******/
/  THIS IS THE STEERING FILE FOR TELEMAC, THE TIDE MODULE USED
TO    /
/   CALCULATE TIDAL BEHAVIOUR IN TELEMAC 2D OR 3D. BELOW ARE
/
/  VARIOUS PARAMETERS AND OPTIONS THAT MAY BE CHANGED AND CHOSEN
/
/  BY THE USER.                                               /
/*************************************************************
*******/

/RELEASE = V7P2r0(use command prompt telemac*d -c sl6 -s
'casfile' or -c sl6mpi for parallel mode)
/
/-------------------------------------------------------------
-------/
/    FILES
/-------------------------------------------------------------
-------/
CHECKING THE MESH          = TRUE
GEOMETRY FILE              = Irish_sea.slf
FORTRAN FILE               = forcing.f
BOUNDARY CONDITIONS FILE   = Irish_Sea.cli
RESULTS FILE               = March_2018.slf
PARALLEL PROCESSORS        = 8
COMPUTATION CONTINUED     = YES
PREVIOUS COMPUTATION FILE = 'February_2018.slf'
/INITIAL TIME SET TO ZERO  = TRUE
/
/---------------------------------------------
/  GENERAL INFORMATIONS - OUTPUTS
/---------------------------------------------
/
TITLE                           = 'IrishSea'
VARIABLES FOR GRAPHIC PRINTOUTS  = 'U,V,S,H'
GRAPHIC PRINTOUT PERIOD          = 900
/NUMBER OF FIRST TIME STEP FOR GRAPHIC PRINTOUTS = 1330200
LISTING PRINTOUT PERIOD          = 900
VALIDATION                       = NO
TIME STEP                        = 2
NUMBER OF TIME STEPS             = 1339200
/VARIABLE TIME-STEP            = YES
```

```
/DESIRED COURANT NUMBER       = 1
MASS-BALANCE                     = YES
INFORMATION ABOUT SOLVER         = YES
/-------------------------------------------
/  COORDINATES
/-------------------------------------------
SPHERICAL COORDINATES          = NO
SPATIAL PROJECTION TYPE        = 2
GEOGRAPHIC SYSTEM              = 2
ZONE NUMBER IN GEOGRAPHIC SYSTEM  = 30
/
/-------------------------------------------
/  INITIAL CONDITIONS
/-------------------------------------------
/
INITIAL CONDITIONS     = 'CONSTANT ELEVATION'
INITIAL ELEVATION      = 0.0
/
/-------------------------------------------
/  BOUNDARY CONDITIONS
/-------------------------------------------
/
OPTION FOR TIDAL BOUNDARY CONDITIONS    = 1;1
TIDAL DATA BASE                      = 2
BINARY DATABASE 1 FOR TIDE              =
'/home/jonathan.demmer/tpxo/h_tpxo7.2'
BINARY DATABASE 2 FOR TIDE              =
'/home/jonathan.demmer/tpxo/u_tpxo7.2'
MINOR CONSTITUENTS INFERENCE        = YES
ORIGINAL DATE OF TIME               = 2015;01;01
ORIGINAL HOUR OF TIME                   = 00;00;00
PRESCRIBED ELEVATIONS               = 2.;2
/
/-------------------------------------------
/  PHYSICAL PARAMETERS
/-------------------------------------------
/
LAW OF BOTTOM FRICTION          = 5
FRICTION COEFFICIENT            = 0.1
TURBULENCE MODEL                = 1
VELOCITY DIFFUSIVITY            = 0.2
CORIOLIS                       = YES
CORIOLIS COEFFICIENT              = 1.15E-4
/
/-------------------------------------------
/  NUMERICAL PARAMETERS
/-------------------------------------------
/
TIDAL FLATS                           = YES
OPTION FOR THE TREATMENT OF TIDAL FLATS = 1
H CLIPPING                                = NO
MINIMUM VALUE OF DEPTH               = 0.05
TREATMENT OF NEGATIVE DEPTHS         = 1
THRESHOLD FOR NEGATIVE DEPTHS        = -0.01
```

```
TYPE OF ADVECTION                    = 1;5
TREATMENT OF THE LINEAR SYSTEM           = 2
FREE SURFACE GRADIENT COMPATIBILITY      = 0.9
SUPG OPTION                          = 1;2
SOLVER ACCURACY                      = 1.E-3
DISCRETIZATIONS IN SPACE             = 12 ; 11
PROPAGATION                          = YES
SOLVER                               = 3
PRECONDITIONING                      = 2
IMPLICITATION FOR DEPTH              = 0.6
IMPLICITATION FOR VELOCITY           = 0.6
BOTTOM SMOOTHINGS                       = 1
MAXIMUM NUMBER OF ITERATIONS FOR SOLVER = 300
/
&FIN
```

Appendix C: Custom Matlab script to create a Particle Tracking Model (PTM).

```
close all
clear all
clc

% Assign the path to your working directory:
cd ('D:\simulation_year_2018\');

% Add path to TelemacTools functions:
addpath ('C:\Matlab_download\TelemacTools\');

% Name the path and file of your TELEMAC results file:
% Grid Mask created to avoid particles on land:
FILE0 = ('D:\simulation_year_2018\GRID_MASK_new.slf');
% Hydrodynamic 2D model from TELEMAC:
FILE1 = ('D:\simulation_year_2018\March_2018.slf');
% Name of velocity files interpolated:
file = 'VELOCITY20181_####.mat';
% Wind Data from CEDA:
M = xlsread('Valley_2014');

% Read in the telemac header information:
m = telheadr (FILE0);

% Number of time step:
N = 2160;

% Read the TELEMAC time step information:
m = telstepr (m,1);

% Limit of the domain of study in UTM:
xmin = 2.6e5;
xmax = 5.3e5;
ymin = 5.782e6;
ymax = 6.094e6;

% Scale of the orthogonal mesh:
dx = 50; dy = 50;
xq = xmin: dx : xmax;
yq = ymin: dy : ymax;

% Distinguish the sea from the land:
MASK = griddata(m.XYZ(:,1),m.XYZ(:,2)',m.RESULT(:,1),xq,yq');
MASK(isnan(MASK))=0;
MASK(MASK>=0.5)=1;
MASK(MASK<0.5)=0;

% Plot the primary mesh:
clf;
pcolor(xq,yq,MASK); shading flat;
colorbar

%% Interpolation of velocity from unstructured .slf file to structured .mat
file:

m = telheadr (FILE1);
m = telstepr (m,1);
file = 'VELOCITY20181_####.mat';
for it = 1:N
```

```
    m = telstepr(m,it);
    file(15:18)=sprintf('%04.0f',it);
    U = griddata(m.XYZ(:,1),m.XYZ(:,2)',m.RESULT(:,1),xq,yq');
    V = griddata(m.XYZ(:,1),m.XYZ(:,2)',m.RESULT(:,2),xq,yq');
    H = griddata(m.XYZ(:,1),m.XYZ(:,2)',m.RESULT(:,3),xq,yq');
    save(file,'U','V','H');
end

%% PTM

m = telheadr (FILE1);
m = telstepr (m,1);

% Initialise value for linear temporal interpolation:
DT1=1800; % Telemac time step (seconds)
DT2=300;  % PTM time step desired (seconds)
DTN=DT1/DT2;
DTinc=DT2/DT1;

% To start the PTM at desired timestep (= first time step):
delay = 215;

% Number of particles:
np = 70000;

% Wind file:
Uwind = M(:,2);
Vwind = M(:,3);

% Initialise larvae position vectors:
clear x; x = zeros(N+1,np);
clear y; y = zeros(N+1,np);

% Initial particle position, assign random release from a fixed point:
for i=1:np
    if i<= 7000 % Position Mostyn
    x(1,i) = 4.836792e5 + rand*1000*cos(2*pi*rand);
    y(1,i) = 5.909780e6 + rand*1000*sin(2*pi*rand);
    elseif i<= 14000 % Position Llandudno
    x(1,i) = 4.45250e5 + rand*500*cos(2*pi*rand);
    y(1,i) = 5.91e6 + rand*500*sin(2*pi*rand);
    elseif i<= 21000 % Position Rhyl Flat
    x(1,i) = 4.56566e5 + rand*1000*cos(2*pi*rand);
    y(1,i) = 5.915076e6 + rand*1000*sin(2*pi*rand);
    elseif i<= 28000 % position Gwynt y mor
    x(1,i) = 4.61547e5 + rand*1000*cos(2*pi*rand);
    y(1,i) = 5.922264e6 + rand*1000*sin(2*pi*rand);
    elseif i<= 35000 % Position North Hoyle
    x(1,i) = 4.70160e5 + rand*1000*cos(2*pi*rand);
    y(1,i) = 5.918976e6 + rand*1000*sin(2*pi*rand);
    elseif i<= 42000 % Position Conwy
    x(1,i) = 4.42e5 + rand*500*cos(2*pi*rand);
    y(1,i) = 5.9056e6 + rand*500*sin(2*pi*rand);
    elseif i<= 49000 % Position Brynsiencyn
    x(1,i) = 4.15e5 + rand*300*cos(2*pi*rand);
    y(1,i) = 5.8908e6 + rand*300*sin(2*pi*rand);
    elseif i<= 56000 % Position Holyhead
    x(1,i) = 3.932e5 + rand*500*cos(2*pi*rand);
    y(1,i) = 5.908e6 + rand*500*sin(2*pi*rand);
    elseif i<= 63000 % Position Red Wharf Bay
    x(1,i) = 4.2e5 + rand*300*cos(2*pi*rand);
    y(1,i) = 5.907e6 + rand*300*sin(2*pi*rand);
    else  % Position Bangor
    x(1,i) = 4.245e5 + rand*200*cos(2*pi*rand);
```

```
    y(1,i) = 5.8993e6 + rand*200*sin(2*pi*rand);
    end
end

% Diffusivity mixing parameters:
K = 5;              % Horizontal diffusion coefficient
R =1.e0/sqrt(6.e0); % Radial diffusion


% Plot design:
clf
hold on;
h=patch('faces',m.IKLE,'vertices',m.XYZ,'FaceVertexCData',m.RESULT(:,3));
set(h,'FaceColor','flat','EdgeColor','none');
axis equal
axis tight
box on
xlabel('East (m)')
ylabel('North (m)')
axis([xmin xmax ymin ymax]);

% Plot at timestep = 0:
h1 = plot(x(1,:),y(1,:),'*r');
h2 = text(4.0e5,5.88e6,['Timestep = ',num2str(1)]);

%% Particle tracking model (PTM) loop:

% Velocity file at first time step::
clear U V H
file(15:18)=sprintf('%04.0f',delay);
load(file,'U','V','H'); U1=U; V1=V; H1=H;

% Wind velocity among U and V at first time step:
Uwind1 = M(delay,2);
Vwind1 = M(delay,3);

it = 0;

% Number of time step according to TELEMAC (2160 = 45 days)
for it1=1:N

    file(15:18)=sprintf('%04.0f',it1+delay);
    load(file,'U','V','H'); U2=U; V2=V; H2=H;

    Uwind2 = M((it1+delay),2);
    Vwind2 = M((it1+delay),3);

 % Temporal interpolation loop
for it2=1:DTN
       it=it+1;
       U = U1 + (it2-1)*DTinc*(U2-U1);
       V = V1 + (it2-1)*DTinc*(V2-V1);
       H = H1 + (it2-1)*DTinc*(H2-H1);
       Uwind = Uwind1 + (it2-1)*DTinc*(Uwind2-Uwind1);
       Vwind = Vwind1 + (it2-1)*DTinc*(Vwind2-Vwind1);

    % Particles loop
    for ip=1:np

    % Spatial bilinear interpolation of velocity:
    clear I J I2 J2 I3 J3 Itemp Jtemp I2temp J2temp incx1 incx2 incy1 incy2
    clear u v u1 u2 u3 u4 v1 v2 v3 v4 utide vtide
```

```
    % Find the limit of the box where the particle is:
    I = find(xq<x(it,ip),1, 'last');
    J = find(yq<y(it,ip),1, 'last');
    I2 = find(xq>x(it,ip),1);
    J2 = find(yq>y(it,ip),1);

    % Avoid model to stop if particles reach the limit of the domain:
    if J == (length(yq))
       x(it+1,ip) = x(it,ip);
       y(it+1,ip) = y(it,ip);
    elseif J2 == 1
        x(it+1,ip) = x(it,ip);
        y(it+1,ip) = y(it,ip);
    else

    % Value of the limit boxes in UTM:
    Itemp = xmin + (dx*I);
    Jtemp = ymin + (dy*J);
    I2temp = xmin + (dx*I2);
    J2temp = ymin + (dy*J2);

    % Index creation for bilinear interpolation:
    incx1 = (x(it,ip)-Itemp)/(I2temp-Itemp);
    incx2 = (I2temp-x(it,ip))/(I2temp-Itemp);
    incy1 = (y(it,ip)-Jtemp)/(J2temp-Jtemp);
    incy2 = (J2temp-y(it,ip))/(J2temp-Jtemp);

    u1 = MASK(J,I).*U(J,I);
    u2 = MASK(J,I2).*U(J,I2);
    u3 = MASK(J2,I).*U(J2,I);
    u4 = MASK (J2,I2).*U(J2,I2);
    v1 = MASK(J,I).*V(J,I);
    v2 = MASK(J,I2).*V(J,I2);
    v3 = MASK(J2,I).*V(J2,I);
    v4 = MASK (J2,I2).*V(J2,I2);

    % Bilinear interpolation according to the value of the corner of the box:
    if MASK(J,I) == 1 & MASK(J,I2) == 1 & MASK(J2,I2) == 1 & MASK (J2,I) ==
1
        utide = u1 + incx1*(u4-u1); %linear interpolation in diagonal
    elseif MASK(J,I)== 1 & MASK(J,I2)== 0 & MASK(J2,I2) == 0 & MASK (J2,I)
== 0
        utide = u1;
    elseif MASK(J,I)== 1 & MASK(J,I2)== 1 & MASK(J2,I2) == 0 & MASK (J2,I)
== 0
        utide = u1 + incx1*(u2-u1); %linear interpolation among X axis the
bottom border of the box
    elseif MASK(J,I)== 1 & MASK(J,I2)== 1 & MASK(J2,I2) == 1 & MASK (J2,I)
== 0
        utide = u1 + incx1*(u4-u1); %linear interpolation in diagonal
    elseif MASK(J,I)== 1 & MASK(J,I2)== 0 & MASK(J2,I2) == 0 & MASK (J2,I)
== 1
        utide = u1 + incy1*(u3-u1); %linear interpolation among Y axis the
left border of the box
    elseif MASK(J,I)== 1 & MASK(J,I2)== 0 & MASK(J2,I2) == 1 & MASK (J2,I)
== 1
        utide = u1 + incx1*(u4-u1); %linear interpolation in diagonal
    elseif MASK(J,I)== 1 & MASK(J,I2)== 1 & MASK(J2,I2) == 0 & MASK (J2,I)
== 1
        utide = u2 + incx2*(u3-u2); %linear interpolation in diagonal
    elseif MASK(J,I)== 0 & MASK(J,I2)== 1 & MASK(J2,I2) == 1 & MASK (J2,I)
== 1
        utide = u2 + incx2*(u3-u2); %linear interpolation in diagonal
```

```
    elseif MASK(J,I)== 0 & MASK(J,I2)== 0 & MASK(J2,I2) == 1 & MASK (J2,I)
== 1
        utide = u4 + incx2*(u3-u4); %linear interpolation among X axis the
top border of the box
    elseif MASK(J,I)== 0 & MASK(J,I2)== 0 & MASK(J2,I2) == 0 & MASK (J2,I)
== 1
        utide = u3;
    elseif MASK(J,I)== 0 & MASK(J,I2)== 1 & MASK(J2,I2) == 0 & MASK (J2,I)
== 1
        utide = u2 + incx2*(u3-u2); %linear interpolation in diagonal
    elseif MASK(J,I)== 0 & MASK(J,I2)== 1 & MASK(J2,I2) == 1 & MASK (J2,I)
== 0
        utide = u4 + incy2*(u2-u4); %linear interpolation among Y axis the
right border of the box
    elseif MASK(J,I)== 0 & MASK(J,I2)== 0 & MASK(J2,I2) == 1 & MASK (J2,I)
== 0
        utide = u4;
    elseif MASK(J,I)== 0 & MASK(J,I2)== 1 & MASK(J2,I2) == 0 & MASK (J2,I)
== 0
        utide = u2;
    elseif MASK(J,I)== 1 & MASK(J,I2)== 0 & MASK(J2,I2) == 1 & MASK (J2,I)
== 0
        utide = u1 + incx1*(u4-u1); %linear interpolation in diagonal
    else
       utide = 0;
    end

    if MASK(J,I) == 1 & MASK(J,I2) == 1 & MASK(J2,I2) == 1 & MASK (J2,I) ==
1
        vtide = v1 + incx1*(v4-v1); %linear interpolation in diagonal
    elseif MASK(J,I)== 1 & MASK(J,I2)== 0 & MASK(J2,I2) == 0 & MASK (J2,I)
== 0
        vtide = v1;
    elseif MASK(J,I)== 1 & MASK(J,I2)== 1 & MASK(J2,I2) == 0 & MASK (J2,I)
== 0
        vtide = v1 + incx1*(v2-v1); %linear interpolation among X axis the
bottom border of the box
    elseif MASK(J,I)== 1 & MASK(J,I2)== 1 & MASK(J2,I2) == 1 & MASK (J2,I)
== 0
        vtide = v1 + incx1*(v4-v1); %linear interpolation in diagonal
    elseif MASK(J,I)== 1 & MASK(J,I2)== 0 & MASK(J2,I2) == 0 & MASK (J2,I)
== 1
        vtide = v1 + incy1*(v3-v1); %linear interpolation amon Y axis the
left border of the box
    elseif MASK(J,I)== 1 & MASK(J,I2)== 0 & MASK(J2,I2) == 1 & MASK (J2,I)
== 1
        vtide = v1 + incx1*(v4-v1); %linear interpolation in diagonal
    elseif MASK(J,I)== 1 & MASK(J,I2)== 1 & MASK(J2,I2) == 0 & MASK (J2,I)
== 1
        vtide = v2 + incx2*(v3-v2); %linear interpolation in diagonal
    elseif MASK(J,I)== 0 & MASK(J,I2)== 1 & MASK(J2,I2) == 1 & MASK (J2,I)
== 1
        vtide = v2 + incx2*(v3-v2); %linear interpolation in diagonal
    elseif MASK(J,I)== 0 & MASK(J,I2)== 0 & MASK(J2,I2) == 1 & MASK (J2,I)
== 1
        vtide = v4 + incx2*(v3-v4); %linear interpolation among X axis the
top border of the box
    elseif MASK(J,I)== 0 & MASK(J,I2)== 0 & MASK(J2,I2) == 0 & MASK (J2,I)
== 1
        vtide = v3;
    elseif MASK(J,I)== 0 & MASK(J,I2)== 1 & MASK(J2,I2) == 0 & MASK (J2,I)
== 1
        vtide = v2 + incx2*(v3-v2); %linear interpolation in diagonal
    elseif MASK(J,I)== 0 & MASK(J,I2)== 1 & MASK(J2,I2) == 1 & MASK (J2,I)
== 0
```

```
        vtide = v4 + incy2*(v2-v4); %linear interpolation among Y axis the
right border of the box
    elseif MASK(J,I)== 0 & MASK(J,I2)== 0 & MASK(J2,I2) == 1 & MASK (J2,I)
== 0
        vtide = v4;
    elseif MASK(J,I)== 0 & MASK(J,I2)== 1 & MASK(J2,I2) == 0 & MASK (J2,I)
== 0
        vtide = v2;
    elseif MASK(J,I)== 1 & MASK(J,I2)== 0 & MASK(J2,I2) == 1 & MASK (J2,I)
== 0
        vtide = v1 + incx1*(v4-v1); %linear interpolation in diagonal
    else
        vtide = 0;
    end

    % Surface velocity approximation:
    usurface = utide*1.15;
    vsurface = vtide*1.15;

    % Wind velocity approximation:
    Uwindnew = Uwind *0.035;
    Vwindnew = Vwind *0.035;

    % Addition of wind velocity:
    u = usurface + Uwindnew;
    v = vsurface + Vwindnew;

    % Total advection:
    ddx = u*DT2;
    ddy = v*DT2;

    % Diffusion:
    r = rand;
    ra = rand;
    if r < 0.5
       RR = -(r*2);
    else
       RR = r*2;
    end
    if ra < 0.5
        RRa = -(ra*2);
   else
        RRa = ra*2;
    end

    angx = 2*pi*RR;
    angy = 2*pi*RR;
    Lx = RRa/R*(cos(angx))*sqrt(2*K*DT2);
    Ly = RRa/R*(sin(angy))*sqrt(2*K*DT2);

    % Total dispersal:
    x(it+1,ip) = x(it,ip)+ ddx + Lx;
    y(it+1,ip) = y(it,ip)+ ddy + Ly;

    I3 = find(xq>=x(it+1,ip),1);
    J3 = find(yq>=y(it+1,ip),1);

    % Reflect particles off land:
    if (MASK(J3,I3)*H(J3,I3)) < 0.1
      x(it+1,ip)= x(it,ip);
      y(it+1,ip)= y(it,ip);
    end % End loop reflect particles
```

```
    end % End loop border

    end % End loop particles

    % plot the patch
    delete(h1);
    delete(h2);
    h1 = plot(x(it+1,:),y(it+1,:),'xr');
    h2 = text(4.3e5,5.89e6,['Time step = ',num2str(it)]);
    drawnow

end % End it2 loop

     U1=U2; V1=V2; H1=H2;
     Uwind1 = Uwind2; Vwind1 = Vwind2;

end % End it1 loop
```

Appendix D: Evaluation of first spawning event in 2014 based on the difference between air temperature and sea surface temperature.

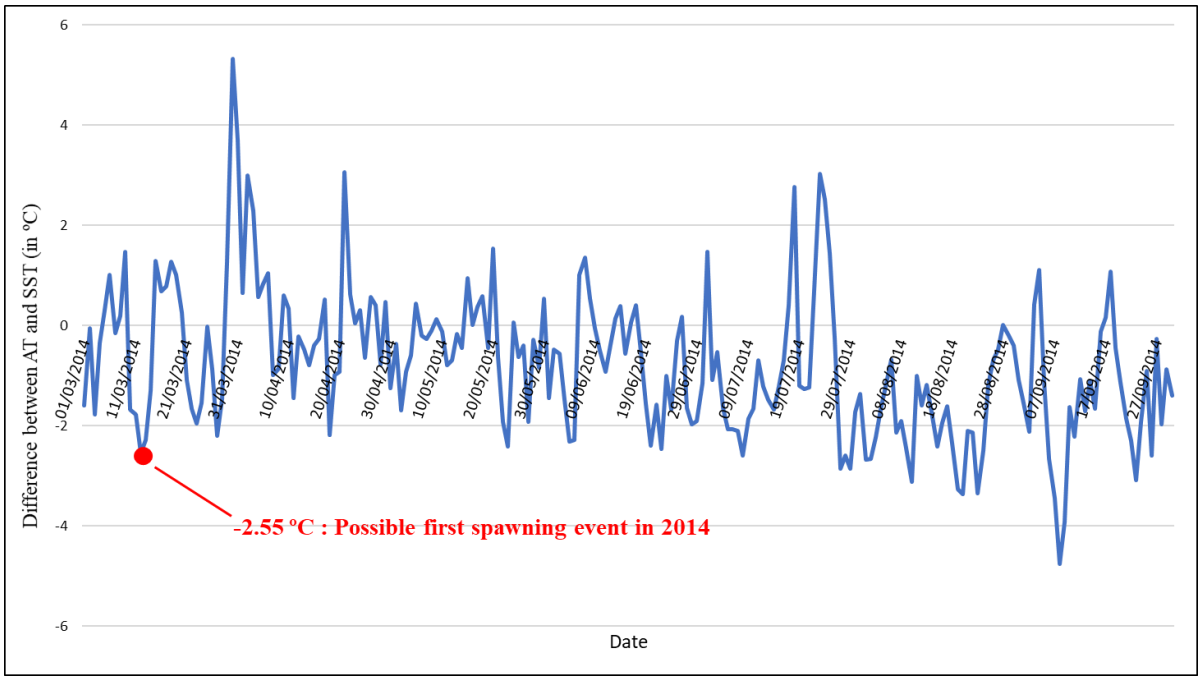

Figure D.1: Graph showing the difference (in ºC) between Air Temperature (AT) and Sea Surface Temperature (SST) during spring and summer 2014.

Appendix E: Results of simulation representing larvae released at mid-water depth during March-April 2014.

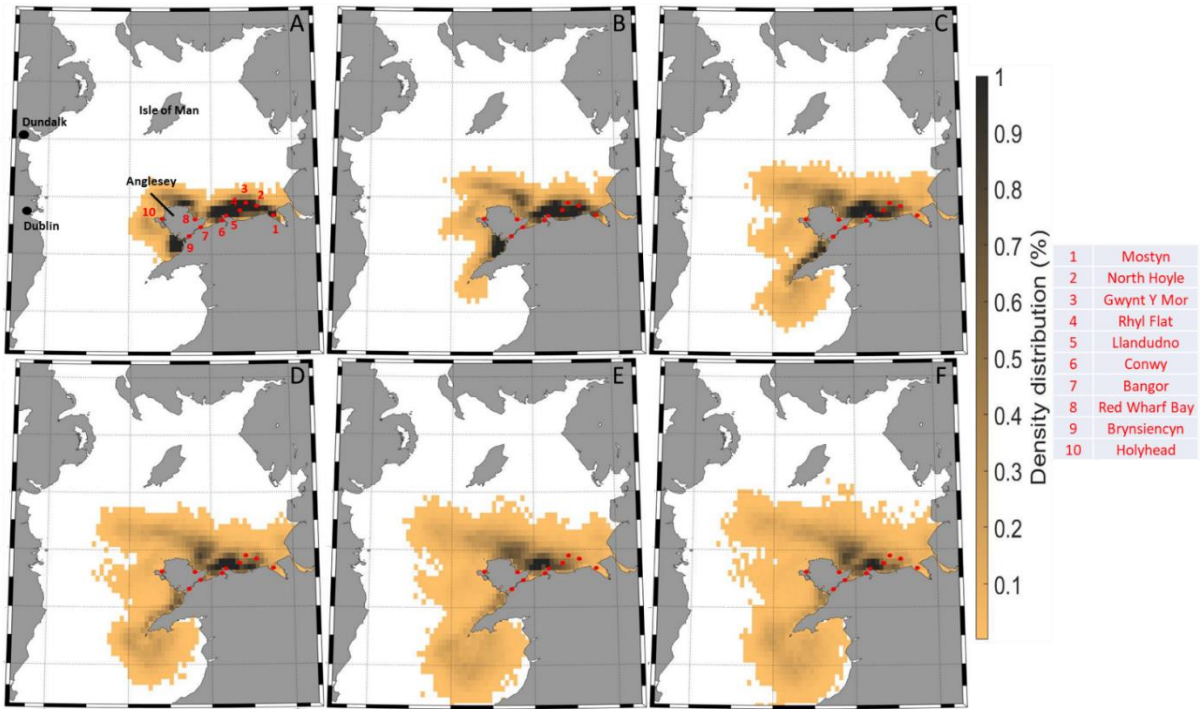

Figure E.1: Maps showing the density distribution of mussel larvae released at the midwater column in March-April 2014 (advected by tide only) from 10 released areas (red dots) during: (A) week 1; (B) week 2; (C) week 3; (D) week 4; (E) week 5 and (F) week 6.

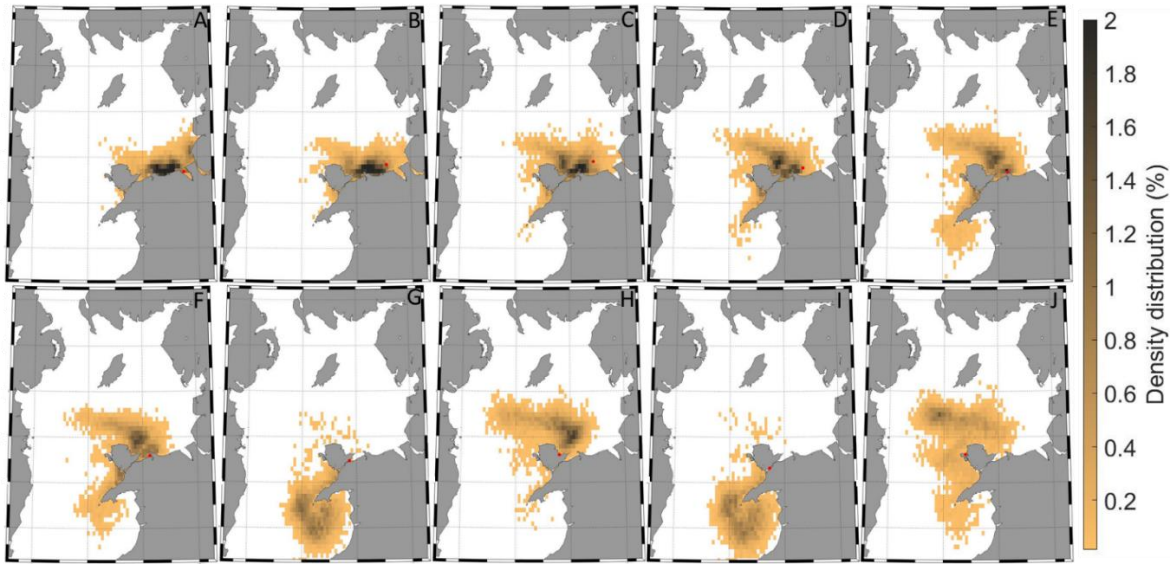

Figure E.2: Maps showing the density distribution of mussel larvae released at the midwater column (advected by tide only) after 6 weeks simulation in March-April 2014 from 10 released areas (red dots): (A) Mostyn; (B) North Hoyle; (C) Gwynt Y Mor; (D) Rhyl Flat; (E) Llandudno; (F) Conwy; (G) Bangor; (H) Red Wharf Bay; (I) Brynsiencyn and (J) Holyhead.

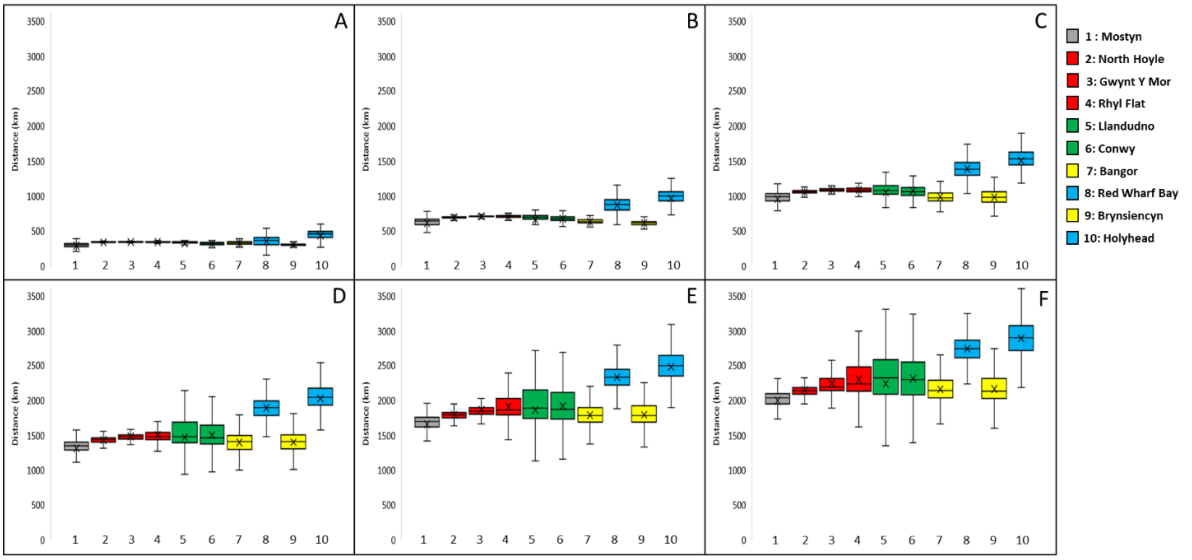

Figure E.3: Cumulative distance (CD) travelled by particles (representing mussel larvae dispersing at mid-waters) during March-April 2014 during week 1 (A), week 2 (B), week 3 (C), week 4 (D), week 5 (5) and week 6 (F). Sites are coloured according to their location: Mostyn (grey), Offshore wind farms (red), Great Orme (green), Menai Strait (yellow), Anglesey (blue). Results are based on 21,000 particles – showing maximum, minimum, median (crossbar) and average (cross) value.

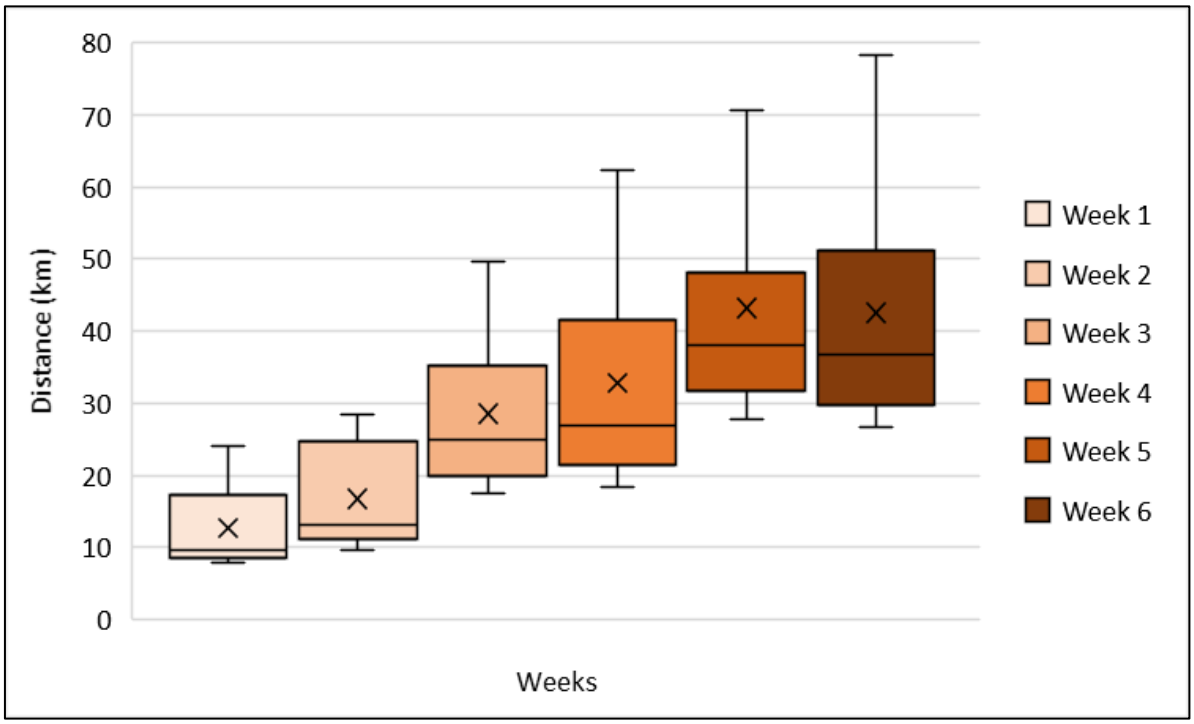

Figure E.4: Net transport (NT) distances of particles per week when released at mid-water depth in March-April 2014. Results are based on: 70,000 particles – showing maximum, minimum, median (crossbar) and average (cross) value.

Table E.1: Cumulative percentage of particles (representing mussel larvae dispersing near the surface in 2014) per release site which were simulated to connect with settlement site, for different PLD: week 3, week 4, week 5 and week 6.

Release site number	1	2	3	4	5	6	7	8	9	10
Release site name	Mostyn	North Hoyle	Gwynt Y Mor	Rhyl Flat	Llandudno	Conwy	Bangor	Red Wharf Bay	Brynsiencyn	Holyhead
Week 3	46.7	51.4	32.3	25.4	32.5	25.9	1.7	0.6	1.1	1.5
Week 4	42.9	43.7	26.4	22.9	26.6	19.2	0.7	0.4	0.4	0.7
Week 5	39.3	35.6	21.0	16.8	20.9	12.2	0.3	0.4	0.2	0.4
Week 6	37.4	31.9	18.7	14.0	19.0	9.5	0.1	0.5	0.1	0.4

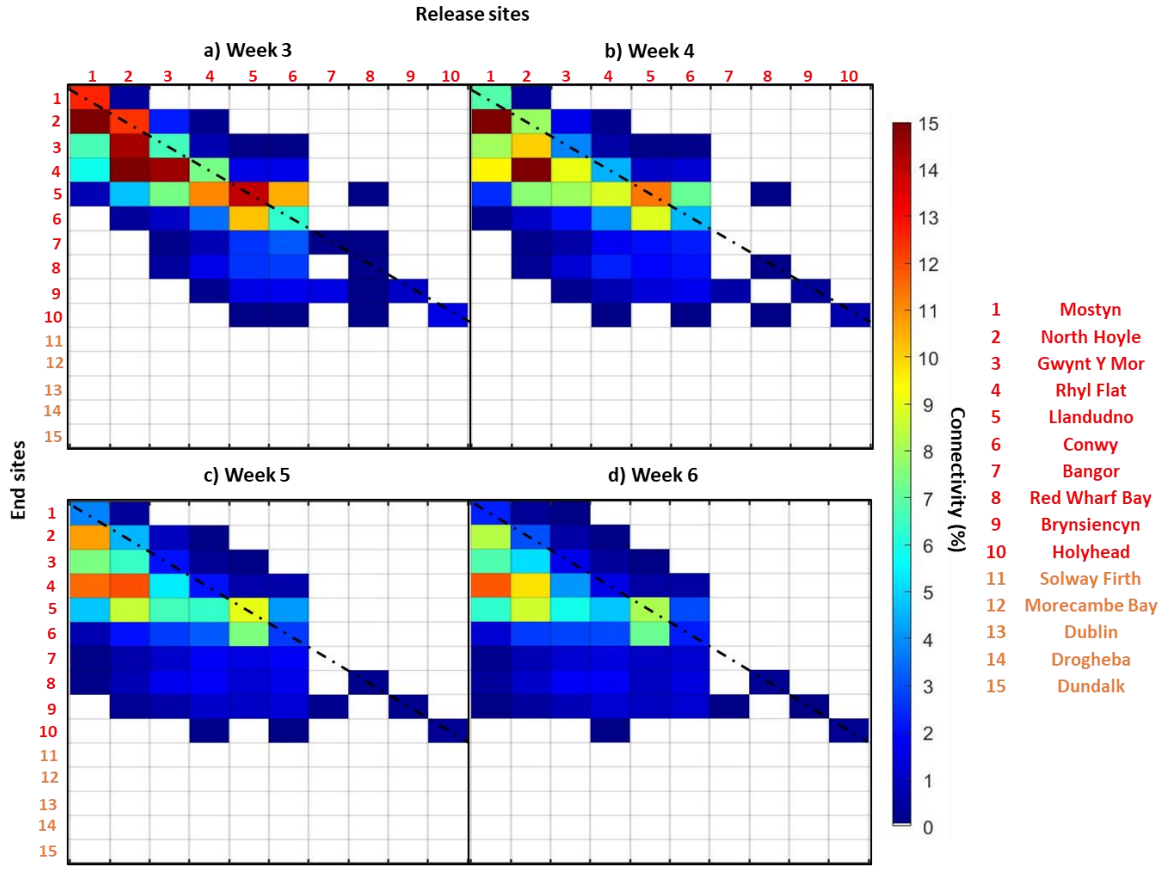

Figure E.5: Connectivity matrices for larvae release in the mid-water column in March-April 2014 during (a) week 3, (b) week 4, (c) week 5 and (d) week 6. Connectivity between larvae from a source (column) with a sink (row) is highlighted by colour scale with high connectivity in red, low connectivity in blue and no connectivity in white. Self-recruitment (e.g. retention within the release site) is indicated by cells that cross the diagonal dashed line. Sites are colour coded as: red = source and sink sites and orange = sink sites only.